Summer 2008

Investigation of (E, 2E) Collisions and Related Phenomena

Jason Manuel Martinez
Old Dominion University

INVESTIGATION OF $(E, 2E)$ COLLISIONS AND RELATED PHENOMENA

by

Jason Manuel Martinez
B.S. May 2001, Reed College
M.S. May 2005, Old Dominion University

A Dissertation Submitted to the Faculty of
Old Dominion University in Partial Fulfillment of the
Requirement for the Degree of

DOCTOR OF PHILOSOPHY

PHYSICS

OLD DOMINION UNIVERSITY
August 2008

Approved by:

Colm T. Whelan (Director)

John A. Adam (Member)

Alexander L. Godunov (Member)

Mark D. Havey (Member)

J. Wallace Van Orden (Member)

ABSTRACT

INVESTIGATION OF (E, $2E$) COLLISIONS AND RELATED PHENOMENA

Jason Manuel Martinez
Old Dominion University, 2008
Director: Dr. Colm T. Whelan

In this thesis I investigate $(e, 2e)$ processes, or electron impact ionization, using several theoretical methods. I first examine the problem using the Born approximations, particularly the Distorted Wave Born Approximation (DWBA), focusing on the underlying processes that dominate for ionization of the $2p$ state of Argon and Magnesium. I investigate as well the ionization of helium and hydrogen and use the simplicity of the approximation to probe the incident particle effects on the Helium cross section. In both cases the results are compared with experiment. I also produce cross section results for ions near threshold, a regime that is currently under experimental investigation. In the second part of this thesis, I develop an *ab initio* method for doing these calculations called the X2e method. This is described in full, including derivation of the important features of the method. Preliminary results are presented in comparison with established theory.

ACKNOWLEDGEMENTS

I would like to thank my advisor Dr. Colm T. Whelan for his guidance and expertise throughout this project. In particular I appreciate his help with the DWBA calculations and in obtaining a collaboration with experimentalists.

I would also like to thank my collaborator Dr. Robert K. Nesbet for his aid in completing the X2e code. His work forms the basis of this method and he has been instrumental in resolving the remaining bugs.

I would also like to thank Dr. Lorenzo Avaldi and his research group for providing us with new data with which to compare our DWBA code and for supplying us with it prior to journal publication.

Of those people who had an indirect impact on my research, I first would like to thank Dr. Nicholas Wheeler for his advice to me when writing my senior thesis. His encouragement to always be writing has made this second experience that much easier.

I would also like to thank my fellow graduate students for their support and advice over the years. Also I thank my other friends for giving me many fun Saturday nights as an outlet for my frustrations.

Lastly I would like to thank my Mom, Dad, Babcia, and my bothers Michael and David for always believing in me.

TABLE OF CONTENTS

LIST OF TABLES

LIST OF FIGURES

CHAPTER I

INTRODUCTION

In recent years there have been great strides in experimental atomic collision physics. It has become possible to perform kinematically complete scattering experiments and to put the experimental data on an absolute scale. Much of the work in the field has been directed to the study of electron impact ionization and photo-double ionization [1]. In these processes an electron or photon, respectively, is incident on an atom or ion, and the collision results in the ionization of the target with two electrons escaping. This form of ionization collision is called an $(e,2e)$ or $(\gamma,2e)$ collision, respectively. Specifically of interest are the measurements of the Triple Differential Cross Sections (TDCS) where the energies and angles of the escaping electrons are resolved. These five-fold differential cross sections contain the most information that can be derived from the collisional system where spin is not accounted for.

There is strong interest in theoretical calculations for these processes, for example with the FAIR project with $(e, 2e)$ collisions with ions [2]. These calculations offer a chance to examine the underlying physics and see what are the dominate contributions to these cross sections. This can be done by looking at the approximations that mostly clearly replicate the experimental data and examining from that what are the necessary physics to include.

Additionally there is the challenge to produce *ab initio* calculations for these reliable experimental results. This still presents a substantial challenge to theory. The difficulty of calculating this process is due to the long range Coulomb interactions between all three particles (i.e. the two escaping electrons and the resulting ion). These interactions do not become negligible except at the most extreme distances and require substantial effort (both computational and analytical) from theory to calculate them. Exacerbating these difficulties is the issue of correctly accounting for the target wave function. In addition to the difficulties of modeling the complex behavior of an atom with multiple electrons, there is also the fact that the target modifies the incident electron wave function as well.

The subject of theoretical calculation of $(e, 2e)$ and $(\gamma, 2e)$ collisions are important for a number of fields in science. In addition to extending the understanding

This dissertation follows the style of *The Physical Review*

of multibody interactions and aiding experimental examination of these collisions, this work is necessary for the calculations of high density plasmas for fusion [3, 4], astrophysical studies [5], and in the developing field of electron momentum spectroscopy [6]. This work, particularly in the development of *ab initio* models, is a stepping stone to more advance calculations for more complex targets in the future.

The benchmark work for electron impact ionization on atomic hydrogen has been resolved experimentally in recent years. Considerable effort is currently being focused on experimentally producing the analogous benchmark data for helium double photo-ionization [7]; results for the simultaneous electron impact excitation and ionization of helium are becoming available [8]. Recent experimental studies of the ionization of molecules and solid surfaces lie still further beyond current theoretical capabilities [1]. While there have been considerable theoretical advances in special cases, a complete *ab initio* theoretical treatment which is applicable to all these problems, is not currently available .

In this thesis we examine the problem initially from a first order perturbation calculation using the Distorted Wave Born Approximation (DWBA). This approach attempts to solve the problem using the simplest approximations that contain the relevant physics. This approximation allows us to derive correct results for a large subset of $(e, 2e)$ processes but is limited in cases where higher order effects dominate, such as near threshold. Despite this we are able to show that it works well in a wide range of cases. In Chapter 2 we will show calculations involving inner and outer shell ionization of Magnesium as well as other elements in comparison with experiment. In Chapter 3 we then extend this method to calculations involving hydrogen-like and helium-like ions near threshold. Because of the simple approximations used we are able to examine the dominate processes within these collisions and understand the underlying physics.

In the second half of this thesis we will develop the variational $\mathcal{R}$-operator approach, or X2e method, which is an *ab initio* calculation applicable to electron impact ionization and double photo-ionization for all kinematics. Ultimately we hope this method will provide an efficient and flexible method of calculating $(e, 2e)$ and $(\gamma, 2e)$ TDCS for a wide variety of systems beyond that of hydrogen or helium. What we present here is essentially a proof of principle that this method is viable and can be extended to much more complex systems than atomic hydrogen or helium. This will be done by comparing our results with those of the simplified Poet-Temkin

model [9, 10].

In this chapter we review the relevant physics needed to understand our methods, both for the DWBA and the $\mathcal{R}$-operator. We first consider basic scattering theory. We discuss the kinematics of the problem and the relevant boundary conditions. We then discuss how one can extract the TDCS from the wave function. Afterwards we examine various perturbation methods for solving the problem and their successes and failures. Then we look at the current *ab initio* solutions that might solve the problem in its entirety and their relative strengths and weaknesses. Lastly we examine the experimental geometries that are relevant to this thesis.

Throughout this thesis we consider only non-relativistic, spin independent interactions. Atomic units are used throughout ($\hbar = e = m_e = 1$).

I.1 SCATTERING THEORY

To get a basic understanding of the problems involved in calculating $(e, 2e)$ processes, we will first review the simpler problem of potential scattering. Indeed, much of the theory of $(e, 2e)$ processes is derived from this earlier work and we will be making use of scattering calculations later when we test our general X2e method.

We begin by describing the basic kinematics. For the $(e, 2e)$ process, we have an electron with momentum $\mathbf{k}_0$ striking the atom or ion. After the collision two electrons escape the ion with momenta $\mathbf{k}_f$ and $\mathbf{k}_s$, for fast and slow respectively. We will be including the effects of exchange so these do not necessarily correspond to the actual scattered or emitted electrons. Using conservation of energy and momenta we can relate the momenta of the escaping electrons to that of the atom's recoil and the incident momenta,

$$k_0^2 = k_f^2 + k_s^2 - 2\epsilon_0 + 2E_{recoil} \tag{1}$$

$$\mathbf{k}_0 = \mathbf{k}_f + \mathbf{k}_s - \mathbf{k}_{recoil} \tag{2}$$

where ϵ_0 is the energy of the ground state (i.e. the energy needed for ionization), which is -0.5 a.u. for hydrogen. An important quantity is the momenta transfer $\mathbf{q}$ from the fast electron to the slow electron and ion,

$$\mathbf{q} = \mathbf{k}_0 - \mathbf{k}_f \tag{3}$$

$$\mathbf{k}_{recoil} = \mathbf{q} - \mathbf{k}_s \tag{4}$$

Note that in a classical collision the momentum transfer for an impact on a stationary electron would directly correspond to the momentum imparted onto the target electron (i.e. $\mathbf{q} = \mathbf{k_s}$). Because we are dealing with a quantum mechanical object however, the target electron has a momentum distribution which allows for it to escape with momentum different from that of the momentum transfer. The momentum transfer is still useful in determining the direction where the electron is most likely to be emitted. We also note that the large mass difference between the incident electron and the nucleus means that E_{recoil} can be neglected in (1).

Our initial state for the wave function can characterized by

$$\Phi(\mathbf{r}_f, \mathbf{r}_s) = \psi_0(\mathbf{r}_s) e^{i\mathbf{k}_0 \cdot \mathbf{r}_f} \tag{5}$$

where the incident electron is treated as a plane wave and ψ_0 is the ground state of the target.

I.1.1 BOUNDARY CONDITIONS

There are several boundary conditions that need to be considered for this problem. The first and simplest is that the outgoing wave functions should be zero when $r_i = 0$. That is to say the electrons cannot overlap with the nucleus.

Another simple condition comes from the consideration of spin. If we take hydrogen as an example, we see that the total spin has to be 0 or 1. This is because the electrons (both the scattered and target) have spin 1/2. Summing their spins gives us this restriction. The limit on the total spin in turn means that if we exchange the positions of the escaping electrons then their wave function must obey the relation $\Psi(\mathbf{r}_f, \mathbf{r}_s) = (-1)^S \Psi(\mathbf{r}_s, \mathbf{r}_f)$. This places an additional restriction of the wave function. It must be symmetric or antisymmetric with respect to the transposition of the electron coordinates. We note that the Hamiltonian is independent of spin and hence we can perform our calculations for each spin state.

The remaining boundary conditions come from the asymptotic forms of the incoming incident and outgoing scattered waves. We can describe the total wave function as a sum of these two parts,

$$\Psi(\mathbf{r}_1, \mathbf{r}_2) \approx \Psi_{in}(\mathbf{r}_1, \mathbf{r}_2) + \Psi_{scat}(\mathbf{r}_1, \mathbf{r}_2) \tag{6}$$

where Ψ_{in} and Ψ_{scat} refer to the incoming and scattered portions respectively. We assume the target is initially in its ground state, denoted by the subscript 0. We can

describe the incoming portion of the wave function as being made up of the ground state wave function of the target electron ψ_0 and a plane wave with momentum $\mathbf{k}_0$

$$\Psi_{in}(\mathbf{r}_1, \mathbf{r}_2) = \frac{1}{\sqrt{2}} \left(\psi_0(\mathbf{r}_2) e^{i\mathbf{k}_0 \cdot \mathbf{r}_1} + (-1)^S \psi_0(\mathbf{r}_1) e^{i\mathbf{k}_0 \cdot \mathbf{r}_2} \right) \tag{7}$$

The scattered wave, Ψ_{scat}, depends on the energy of the escaping electron(s). We can view this wave function as a set of channels, or possible final states, which depend on the energy of the final state atom and the scattered electron. In the simplest case, the electron scatters elastically, leaving the atom in its ground state and no energy is lost. Another possible channel is inelastic scattering where the incident electron excites the target to a higher energy state and leaves with a lower energy. These channels are called 'open' and 'closed' depending on whether the incident electron has sufficient energy to excite the target electron to that particular state or not. Obviously the elastic scattering channel is always open. We can determine the status of the other channels by considering the energies

$$k_\mu^2 = k_i^2 + 2\epsilon_i - 2\epsilon_\mu \tag{8}$$

where k is the momentum of the scattered electron, ϵ is the energy of the bound electron, and the subscripts μ and i denote the final and initial channels respectively. If $k_\mu^2 > 0$ then the channel is open, otherwise it is closed.

The wave function for Ψ_{scat}, when the energies are below the ionization threshold can be described by an expansion in terms of a scattered wave and a bound wave function. In the limit where either $r_1 \to \infty$ or $r_2 \to \infty$ (to account for exchange) this is

$$\lim_{r_1, r_2 \to \infty} \Psi_{scat}(\mathbf{r}_1, \mathbf{r}_2) = \sum_\mu \frac{1}{\sqrt{2}} \left(f_\mu(\hat{\mathbf{r}}_1) \psi_\mu(\mathbf{r}_2) \frac{e^{i\mathbf{k}_0 \cdot \mathbf{r}_1}}{r_1} + (-1)^S g_\mu(\hat{\mathbf{r}}_2) \psi_\mu(\mathbf{r}_1) \frac{e^{i\mathbf{k}_0 \cdot \mathbf{r}_2}}{r_2} \right) \tag{9}$$

where $f_\mu(\hat{\mathbf{r}}_1)$ and $g_\mu(\hat{\mathbf{r}}_2)$ are the direct scattering and exchange amplitudes respectively. ψ_μ refers to the wave function of the other electron after impact, whether that is the ground state or an excited state. In this case each channel is described by a spherically outgoing wave coupled to an excited or ground state with the angular dependance determined by the scattering amplitude.

The case of most interest to us however is that of ionization. When the incident energy is sufficiently large to excite the bound electron to the continuum we must include an additional term to the asymptotic form of the scattered wave function, Ψ_{scat}. Peterkop [11], Rudge and Seaton [12] derived the ionization term in the far

asymptotic region, when all particles are far apart from one another. This derivation is given later in Chapter 7 when we discuss the Rudge, Seaton, and Peterkop (RSP) formalism. For now we will simply note that one can describe the wave function, in hyperspherical notation (where $\rho = \sqrt{r_1^2 + r_2^2}$ and $\alpha = \arctan(r_1/r_2)$) as

$$\lim_{\rho\to\infty} \Psi_{ion}(\mathbf{r}_1, \mathbf{r}_2) = -\sqrt{\frac{i\kappa^3}{\rho^5}} \exp i\left(\kappa\rho + \frac{\zeta(\hat{\mathbf{r}}_1, \hat{\mathbf{r}}_2, \alpha)}{\kappa} \ln(\kappa\rho)\right) \Big(f(\mathbf{k}_f, \mathbf{k}_s) + (-1)^S f(\mathbf{k}_s, \mathbf{k}_f)\Big) \tag{10}$$

where

$$\zeta(\hat{\mathbf{r}}_1, \hat{\mathbf{r}}_2, \alpha) = \frac{Z}{\sin\alpha} + \frac{Z}{\cos\alpha} - \frac{1}{\sqrt{1 - \hat{\mathbf{r}}_1 \cdot \hat{\mathbf{r}}_2 \sin 2\alpha}} \tag{11}$$

or

$$\frac{\zeta(\hat{\mathbf{r}}_1, \hat{\mathbf{r}}_2, \alpha)}{r} = \frac{Z}{r_1} + \frac{Z}{r_2} - \frac{1}{|\mathbf{r}_1 - \mathbf{r}_2|} \tag{12}$$

and $\kappa = \sqrt{k_1^2 + k_2^2} = \sqrt{2E}$. Z is the charge of the resulting ion. It can also be shown [11, 12] that the direct and exchange amplitudes for ionization are related by $f(\mathbf{k}_f, \mathbf{k}_s) = g(\mathbf{k}_s, \mathbf{k}_f)$ (This will be show explicitly in Chapter 7). This allows us to reexpress (10) as

$$\lim_{\rho\to\infty} \Psi_{ion}(\mathbf{r}_1, \mathbf{r}_2) = -\sqrt{\frac{i\kappa^3}{\rho^5}} \exp i\left(\kappa\rho + \frac{\zeta(\hat{\mathbf{r}}_1, \hat{\mathbf{r}}_2, \alpha)}{\kappa} \ln(\kappa\rho)\right) \Big(f(\mathbf{k}_f, \mathbf{k}_s) + (-1)^S g(\mathbf{k}_f, \mathbf{k}_s)\Big) \tag{13}$$

Our concern now is to determine the cross sections for a given process. As will be shown in the next section one way of doing this is to determine the ionization amplitude $f(\mathbf{k}_f, \mathbf{k}_s)$.

I.2 EXTRACTING THE IONIZATION CROSS SECTION

In this section we will examine methods of extracting the ionization cross section. Specifically we are interested in deriving the Triple Differential Cross Section (TDCS). The cross section is defined as the ratio of the number of events per unit time per unit scatterer, to the flux for a given scattering event. In the case of TDCS these events are those that occur when the electrons escape at specific angles to the target and with specific energies, thus getting a complete kinematical picture. The methods we will examine include calculating the scattering amplitudes by projecting out the flux as well as directly calculating the flux ratio from the computation of the wave

function. In constructing the $\mathcal{R}$-operator we have tested both of these methods while for our DWBA calculations we have made use of the scattering amplitudes.

Before discussing either of these we will first quickly discuss the basic methods used for scattering, i.e. the **S**-matrix and related matrices. These matrices allow us to relate features of the scattering channels in the asymptotic region. These matrices will be used when we apply the X2e method to scattering as well as when we construct our final wave function. This will be discussed in detail in Chapter 7. As mentioned in the preceding section we can envision a scattering event occurring in discreet channels. One channel would be elastic scattering where the electron simply scatters off the target with no loss of energy or momentum. Other channels in scattering refer to inelastic scattering where the collision results in the target electron being excited to a higher energy state. In either case we can refer to a channel wave function, $u_\mu(r)$, to describe the scattered electron, where μ is an index that refers to the channel in question.

I.2.1 S-MATRIX METHOD

We begin with the **S**-matrix, or scattering matrix, which relates the amplitude of the incoming waves to that of the outgoing waves. For example we can break up a wave function into

$$\lim_{r\to\infty} u_\mu(r) \to A_\mu f_\mu^{in}(r) + B_\mu f_\mu^{out}(r) \tag{14}$$

where f indicates the incoming and outgoing parts of the channel function. We can then relate the coefficients A_μ and B_μ via the **S**-matrix,

$$B_\mu = \sum_{\mu'} S_{\mu\mu'} A_{\mu'}. \tag{15}$$

The **S**-matrix may be used to construct a **T**-matrix. The **T**-matrix, or transmission matrix, tells us what portion of the wave function is transmitted from one state to another. In our case we are interested in the transmission from the ground state to the final state, whether that is excitation or elastic scattering. The **T**-matrix is derived by removing the incoming waves (which in the formalism we have adopted have a value of unity). In matrix notation this is

$$\mathbf{T} = \frac{\mathbf{S} - \mathbf{I}}{2i} \tag{16}$$

where **I** is the identity matrix representing the incident flux and a factor of $1/2i$ is introduced for ease of computation later. Essentially this is removing the incoming

portion of the wave function to get only the outgoing probability. Using the **T**-matrix one can then construct the scattering cross sections [13]:

$$\sigma_{ij} = \frac{(2S+1)(2L+1)}{(2l_j+1)k_j^2}|T_{ij}|^2 \tag{17}$$

where S is the total spin, L is the total angular momentum, k_j is the momentum of the final channel, and l_j is the angular momentum of the final channel. A full derivation will be shown in Chapter 7 when we discuss the scattering problem in relation to the X2e method.

Another useful quantity is the **K**-matrix, or reactance matrix, that relates the even and odd portions of the wave function. If we divide the asymptotic form of the wave function into sines and cosines we get

$$\lim_{r_1\to\infty} u_\mu(r) = \frac{1}{\sqrt{k_\mu}}(C_\mu \sin\theta_\mu + D_\mu \cos\theta_\mu) \tag{18}$$

where $\theta_\mu = k_\mu r - l_\mu \pi/2 - \eta \log 2k_\mu r + \sigma_{l_\mu}$. $\sigma_l = \arg[\Gamma(l+1-i\eta)]$, $\eta = Z/k_\mu$, and l is the angular momentum. Z is the charge of the resulting ion. The **K**-matrix then relates the coefficients of the even and odd parts of the asymptotic wave function:

$$D_\mu = \sum_{\mu'} K_{\mu\mu'} C_{\mu'}. \tag{19}$$

The **K**-matrix can then be used to determine the scattering phase shifts by spectrally decomposing the **K**-matrix [13],

$$K_{ij} = \sum_{k}^{n} x_{ik} x_{jk} \tan\delta_k \tag{20}$$

where x_{ij} is the jth element of the ith eigenchannel. $\tan\delta_k$ are the eigenvalues for the **K**-matrix. δ_k are the eigenphases corresponding to the scattering phase shifts.

These matrices are discussed in further detail in Chapter 7 when we examine how the X2e method can be used for electron scattering calculations. We also show how one can relate the **S**-matrix to the **K**-matrix.

I.2.2 FLUX PROJECTOR METHOD

The Flux Projector Method works by projecting out the outgoing flux at some large radius. From the outgoing flux one can calculate the ionization amplitude $f(\mathbf{k}_f, \mathbf{k}_s)$. This can then be used to calculate the TDCS. The following derivation comes from

Rudge and Seaton [12]. To determine the ionization amplitude $f(\mathbf{k}_0, \mathbf{k})$, we examine the flux over the hypersphere:

$$\begin{aligned}\mathcal{L} &= \int \Phi(H-E)\Psi d^3\mathbf{r}_1 d^3\mathbf{r}_2 \\ &= \frac{1}{2}\int \left(\Psi\frac{\partial\Phi}{\partial\rho} - \Phi\frac{\partial\Psi}{\partial\rho}\right)\rho^5 \sin^2\alpha\cos^2\alpha d\alpha d\Omega_1 d\Omega_2 \end{aligned} \tag{21}$$

where Φ is our projector and Ψ is the full wave function. Ω stands in for the usual angular coordinates θ, ϕ. As noted earlier $\rho = \sqrt{r_1^2 + r_2^2}$ and $\alpha = \arctan(r_1/r_2)$. In equation (21) we have used Green's theorem to simplify the 6-dimensional volume integral to one over a 5-dimensional surface. In Appendix A, a derivation can be found for the differential surface element.

We next proceed by introducing a projector that asymptotically behaves like two Coulomb waves with effective charges and outgoing waves,

$$\lim_{\rho\to\infty}\Phi \sim \chi(z_1, -\mathbf{k}_1, \mathbf{r}_1)\chi(z_2, -\mathbf{k}_2, \mathbf{r}_2) \tag{22}$$

$$\chi(z, -\mathbf{k}, \mathbf{r}) = e^{-i\mathbf{k}\cdot\mathbf{r}}\phi(z/\kappa, kr + \mathbf{k}\cdot\mathbf{r}) \tag{23}$$

$$\begin{aligned}\lim_{y\to\infty}\phi(\gamma, y) \sim\ & y^{-i\gamma}\left[1 - \frac{i\gamma^2}{y} + \ldots\right] + \frac{\gamma e^{2i\eta_0}e^{i\gamma}}{y^{1-i\gamma}} \\ & \times\left[1 - \frac{i(1-i\gamma)^2}{y} + \ldots\right]\end{aligned} \tag{24}$$

where we are keeping only those terms in the leading order in ρ.

We are assuming that all the particles are very far from each other and that the electron-electron interaction can be accounted for via the effective charges z_1 and z_2. Using the asymptotic expansions above in (21) as well as our solution from the RSP derivation (13), we get

$$\begin{aligned}\mathcal{L} = & -\frac{i^{3/2}}{2}(\kappa\rho)^{5/2}\int f(\mathbf{k}_2, \mathbf{k}_1)\phi_1\phi_2(2\kappa\rho)^{i\zeta/\kappa}(1 + \mu_1\sin\alpha\sin\beta \\ & + \mu_2\cos\alpha\cos\beta)\exp\left[i\kappa\rho(1 - \mu_1\sin\alpha\sin\beta - \mu_2\cos\alpha\cos\beta)\right] \\ & \times\sin^2\alpha\cos^2\alpha d\alpha d\Omega_1 d\Omega_2\end{aligned} \tag{25}$$

with

$$\mu = \hat{\mathbf{k}}\cdot\hat{\mathbf{r}} \tag{26}$$

$$k_1 = \kappa\sin\beta \tag{27}$$

$$k_2 = \kappa\cos\beta. \tag{28}$$

Next we make use of the stationary phase theorem. Jeffreys and Jeffreys [14] showed that if $\xi(k)$ and $\chi(k)$ are continuous in (a,b), where $\xi' = d\xi/dk$ and $\xi'' = d^2\xi/dk^2$, then:

Theorem 1.

$$\lim_{R\to\infty}\int_a^b \chi(k)e^{iR\xi(k)}\,dk \sim \Big\{\frac{\chi(k)e^{iR\xi(k)}}{iR\xi'(k)}\Big\}\Big|_{k=a}^{k=b} \tag{29}$$

if $\xi' \neq 0$ in (a,b). Also:

Theorem 2.

$$\lim_{R\to\infty}\int_a^b \chi(k)e^{iR\xi(k)}dk \sim \chi(k_0)\{\frac{2\pi}{R|\xi''(k_0)|}\}^{1/2}e^{i(R\xi(k_0)+\frac{\pi}{4}\mathrm{sign}(\xi''(k_0)))} \tag{30}$$

where $\xi' = 0$ at k_0, k_0 being in (a,b).

We make use of the second theorem here. The key equation is:

$$\xi' = \frac{\partial}{\partial\alpha}(1-\mu_1\sin\alpha\sin\beta-\mu_2\cos\alpha\cos\beta) = -\mu_1\cos\alpha\sin\beta+\mu_2\sin\alpha\cos\beta. \tag{31}$$

For this to be 0 for all values of α we see that $\mu_1 = \mu_2 = 1$ and $\alpha = \beta$. This means

$$\phi_1 \sim (2\kappa\rho\sin^2\beta)^{-iz_1/k_1} \tag{32}$$

$$\phi_2 \sim (2\kappa\rho\cos^2\beta)^{-iz_2/k_2}. \tag{33}$$

Thus our flux has the form:

$$\mathcal{L} = -(2\pi)^{5/2}f(\mathbf{k}_2,\mathbf{k}_1)(2\kappa\rho)^{i(\frac{\zeta(\beta)}{\kappa}-\frac{z_1}{k_1}-\frac{z_2}{k_2})}\left(\frac{k_1}{\kappa}\right)^{-2iz_1/k_1}\left(\frac{k_2}{\kappa}\right)^{-2iz_2/k_2}. \tag{34}$$

Next we can use the definition of ζ, equation (11), as well as (27) and (28) to show

$$\begin{aligned}\frac{\zeta(\Omega_1,\Omega_2,\beta)}{\kappa} &= \frac{Z}{\kappa\sin\beta}+\frac{Z}{\kappa\cos\beta}-\frac{1}{\kappa\sqrt{1-\hat{\mathbf{r}}_\mathbf{1}\cdot\hat{\mathbf{r}}_\mathbf{2}\sin 2\beta}} \\ &= \frac{Z}{k_1}+\frac{Z}{k_2}-\frac{1}{k_{12}}.\end{aligned} \tag{35}$$

where $\hat{\mathbf{r}}_\mathbf{i} = \hat{\mathbf{k}}_\mathbf{i}$ due to $\mu_i = 1$. Thus if we allow

$$\frac{z_1}{k_1}+\frac{z_2}{k_2} = \frac{\zeta}{\kappa}, \tag{36}$$

the factor reliant on ρ vanishes in equation (34). This is known as the Peterkop relation and allows us to set effective charges. Looking at equation (34) we see that without this restriction we would have an infinite phase at $\rho = \infty$. By establishing

these effective charges we are able to examine the ionization amplitude and not merely its modulus.

Using (21) and (34), as well as (36), we can show that the ionization amplitude can be derived using

$$\begin{aligned} f(\mathbf{k}_f, \mathbf{k}_s) &= -(2\pi)^{-5/2} e^{i\Delta(\mathbf{k}_f, \mathbf{k}_s)} \\ &\quad \times \int \Psi(H - E)\Phi d^3\mathbf{r}_f d^3\mathbf{r}_s \end{aligned} \tag{37}$$

where $\Delta = \frac{2z_1}{k_f}\ln(k_f/\kappa) + \frac{2z_2}{k_s}\ln(k_s/\kappa)$. We can simplify this equation by noting that Φ is an asymptotic solution to $\tilde{H} = -\frac{1}{2}\nabla_1^2 - \frac{1}{2}\nabla_2^2 - z_1/r_1 - z_2/r_2$. That is

$$(H - E)\Phi(\mathbf{r}_1, \mathbf{r}_2) = V\Phi(\mathbf{r}_1, \mathbf{r}_2) \tag{38}$$

where

$$V = \frac{1}{|\mathbf{r}_1 - \mathbf{r}_2|} - \frac{Z - z_1}{r_1} - \frac{Z - z_2}{r_2} \tag{39}$$

Using (38) we can rewrite (37) as

$$f(\mathbf{k}_f, \mathbf{k}_s) = -\frac{1}{(2\pi)^{5/2}} \int e^{i\Delta}\Psi(\mathbf{r}_1, \mathbf{r}_2) V\Phi(\mathbf{r}_1, \mathbf{k}_f, \mathbf{r}_2, \mathbf{k}_s) d\tau \tag{40}$$

The exchange term is simply

$$g(\mathbf{k}_f, \mathbf{k}_s) = -\frac{1}{(2\pi)^{5/2}} \int e^{i\Delta}\Psi(\mathbf{r}_1, \mathbf{r}_2) V\Phi(\mathbf{r}_1, \mathbf{k}_s, \mathbf{r}_2, \mathbf{k}_f) d\tau \tag{41}$$

where we have included the momenta to emphasize the effects of exchange.

Once we have calculated the ionization and exchange amplitude we can derive the TDCS,

$$\frac{d^3\sigma}{d\Omega_1 d\Omega_2 dE_1} = \frac{k_f k_s}{k_0} |f(\mathbf{k}_f, \mathbf{k}_s) + (-1)^S g(\mathbf{k}_f, \mathbf{k}_s)|^2 \tag{42}$$

The spin averaged TDCS is given by

$$\frac{d^3\sigma}{d\Omega_1 d\Omega_2 dE_1} = \frac{k_f k_s}{k_0} \left(\frac{1}{4} |f(\mathbf{k}_f, \mathbf{k}_s) + g(\mathbf{k}_f, \mathbf{k}_s)|^2 + \frac{3}{4} |f(\mathbf{k}_f, \mathbf{k}_s) - g(\mathbf{k}_f, \mathbf{k}_s)|^2 \right) \tag{43}$$

This is the method used to calculate the TDCS in the distorted wave Born approximation as well as was tested on the X2e method.

I.2.3 PURE FLUX METHOD

The Pure Flux Method works by calculating the flux directly from the wave function thus avoiding the issue of needing to project out the ionization amplitude [15]. We

begin with a wave function in the far asymptotic regime, i. e. where contributions from elastic and inelastic scattering are negligible and the distances between the particles are large. The current density vector $\mathbf{j}$ for the wave function Ψ is defined

$$\mathbf{j} = \frac{1}{2i}(\Psi^* \nabla \Psi - \Psi \nabla \Psi^*) \tag{44}$$

where Ψ^* is the complex conjugate of Ψ. In hyperspherical coordinates the Laplacian ∇ is to first order

$$\nabla = \frac{\partial}{\partial \rho}\hat{\rho} + O(1/\rho) \tag{45}$$

and the surface element through which one measures the flux is

$$d\Sigma = \rho^5 \sin^2\alpha \cos^2\alpha d\alpha d\Omega_1 d\Omega_2 \tag{46}$$

or equivalently (see Appendix A)

$$d\Sigma = \rho^5 \sin 2\alpha dE_1 d\Omega_1 d\Omega_2 / 4E \tag{47}$$

We can use (45) in (44) to calculate the current density associated with the wave function Ψ_{ion}, equation (13). This gives to leading order in ρ,

$$\mathbf{j} = \frac{\kappa^4}{\rho^5}|f(\mathbf{k}_f, \mathbf{k}_s) + (-1)^S g(\mathbf{k}_f, \mathbf{k}_s)|^2 \tag{48}$$

Examining (13) more closely we see that if we ignore the exponential terms (which vanish when the modulus is taken), equation (48) is equivalent to

$$\mathbf{j} = \kappa |\Psi_{ion}|^2 \tag{49}$$

Next we note that the flux $\mathcal{F}$ through a hypersurface Σ at hyperradius ρ is defined

$$\mathcal{F} = \int_{\Sigma_\rho} \mathbf{j} \cdot \mathbf{n} d\Sigma \tag{50}$$

where $\mathbf{n}$ is the normal to the hypersurface. The outgoing flux at infinite hyperradius is therefore

$$\mathcal{F}_{out} = \frac{\kappa}{4E} \lim_{\rho \to \infty} \rho^5 \int_{\Sigma_\rho} dE_1 d\Omega_1 d\Omega_2 |\Psi_{ion}|^2 \sin 2\alpha \tag{51}$$

where we can use $\mathcal{F}_{out}$ because our Ψ_{ion} wave function consists of only outgoing waves. If we are using the asymptotic form established in equation (6), then in the far asymptotic region the incoming portion of the wave function which is coupled to the ground state, Ψ_{in}, has died off as we approach infinity. This is due to the

ground state rapidly falling to zero by that point. The same also holds for the excited channels. We can relate equation (51) to the cross section by dividing by the incoming flux $\mathcal{F}_{in}$

$$\sigma = \frac{\kappa}{4E\mathcal{F}_{in}} \lim_{\rho\to\infty} \rho^5 \int_{\Sigma_\rho} dE_1 d\Omega_1 d\Omega_2 |\Psi_{ion}|^2 \sin 2\alpha \tag{52}$$

The incident electron can be represented by a plane wave, which has a current density $\mathbf{j} = k_0\hat{\mathbf{z}}$. The incident flux therefore is

$$\mathcal{F}_{in} = k_0 \tag{53}$$

The total spin dependent cross section is thus

$$\sigma = \frac{\kappa}{4Ek_0} \lim_{\rho\to\infty} \rho^5 \int_0^E \sin 2\alpha dE_1 \int |\Psi_{ion}|^2 d\Omega_1 d\Omega_2 \tag{54}$$

This allows us to derive the spin dependent TDCS,

$$\frac{d^3\sigma}{d\Omega_1 d\Omega_2 dE_1} = \lim_{\rho\to\infty} \frac{\kappa}{4Ek_0} \rho^5 |\Psi_{ion}|^2 \sin 2\alpha \tag{55}$$

This is one of the methods tested in the calculation of the TDCS for the X2e method.

I.3 SOLVING THE DOUBLE IONIZATION PROBLEM

In this section we will give a short review of some of the approaches to solving the $(e, 2e)$ problem for TDCS. First we will discuss the Born approximations which are among the simplest and most successful models. In Chapter 2 we will discuss the highly successful distorted wave Born approximation (DWBA) at length when we show new results with Magnesium and in Chapter 3 for atoms and ions at low energy.

In the second part of this section we will discuss the *ab initio* numerical solutions to the problem. We will review the major contributions to this area. We will discuss the Convergent Close Coupling (CCC) method of McCurdy and Rescigno, the extension of this method to Exterior Complex Scaling (ECS) of Bray and Stelbovics, the general **R**-matrix method, and the Hyperspherical **R**-Matrix with Semiclassical Outgoing Waves (HRM-SOW) method of Malegat. We will look at the general methods and focus the relative strengths and weaknesses of these various theories. Additionally in Chapters 4 through 7 we will describe in full detail a new and more flexible method called the X2e method.

I.3.1 BORN APPROXIMATIONS

The Born approximation works by solving the integral form of Schrödinger's equation in the perturbation regime. By this we mean that the wave function is not substantially modified by the electron interaction potential to some order. The methods work from the flux projector method of extracting the ionization amplitude. We will discuss this method in greater detail in the next chapter in reference to the Distorted Wave Born Approximation (DWBA). Here we will give a brief overview.

In a first order Born calculation the waves interact with the electron interaction potential once and the formula is of the form

$$f(\mathbf{k}_f, \mathbf{k}_s) = \langle \chi_f \chi_s | \frac{1}{r_{sf}} | \chi_i \Psi_0 \rangle \tag{56}$$

where χ is the wave function for the free electrons (f and s for the escaping electrons, i for the incident electron) and Ψ_0 is the target state. This corresponds to our flux projector result, equation (40), neglecting of the Peterkop phase factor. This phase factor can be accounted for in the effective charges for the final state electron wave functions χ_f and χ_s.

The differences between the various first Born approximations is in how the electron wave functions are treated. The simplest approximation one could make is to treat all the free electrons (both the incident and escaping electrons) as plane waves. This plane wave Born approximation (PWBA) results in an integral of the form,

$$\begin{aligned} f^{PWBA}(\mathbf{k}_f, \mathbf{k}_s) &= (2\pi)^{-\frac{9}{2}} \int d^3r_s d^3r_f e^{-i\mathbf{k_f}\cdot\mathbf{r_f}} e^{-i\mathbf{k_s}\cdot\mathbf{r_s}} \\ &\quad \times \frac{1}{|\mathbf{r_f} - \mathbf{r_s}|} e^{i\mathbf{k_0}\cdot\mathbf{r_f}} \psi_0(\mathbf{r_s}) \end{aligned} \tag{57}$$

As will be shown in the next chapter this results in completely incorrect behavior near $\mathbf{q} = 0$, which is when the system is slightly perturbed. As the Born approximations are a perturbative approach this is a gross failure. Next we will look at improvements on this approach that resolve this and other problems.

First Born Approximation

The First Born Approximation (FBA) overcomes the flaw of the plane wave approach by treating the wave function of the slow electron, the one with momentum $\mathbf{k}_s$, as distorted by the potential of the ion. In the notation we used above,

$$f^{FBA}(\mathbf{k}_f, \mathbf{k}_s) = (2\pi)^{-9/2} \int d^3r_s d^3r_f$$

$$\times \quad e^{-i\mathbf{k_f}\cdot\mathbf{r_f}}\chi^{-}(\mathbf{k_s},\mathbf{r_s})\frac{1}{|\mathbf{r_f}-\mathbf{r_s}|}e^{i\mathbf{k_0}\cdot\mathbf{r_f}}\psi_0(\mathbf{r_s}) \tag{58}$$

where χ is a distorted wave constructed in the field of the ion. This is done by treating the slow ejected electron as moving in the static exchange potential of the ion and orthogonalizing this state to the bound state, i.e. the slow electron is treated as a continuum state for the target. The fast and incident electrons are still treated as plane waves.

While this results in an approximation that is good for many cases (see Chapter 2 for some comparisons with experiment and the DWBA method), it still fails for cases, such as inner shell ionization, where interactions between the nucleus and the incident or fast electron dominate. In Zhang *et al* [16], they showed that this was extremely important for the recoil direction where FBA underestimated the ratio of the size of the recoil peak to the binary peak as well as failing to account for its asymmetry. Additionally Walters [17, 18] showed that the FBA loses accuracy in overall amplitude when dealing with heavy atoms such as potassium.

Zhang *et al* [16] argued that the distorting effect of the atom, primarily the Coulomb interaction with nucleus could not be neglected for any of the electrons. In the next chapter, we will present comparisons of FBA to the DWBA, which does account for these interactions and show the flaws in this approximation.

Distorted Wave Born Approximation

The Distorted Wave Born Approximation (DWBA) is a highly successful method that was first applied to $(e, 2e)$ of helium [19]. It has been used to calculate the TDCS of a wide range of targets including Helium, Hydrogen, noble gases, Lithium, and Magnesium (In this thesis we examine Helium, Hydrogen, Magnesium, Argon, and Hydrogen-like and Helium-like ions up to $N = 10$).

The DWBA uses distorted waves for all free electrons to properly account the interactions between the electrons and the ions. That is, it accounts for elastic scattering of the electrons to all orders but considers the electron-electron scattering only to first order, which is an important limitation. Here we will give a brief derivation in the finite range formalism [20]. By finite range we mean that the potentials (and thereby interactions) become negligible at some large but finite radius. There are other equivalent methods but this presents the clearest derivation. We begin with the result of our derivation of the ionization amplitude, equation (40), expressed in

bracket notation

$$f(\mathbf{k}_s, \mathbf{k}_f) = \langle \Phi | V_b | \Psi_a^+ \rangle \tag{59}$$

where $V_b = 1/r_s + 1/r_f - 1/r_{sf}$. Next we introduce some interaction W_b into the left hand side of (59),

$$f(\mathbf{k}_s, \mathbf{k}_f) = \langle \psi_b^- | V_b - W_b | \Psi_a^+ \rangle - \langle \psi_b^- | V_a - V_b + W_b | \Phi \rangle \tag{60}$$

where $V_a = 1/r_f - 1/r_{sf}$. ψ_a^- is the wave function for scattering initially free electrons with momenta k_s, k_f. This means it satisfies

$$\psi_b^- = [1 + (E - H_b - W_b - i\eta)^{-1} W_b] \Phi_b \tag{61}$$

where $H_b = \nabla_1^2/2 + \nabla_2^2/2$ or the free electron Hamiltonian. If we take $W_b = V_b$ then the ionization amplitude in equation (60) reduces to

$$f(\mathbf{k}_s, \mathbf{k}_f) = \langle \Psi_b^- | V_a | \Phi \rangle \tag{62}$$

This is merely the standard post prior equivalence. The subscript b denotes the final potentials while a includes only the initial potentials. At this stage no approximations have yet been made. The distorting potential is totally arbitrary. When we do make an approximation we will lose our post prior equivalence.

In deriving the DWBA we assume that $W_b(r_s, r_f)$ is separable

$$W_b(\mathbf{r}_s, \mathbf{r}_f) = V_1(\mathbf{r}_f) + V_2(\mathbf{r}_s) \tag{63}$$

This implies that the wave function for the escaping electrons Φ can be represented by two separate wave function $\chi^-(\mathbf{r}_f)$ and $\chi^-(\mathbf{r}_s)$ dependent on the potentials V_1 and V_2. Thus equation (60) is

$$f(\mathbf{k}_s, \mathbf{k}_f) = \langle \chi^-(z_f, \mathbf{k}_f, \mathbf{r}_f) \chi^-(z_s, \mathbf{k}_s, \mathbf{r}_s) | V_b - V_1 - V_2 | \Psi_a^+ \rangle \tag{64}$$

The second term can be shown to vanish [21]. Next we approximate Ψ^+

$$\Psi_a^+(\mathbf{r}_s, \mathbf{r}_f) = \chi_0^+(\mathbf{k}_0, \mathbf{r}_f) \psi(\mathbf{r}_s) + (-1)^S \chi_0^+(\mathbf{k}_0, \mathbf{r}_s) \psi(\mathbf{r}_f) \tag{65}$$

where we have indicated the effects of spin. This approximation is at the heart of the DWBA [21, 22, 23]. The approximation for Ψ^+ is where we have set our method as a first order approximation in the $1/r_{sf}$ potential. By making this approximation we note that the functions $\chi^-(\mathbf{r}_f)$ and $\chi^-(\mathbf{r}_s)$ are no longer mere projectors, as they

have been constructed with the potential $W_b(r_s, r_f)$ in mind and are intrinsic to approximation. Thus we will want to include as much physics as possible into the choice of their their effective potentials V_1 and V_2.

The choice we take (which is perfectly reasonable for the case when $E_f \approx E_s$) is

$$V_1(\mathbf{r}_f) = -1/r_f, V_2(\mathbf{r}_s) = -1/r_s \tag{66}$$

With this choice of DWBA, the direct and exchange amplitudes become

$$f^{\mathrm{DWBA}}(\mathbf{k}_s, \mathbf{k}_f) = \langle \chi^-(z_f, \mathbf{k}_f, \mathbf{r}_f)\chi^-(z_s, \mathbf{k}_s, \mathbf{r}_s)|\frac{1}{r_{sf}}|\chi_0^+(\mathbf{k}_0, \mathbf{r}_f)\psi(\mathbf{r}_s)\rangle \tag{67}$$

$$g^{\mathrm{DWBA}}(\mathbf{k}_s, \mathbf{k}_f) = \langle \chi^-(z_f, \mathbf{k}_s, \mathbf{r}_f)\chi^-(z_s, \mathbf{k}_f, \mathbf{r}_s)|\frac{1}{r_{sf}}|\chi_0^+(\mathbf{k}_0, \mathbf{r}_f)\psi(\mathbf{r}_s)\rangle \tag{68}$$

These can then be used to derive the TDCS via equation (43).

In the actual calculation we use the following methods. For complex atoms with N electrons the incoming distorted waves are generated in the static exchange potential for the target, asymptotically the electron sees a Coulombic potential of charge $Z - N+1$ where Z is the nuclear charge. The distorted waves of the two outgoing electrons are identical, being generated in the static exchange potential of the residual ion, i. e. with an asymptotic charge of $Z - N + 1$. Both final state distorted waves are orthogonalized to the ground state. The Hartree Fock wave functions of Clementi [24] are used for the target wave functions ψ_{nlm}.

Furness-McCarthy local potentials are used for exchange in each of the channels. For the final channel we use an 'average' form. A local exchange approximation of Furness-McCarthy type, [25, 26], is used to simplify the static exchange calculation. Also no final state electron-electron interaction is included, i. e. the approach is strictly first order in $1/r_{sf}$. This has been shown to have negligible effect [21].

Despite the method's great success, there remain several weaknesses due to its nature as a first order approximation. For example it does not include the possibility of recapture for the emitted electron. Also as mentioned earlier it suffers at low energies, such as near threshold, where the effects of higher order interactions dominate. This would correspond to where post collisional interaction between the escaping electrons dominates.

It is for these reasons as well as the challenge of a complete *ab initio* solution that the following methods have been pursued.

I.3.2 CONVERGENT CLOSE COUPLING

Convergent Close Coupling (CCC) [27] is based on the widely used close coupling approximation. The idea behind the close coupling approximation is that the total wave function for the system can be expanded in terms of a complete set of eigenstates or pseudostates of the target Hamiltonian. The pseudostates are a set of states that approximate the behavior of the (often much) larger set of eigenstates of the system. That is

$$\Psi(\mathbf{r}_1,\mathbf{r}_2)=\sum_{\mu}\left(\frac{u_\mu(r_1)\phi_\mu(r_2)}{r_1}\Xi^L_\mu(\Omega_1,\Omega_2)+(-1)^S\frac{u_\mu(r_2)\phi_\mu(r_1)}{r_2}\Xi^L_\mu(\Omega_2,\Omega_1)\right) \quad (69)$$

where ϕ_μ are the target wave functions, u_μ are the channel wave functions, and Ξ are the coupled spherical harmonics. μ denotes $\{nkl_1l_2LM_LSM_S\}$, following the notation of Percival and Seaton [28]. n and l_1 are the principal quantum number of the atomic electron, k and l_2 are the wave number and orbital angular momentum of the scattered electron. L and M are the total angular momentum and its z projection for the system. the same applies to the spin S and its z projection M_S.

The summation in (69) should include an integral over the continuum energies. As this is not practical, this is approximated by a smaller number states, called pseudostates. Curran and Walters [29] first successfully applied pseudostate close coupling to the calculation of TDCS for the electron impact ionization of ground state hydrogen. In addition to CCC, this method is also used extensively in **R**-matrix calculations [30].

The Convergent Close Coupling uses this method to calculate not only discrete and excitation cross sections but also total ionization. Where it differs from traditional close coupling is by its use of numerical basis functions instead of the target eigenstates. As the size of the basis is increased these basis functions and their eigenvalues converge on the true wave functions of for the target and their associated energies. The total number of states is increased until the cross section has converged.

The problems with this method are that by construction it is more suited to asymmetric kinematics, such as scattering and ionization calculation where one electron has a small energy relative to the other. This is due the fact that the slow electron is considered to be some bound, but positive energy, pseudostate and not in a true continuum state. For highly asymmetric kinematics this works well [31]. For calculations involving low energy more symmetrical kinematics it does poorly,

oscillating about the true result [32].

Rescigno *et al* [33] however showed that the difficulty lay with how the cross section was extracted and that by obtaining their results by projecting the flux through a hypersurface of sufficiently large radii, they could get good results with their related Exterior Complex Scaling method.

I.3.3 EXTERIOR COMPLEX SCALING

Exterior Complex Scaling (ECS), as applied to $(e, 2e)$, was first pioneered by Rescigno *et al* [33]. While it generates good agreement with experiment, the method is very computationally intensive [34], even when applied to $(e, 2e)$ on Hydrogen.

In the ECS method, the scattered outgoing wavefunction $\Psi_{\rm SC}^{(+)}$ is solved directly from a rearranged Schrödinger's equation:

$$(E - \hat{H})\Psi_{\rm SC}^{(+)} = (\hat{H} - E)\Psi_{\mathbf{k_0}}(\mathbf{r}_1, \mathbf{r}_2) \tag{70}$$

Where $\Psi_{\mathbf{k_0}}$ is an initial state symmetrized wavefunction consisting of a plane wave and the target state (the ground state of Hydrogen in the current version of the method).

$\Psi_{\rm SC}^{(+)}$ is then expanded in partial waves:

$$\Psi_{\rm SC}^{(+)} = \frac{1}{r_1 r_2} \sum_{l_1 l_2 LM} \psi_{l_1 l_2}^{LMS}(r_1, r_2)\Xi_{l_1 l_2}^{LM}(\hat{\mathbf{r}}_1, \hat{\mathbf{r}}_2) \tag{71}$$

where $\Xi_{l_1 l_2}^{LM}$ are bispherical harmonics. Note that $|l_1 - l_2| \leq L \leq l_1 + l_2$ and $L + l_1 + l_2$ must be even due to parity conservation. Also for a ground state collision $M = 0$. They solve for each partial wave via projection.

The partial wave equation is solved on a finite grid using exterior complex scaling, where the radial coordinates are rotated into the complex plane at a boundary radius R_0:

$$z(r) = \begin{cases} r, & r < R_0 \\ R_o + (r - R_0)e^{i\theta}, & r \geq R_0. \end{cases} \tag{72}$$

This transformation causes the outgoing waves to diminish exponentially, setting the boundary condition at $r_1, r_2 = R_{\rm max} > R_0$ to be $\psi_{l_1 l_2}^{LS}(r_1, r_2) = 0$. On the other hand, the incoming waves now diverge and $\psi_{l_1 l_2}^{LS}(r_1, r_2)$ must be truncated for $r_1, r_2 > R_0$. This is the only systematic approximation in the method.

The afore mentioned computational intensity spurred the development of the Propagating Exterior Complex Scaling (PECS) method, to reduce computational

complexity so the method could be applied to more complex systems. The PECS works with the same underlying equations of ECS above but uses a Numerov scheme first devised by Poet [35], modified to include certain inhomogeneous terms. This simplifies the process of propagating to large radii and has allowed the computation of several difficult kinematics such as near threshold [36].

ECS and PECS resolve the issues with the CCC. With improvements in the extraction of the cross section it is no longer limited to asymmetric geometries. There is however the requirement of a good approximation for the ground state for the target. For more complex systems than Hydrogen PECS will require more complex ground states and necessarily be more computationally complex. For a method that already requires a large amount of computational resources, this will certainly hinder future development and expansion of this method to more complex targets has been only recently been achieved [37, 38].

I.3.4 CONVENTIONAL R-MATRIX CALCULATIONS

The **R**-matrix method was originally developed by Wigner and Eisenbud [39] in the area of nuclear physics and later extended to electron scattering in atomic physics by Burke and Robb [30]. The principle behind the **R**-matrix approach is to divide the problem into an inner and outer region. The inner region, defined where the escaping particles are within some radius $\bar{r}$, is where all possible interactions, including exchange, are taken into account. In the outer region, exchange effects are ignored. This allows for different computational models to be used in each region thereby allowing for a great potential simplification of the problem. The **R**-matrix, itself, allows one to connect the interior region's solutions to the exterior region's.

In the X2e method we use an $\mathcal{R}$-operator approach. The $\mathcal{R}$-operator is a generalization of the **R**-matrix and thus we detail the basic **R**-matrix derivation here. We begin with the Schrödinger's equation with some solution Ψ

$$(H - E)\Psi = 0 \tag{73}$$

We then derive a set of basis functions for this problem by diagonalizing the Hamiltonian so that

$$\langle \Psi_k | H | \Psi_{k'} \rangle = E_k \delta_{k,k'} \tag{74}$$

where Ψ_k are the basis elements and E_k are their eigenenergies. In the traditional non-variational **R**-matrix method, we divide the basis functions into a set of radial

functions $u_{ik}(r)$, where $\Psi_k = \sum_i c_i u_{ik}$, such that they satisfy the **R**-matrix boundary equation

$$\frac{\bar{r}}{u_{ik}(\bar{r})} u'_{ik}(r)\Big|_{r=\bar{r}} = b \tag{75}$$

where $'$ refers to a derivative with respect to r, and $\bar{r}$ is the boundary radius. b, the logarithmic derivative of $u_{ik}(r)$, is an arbitrary parameter, which is most commonly set to zero. This is not the case however in variational **R**-matrix methods which will be examined in detail in Chapter 5.

We note that we are omitting the angular portion of the problem for the moment. In an actual calculation we would project out the angular portion of the wave function and solve the problem in the radial space of the escaping electron(s).

As for $\bar{r}$ this is chosen to be just large enough to contain the important bound electron information while minimizing the computation. Inside the region bounded by $\bar{r}$ all effects (such as exchange and correlation) are taken into account. Outside this region they are considered negligible and only the long range effects like the Coulomb potential are considered.

Our next step is to expand the full solution Ψ in terms of the basis functions

$$\Psi = \sum_{k=1}^{\infty} a_k \Psi_k \tag{76}$$

Next we consider the identity

$$\langle (H - E)\Psi_k | \Psi \rangle - \langle \Psi_k | H - E | \Psi \rangle = 0 \tag{77}$$

Using (73) and (74), we can rearrange (77),

$$\begin{aligned} \langle H\Psi_k | \Psi \rangle - E_k \langle \Psi_k | \Psi \rangle - \langle \Psi_k | H\Psi \rangle + E\langle \Psi_k | \Psi \rangle = 0 \\ \langle H\Psi_k | \Psi \rangle - \langle \Psi_k | H\Psi \rangle = E_k \langle \Psi_k | \Psi \rangle - E\langle \Psi_k | \Psi \rangle \\ \langle \Psi_k | H\Psi \rangle - \langle H\Psi_k | \Psi \rangle = (E - E_k)\langle \Psi_k | \Psi \rangle \end{aligned} \tag{78}$$

Next we can expand the wave function as $\Psi = \sum_i F_i(r) c_i$, using the basis expansion from earlier ($\Psi_k = \sum_i u_{ik}(r) c_i$). We then use equation (76) and apply Green's theorem to left hand side of (78) to get

$$\frac{1}{2} \sum_i [u_{ik}(r) F'_i(r) - F_i(r) u'_{ik}(r)]|_{r=\bar{r}} = (E_k - E) a_k \tag{79}$$

At this point we can insert the **R**-matrix boundary condition (75) into (79)

$$\frac{1}{2} \sum_i \frac{u_{ik}(r)}{\bar{r}} [\bar{r} F'_i(r) - b F_i(r)]|_{r=\bar{r}} = (E_k - E) a_k \tag{80}$$

This allows us to solve for the expansion coefficients a_k

$$a_k = \frac{1}{2(E_k - E)} \sum_i \frac{u_{ik}(r)}{\bar{r}} [\bar{r}F_i'(r) - bF_i(r)]|_{r=\bar{r}} \tag{81}$$

From the expansion of Ψ and Ψ_k in terms of F_i and u_{ik} it is clear that

$$F_i(r) = \sum_{k=1}^{\infty} u_{ik}(r) a_k \tag{82}$$

Placing (81) into (82) and setting $r = \bar{r}$ we get

$$F_i(\bar{r}) = \sum_j \sum_{k=1}^{\infty} \frac{1}{2\bar{r}} \frac{u_{ik}(\bar{r}) u_{jk}(\bar{r})}{E_k - E} [\bar{r}F_i'(r) - bF_i(r)]|_{r=\bar{r}} \tag{83}$$

At this point we define the **R**-matrix on the boundary $r = \bar{r}$ as

$$R_{ij} = \frac{1}{2\bar{r}} \sum_{k=1}^{\infty} \frac{u_{ik}(\bar{r}) u_{jk}(\bar{r})}{E_k - E} \tag{84}$$

Thus the radial functions on the boundary can be expressed

$$F_i(\bar{r}) = \sum_j R_{ij} [\bar{r}F_i'(r) - bF_i(r)]|_{r=\bar{r}} \tag{85}$$

or with the conventional choice for $b = 0$,

$$F_i(\bar{r}) = \sum_j R_{ij} \bar{r} F_i'(r)|_{r=\bar{r}} \tag{86}$$

To obtain useful results from this method, the solutions at the bounding surface must be matched up to those on the outer region. This can be done by calculating the **T**-matrix. Details of how that calculation is done can be found in Chapter 7.

I.3.5 HYPERSPHERICAL R-MATRIX METHOD WITH SEMICLASSICAL OUTGOING WAVES

Lastly we discuss the hypersphrical **R**-matrix with semiclassical outgoing waves (HRM-SOW) [40, 41, 42] developed by Malegat for photo-double ionization $(\gamma, 2e)$ of Helium. This method uses the **R**-matrix method in hyperspherical coordinates and then connects the results to semiclassical outgoing waves.

They begin with Schrödinger's equation in hyperspherical coordinates

$$\left(-\frac{1}{2}\frac{\partial^2}{\partial \rho^2} + \frac{1}{2}\delta(\rho - \rho_0)\frac{\partial}{\partial R} + T(\Omega_5) + V(\rho, \Omega_5) - E) \right) \Psi(\rho, \Omega_5) = 0 \tag{87}$$

and solve for Ψ. Ω_5 denotes the various angular coordinates α, Ω_1, and Ω_2. T is the kinetic energy of angular coordinates, V is the usual $(e, 2e)$ potential $1/r_s + 1/r_f + 1/r_{sf}$, and the delta function is part of the Bloch operator term that ensures the Hamiltonian is hermitian in the inner region. The Bloch operator will be discussed in detail in Chapter 4.

Equation (87) is then solved for a set of pseudostates Φ_k which are expanded into partial waves, $\Phi_k = \sum_\mu f_{k\mu}(\rho)x_\mu(\Omega_5)$. The functions f_μ are then used to build the **R**-matrix at some radius ρ_0 via

$$f_{k\mu} = \sum_{\mu'} R_{\mu\mu'} f'_{k\mu'} + \mathcal{I}_{\mu'} \tag{88}$$

where

$$R_{\mu\mu'}(\rho_0) = \frac{1}{2}\sum_k \frac{f_{k\mu}(\rho_0) f_{k\mu'}(\rho_0))}{E_k - E} \tag{89}$$

and $\mathcal{I}$ is an inhomogeneous term due dipole interaction from the incident photon.

After obtaining the **R**-matrix they next derive semiclassical outgoing waves to be matched to the inner region. These satisfy

$$\left(-\frac{1}{2}\frac{\partial^2}{\partial\rho^2} + E_M(\rho) - E)\right) F_M(\rho) = 0 \tag{90}$$

and have the form

$$F_M(\rho) = \frac{1}{\sqrt{|p_M(\rho)|}} \tilde{F}_M(\rho) \exp\left(i\int_{\rho_0}^{\rho} p_M(\rho')d\rho'\right) \tag{91}$$

$$p_M(\rho) = \sqrt{2[E - E_M(\rho)]} \tag{92}$$

$$\frac{d^2\tilde{F}_M}{d\rho^2} \ll 1 \text{ and } \left|\frac{1}{p_M^2}\frac{dp_M}{d\rho}\right| \ll 1 \tag{93}$$

were $p_M(\rho)$ are the local momenta of the escaping electrons. These solutions F_M are then solved for via the propagation equation

$$i\frac{\partial}{\partial\tau}\tilde{F}_M(\tau) = (\rho(\tau)H_0(\rho))\,\tilde{F}_M(\tau) \tag{94}$$

where τ is a false time defined by $p(\rho)\rho d\tau = d\rho$. These results are propagated to some large radius (up to millions of a.u.). Once propagated these waves are then matched to the inner region using

$$(i\mathbf{p}\cdot\mathbf{U}\cdot\mathbf{R}\cdot\mathbf{U}\cdot\mathbf{p} - \mathbf{p})F = -\mathbf{p}\cdot\mathbf{U}\cdot\mathcal{I} \tag{95}$$

where U is a unitary transformation matrix and p is the diagonal matrix of semiclassical momenta in each channel. The cross section then is extracted via the pure flux method as outlined earlier.

While highly successful for photo double-ionization of Helium, this method has yet to be applied to other more complex targets, nor to electron impact ionization. Since its inner region is constructed, by default, as a two electron system, it is hard to see how the method could easily be generalized to other systems with differing numbers of electrons. It also has the lacks a fully quantum treatment for the outer region which would be preferred from an *ab initio* theory.

I.4 EXPERIMENTAL GEOMETRIES

In comparing the results of our $(e, 2e)$ and $(\gamma, 2e)$ processes to experiment, it is important to note the common experimental geometries. As noted earlier, in an single ionization process such as $(e, 2e)$, an electron ionizes the target and two electrons are detected in coincidence with their position and energies resolved. This gives us a complete kinematical picture of a given collision. For $(\gamma, 2e)$ for the final state of the system is similar, though of course the initial double ionization of the target electrons occurs by different means.

Our coordinates are outlined in Fig. 1. As mentioned earlier the incident electron comes in with momentum k_0. Two electrons escape with momenta k_f and k_s where the subscripts f and s refer to fast and slow respectively. In a classical collision without the possibility of exchange, this would correspond to the scattered and ejected electrons. The differences between the various experimental geometries depend on the angles made by the escaping electron momenta with the incident particle. These angles are noted in the figure. In this work we will examine four different geometries:

Coplanar Symmetric: In coplanar symmetric geometry the detected final state electrons exit in the same plane as the incident projectile ($\Phi = 0$) and with equal (but opposite) angles relative to the incident projectile ($\theta_f = -\theta_s$). Typically the angle to the left of the beam direction is labeled negative. In this somewhat "Y" shaped geometry the angle of each detector makes with the incident particle is varied by the same amount (i.e. θ_f and θ_s remain equal in magnitude and opposite in sign as they vary).

Coplanar Asymmetric: In coplanar asymmetric geometry the detected final state electrons exit in the same plane as the incident projectile ($\Phi = 0$) and with different

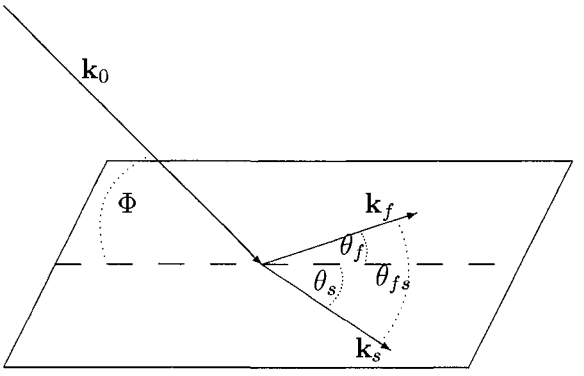

FIG. 1: The general experimental set up envisaged for the $(e, 2e)$ processes considered in this thesis. $\mathbf{k_0}, \mathbf{k_f}, \mathbf{k_s}$ denote, respectively, the wave-vectors of the incident and final state electrons. It is assumed that $\mathbf{k_f}$ and $\mathbf{k_s}$ are coplanar and that $\mathbf{k_0}$ makes an angle Φ with the scattering plane. The exiting electrons are detected with angles θ_f, θ_s left and right of the line defined by $\Phi = 0$ degrees. Their angle of mutual separation is given by θ_{fs}.

angles relative to the incident projectile ($\theta_f \neq \theta_s$). One detector (typically the one detecting the more energetic electron) is kept at a fixed angle and the position of other detector is then varied (i.e. θ_f is held constant while θ_s is varied).

Constant θ_{fs}: Another coplanar geometry ($\Phi = 0$), in constant θ_{fs} geometry, the angle between the detected final state electrons θ_{fs} is kept fixed and the two detectors are rotated in the plane of the incident projectile. In other words θ_f and θ_s are varied such that $\theta_{fs} = \theta_f - \theta_s$ is constant.

Perpendicular Plane: In this case the incident projectile is perpendicular to the plane of the detected electrons ($\Phi = \pi/2$). One detector is fixed and the other rotated about the plane. For example θ_f might be held at 0 degrees and θ_s rotated about the target.

I.5 SUMMARY

In this chapter, we reviewed basic scattering theory, discussing the basic kinematics of the problem and the relevant boundary conditions. We then examined how one can extract the TDCS from the wave function via both a flux projection and pure flux method. Afterwards we examined the several perturbation methods for solving the problem and their successes and failures. We then looked at the current *ab initio* solutions that might solve the problem in its entirety and their relative strengths and weaknesses. Lastly we examined the experimental geometries that are relevant to this thesis.

In Chapter 2 we will discuss the DWBA in greater detail and show new results in comparison with experiment. In Chapter 3 we will expand on this to examine $(e, 2e)$ collisions with hydrogen-like and helium-like ions to determine the dominate contributions to the cross section.

Afterwards we will develop a full *ab initio* solution using the $\mathcal{R}$-operator formalism, the X2e method. This will done in Chapters 4 through 7. In Chapter 4 we will outline the method and discuss the interior region calculations. In Chapter 5 we will discuss the **R**-matrix is greater detail and derive the $\mathcal{R}$-operator. Chapter 6 we will deal with the resolution of certain problems with reaching the correct asymptotic region and the work done to resolve that. In Chapter 7 we will detail how we connect to the asymptotic region. This will include a full review of the **S**-matrix and how it relates to the **R** and **K**-matrices. It will also show how we calculated the surface integral to project out the flux and derive the ionization amplitude. In Chapter 8 we will show preliminary results for the X2e method using a simplified model called the Poet-Temkin model. Additionally results for elastic scattering will be shown. Lastly in Chapter 9 we will detail the remaining work needed to complete this method to generate full TDCS.

CHAPTER II

DWBA AND $(E, 2E)$ ON MG AND AR

In Chapter 1, we briefly discussed the Distorted Wave Born Approximation, or DWBA, [22, 25, 43] and its related approximations. In this chapter we will more closely examine this method and its advantages over other first order approaches. The DWBA offers a straightforward and flexible approach to the calculation of $(e, 2e)$ processes. It has proved particularly useful in identifying targets and kinematics where multiple scattering effects are important [16, 22]. In this chapter, we will show results in comparison with experiment for inner and outer shell electron impact ionization on Magnesium and Argon as well as $(e, 2e)$ on Helium. We will use the full flexibility of the approximation to explore the ionization mechanisms.

By inner shell ionization we mean that the electron interacts with and ionizes an electron in one of the inner shells of the target atom or ion. For example, $(e, 2e)$ on $Ar(2p)$ refers to the case where the incident electron knocks off an electron in the $2p$ shell of Argon, or equivalently

$$e^- + Ar(1s^2, 2s^2, 2p^6, 3s^2, 3p^6) \rightarrow 2e^- + Ar(1s^2, 2s^2, 2p^5, 3s^2, 3p^6) \qquad (96)$$

The first $(e, 2e)$ measurement on $Ar(2p)$ were made by Lahmam-Bennani *et al* [44] at an impact energy of $8keV$ with further results being reported by [45, 46, 47], and at significantly lower impact energies by [16]. Very recently new experimental data has become available for $Ar(3s), Mg(2s)$ and $Mg(2p)$, at impact energies of the order of $1keV$ [48].

In this chapter we will begin by reviewing the basic Born approximation theory. Then we will examine the various choices for the continuum electron wave functions within the theory, starting with the plane wave model and then working to the First Born Approximation (FBA). Finally we will review the DWBA approach as we use it in our calculations. Then we will compare the results of the FBA and DWBA to experiment [48] for the cases of $(e, 2e)$ on helium, $Mg(2p)$, $Mg(3s)$ and $Ar(3s)$ at a variety of angles. We will propose how the differences between FBA and DWBA can be shown in experiment using $Mg(2p)$ as the target. In Chapter 3 we will examine the cases of $(e, 2e)$ on helium and hydrogen at low energies, just a few eV above threshold, and examine the results for ions at similar energies.

II.1 THEORY

As described in Chapter 1, the Born approximation works by solving the integral form of Schrödinger's equation in the perturbative regime. All of the methods discussed in here are first order Born approximations where the electron-electron interactions are only evaluated once. That is we do not use the possibility of multiple interactions between the electrons. Elastic collisions with the nucleus are evaluated to all orders of magnitude.

Using the flux projector method of extracting the cross section, equation (43), the TDCS, for a Born approximation is of the form, [20, 22, 25]

$$\frac{d^3\sigma}{d\Omega_1 d\Omega_2 dE} = (2\pi)^4 \frac{k_f k_s}{k_0} \sum_m \left[|f_{nlm}|^2 + |g_{nlm}|^2 - \mathrm{Re}(f^*_{nlm} g_{nlm}) \right] \tag{97}$$

where we have corrected for the possibility of inner shell ionization (hence the subscripts nlm to indicate the target state). The direct and exchange amplitudes are respectively

$$f_{nlm} = \langle \chi_1^-(\mathbf{k}_f, \mathbf{r}_1) \chi_2^-(\mathbf{k}_s, \mathbf{r}_2) | \frac{1}{|\mathbf{r}_1 - \mathbf{r}_2|} | \chi_0^+(\mathbf{k}_0, \mathbf{r}_1) \psi_{nlm}(\mathbf{r}_2) \rangle \tag{98}$$

$$g_{nlm} = \langle \chi_1^-(\mathbf{k}_s, \mathbf{r}_1) \chi_2^-(\mathbf{k}_f, \mathbf{r}_2) | \frac{1}{|\mathbf{r}_1 - \mathbf{r}_2|} | \chi_0^+(\mathbf{k}_0, \mathbf{r}_1) \psi_{nlm}(\mathbf{r}_2) \rangle \tag{99}$$

where the subscripts 1 and 2 refer to the escaping electrons and 0 refers to the incident electron. ψ_{nlm} is the target state. The functions χ describe the behavior of the free electrons and the approximations used for them constitute the major differences between the theories.

II.2 PLANE WAVE BORN

In the absence of any distorting potentials, the wave functions χ reduce to plane waves. In the extreme case when there is no distorting potentials acting on any of the electrons then we have the plane wave Born approximation (PWBA). The direct ionization amplitude can be expressed as

$$\begin{aligned} f^{PWBA}_{nlm} &= (2\pi)^{-\frac{9}{2}} \int d^3r_1 d^3r_2 e^{-i\mathbf{k}_f \cdot \mathbf{r}_1} e^{-i\mathbf{k}_s \cdot \mathbf{r}_2} \\ &\quad \times \frac{1}{|\mathbf{r}_1 - \mathbf{r}_2|} e^{i\mathbf{k}_0 \cdot \mathbf{r}_1} \psi_{nlm}(\mathbf{r}_2) \end{aligned} \tag{100}$$

We can simplify this integral by making use of the Bethe integral relation [49]. This states

$$\int d^3r_1 \frac{e^{i\mathbf{q}\cdot\mathbf{r}_1}}{|\mathbf{r}_1 - \mathbf{r}_2|} = \frac{4\pi}{q^2} e^{i\mathbf{q}\cdot\mathbf{r}_s} \tag{101}$$

Using this in (100) we get

$$f_{nlm}^{PWBA} = \frac{4\pi}{(2\pi)^{\frac{9}{2}} q^2} \int d^3r e^{i\mathbf{p}\cdot\mathbf{r}} \psi_{nlm}(\mathbf{r}) \tag{102}$$

Where $\mathbf{q} = \mathbf{k}_0 - \mathbf{k}_f$ is the momentum transfer and $\mathbf{p} = \mathbf{q} - \mathbf{k}_s$ is the momentum of the target electron. If we can neglect the exchange amplitude then we have

$$\frac{d^3\sigma^{PWBA}}{d\Omega_1 d\Omega_2 dE} = (2\pi)^4 \frac{k_f k_s}{k_0} \sum_m (|f_{nlm}^{PW}|^2) \tag{103}$$

$$= \frac{k_f k_s}{2\pi^3 q^4 k_0} \sum_m |\int d^3r_2 e^{i\mathbf{p}\cdot\mathbf{r}_s} \psi_{nlm}(\mathbf{r}_2)|^2 \tag{104}$$

We immediately recognize the term

$$\int d^3r_2 e^{i\mathbf{p}\cdot\mathbf{r}_2} \psi_{nlm}(\mathbf{r}_2) \tag{105}$$

as the atomic wave function in momentum space, i. e. $\hat{\psi}_{nlm}(\mathbf{p})$. Equation (104) defines the plane wave Born approximation. The TDCS in the PWBA is thus crucially dependent on the norm of the target wave function summed over the magnetic quantum numbers m, and the vector $\mathbf{p}$. As is well known, [50, 51], the momentum space wave function may be written

$$\hat{\psi}_{nlm}(\mathbf{p}) = F_{nl}(p) Y_{lm}(\hat{\mathbf{p}}) \tag{106}$$

where the angular dependence is entirely in the spherical harmonics, and F_{nl} is independent of m. Consequently (104) may be written:

$$\frac{d^3\sigma^{PWBA}}{d\Omega_1 d\Omega_2 dE} = \frac{k_f k_s (|F_{nl}(p)|^2)}{2\pi^3 q^4 k_0} \sum_m |Y_{lm}|^2 \tag{107}$$

Now from equation (588) in Appendix G we know that

$$\sum_m |Y_{lm}|^2 = \frac{2l+1}{4\pi} \tag{108}$$

This means

$$\frac{d^3\sigma^{PWBA}}{d\Omega_1 d\Omega_2 dE} = \frac{k_f k_s (2l+1)}{4\pi^3 q^4 k_0} (|F_{nl}(p)|^2) \tag{109}$$

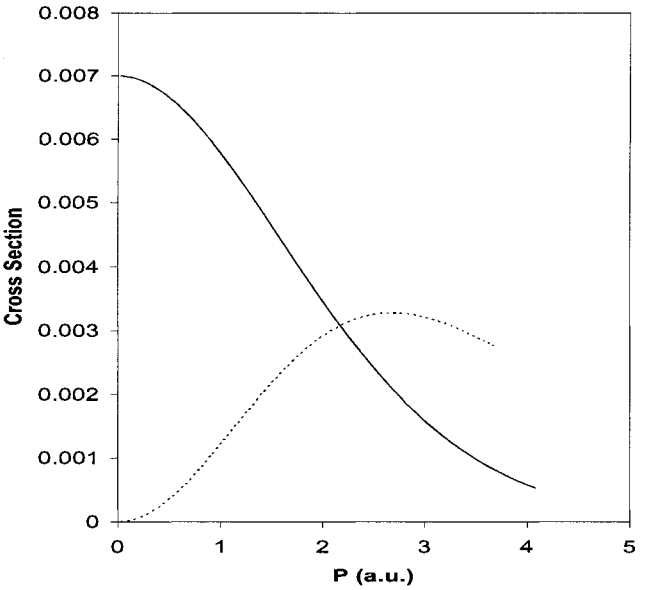

FIG. 2: The TDCS in πa_0^2 calculated in the PWBA approximation, (100) for coplanar asymmetric geometry plotted as a function of $p = |\mathbf{k}_0 - \mathbf{k}_f - \mathbf{k}_s|$ where the fast electron has an energy of 500 eV. The solid curve is Argon $2s$, with a slow electron energy of $56eV$ and $\theta_f = 4\,\text{deg}$. The dotted curve is Argon $2p$, with a slow electron energy of $46eV$ and $\theta_f = 8\,\text{deg}$.

Thus we can see that the TDCS depends only on the magnitude of $\mathbf{p}$ through $F_{nl}(p)$. The character of the target wave function is most clearly seen in the region of $\mathbf{p} = \mathbf{0}$. This corresponds to

$$\mathbf{q} - \mathbf{k}_s = \mathbf{0} \Rightarrow \mathbf{k}_s = \mathbf{k}_0 - \mathbf{k}_f \tag{110}$$

or zero recoil of the ion. We take (110) as the defining equation for the Bethe Ridge.

In Fig. 2 we present the TDCS as a function of $p = |\mathbf{p}|$ calculated in the PWBA Approximation, (100), for $Ar(2s)$ and $Ar(2p)$. The cross section has a minimum at $p = 0$ for the $2p$ case but a maximum for $2s$ at the same point. This behavior is characteristic of the state of the target, that is for an electron in an s state the most

probable momentum is zero, while this is the least probable momentum value for a p electron [1, 50]. The hydrogenic momentum space wave functions are known in closed analytic form e.g. [50] $F_{10}(p) = N_{10}(1+p^2)^{-2}$; $F_{21}(p) = N_{21}(1+4p^2)^{-3}$ where the N's are normalization constants. We can see at once that $F_{21}(p)$ is exactly 0 at $p = 0$ while $F_{10}(0)$ is at its maximum value. The $2p$ case exhibits a maximum for some value of $p = p_0$ and then declines uniformly. If the kinematics of our experiment are such that we can reach values of $p > p_0$ and p_{max} is the maximum value of p that can be obtained then we will find a local minimum in the TDCS for $\mathbf{k}_s = \tilde{\mathbf{k}}$ at which

$$p_{max} = |\mathbf{q} - \tilde{\mathbf{k}}| \tag{111}$$

Equation (104) reveals the major problem with the PWBA. Examining the formula, we see that the cross section is symmetric about the direction of momentum transfer, $\mathbf{q}$, and goes like $1/q^4$ as $q \to 0$. This is in contradiction to the experimentally observed behavior of $1/q^2$ as $q \to 0$ [23, 26, 52]. This spurious behavior arises because we have neglected the effect of the atomic nucleus on the slow electron in the final state but included it in the initial. Indeed in the absence of this interaction the initial and final states are not orthogonal and we have therefore included a non-physical auto-ionizing contribution. This incorrect behavior at $\mathbf{q} = 0$, which is the case of minimal perturbation of the system, shows that PWBA is a poor approximation for $(e, 2e)$ collisions.

II.3 FIRST BORN APPROXIMATION

To correct for the flaws of the PWBA we can assume that the outgoing slow electron is in a continuum state of the ion. We calculate this by treating the slow ejected electron as moving in the static exchange potential of the ion and orthogonalize this state to the bound state. This is the First Born Approximation (FBA), with a distortion only on the slow electron. In this approximation the direct scattering amplitude becomes

$$\begin{aligned} f^{FBA} &= (2\pi)^{-9/2} \int d^3r_1 d^3r_2 e^{-i\mathbf{k}_f\cdot\mathbf{r}_1} \chi^-(\mathbf{k}_s, \mathbf{r}_2) \\ &\quad \times \frac{1}{|\mathbf{r}_1 - \mathbf{r}_2|} e^{i\mathbf{k}_0\cdot\mathbf{r}_1} \psi_{nlm}(\mathbf{r}_2) \end{aligned} \tag{112}$$

To illustrate the improvements over the PWBA we apply the Bethe integral relation (101) to get

$$f^{FBA} = \frac{4\pi}{(2\pi)^{9/2} q^2} \int d^3r_2 \chi^-(\mathbf{k}_s, \mathbf{r}_2) e^{i\mathbf{q}\cdot\mathbf{r}_2} \psi_{nlm}(\mathbf{r}_2) \tag{113}$$

If we again neglect exchange amplitude we get

$$\frac{d^3\sigma^{FBA}}{d\Omega_1 d\Omega_2 dE} = (2\pi)^4 \frac{k_f k_s}{k_0} \sum_m |f_{nlm}^{FBA}|^2 \tag{114}$$

We see immediately that the symmetry about the direction of momentum transfer is maintained. Also if we expand

$$e^{i\mathbf{q}\cdot\mathbf{r}} = 1 + qr\cos\mu + O(q^2) \tag{115}$$

where $\mathbf{q}\cdot\mathbf{r}_s = qr\cos\mu$, then we see that the orthogonality of $\psi_{nlm}(\mathbf{r}_2)$ and $\chi^-(\mathbf{k}_s, \mathbf{r}_2)$ means that the first term of the expansion is zero. The second term gives us a factor of q which is squared as we pull it out of the modulus. This gives the TDCS the correct $1/q^2$ behavior as $q \to 0$.

This method still presents problems, which we outlined in Chapter 1. Further proof of the method's flaws can be seen later in this chapter when we compare our results using both the FBA and DWBA to experiment.

II.4 DISTORTED WAVE BORN APPROXIMATION

In Zhang *et al* [16] it was argued that the distorting effect of the atom, primarily the Coulomb interaction with nucleus could not be neglected for any of the electrons. These interactions can be represented by calculating the wave functions of all of the free electrons in the static exchange potential of the atom or ion. This distortion for all the wave functions is what defines the Distorted Wave Born Approximation (DWBA).

The derivation of the DWBA was given in Chapter 1, using a finite range formalism. Here we will discuss the details of the calculations as they are used for the results later in this and the next chapter. In addition to the methods noted in Chapter 1, we will briefly review the Hartree-Fock wave functions, the Furness-McCarthy local exchange approximation, and issue of post collisional impact.

II.4.1 HARTREE-FOCK WAVE FUNCTIONS

The Hartree-Fock wave functions are approximation of the true N-body electron wave functions for an atomic system. Developed by Hartree [53] and Fock in the early days of quantum mechanics, it can be applied to multiple electron systems for both atoms and molecules. In this method the true electron wave functions are approximated

by a single Slater determinate [54] of N spin orbitals. That is we separate the wave function of all the atom's electrons into individual spin orbital functions ϕ,

$$\Psi(\mathbf{r}_1, \mathbf{r}_2, ...\mathbf{r}_n) = \prod_{i=1}^{n} \phi_i(\mathbf{r}_i) \tag{116}$$

We note that the above wave function has the wrong behavior for electrons, as the total wave function should be antisymmetric. This is where the Slater determinate is used. This is represents the function Ψ as the determinate of a matrix made up of all the spin orbitals ϕ_i associated with each of the electron positions r_i. A simple two electron example is,

$$\Psi(\mathbf{r}_1, \mathbf{r}_2) = \frac{1}{\sqrt{2}} \begin{vmatrix} \phi_1(\mathbf{r}_1) & \phi_1(\mathbf{r}_2) \\ \phi_2(\mathbf{r}_1) & \phi_2(\mathbf{r}_2) \end{vmatrix} = \frac{1}{\sqrt{2}} \{\phi_1(\mathbf{r}_1)\phi_2(\mathbf{r}_2) - \phi_1(\mathbf{r}_2)\phi_2(\mathbf{r}_1)\} \tag{117}$$

This ensures that the wave function is correctly anti-symmetrized. The spin orbitals ϕ_i are Slater-type orbitals that have the form

$$\phi_i(r) = N_i r^{n_i - 1} e^{-\zeta_i r} \tag{118}$$

in the radial component, where n acts as the principal quantum number, N is a normalization constant, and ζ is a constant related to the effective charge of the nucleus with the nuclear charge being partly shielded by electrons. These constants are solved for by finding the eigenfunctions of the Fock operator $\hat{F}$, which is an approximate Hamiltonian that is broken down into a sum of one electron operators. A more detailed treatment of this method can be found in [55].

In our calculations the Hartree Fock wave functions of Clementi [24] are used for the target wave functions ψ_{nlm}. In Chapter 3, we examine some other choices for the target wave function while investigating the effects of correlation within the target.

II.4.2 LOCAL EXCHANGE APPROXIMATIONS

The Furness-McCarthy local exchange approximation, [25, 26, 56, 57] is commonly used for DWBA studies. Its use greatly simplifies the static exchange calculations in that one needs only solve differential equations rather than integro-differential equations. For a helium target in the incident channel it is give by

$$V_{\text{local}} = \frac{1}{2}\left[\frac{k_0^2}{2} - V_{\text{static}}^{\text{He}} - \sqrt{(\frac{k_0^2}{2} - V_{\text{static}}^{\text{He}})^2 + 2|R_{1s}|^2}\right] \tag{119}$$

where $V_{\text{static}}^{\text{He}}$ is the static potential of the helium atom and R_{1s} is the radial part of the ground state. Because we treat each of the exiting electrons as moving in the field of an one electron ion, there is an ambiguity in the choice of final state exchange potential, (for a full discussion see [25]). For an outgoing wave number k_{out} we have

$$V_{\text{local}} = \frac{1}{2}\left[\frac{k_{\text{out}}^2}{2} - V_{\text{static}}^{\text{He+}} - \sqrt{(\frac{k_0^2}{2} - V_{\text{static}}^{\text{He+}})^2 + \beta|R_{1s}^+|^2}\right] \tag{120}$$

where $V_{\text{static}}^{\text{He+}}$ is the static potential of the helium ion, R_{1s}^+ is the radial part of the $1s$ orbital of He^+. The parameter β defines the spin type of the exchange interaction. If $\beta = 2$ then we have a triplet interaction, $\beta = -2$ a singlet potential. A third somewhat ad-hoc choice $\beta = 1$ is in common use and in this case we talk about an "average exchange potential." When considering $(e, 2e)$ on the hydrogen-like isoelectronic sequence we only have an exchange term in the incident channel and one uses a local exchange potential analogous to (119)

$$V_{\text{local}}^{\mp} = \frac{1}{2}\left[\frac{k_{\text{out}}^2}{2} - V_{\text{static}}^{[\text{H}]} - \sqrt{(\frac{k_0^2}{2} - V_{\text{static}}^{[\text{H}]})^2 + \mp 2|R_{1s}^+|^2}\right] \tag{121}$$

where $V_{\text{static}}^{[\text{H}]}$ is the static potential of the hydrogen-like ion, R_{1s}^+ is the radial part of its $1s$ orbital. For the triplet case V_{local}^+ is attractive and real, whereas for the singlet case V_{local}^- is repulsive and can become complex depending on the energy. The possibility of a complex exchange potential is discussed by Rasch [25] but in our own calculations this problem never arose. Following [25] we will modify (99):

$$\frac{d^3\sigma^{DWBA}}{d\Omega_f d\Omega_s dE} = (2\pi)^4 \frac{k_f k_s}{4k_0}(|f^s + g^s|^2 + 3|f^t - g^t|^2) \tag{122}$$

where the superscripts s and t indicate that the singlet or triplet form of the local exchange potential is in use. The form (122) has the advantage of being unambiguous. For the two electron target (120) the ambiguity is unavoidable and one is forced to make a choice.

In this chapter we will use the triplet form of the exchange potential for our calculations. In Chapter 3 we examine the choice of exchange potential when we consider the dominate contributions to the TDCS at low energies.

II.4.3 POST COLLISIONAL IMPACT

By default, the DWBA does not include any calculation of post collisional impact (pci). This is implicit in the limit of first order electron-electron interaction. We can

however include a geometrical factor N_{ee} to account for the repulsion between the two electrons as they escape [21, 22]. The N_{ee} or Gamov factor is applied to the final TDCS as follows

$$\frac{d^3\sigma^{Nee}}{d\Omega_f d\Omega_s dE} = N_{ee}\frac{d^3\sigma^{DWBA}}{d\Omega_f d\Omega_s dE} \tag{123}$$

where

$$N_{ee} = \frac{\gamma}{e^{\gamma}-1};\ \gamma = \frac{2\pi}{|\mathbf{k}_f - \mathbf{k}_s|} \tag{124}$$

This factor is derived from the geometrical analysis of the Coulomb interaction between the two electrons. This is done in the approximation where the interaction is separable, that is where the interaction can be represented via a Coulomb wave function. The inclusion of N_{ee} factor has the effect of bringing the DWBA into close accord with the Wannier fit [58]. It has the unfortunate side effect however of effecting the overall normalization of the TDCS, throwing doubt on the absolute size. For this chapter we will avoid the use of this approximation, though we make some use of it in Chapter 3.

II.5 COMPARISON WITH EXPERIMENT

Here we show some basic calculations with the DWBA [59] in comparison with some recent experiments by Avaldi [48, 60]. Figure 3 shows results for $(e, 2e)$ on helium and $Mg(3s)$ at relatively asymmetric energies: $E_0 = 1044.6eV, E_f = 1000eV, E_s = 20eV$ for helium and $E_0 = 1027.6eV, E_f = 1000eV, E_s = 20eV$ for $Mg(3s)$. This is done for several different angles in the asymmetric coplanar geometry (with fixed θ_f). In Fig. 4 we see another TDCS this time for $Mg(3s)$ with θ_s fixed at 80 degrees and θ_f varied. As can be seen in all cases there is excellent agreement between theory and experiment. Because we are examining the s state however the TDCS are relatively structureless, exhibiting only a peak in the direction of momentum transfer. We also note that the experimental data is not absolute.

For more interesting results we need to look at the p state. Figure 5 shows a comparison between the older experiments from Hink and his collaborators [16] on $Ar(2p)$ and the DWBA. We see for Ar that the theory correctly predicts a binary peak which is split in the forward direction and a recoil peak which is much larger than the binary and also split. We can understand the splitting of the binary in that the minimum value occurs in the region of $\mathbf{0} = \mathbf{k_0} - \mathbf{k_f} - \mathbf{k_s}$ exactly as we would

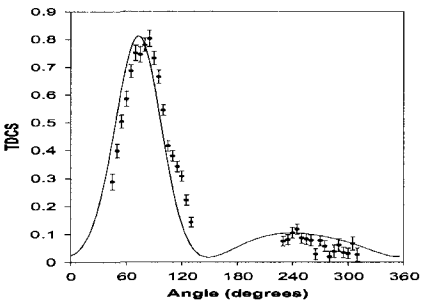

(a)

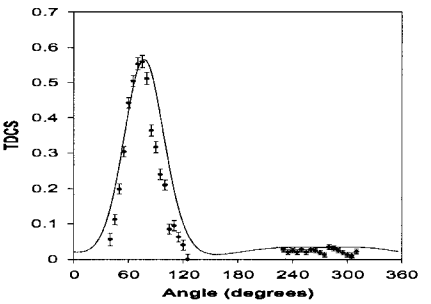

(b)

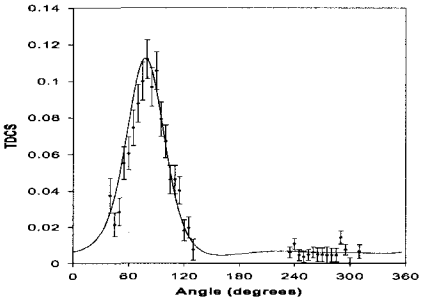

(c)

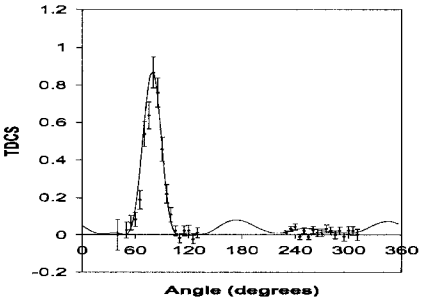

(d)

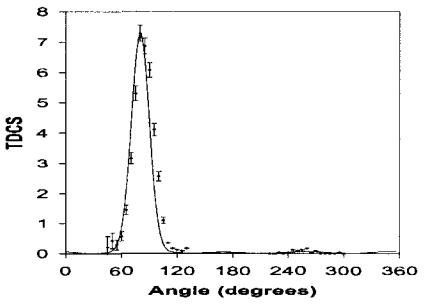

(e)

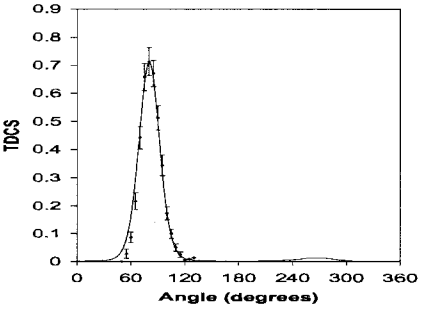

(f)

FIG. 3: TDCS in atomic units for He(1s) $E_0 = 1044.6eV, E_f = 1000eV$ with angles of (a) $\theta_f = 5^0$, (b) $\theta_f = 7^0$, and (c) $\theta_f = 12^0$, and TDCS in atomic units for Mg(3s) $E_0 = 1027.6eV, E_f = 1000eV$ with angles of (a) $\theta_f = 5^0$, (b) $\theta_f = 7^0$, and (c) $\theta_f = 12^0$. Experiment is from [60]. The solid curve is DWBA for all cases.

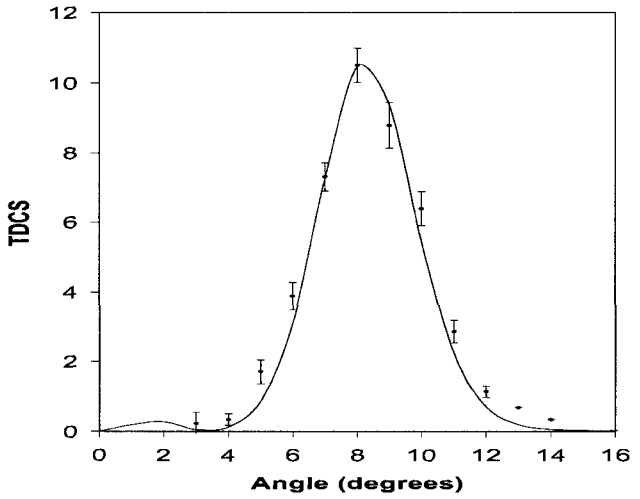

FIG. 4: TDCS in atomic units for coplanar asymmetric geometry for $Mg(3s)$: $E_0 = 1027.6eV, E_f = 1000eV, \theta_s = 80^0$. Experiment is from [60]. The solid curve is DWBA.

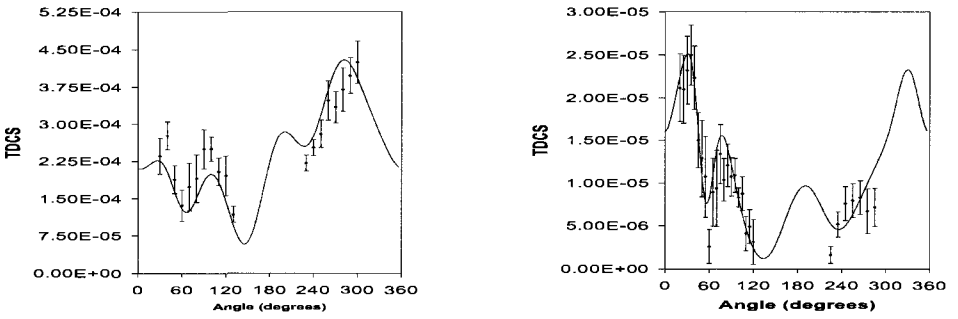

(a) (b)

FIG. 5: TDCS in atomic units for (a) Ar(2p) $E_0 = 1949eV, E_f = 1550eV, \theta_f = 15.6^0$ and (b) TDCS for $Ar(2p)$ $E_0 = 1949eV, E_f = 1200eV, \theta_f = 30^0$. Experiment and theory are from [16]. Solid curve is DWBA for both cases.

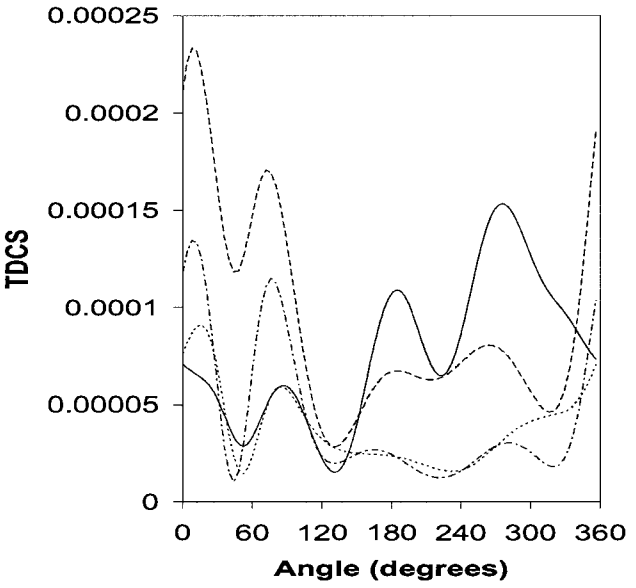

FIG. 6: TDCS in atomic units for $Ar(2p),$: $E_f = 500eV, \theta_f = 25^0, E_s = 200eV$. Solid curve is DWBA, dotted is DWPWDW (distorted waves in the incident and fast channels), dashed is FBA, and dash and dotted is a PWBA calculation.

expect for a p state. For the curves in Fig. 3, we have a maximum at this point since the target electron is in an s state.

In order to better understand the competing processes for ionization from a $2p$ state we look at a series of model calculations. By switching on and off the distorting potentials we can look at the effect of elastic scattering on the incident, slow and fast electrons. In Fig. 6 we use equation (98) and define a series of model calculations for $Ar(2p)$: $E_f = 500eV, \theta_f = 25\,\mathrm{deg}, E_s = 200eV$. These calculations consist of the PWBA, the DWBA, FBA, and DWPWPW. The DWPWPW is where we have put a distortion of the fast electron but left the slow and incoming electron as plane waves. Note that in all cases we include exchange and that the distorted waves are orthogonalized to the ground state but the plane waves are not.

We can see that the PWBA case has a local minima when $\mathbf{k_s}$ is in the $\mathbf{q}$ and $-\mathbf{q}$

directions, that is along the direction of momentum transfer. These minima arise solely from the $2p$ character of the wave function, as discussed above. The effect of switching on the elastic scattering on the slow ejected electron is to significantly enhance the recoil peak in the FBA case. If however we allow only for elastic scattering of the incoming and fast electrons but not the slow (DWPWDW) the recoil remains small but the binary is reduced. The effect of including elastic scattering on all free particles, (DWBA), is to further enhance the recoil over the binary, as compared to the FBA case. The splitting of the recoil peak is a much clearer structure in the DWBA and should be readily visible in an experiment. The split binary and recoil is seen in all the calculations. We see that distortion is needed in all channels to maximize this effect. It should be remembered that when we included distorted waves in all channels we allow not only for elastic collisions in these channels but also for the distorted waves to interfere [61]. The structures predicted here are similar to those found in the DWBA calculations of Zhang *et al* [16]. The experimental results of Hink [16] and Avaldi [48] are certainly consistent with the DWBA as we can see in Fig. 5 and Fig. 7. Unfortunately for the choice of kinematics used by Avaldi [48] it is impossible to distinguish between the simple FBA and the DWBA with a relative measurement.

Figure 7 shows a comparison between the DWBA and FBA calculations and the experimental data of Avaldi [48], for $Ar(2s)$ and $Mg(2p)$. We have normalized the relative experimental data to the DWBA. Agreement with the DWBA is good, but had we fitted to the FBA agreement would have been equally good. There is a large difference in absolute size between the two approximations in the $Ar(2s)$ case but the results for the $Mg(2p)$ are remarkably close both in shape and magnitude. However by making a relatively small change in parameters we can produce cross sections which should be easily distinguishable. This is shown in Fig. 8. With these kinematics, we can clearly see a difference in the recoil peak between the FBA and DWBA theories. If this experiment was performed it would illustrate the flaws in the FBA.

Another way to determine the validity of the FBA would be to compare it (and the DWBA) with experimental measurements in terms of absolute size. Thus it would be extremely useful to have such data on an absolute scale. However this is probably beyond present experimental capabilities. Hence it is of value to seek out kinematics where the difference between the different theoretical approaches are

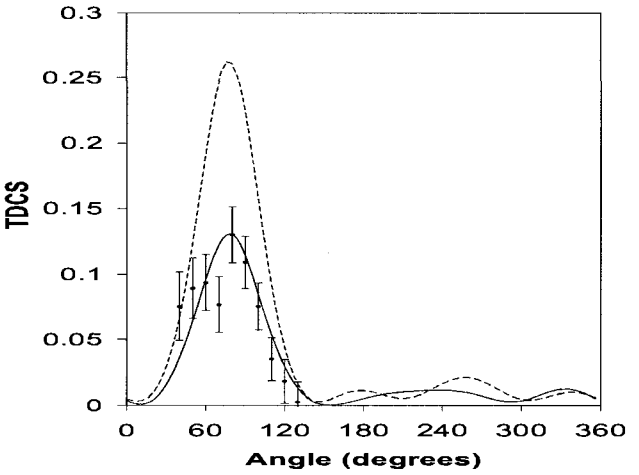

(a)

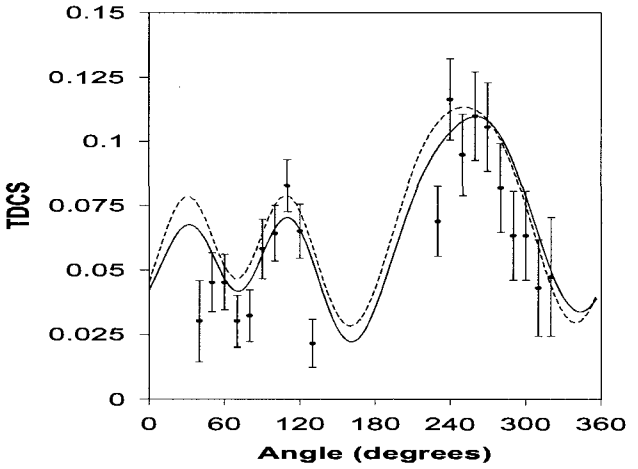

(b)

FIG. 7: TDCS in atomic units for (a) $Ar(2s) : E_f = 1000eV, \theta_f = 12^0, E_s = 20eV$ and (b)$Mg(2p) : E_0 = 1078eV, E_f = 1000eV, \theta_f = 7^0$. The solid line is DWBA and the dotted is PWBA. Experiment is from [48].

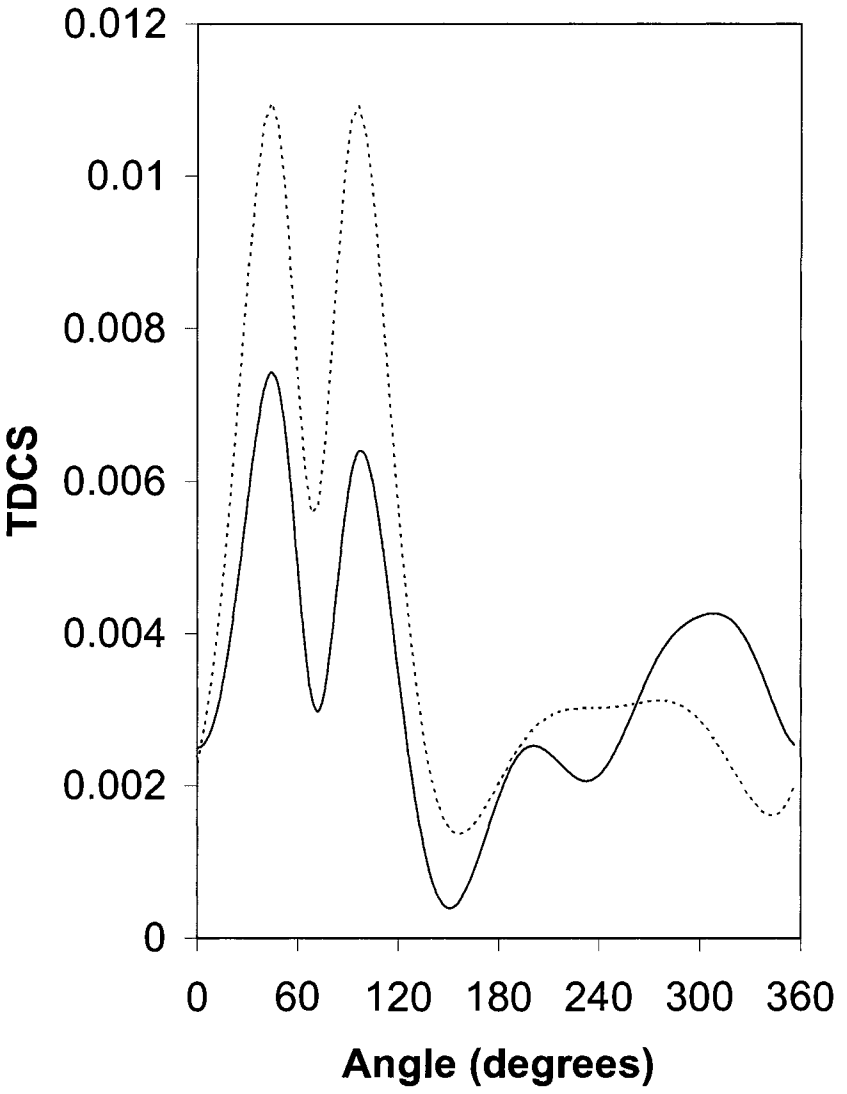

FIG. 8: TDCS in atomic units for coplanar asymmetric geometry for $Mg(2p) : E_0 = 1153eV, E_f = 1000eV, \theta_f = 15\,\text{deg}$. The solid curve is DWBA and the dotted curve is FBA.

apparent in the shape of the TDCS, as we have done above. It is also important however to look for a way to systematically inter-normalize different relative measurements. This particularly true for s states where even in the DWBA the TDCS is relatively structureless. Here the difference between the theories must of course lie in the relative size of the cross section. Several methods for accomplishing this have been suggested [62] in the past. We suggest working in the coplanar constant θ_{fs} geometry [63] described in Chapter 1. The effect of performing such an experiment would allow one to place all the coplanar asymmetric measurements done for the same impact and exiting energies on the same scale and thus permit a welcome if more severe test of theory.

II.6 SUMMARY

In this chapter we have reviewed the underlying theory for the various Born approximations and examined their strengths and weaknesses. We have examined the Distorted Wave Born Approximation in particular and shown that it generally gives good agreement with the available experimental data. We note that since this data is both relative and over a limited angular range, we are not always able to unambiguously distinguish between the different theoretical models. We examined the very recent experimental results, [48], where the available experimental data is in good agreement with both the FBA and the DWBA and showed that by relatively small changes in the parameters we could arrive at a situation where a relative experiment should be able to clearly differentiate between the two theories. We further suggest performing complementary measurements in both coplanar asymmetric and coplanar constant θ_{fs} geometries, which would allow an inter-normalization between different measurements. In the next chapter we will examine the choices made in calculations involving the DWBA in relation to hydrogen and helium at low energies to determine the dominate contributions to those TDCS.

CHAPTER III

DWBA AND $(E, 2E)$ ON HYDROGEN, HELIUM, AND IONS

It is only very recently that advances in experimental techniques have opened up the possibility of making accurate multiply differential measurements of ionic targets. Advances in storage ring technology are likely to facilitate further progress in this area. Müller [64] has used a heavy ion storage ring to perform high resolution studies of ionization and recombination of highly charged ions. The new Facility for Antiproton and Ion Research (FAIR) [2], for which construction has just begun, will provide a wide range of particle beams of ions up to bare uranium, as well as intense electron and antiproton beams, and it is envisaged that $(e, 2e)$ experiments will be performed on ions to complement the existing neutral experiments [65].

In this chapter we are concerned with the study of the electron impact ionization of atoms and ions close to the ionization threshold. For some time now accurate experimental data has been available for the ionization of hydrogen and helium [66, 67, 68]. We will first study the ionization of neutral hydrogen and helium in the near threshold region and compare with the available experimental data. We will show that very good agreement with experiment can be obtained using a variant of the Distorted Wave Born Approximation (DWBA). It is relatively straightforward to extend these calculations to one or two electron ions. We present here calculations on the isoelectronic sequence of hydrogen-like and helium-like ions corresponding to the first row of the periodic table, i.e. up to neon.

III.1 CHOICES FOR THE DISTORTING AND EXCHANGE POTENTIALS

As stressed in Chapter 1, we have a great deal of freedom in choosing the distorting potential. In this chapter we will consider several choices.

First we define our "standard" DWBA, DWBAS. For N electron targets, the incoming distorted wave is generated in the static exchange potential for the target and asymptotically the electron sees a Coulombic potential of charge $Z - N + 1$ where Z is the nuclear charge. The distorted waves of the two outgoing electrons are identical and are generated in the static exchange potential of the residual ion, i. e. with an asymptotic charge of $Z - N + 1$. For a hydrogen-like targets the TDCS

is given by (122). For helium-like targets, the TDCS is given by (97) and we use Furness-McCarthy local potentials for exchange in each of the channels. For the final channel we use an 'average' form. Next we define DWBA with Peterkop asymptotics, DWBAP, to be identical to our standard model except that the asymptotic charges seen by the outgoing electrons obey the Peterkop relation (36).

Our third choice is the Coulomb Born, CB, approximation. This derived by taking the distorting potentials in both the incident and final channels to be the unscreened Coulomb potential of the nucleus, Z/r. Similar to the DWBAP, we define the Coulomb Born Peterkop, CBP, approximation by taking the incident distorted wave to be that of an electron moving in the field of the unscreened Coulomb potential of the nucleus, Z/r while the outgoing electrons experience a Coulomb field given by effective charges $z_s = z_f$ which obey (36).

We note that while there is a closed analytic form for the one electron wave function the same is not the case for the two electron target. The target wave function enters our model both explicitly in (98) and (122) and implicitly in the calculation of the local potential, (119), (120), (121). It is thus possible that the TDCS will be sensitive to the level of correlation in the target wave-function.

III.2 $(E, 2E)$ NEAR THRESHOLD

Naively one might assume that close to threshold the TDCS would be dominated by post collisional electron-electron interactions and that incident channel effects would not be too significant [69]. One would assume that the electrons would escape back to back, i.e. with $\theta_{fs} = \pi$. Ehrhardt and his collaborators [66, 67, 68] have performed absolute experimental measurements in coplanar constant $\theta_{fs} = \pi$ geometry, which is outlined in Chapter 1. The TDCS is given as a function of θ_f. Figure 9 shows this TDCS in comparison with various theoretical models. In particular, our DWBAS and DWBAP approximations are in remarkably good agreement, especially when one remembers that both these approximations are first order in the electron-electron interactions. Adding the Peterkop asymptotics, (36), makes a negligible difference to the calculation. In this very particular geometry all 3 final state particles are collinear and one might assume that it is most favorable for incorporating final state interactions via (36).

Figure 10 shows theory and experiment in the same geometry for a helium target. Again agreement is good and there is little or difference between the DWBAS and

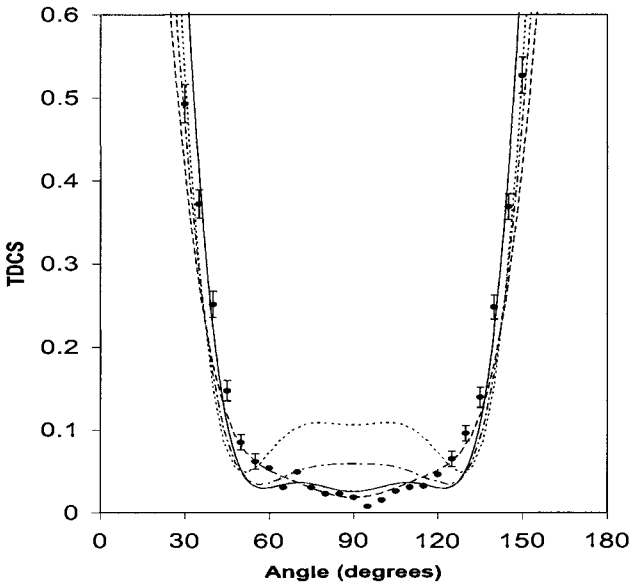

FIG. 9: TDCS in atomic units ($a_0\pi^2$), plotted against θ_f for hydrogen. Using the constant θ_{fs} geometry, $\theta_{fs} = \pi; E_f = E_s = 1eV$. The absolute experimental data of Ehrhardt [68] is plotted against θ_f. The solid line is the DWBAS, long dashed DWBAP, short dashed CB, and the dashed dotted CBP.

DWBAP calculations.

Pan and Starace [70] have also considered these experiments in a model identical to our DWBAP approach except that they did not make use of the local exchange approximation, i.e. they solved the appropriate integro-differential equations. In Fig. 11 the DWBA [71] is compared to the theoretical results of Pan and Starace [70] and Jones and Madison [72]. There is little difference between the results of Pan and Starace and ours. The good accord between our two calculations encourages us in the use of our local exchange approximation. Jones and Madison's [67, 72] approach is similar to ours except that they use effective charges which obey a different asymptotic form to (36). We have performed several DWBA calculations using a local exchange approximation but with a different choice of asymptotic effective

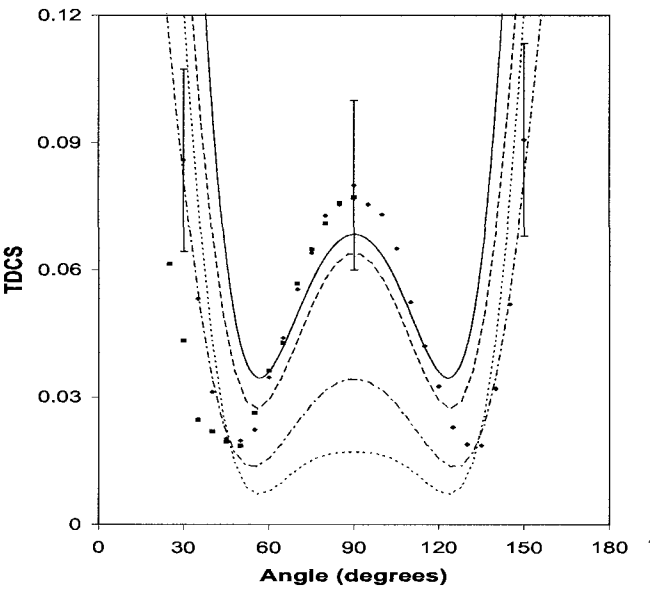

FIG. 10: TDCS in atomic units ($a_0\pi^2$), plotted against θ_f for helium. $\theta_{fs} = \pi; E_f = E_s = 1eV$. The circles are the absolute experimental data from [68]. The squares are the relative experimental data of [58]. The solid line is DWBAS, long dashed DWBAP, short dashed CB, and the dashed dotted CBP.

charges. Despite this the agreement with experiment remains very good. In other words the use of effective charges contributes nothing over the DWBAS.

Unlike the hydrogen case the TDCS for helium exhibits some structure. There is a local maximum at $\theta_f = \frac{\pi}{2}$. We have used the freedom inherent in the DWBA approach to explore the origin of this feature. Figure 12 shows the same experimental arrangement for helium, where we examine the effect of exchange in the incident and final channels potentials.

We find that the structure persists for any choice of final state exchange potentials but in the absence of incident channel exchange it is significantly reduced. This suggests that in contrast to the naive picture, incident channel effects may be significant. To further explore this we have considered the role of the target wave function.

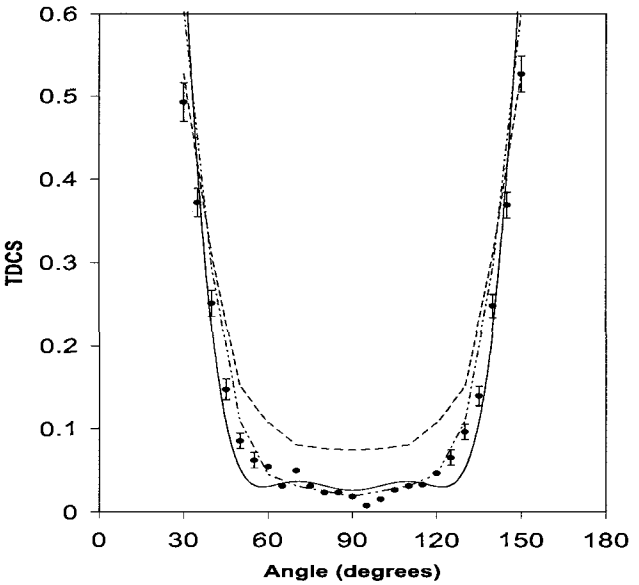

FIG. 11: TDCS in atomic units ($a_0\pi^2$), plotted against θ_f for hydrogen with $\theta_{fs} = \pi; E_f = E_s = 1eV$. The absolute experimental data of [68] is plotted against θ_f. The solid line is DWBAS, the theoretical curves of Pan and Starace [70] are the dashed line, and Jones and Madison [72] are the dashed and double dotted line. Pan and Starace is almost identical to DWBAS.

It enters our calculations explicitly in (98) and also implicitly in generating the static exchange potential. In Fig. 13 we present results using four different wave functions for the helium target: a simple variational uncorrelated choice, VUC [73], the Byron-Joachain, B-J, wave function [74], the Clementi-Roetti, C-R, wave function [24] and the wave function of Koga [75], K. Each set of wave functions is constructed in the Hartree Fock form as outlined in Chapter 2. These wave functions give progressively better ground state energies: VUC is within 2% of the correct energy and B-J within 0.4%. C-R gives the correct answer to 6 decimal places while the Koga form is even better (10 places of decimal places of accuracy). The TDCS becomes progressively

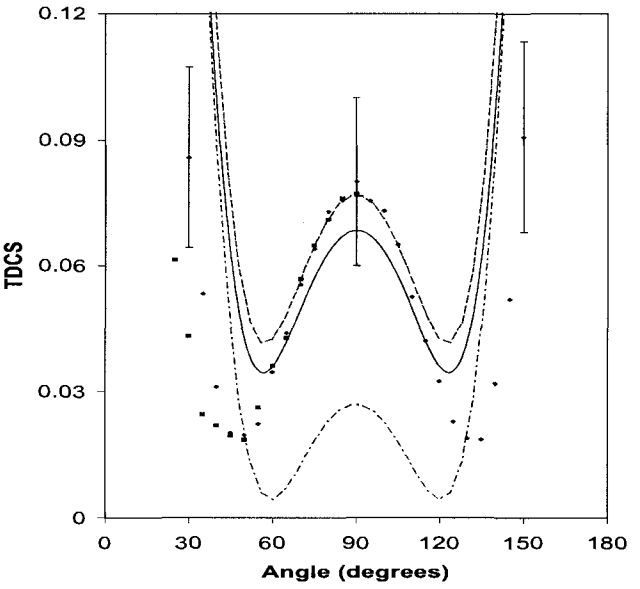

FIG. 12: TDCS in atomic units ($a_0\pi^2$) for helium for $\theta_{fs} = \pi$ and $E_f = E_s = 1eV$ comparing various exchange potentials. The solid curve is the standard model used, DWBAS. The dashed dotted curve is with exchange turned off in the incident channel. The dashed curve is with a triplet exchange potential, the singlet is given by a dotted curve which is indistinguishable from the triplet, experimental data as in Fig. 10.

closer to the experiment as we increase the level of correlation in our target. However while these results reinforce the importance of incident channel effects we note that the CR [24] is just as effective as the more correlated Koga wave function. The results suggest that the relative size of the central peak may be linked to the degree of correlation in the target wave function.

In [76], experimental results were presented for helium for the same energies as Ehrhardt [68] but in perpendicular plane geometry, i.e. $\Phi = 90^0, \theta_f = \theta_s$. These measurements are relative but share a point in common with the Ehrhardt [68] data and can thus be placed on an absolute scale. In Fig. 14 we compare with our DWBAS approach. Also shown is the Selles [58] parameterized fit, based on the Wannier

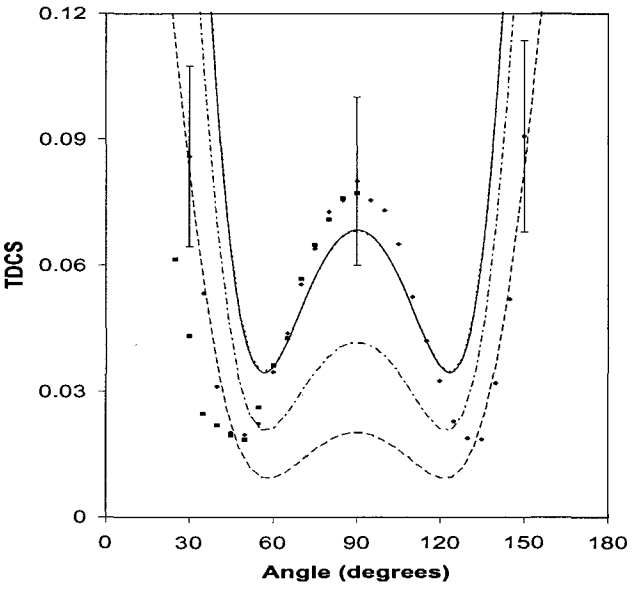

FIG. 13: TDCS in atomic units ($a_0\pi^2$) for helium for $\theta_{fs} = \pi$ and $E_f = E_s = 1eV$ using various models for the target wavefunction. The solid curve is C-R, dotted K (note it is indistinguishable from C-R), dashed-dotted B-J, and dotted VUC. The experimental data as in Fig. 10.

model [69]. While the DWBAS agrees quite well both in shape and absolute size with experiment it is slightly broader than the fit. This suggests that post collisional interactions (pci) might be playing more of a role than in the coplanar case. To test this we have used the N_{ee} factor on DWBA calculation, as discussed in Chapter 2. The inclusion of N_{ee} brings the DWBA into close accord with the Wannier fit [58]. This indicates that pci may indeed play a role but it has to be stressed that the DWBA without any attempt to include its effect is in good accord with both the shape and the absolute size of the TDCS. As we noted earlier, the introduction of the Gamov factor generally destroys the normalization of the TDCS. Still the inclusion of the N_{ee} factor does seem to improve the correspondence of DWBA to the experiment.

In summary, we note that there is very little difference between our DWBAS

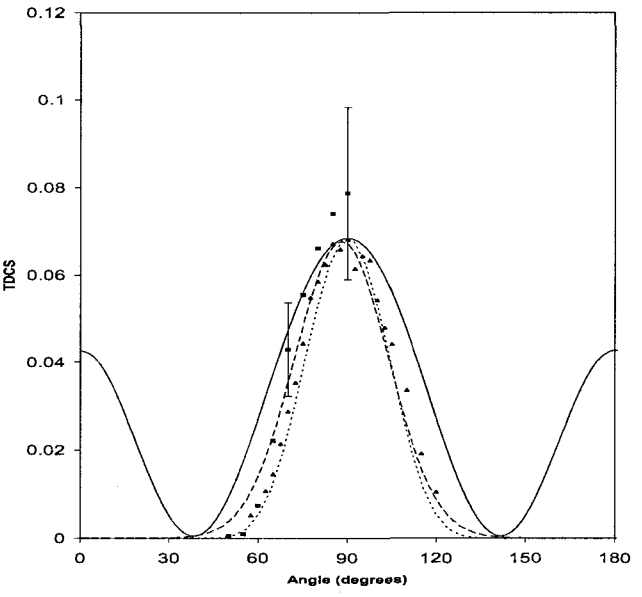

FIG. 14: TDCS in atomic units ($a_0\pi^2$) for helium, in the perpendicular plane, $\phi = \pi/2, \theta_f = \theta_s, E_f = E_s = 1eV$. The solid curve is DWBAS, the dashed curve is DWBA+N_{ee}, and the dotted curve is a fitting using the form given by Selles [58]. The triangles are the relative data of [76] while the squares are absolute experimental data from [68].

and DWBAP calculations, indicating that the choice of effective charges is not a significant factor. We also see that if we turn off exchange in the final channel it has little effect on the TDCS. In contrast turning off exchange in the incident channel does significantly reduce the local maximum away from experiment. We also note that the TDCS does exhibit a sensitivity to the choice of target wavefunction, with VUC giving the worst agreement and K and C-R being largely indistinguishable and giving the best agreement with experiment. These two factors, exchange in the incident channel and correlation in the target wave function, indicate that incident channel effects play an important role near threshold.

This is surprising when one considers the work of Wannier [69]. Wannier determined the scaling law for the total cross section for an atom near threshold. Experiment [77] and later theory [11, 78] have supported his threshold laws. However his derivation specifically ignores incident channel effects and is derived using an idea of Wigner's [79], that in the case of threshold ionization one can neglect the interior region of the problem, the reaction region, and that the threshold behavior arises from the escape process where the two electrons can be treated classically.

Clearly then we must conclude that while the total cross section may depend only on the far asymptotic region where the electrons behave classically, the shape of the TDCS is dependent on the incident channel effects. We note that we found excellent agreement with experiment using what was essentially the DWBAS. By lowering the energy one would expect that post-collisional electron-electron interactions would become important and hence a decreased accuracy of the DWBAS. But overall the DWBAS works remarkably well at these low energies.

III.3 $(E, 2E)$ ON IONS

For a multi-charged ion, one can reasonably expect the DWBA to be even better, as pci will be even less significant as the charge on the residual ion increases, dominating the interactions between the three charged particles. Here we present the TDCS for the isoelectronic sequences of hydrogen-like and helium-like ions up to $Z = 10$, i.e. up to Ne^{8+} and Ne^{9+}. Figure 15 shows the hydrogen-like sequence in coplanar constant $\theta_{fs} = \pi$ geometry with $E_s = E_f$. The shape of the cross section varies only a small amount with Z but its absolute size decreases significantly. This is as one would expect when dealing with the increasingly large charge of the initial ion.

Figure 16 shows the helium-like sequence in coplanar constant $\theta_{fs} = \pi$ geometry with $E_s = E_f$. Again the shape of the cross section varies only a small amount but its absolute decreases significantly with increasing Z. As we increase Z the local maximum around $\theta_f = 90$ degrees begins to disappear. We interpret this as indicating that the target wave function and exchange in the incident channel effects become less important with increasing nuclear charge. The nuclear charge comes dominate the process and the collision becomes hydrogen-like.

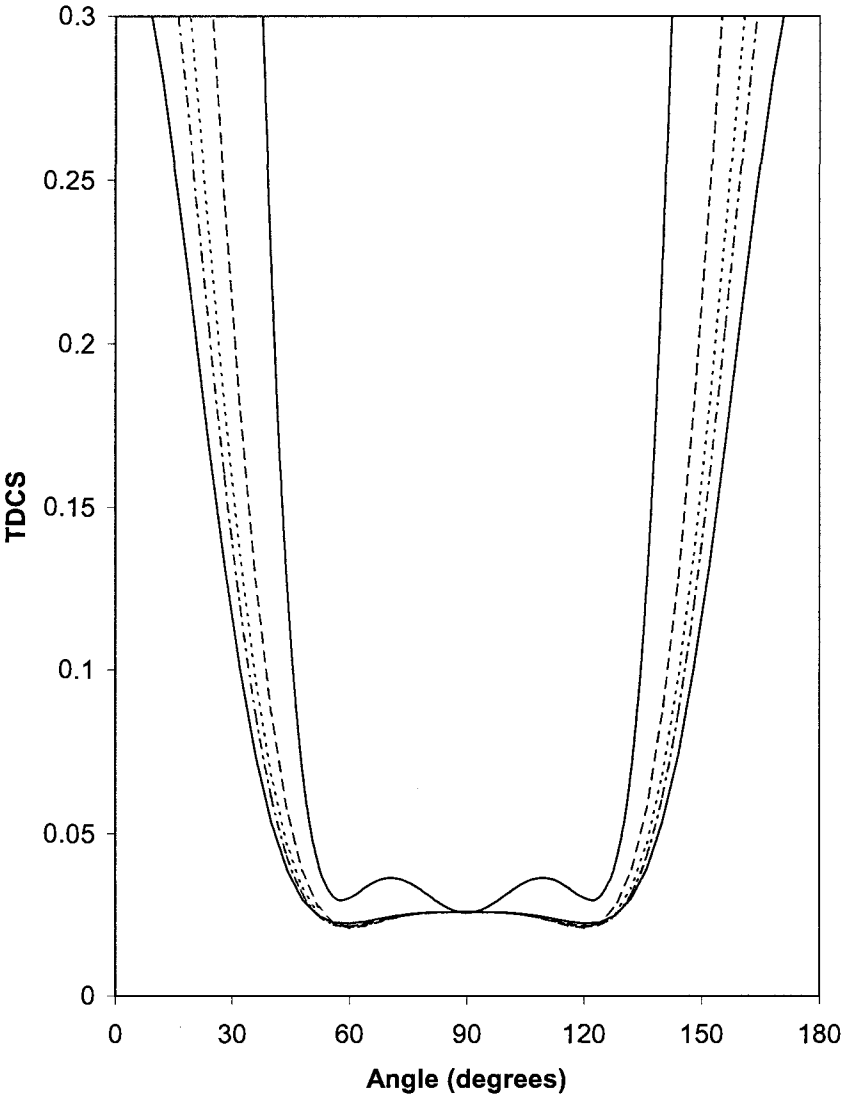

FIG. 15: TDCS in atomic units ($a_0\pi^2$) for hydrogen-like ions, $\theta_{fs} = \pi; E_f = E_s = 1eV$. The upper most solid curve is hydrogen itself, followed by He^+ (dashed), Li^{2+} (dotted), Be^{3+} (dashed and dotted), and Ne^{9+} the lowermost solid curve. All have been scaled to the hydrogen value at $\theta = \pi/2$. The scaling factors are: 18.6 (He^+), 181 (Li^{2+}), 978, (Be^{3+}), and 23700, Ne^{9+}.

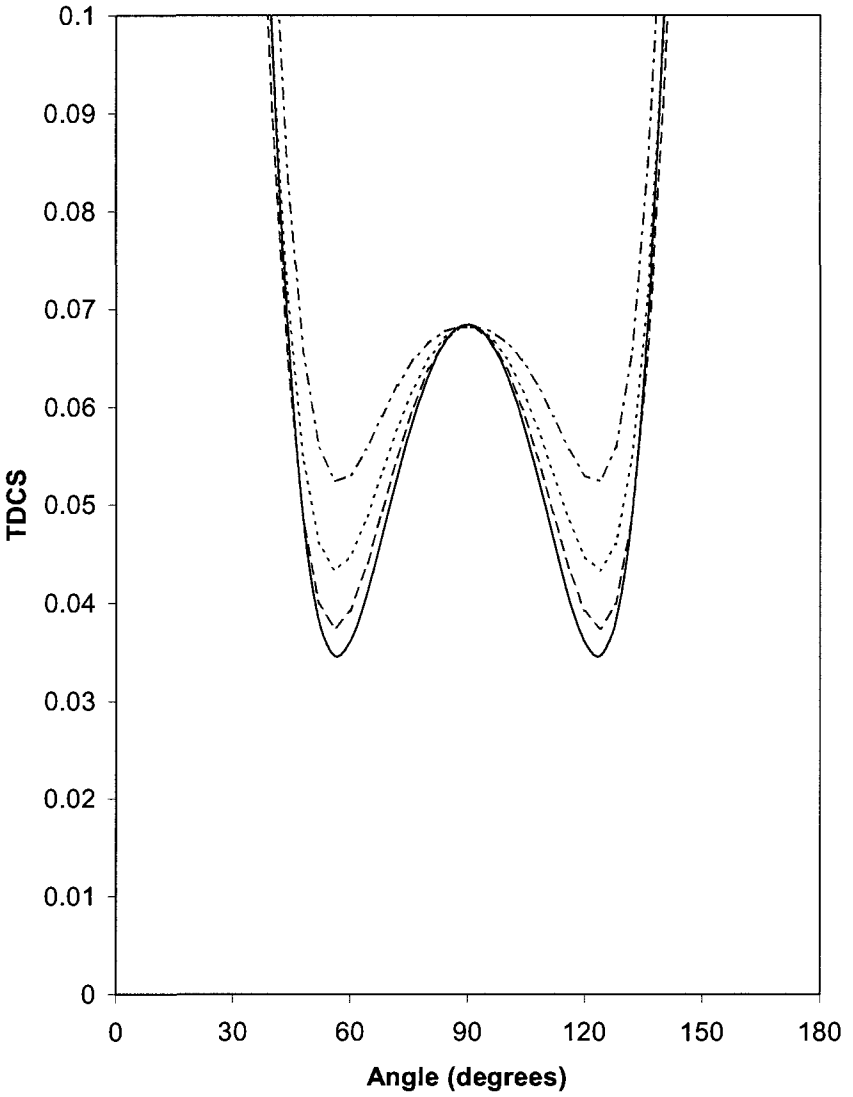

FIG. 16: TDCS in atomic units ($a_0\pi^2$) for helium-like ions, $\theta_{fs} = \pi; E_f = E_s = 1eV$. The lower most solid curve is helium itself, followed by Li^+ (dashed), Be^{2+} (dotted), and Ne^{8+} (dashed and dotted). All have been scaled to the helium value at $\theta = \pi/2$. The scaling factors are: 28.5, (Li^+), 257 (Be^{2+}), and 16700, (Ne^{8+}).

III.4 CONCLUSIONS

In this chapter we have examined the near threshold region for the electron impact ionization of hydrogen and helium and we have shown that while we are working in a regime where the total cross section obeys the Wannier scaling law [80], the TDCS in energy sharing $\theta_{fs} = 180$ degrees geometry shows a marked dependence on incident channel effects. We found that using effective charge asymptotics made very little difference to our Distorted Wave calculations and we remain skeptical about their utility. We have also performed calculations on the simplest isoelectronic sequence of multi-charged ions and found cross sections that differ only a little from the neutral case in shape but whose absolute size decreases sharply with increasing charge.

CHAPTER IV

X2E

In this chapter we outline a new *ab initio* method of calculating $(e, 2e)$ processes, called the X2e method. In the following chapters we will describe the method in full and provide a proof of principle that this technique can be applied to the full problem. The X2e method is an $\mathcal{R}$-operator based method. Much like the **R**-matrix method detailed in Chapter 1, the X2e method breaks up the problem into an inner and outer region. The inner region is where the problem is treated completely with all the relevant interactions accounted for. The outer region is where we match to the asymptotic forms of the process we are interested in, whether they be scattering or double escape of the electrons. One of the strengths of the X2e method is its flexibility. Despite the fact that we focus in this thesis on hydrogenic ions, we could if we wish model the interactions of more complicated systems by adjusting the calculations in the inner region. The $\mathcal{R}$-operator method allows us to connect the inner region, whatever it may be, to the asymptotic region of up to two escaping electrons about an ion.

We begin with an overview of the X2e method, from the inner region to the final calculation of the cross sections. We then discuss the inner region, describing the basis elements we use, and then showing how these are used to construct the pseudostates within the inner region.

IV.1 OVERVIEW

As shown in Fig. 17, the X2e method is subdivided into several regions. It begins in the inner region. This is the region we mentioned above, where we take into account all the relevant physics, including exchange and target correlation. In this region we construct a close coupling expansion of the wave function using the full Hamiltonian. The expansion is done using a basis set of spherical harmonics and Sturmian radial functions. The basis set is used to calculate the pseudostates within this region using a $1e^-$ Hamiltonian. By pseudostates we mean a set of states that span both the bound energies and the continuum. If we had an infinite number of these states they would converge on the true wave functions for the target atom. The basis is also used to construct pseudostates of coupled electron wave functions using

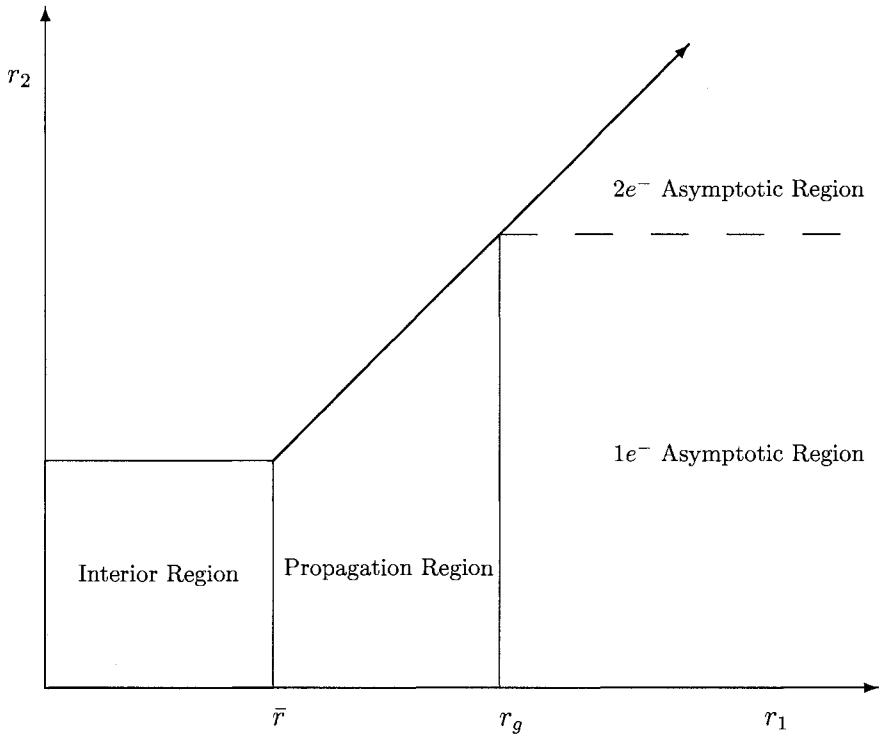

FIG. 17: A conceptual image of the X2e method displayed in the radial spaces of the two escaping electrons. $\bar{r}$ is the boundary between the interior region and the propagation region. r_g, the Gailitis radius, is the final asymptotic radius where the **R**-matrix is used to construct cross sections and phase shifts. The diagonal line is where $r_1 = r_2$ and is the line of symmetry in the problem.

a full $2e^-$ Hamiltonian. The details of this construction are in the second section of this chapter. The close coupling expansion is explored in the Chapter 5, though the relevant matrix elements and pseudostates are derived in this chapter.

Once we have our pseudostates from this expansion and the relevant $2e^-$ Hamiltonian matrix elements, we can construct our $\mathcal{R}$-operator. This is done on the boundary $\bar{r}$. This radius arises because in all numerical calculations there is an upper limit to accuracy based on the number of decimal places available[1]. This loss of accuracy results in false linear dependencies cropping up in the Sturmian basis set as the radial coordinates increase and consequentially forcing an increase in the size of the basis set. Once accounting for these becomes too inefficient in terms of computational effort we move into the next region, the propagation region. At that radius, $\bar{r}$, the $\mathcal{R}$-operator is constructed and projected into the space where $r_1 \geq r_2$ in the form of an **R**-matrix. We make use of the symmetry about the line $r_1 = r_2$ to account for the region where $r_2 \geq r_1$. The details of this calculation as well as the derivation of the $\mathcal{R}$-operator can be found in Chapter 5.

Once we are in the propagation region, we must first account for the linear dependencies arising in the Sturmian basis. We do this by translating to a more robust basis, the spline delta basis, which is explicitly linearly independent and defined in the region $0 \leq r \leq r_g$, where r_g is an asymptotic radius. After a linear translation of bases we then make use of a modified Light Walker propagation scheme, which propagates the **R**-matrix from $\bar{r}$ out to the asymptotic radius r_g, called the Gailitis radius. r_g is determined when our electrons are sufficiently far out to be treated asymptotically. The details of the spline delta basis and the propagation technique can be found in Chapter 6.

Finally we can connect our results to the asymptotic regions. In the $1e^-$ asymptotic region, one electron remains close to the atom and the essential problem is that of elastic scattering and excitation. We calculate the **S**, **K**, and **T**-matrices. These are used to calculate the scattering phase shifts as well as cross sections for elastic scattering and excitation. In the $2e^-$ asymptotic region, we calculate the TDCS in whatever geometry we are interested in. We do this by projecting out our results on the asymptotic forms for the wave functions of the escaping electrons. The details of the $1e^-$ and $2e^-$ asymptotic region calculations can be found in Chapter 7 as well

[1]In our calculations we make use of Fortran*8 which means approximately 16 significant figures are retained.

as the discussion of the ideal projector to use in the $2e^-$ asymptotic region. Further details on projectors that were considered at one point may be found in Appendix H.

IV.2 INTERIOR REGION

Here we will describe the method used in the interior region for $(e, 2e)$ on one electron targets. We begin in the interior region where the electrons are still close to the ion. In this region we construct a set of pseudostates which characterize the behavior of the electrons in that region using the $1e^-$ Hamiltonian and a basis of Sturmian functions and spherical harmonics. These are used in the close coupling expansion and the calculation of the channel wave functions, using the same basis. We also derive coupled two electron pseudostates using the elements the matrix elements for the $2e^-$ Hamiltonian and a basis of coupled one electron bases. These are used in our derivation of the **R**-matrix in Chapter 5. We assume that relativistic effects including spin-orbit coupling can be neglected.

For the systems we are interested in, Schrödinger's equation is

$$H = -\frac{1}{2}\nabla_1^2 - \frac{1}{2}\nabla_2^2 - \frac{Z}{r_1} - \frac{Z}{r_2} + \frac{1}{r_{12}} \tag{125}$$

where Z is the charge of the nucleus. The subscripts denote the electrons and $r_{12} = |\mathbf{r}_1 - \mathbf{r}_2|$. This can be broken up into a $1e^-$ Hamiltonian and a $2e^-$ portion by rewriting it into

$$H = H_1 + H_{12} \tag{126}$$

where

$$H_1 = -\frac{1}{2}\nabla_1^2 - \frac{Z}{r_1} \tag{127}$$

$$H_{12} = -\frac{1}{2}\nabla_2^2 - \frac{Z}{r_2} + \frac{1}{r_{12}} \tag{128}$$

The total state of the system is determined by considering the quantum numbers of the two electrons. The electrons' quantum states are denoted by subscripts, a and b, representing the set of quantum numbers $\{n_a, l_a m_a m_a^s\}$ and $\{n_b, l_b m_b m_b^s\}$, with electrons in the continuum having the index n replaced by the wave number k. We know from standard quantum mechanics [50, 81] that the two electron Hamiltonian commutes with the total orbital and spin angular momentum operators and their respective z-components as well as the parity operator. This means we should be

able to derive a wave function which is an eigenfunction of all five operators. The state of the total system can then be specified by a set of quantum numbers (using the notation of Percival and Seaton [28]) $\Gamma = n_a, n_b, l_a, l_b, L, S, M_L, M_S, P$.

The total wave function is described by the expansion:

$$\Psi^{LSP}(\mathbf{r}_1, \mathbf{r}_2) = \sum_{l_a, l_b} \psi^{LSP}_{l_a l_b}(r_1, r_2) \Xi^{LM_L}_{l_a l_b}(\Omega_1, \Omega_2) \tag{129}$$

where the couple spherical harmonics, $\Xi^{LM_L}_{l_a l_b}$, are

$$\Xi^{LM_L}_{l_a l_b}(\Omega_1, \Omega_2) = \sum_{m_a, m_b} c(l_a l_b m_a m_b; LM_L) Y_{l_a m_a}(\Omega_1) Y_{l_b m_b}(\Omega_2). \tag{130}$$

Y_{lm} are the usual spherical harmonics and $c(l_a l_b m_a m_b; LM_L)$ are the Clebsch-Gordon coefficients as discussed in Appendix B. Ω is our short hand for the angular components ϕ and θ.

The function $\psi^{LSP}_{l_a l_b}$ is expanded into a product of pseudostates and radial channel functions. The pseudostates are a basis of states constructed from the Hamiltonian for a one electron target. In the limit of an infinite basis, this basis would become the full set of hydrogenic wave functions but in our case we span the continuum with a finite number of states. Hence the term pseudostate.

For much of our actual work instead of ψ we make use of the more convenient function F which is equal to ψ multiplied by the two radial coordinates, r_1 and r_2. This eases the relevant integrations. F (and ψ) are defined:

$$F^{LSP}_{l_a l_b}(r_1, r_2) = r_1 r_2 \psi^{LSP}_{l_a l_b}(r_1, r_2) = \sum_n u_{nl_2, l_1}(r_1) \phi_{nl_2}(r_2) = \sum_{\mu'} u_{\mu\mu'}(r_1) \phi_{\mu'}(r_2) \tag{131}$$

where the functions u are the channel wave function of the scattered particle and the functions ϕ are the pseudostates of the target. The subscripts μ denote the relevant quantum number $\{n, l_a, l_b\}$ for the channel. Prime indicates the scattering channels while unprime refers to the incident channel. The derivation of the channel wave functions u is done by solving the following series of integro-differential equations:

$$\left(\frac{d^2}{dr_1^2} - \frac{l_\mu(l_\mu + 1)}{r_1^2} + \frac{2Z}{r_1} + k_\mu^2 \right) u_{\mu\mu'}(r_1) = 2 \sum_\nu V_{\mu\nu} u_{\nu\mu'} \tag{132}$$

where

$$V_{\mu\nu} = \langle \phi_\mu \Xi_\mu | \frac{1}{r_{12}} | \phi_\nu \Xi_\nu \rangle \tag{133}$$

The channel wave functions will be derived in Chapter 5 by solving the full the $2e^-$ Hamiltonian, making use of the pseudostates as solutions of the $1e^-$ Hamiltonian, H_1.

Our first task is to calculate the pseudostates. To do this we need to construct the $1e^-$ and $2e^-$ Hamiltonians and then determine the eigenstates for each. The $1e^-$ eigenstates will then become the pseudostates for our method. First we will examine the basis elements for the $1e^-$ and $2e^-$ cases. Then we will look at a mathematical result that we can use to simplify our construction of the various Hamiltonian matrix elements. This result will also allow us to naturally include a Bloch modification to Schrödinger's equation. Then we will construct the various matrix elements for H_1, the $1e^-$ Hamiltonian, using this basis. We will also calculate the matrix elements for H_{12}, the $2e^-$ Hamiltonian in the $2e^-$. Lastly we show how the pseudostates are calculated.

IV.2.1 $1e^-$ BASIS ELEMENTS

As mentioned the basis for the interior is broken up into angular and radial parts, consisting of spherical harmonics and Sturmian functions. The Sturmian functions used are of the form:

$$\chi_a(r) = r^{n_a-1}e^{-\alpha r} \tag{134}$$

where $n_a > 0$ and the damping parameter α is an arbitrary positive number. These Sturmian functions are a complete (in the limit of an infinite basis set), discrete and regular linearly independent set on any closed interval $(0, \bar{r})$. As will be shown in the Chapter 5, the $\mathcal{R}$-operator method requires a basis that is linearly independent.

The virtue of the Sturmian basis is the ease with which the radial integrals can be conducted. The details of the radial integrals can be found in Appendix C.

The full $1e^-$ basis elements can be expressed as

$$\varphi_a(\mathbf{r}) = N_a\chi_{n_a}(r)Y_{l_am_a}(\theta,\phi) \tag{135}$$

where N_a is a normalization factor and Y_{lm} are the standard spherical harmonics.

IV.2.2 $2e^-$ BASIS ELEMENTS

In the case of solving the full $2e^-$ Hamiltonian for the coupled pseudostates, we will use a two electron basis constructed out of the $1e^-$ radial basis elements χ_a and coupled spherical harmonics as defined in equation (130). These coupled spherical harmonics form an orthonormal set as can be seen by looking at equation (509) in Appendix B.

We must ensure that the basis is properly anti-symmetrized with relation to the Pauli exclusion principle. This requires that the wave function should be antisymmetric with respect in the combined space and spin coordinates of the particles. For our $2e^-$ basis this means for the singlet state, which is symmetric in spin ($S = 0$), the spatial part is antisymmetric. The triplet state ($S = 1$) is antisymmetric in spin and thus must be symmetric in the spatial part.

We incorporate this into the construction of our $2e^-$ basis by using a linear combinations of the $1e^-$ basis elements of the form

$$\Pi_{ab}(\mathbf{r}_1,\mathbf{r}_2) = \frac{1}{\sqrt{2}}N_aN_b\Big(\chi_a(r_1)\chi_b(r_2)\sum_{m_a,m_b} c(l_al_bm_am_b;LM_L)Y_{l_am_a}(\Omega_1)Y_{l_bm_b}(\Omega_2) \\ +(-1)^S\chi_b(r_1)\chi_a(r_2)\sum_{m_a,m_b} c(l_bl_am_bm_a;LM_L)Y_{l_bm_b}(\Omega_1)Y_{l_am_a}(\Omega_2)\Big) \quad (136)$$

where Π_{ab} is the $2e^-$ basis element. This result can be simplified somewhat by examining how the coupled spherical harmonics transform under an interchange of coordinates. For the spherical harmonics $\Xi^{LM_L}_{l_al_b}$, this gives us

$$\begin{aligned}\Xi^{LM_L}_{l_bl_a}(\Omega_1,\Omega_2) &= \sum_{m_a,m_b} c(l_bl_am_bm_a;LM_L)Y_{l_bm_b}(\Omega_1)Y_{l_am_a}(\Omega_2) \\ &= (-1)^{l_a+l_b-L}\sum_{m_a,m_b} c(l_al_bm_am_b;LM_L)Y_{l_bm_b}(\Omega_1)Y_{l_am_a}(\Omega_2) \quad (137)\end{aligned}$$

Now using (137) in equation (136) we can see how this allows us to introduce the coupled spherical harmonics,

$$\begin{aligned}\Pi_{ab}(\mathbf{r}_1,\mathbf{r}_2) &= \frac{1}{\sqrt{2}}N_aN_b\Big(\chi_a(r_1)\chi_b(r_2)\sum_{m_a,m_b} c(l_al_bm_am_b;LM_L)Y_{l_am_a}(\Omega_1)Y_{l_bm_b}(\Omega_2) \\ &\quad +(-1)^{l_a+l_b-L+S}\chi_b(r_1)\chi_a(r_2) \\ &\quad \times\sum_{m_a,m_b} c(l_al_bm_am_b;LM_L)Y_{l_bm_b}(\Omega_1)Y_{l_am_a}(\Omega_2) \\ &= \frac{1}{\sqrt{2}}N_aN_b\Big\{\chi_a(r_1)\chi_b(r_2)\Xi^{LM_L}_{l_al_b}(\Omega_1,\Omega_2) \\ &\quad \times(-1)^{l_a+l_b-L}(-1)^S\chi_b(r_1)\chi_a(r_2)\Xi^{LM_L}_{l_bl_a}(\Omega_1,\Omega_2)\Big\} \quad (138)\end{aligned}$$

Additionally if we look at the effect of the parity operator on the coupled spherical harmonics, we see that for a single spherical harmonic

$$\mathcal{P}[Y_{lm}(\theta,\phi)] = Y_{lm}(\pi-\theta,\phi+\pi) = (-1)^lY_{lm}(\theta,\phi). \quad (139)$$

Hence the effect of the parity operator on $\Xi^{LM_L}_{l_al_b}$ is to add a factor of $(-1)^{l_a+l_b}$. We rewrite (138) as

$$\Pi_{ab}(\mathbf{r}_1,\mathbf{r}_2) = \frac{1}{\sqrt{2}}N_aN_b\Big\{\chi_a(r_1)\chi_b(r_2)\Xi^{LM_L}_{l_al_b}(\Omega_1,\Omega_2)$$

$$\times(-1)^{L+S+P}\chi_b(r_1)\chi_a(r_2)\Xi_{l_b l_a}^{LM_L}(\Omega_1,\Omega_2)\Big\} \tag{140}$$

where $P = l_a + l_b$ and we use $(-1)^{-L} = (-1)^L$.

It should be noted that parity also limits the number of coupled states by limiting the values of allowed orbital momenta (those that yield non-zero results). In our calculations we choose a parity prior to calculation and then work out the allowed 2-electron configurations. A list is derived of these configurations by using the convention that $l_a \geq l_b$, $n_a \geq n_b$ for $|l_a - l_b| \leq L \leq l_a + l_b$.

IV.2.3 MATHEMATICAL RESULTS

In this section we derive a key mathematical theorem that we will need both in the derivation of the Bloch modified Hamiltonian and later in our derivation of the $\mathcal{R}$-operator (which is done in Chapter 5). First we will present and prove the lemma then proceed to examine its effects on our Schrödinger's equation.

Lemma 1

For any two sufficiently 'well behaved' functions $\phi(\mathbf{r})$ and $\psi(\mathbf{r})$ defined on a volume Ω with a surface Σ then [13]

$$\begin{aligned}\int_\Omega \phi(\mathbf{r})\Big\{-\frac{1}{2}\nabla^2 + V(\mathbf{r}) - E\Big\}\psi(\mathbf{r})\,d\tau &= -\frac{1}{2}\int_\Sigma \phi(\mathbf{r})\nabla_n\psi(\mathbf{r})\,d\sigma \\ &+ \int_\Omega \Big\{\frac{1}{2}\nabla\phi(\mathbf{r})\cdot\nabla\psi(\mathbf{r}) + \phi(\mathbf{r})(V(\mathbf{r}) - E)\psi(\mathbf{r})\Big\}\,d\tau\end{aligned} \tag{141}$$

where V is real and ∇_n is the outward normal gradient.

Proof: *Using the vector identity $\phi\nabla^2\psi = \nabla\cdot(\phi\nabla\psi) - \nabla\phi\cdot\nabla\psi$:*

$$\begin{aligned}&\int_\Omega \phi(\mathbf{r})\Big\{-\frac{1}{2}\nabla^2 + V(\mathbf{r}) - E\Big\}\psi(\mathbf{r})\,d\tau \\ &= \int_\Omega \Big\{-\frac{1}{2}\nabla\cdot(\phi(\mathbf{r})\nabla\psi(\mathbf{r})) + \frac{1}{2}\nabla\phi(\mathbf{r})\cdot\nabla\psi(\mathbf{r})\Big\}\,d\tau \\ &\quad + \int_\Omega \phi(\mathbf{r})(V(\mathbf{r}) - E)\psi(\mathbf{r})\,d\tau \qquad (142) \\ &= \int_\Omega \Big\{\frac{1}{2}\nabla\phi(\mathbf{r})\cdot\nabla\psi(\mathbf{r}) + \phi(\mathbf{r})(V(\mathbf{r}) - E)\psi(\mathbf{r})\Big\}\,d\tau \\ &\quad - \int_\Omega \frac{1}{2}\nabla(\phi(\mathbf{r})\nabla\psi(\mathbf{r}))\,d\tau. \qquad (143)\end{aligned}$$

Using Green's theorem to convert the second volume integral into a surface integral, we arrive at the result:

$$\int_\Omega \phi(\mathbf{r})\Big\{-\frac{1}{2}\nabla^2 + V(\mathbf{r}) - E\Big\}\psi(\mathbf{r})\,d\tau = -\frac{1}{2}\int_\Sigma \phi(\mathbf{r})\nabla_n\psi(\mathbf{r})\,d\sigma + \int_\Omega \Big\{\frac{1}{2}\nabla\phi(\mathbf{r})\cdot\nabla\psi(\mathbf{r}) + \phi(\mathbf{r})(V(\mathbf{r}) - E)\psi(\mathbf{r})\Big\}\,d\tau \tag{144}$$

where ∇_n is the outward normal gradient relative to the boundary surface Σ.

Corollary 1: *If $\phi(\mathbf{r})$ is a well behaved function within the volume Ω and if $\Psi(\mathbf{r})$ is a regular solution of the time independent Schrödinger equation, $(H-E)\psi(\mathbf{r}) = 0$, subject to the boundary condition $\nabla_n\psi(\mathbf{r}) = \zeta(\mathbf{r})$ where $\zeta(\mathbf{r})$ is an arbitrary defined function on an arbitrary surface Σ enclosing a volume Ω, then using Lemma 1:*

$$\int_\Omega \phi(\mathbf{r})(H-E)\psi(\mathbf{r})\,d\tau = A - \frac{1}{2}\int_\Sigma \phi(\mathbf{r})\nabla_n\psi(\mathbf{r})\,d\sigma \tag{145}$$

where

$$A = \int_\Omega \Big\{\frac{1}{2}\nabla\phi(\mathbf{r})\cdot\nabla\psi(\mathbf{r}) + \phi(\mathbf{r})(V(\mathbf{r}) - E)\psi(\mathbf{r})\Big\}\,d\tau. \tag{146}$$

Then if $\psi(\mathbf{r})$ is a solution of Schrödinger equation, the first term on the left hand side vanishes irrespective of $\phi(\mathbf{r})$:

$$A = \frac{1}{2}\int_\Sigma \phi(\mathbf{r})\nabla_n\psi(\mathbf{r})\,d\sigma. \tag{147}$$

Bloch Modification to Schrödinger's equation

Lemma 1 breaks our integral over Schrödinger's equation into a volume integral and a surface integral. It is important to note that the volume integral on the right hand side of equation (141) is Hermitian while the left hand side volume integral is not (assuming we are discussing a finite volume). The issue of ensuring that the Hamiltonian is Hermitian in an integral over a finite region has been thought over for a long time.

A standard solution is to introduce a Bloch operator [82, 83] that eliminates the surface terms. This operator has the form:

$$L = \frac{1}{2}\delta(r - \bar{r})\left(\nabla_n - \frac{b}{r}\right) \tag{148}$$

where b is an adjustable parameter and $\bar{r}$ defines some surface σ. In equation (141) we have already separated the surface terms from the main integral. In fact the integral over the surface in (141) has the form of the Bloch operator with $b = 0$.

Thus the natural alteration to ensure the proper form for the Hamiltonian is to drop the surface integral.

Thus the integral over the Hamiltonian can replace with an integral over a Bloch modified Hamiltonian, H_B,

$$\int_\Omega \phi(\mathbf{r}) H_B \psi(\mathbf{r}) d\tau = \int_\Omega \left\{ \frac{1}{2} \nabla\phi(\mathbf{r}) \cdot \nabla\psi(\mathbf{r}) + \phi(\mathbf{r}) V(\mathbf{r}) \psi(\mathbf{r}) \right\} d\tau \tag{149}$$

This is the form we use for our interior region calculations. The surface terms as defined by the right hand side of equation (147) are made to vanish, just as if we had applied the Bloch operator.

We express the Bloch modified hamiltonian H_B as an operator of the form

$$H_B = T_B + V(\mathbf{r}) \tag{150}$$

where T_B is the Bloch modified kinetic energy operator which acts as

$$\int_\Omega \phi(\mathbf{r}) T_B \psi(\mathbf{r}) d\tau = \int_\Omega \frac{1}{2} \nabla\phi(\mathbf{r}) \cdot \nabla\psi(\mathbf{r})\, d\tau \tag{151}$$

IV.2.4 $1e^-$ HAMILTONIAN MATRIX

We start with the $1e^-$ Hamiltonian. These results are used to calculated the target pseudostates. They also serve as the building blocks for the more complicated $2e^-$ Hamiltonian matrix elements.

$1e^-$ radial overlap matrix elements

We begin by calculating the $1e^-$ radial overlap matrix elements. These elements are the basis for all the matrix elements that follow and are needed for the calculation of the pseudostates as shown later. They consist of integrals of the form:

$$\langle \chi_a | \chi_b \rangle = \int_0^{\bar{r}} dr r^{n_a + n_b} e^{-2\alpha r} \tag{152}$$

where the r^2 factor from the volume element has been incorporated. In Appendix C, we explicitly derive the analytic formula for the solving integrals of this type. The result is described by the function:

$$\langle \chi_a | \chi_b \rangle = U_{\bar{r}}(n_a + n_b, 2\alpha) \tag{153}$$

The angular portion of this integral yields either unity or zero, due to the orthonormality of the spherical harmonics.

$1e^-$ radial Coulomb matrix elements

Having looked at the overlap matrix elements, we can see that the integrals for the $1e^-$ Coulomb potential are simply

$$\langle \chi_a | \frac{Z}{r} | \chi_b \rangle = Z U_{\bar{r}}(n_a + n_b - 1, 2\alpha) \tag{154}$$

since the they differ only by a factor of $1/r$.

$1e^-$ radial kinetic energy operator matrix elements

Using the results of Lemma 1, we can make use of the Bloch modified Hamiltonian in equation (149). This simplifies our calculation the integral over the $1e^-$ Bloch modified kinetic energy operator, which is

$$\langle \chi_a | T_B | \chi_b \rangle = \frac{1}{2} \int_0^{\bar{r}} dr \left\{ r^2 \frac{d\chi_a}{dr} \frac{d\chi_b}{dr} + l_a(l_a+1)\chi_a \chi_b \right\} \tag{155}$$

The angular term $l_a(l_a+1)$ comes from the $1e^-$ spherical harmonics. The orthogonality of the spherical harmonics ensures that $l_b = l_a$. T_B is the kinetic energy operator with a Bloch modification as shown in (151).

We next look at the derivative of the Sturmian function:

$$\frac{d\chi}{dr} = (n-1)r^{n-2}e^{-\alpha r} - \alpha r^{n-1} e^{-\alpha r} \tag{156}$$

Using (156) in (155) yields

$$\begin{aligned}
\langle \chi_a | T_B | \chi_b \rangle &= \frac{1}{2} \int_0^{\bar{r}} dr \left\{ r^2 \frac{d\chi_a}{dr} \frac{d\chi_b}{dr} + l_a(l_a+1)\chi_a\chi_b \right\} \\
&= \frac{1}{2} \int_0^{\bar{r}} dr \Big\{ r^2 \left((n_a-1) r^{n_a-2} e^{-\alpha r} - \alpha r^{n_a-1} e^{-\alpha r} \right) \\
&\quad \times \left((n_b-1) r^{n_b-2} e^{-\alpha r} - \alpha r^{n_b-1} e^{-\alpha r} \right) \\
&\quad + l_a(l_a+1) r^{n_a+n_b-2} e^{-2\alpha r} \Big\} \\
&= \frac{1}{2} \int_0^{\bar{r}} dr \Big\{ (n_a-1)(n_b-1) r^{n_a+n_b-2} e^{-\alpha r} \\
&\quad + l_a(l_a+1) r^{n_a+n_b-2} e^{-2\alpha r} + \alpha^2 r^{n_a+n_b} e^{-2\alpha r} \\
&\quad - \alpha(n_a+n_b-2) r^{n_a+n_b-1} e^{-2\alpha r} \Big\} \\
&= \frac{1}{2} \Big\{ \left((n_a-1)(n_b-1) + l_a(l_a+1) \right) U_{\bar{r}}(n_a+n_b-1, 2\alpha) \\
&\quad - \alpha(n_a+n_b-2) U_{\bar{r}}(n_a+n_b-1, 2\alpha) \\
&\quad + \alpha^2 U_{\bar{r}}(n_a+n_b, 2\alpha) \Big\}
\end{aligned} \tag{157}$$

Combined with our earlier results this allows us to calculate the $1e^-$ Hamiltonian matrix elements:

$$\langle \chi_a | h_1^B | \chi_b \rangle = \langle \chi_a | T_B | \chi_b \rangle + Z \langle \chi_a | \frac{1}{r} | \chi_b \rangle \tag{158}$$

IV.2.5 $2e^-$ HAMILTONIAN MATRIX ELEMENTS

Here we will derive the $2e^-$ Hamiltonian matrix elements that we will use to determine the channel wave functions in Chapter 5 as well as the coupled two electron pseudostates. Before we move to the full $2e^-$ calculations we will first look at the integration of the Coulomb interaction using the $1e^-$ basis elements. Once we have examined this term we will then look at each term of the Hamiltonian again in the case of two electrons to construct the full $2e^-$ Hamiltonian matrix.

Coulomb Interaction using $1e^-$ basis elements

Before engaging the derivation of the $2e^-$ Hamiltonian matrix elements, we will first the determine the radial portions of the Coulomb interaction potential, $1/r_{12}$, in terms of the $1e^-$ basis elements. This will be used in Chapter 5 in the construction of the channel functions as well as the derivation of the equivalent $2e^-$ Hamiltonian matrix.

In Appendix D, we perform the angular portion of the integral for the $2e^-$ Coulomb interaction potential between the two electrons. The potential can be expressed as

$$\frac{1}{r_{12}} = \frac{1}{|\mathbf{r}_1 - \mathbf{r}_2|} = \sum_{\lambda=0}^{\infty} \sum_{m=-\lambda}^{+\lambda} \frac{4\pi}{2\lambda+1} \frac{r_<^\lambda}{r_>^{\lambda+1}} Y_{\lambda m}(\Omega_1) Y_{\lambda m}^*(\Omega_2) \tag{159}$$

where $r_>$ and $r_<$ refer to the greater and lesser radial coordinate of the two electrons respectively. The radial portion of this integral consists of terms of the form:

$$\langle \chi_a \chi_b | \left[\frac{1}{r_{12}}\right]_\lambda | \chi_c \chi_d \rangle = \int_0^{\bar{r}} r_1^2 dr_1 \int_0^{\bar{r}} r_2^2 dr_2 \chi_a(r_1) \chi_c(r_1) \frac{r_<^\lambda}{r_>^{\lambda+1}} \chi_b(r_2) \chi_d(r_2) \tag{160}$$

where $[1/r_{12}]_i$ refers to the ith element in the sum over λ. To simplify our notation we denote the $2e^-$ radial Coulomb matrix elements by

$$[ab|cd]^\lambda = \langle \chi_a \chi_b | \left[\frac{1}{r_{12}}\right]_\lambda | \chi_c \chi_d \rangle \tag{161}$$

Next we substitute the explicit form for the Sturmian functions into (160) to get

$$\begin{aligned}[ab|cd]^{\lambda} &= \int_0^{\bar{r}} r_1^2 dr_1 \int_0^{\bar{r}} r_2^2 dr_2 \left(r_1^{n_a+n_c-2} e^{-2\alpha r_1}\right) \frac{r_<^{\lambda}}{r_>^{\lambda+1}} \left(r_2^{n_b+n_d-2} e^{-2\alpha r_2}\right) \\ &= \int_0^{\bar{r}} dr_1 \int_0^{\bar{r}} dr_2 \left(r_1^{N_p} e^{-2\alpha r_1}\right) \frac{r_<^{\lambda}}{r_>^{\lambda+1}} \left(r_2^{N_q} e^{-2\alpha r_2}\right) \end{aligned} \tag{162}$$

where $N_p = n_a + n_c$ and $N_q = n_b + n_d$. We solve this double integral by turning into the sum of two integrals, one where $r_2 \leq r_1 \leq \bar{r}$ and one where $r_1 \leq r_2 \leq \bar{r}$. These are denoted as W_{12}^{λ} and W_{21}^{λ}, respectively, where the subscripts indicate the region (i.e. the first subscript corresponds to the larger of the two radial coordinates). With this we can rewrite (162) as

$$[ab|cd]^{\lambda} = W_{12}^{\lambda} + W_{21}^{\lambda} \tag{163}$$

Considering for the moment only the region where $r_2 \leq r_1 \leq \bar{r}$, we see $r_2 < r_1$ and hence $r_<^{\lambda}/r_>^{\lambda+1} = r_2^{\lambda}/r_1^{\lambda+1}$. Thus we can express W_{12}^{λ} as

$$\begin{aligned} W_{12}^{\lambda} &= \int_0^{\bar{r}} dr_1 \int_0^{r_1} dr_2 \left(r_1^{N_p} e^{-2\alpha r_1}\right) \frac{r_2^{\lambda}}{r_1^{\lambda+1}} \left(r_2^{N_q} e^{-2\alpha r_2}\right) \\ &= \int_0^{\bar{r}} dr_1 \left(r_1^{N_p-\lambda-1} e^{-2\alpha r_1}\right) \int_0^{r_1} dr_2 \left(r_2^{N_q+\lambda} e^{-2\alpha r_2}\right) \\ &= \int_0^{\bar{r}} dr_1 \left(r_1^{N_p-\lambda-1} e^{-2\alpha r_1}\right) U_{r_1}(N_q+\lambda, 2\alpha). \end{aligned} \tag{164}$$

Next we use the finite series expansion from Appendix C, equation (529), for $U_{\bar{r}}(n,\alpha)$ in equation (164) to yield

$$W_{12}^{\lambda} = \frac{(N_q+\lambda)!}{(2\alpha)^{N_q+\lambda+1}} \left[U_{\bar{r}}(N_p-\lambda-1, 2\alpha) - \sum_{i=0}^{N_q+\lambda} \frac{(2\alpha)^i}{i!} U_{\bar{r}}(N_p+i-\lambda-1, 4\alpha) \right] \tag{165}$$

W_{21}^{λ} can be derived by simply exchanging the indices 1 and 2 in equation (165) as the difference is only in the relative size of the two coordinates. This means we are essentially switching the two indices N_p and N_q.

$2e^-$ overlap matrix elements

Now we consider the full $2e^-$ Hamiltonian. In the same fashion as before we first look at the $2e^-$ overlap matrix elements Π_{ab}^{LSP}. These elements are important for calculations of the form $H - E$ to accurately represent the energy portion of the

matrix. We begin with

$$\langle \Pi_{ab}^{LSP} | \Pi_{cd}^{LSP} \rangle = \frac{\mathcal{N}}{2} \int_\tau d^3r_1 d^3r_2 \left(\chi_a(r_1)\chi_b(r_2)\Xi_{ab}^L + (-1)^{L+S+P}\chi_b(r_1)\chi_a(r_2)\Xi_{ba}^L \right)^* \times \left(\chi_c(r_1)\chi_d(r_2)\Xi_{cd}^L + (-1)^{L+S+P}\chi_d(r_1)\chi_c(r_2)\Xi_{dc}^L \right) \quad (166)$$

where $\mathcal{N} = N_a N_b N_c N_d$ and $d^3r = r^2 dr d\Omega$ denotes the 3-dimensional volume element. Continuing, we multiply out our terms

$$\begin{aligned} \langle \Pi_{ab}^{LSP} | \Pi_{cd}^{LSP} \rangle &= \frac{\mathcal{N}}{2} \int_\tau d^3r_1 d^3r_2 \Big\{ \Big(\chi_a(r_1)\chi_c(r_1)\chi_b(r_2)\chi_d(r_2)\Xi_{ab}^{L*}\Xi_{cd}^L \\ &\quad + \chi_b(r_1)\chi_d(r_1)\chi_a(r_2)\chi_c(r_2)\Xi_{ba}^{L*}\Xi_{dc}^L \Big) \\ &\quad + (-1)^{L+S+P} \Big(\chi_a(r_1)\chi_d(r_1)\chi_b(r_2)\chi_c(r_2)\Xi_{ab}^{L*}\Xi_{dc}^L \\ &\quad + \chi_b(r_1)\chi_c(r_1)\chi_a(r_2)\chi_d(r_2)\Xi_{ba}^{L*}\Xi_{cd}^L \Big) \Big\} \end{aligned} \quad (167)$$

where the radial basis elements are purely real. Next we use of two symmetry relations

$$\int_\tau d^3r_1 d^3r_2 \chi_a(r_1)\chi_c(r_1)\chi_b(r_2)\chi_d(r_2)\Xi_{ab}^{L*}\Xi_{cd}^L = \int_\tau d^3r_1 d^3r_2 \chi_b(r_1)\chi_d(r_1)\chi_a(r_2)\chi_c(r_2)\Xi_{ba}^{L*}\Xi_{dc}^L \quad (168)$$

and

$$\int_\tau d^3r_1 d^3r_2 \chi_a(r_1)\chi_d(r_1)\chi_b(r_2)\chi_c(r_2)\Xi_{ab}^{L*}\Xi_{dc}^L = \int_\tau d^3r_1 d^3r_2 \chi_b(r_1)\chi_c(r_1)\chi_a(r_2)\chi_d(r_2)\Xi_{ba}^{L*}\Xi_{cd}^L \quad (169)$$

to rewrite equation (167) as

$$\begin{aligned} \langle \Pi_{ab}^{LSP} | \Pi_{cd}^{LSP} \rangle &= \mathcal{N} \int_\tau d^3r_1 d^3r_2 \Big\{ \chi_a(r_1)\chi_c(r_1)\chi_b(r_2)\chi_d(r_2)\Xi_{ab}^{L*}\Xi_{cd}^L \\ &\quad + (-1)^{L+S+P}\chi_a(r_1)\chi_d(r_1)\chi_b(r_2)\chi_c(r_2)\Xi_{ab}^{L*}\Xi_{dc}^L \Big\} \end{aligned} \quad (170)$$

We now carry out the integration over all space. We make use of the fact that the coupled spherical harmonics, Ξ_{ab}^L, form an orthonormal set and use the notation $\langle | \rangle$ to denote the radial integrals we derived earlier for the $1e^-$ overlap matrix elements. This gives us a final result of

$$\begin{aligned} \langle \Pi_{ab}^{LSP} | \Pi_{cd}^{LSP} \rangle = \mathcal{N} \Big\{ &\langle \chi_a | \chi_c \rangle \langle \chi_b | \chi_d \rangle \delta_{l_a l_c} \delta_{l_b l_d} \\ &+ (-1)^{L+S+P} \langle \chi_a | \chi_d \rangle \langle \chi_b | \chi_c \rangle \delta_{l_a l_d} \delta_{l_b l_c} \Big\} \end{aligned} \quad (171)$$

$2e^-$ Hamiltonian matrix elements

We can break up the $2e^-$ Hamiltonian for hydrogenic ions into three parts, $H = h_1 + h_2 + V_{12}$, where $h_1 = -\frac{1}{2}\nabla_1^2 + \frac{Z}{r_1}$, $h_2 = -\frac{1}{2}\nabla_2^2 + \frac{Z}{r_2}$, and V_{12} is the Coulomb interaction between the escaping electrons. We have seen previously how to construct these in the $1e^-$ case, now we look at how these terms are constructed in the $2e^-$ case. We begin with $H_B = h_1^B + h_2^B$, which as before has been Bloch modified,

$$\begin{aligned}\langle \Pi_{ab}^{LSP}|H_B|\Pi_{cd}^{LSP}\rangle = \frac{\mathcal{N}}{2}\int_\tau d^3r_1 d^3r_2 \Big(&\chi_a(r_1)\chi_b(r_2)\Xi_{ab}^L \\ &+(-1)^{L+S+P}\chi_b(r_1)\chi_a(r_2)\Xi_{ba}^L\Big)^*\left(h_1^B + h_2^B\right) \\ &\times\left(\chi_c(r_1)\chi_d(r_2)\Xi_{cd}^L + (-1)^{L+S+P}\chi_d(r_1)\chi_c(r_2)\Xi_{dc}^L\right)\end{aligned} \tag{172}$$

We then perform the angular integrals, making use of the symmetry relations (168) and (169), to rewrite the integral as

$$\begin{aligned}\langle \Pi_{ab}^{LSP}|H_B|\Pi_{cd}^{LSP}\rangle = \mathcal{N}\int_\tau dr_1 dr_2 \Big\{&\chi_a(r_1)\chi_b(r_2)(h_1^B + h_2^B)\chi_c(r_1)\chi_d(r_2)\delta_{l_a l_c}\delta_{l_b l_d} \\ &+(-1)^{L+S+P}\chi_a(r_1)\chi_b(r_2)(h_1^B + h_2^B)\chi_d(r_1)\chi_c(r_2)\delta_{l_a l_d}\delta_{l_b l_c}\Big\}\end{aligned} \tag{173}$$

Lastly we make use of the $\langle|\rangle$ notation for the radial integrals to simplify this result, and express the $2e^-$ Hamiltonian matrix elements as

$$\begin{aligned}\langle \Pi_{ab}^{LSP}|H_B|\Pi_{cd}^{LSP}\rangle = \mathcal{N}\Big\{&\Big(\langle\chi_a|h_1^B|\chi_c\rangle\langle\chi_b|\chi_d\rangle + \langle\chi_a|\chi_c\rangle\langle\chi_b|h_2^B|\chi_d\rangle\Big)\delta_{l_a l_c}\delta_{l_b l_d} \\ &+(-1)^{L+S+P}\Big(\langle\chi_a|h_1^B|\chi_d\rangle\langle\chi_b|\chi_c\rangle + \langle\chi_a|\chi_d\rangle\langle\chi_b|h_2^B|\chi_c\rangle\Big)\delta_{l_a l_d}\delta_{l_b l_c}\Big\}\end{aligned} \tag{174}$$

The terms of $\langle\chi|h_1^B|\chi\rangle$ and $\langle\chi|h_2^B|\chi\rangle$ are merely the $1e^-$ Hamiltonian elements we derived earlier in equation (158).

$2e^-$ Coulomb interaction matrix elements

The $2e^-$ Coulomb interaction matrix elements are derived much as we did for the $1e^-$ case but now we need to take into account the angular integrals. We begin with the basic integral:

$$\begin{aligned}\langle \Pi_{ab}^{LSP}|V|\Pi_{cd}^{LSP}\rangle \;=\; &\frac{\mathcal{N}}{2}\int_\tau d^3r_1 d^3r_2\Big\{\Big(\chi_a(r_1)\chi_b(r_2)\Xi_{ab}^L + (-1)^{L+S+P}\chi_b(r_1)\chi_a(r_2)\Xi_{ba}^L\Big)^* \\ &\times\;\left(\frac{1}{r_{12}}\right)\Big(\chi_c(r_1)\chi_d(r_2)\Xi_{cd}^L + (-1)^{L+S+P}\chi_d(r_1)\chi_c(r_2)\Xi_{dc}^L\Big)\Big\}\end{aligned} \tag{175}$$

We then expand this to give

$$\begin{aligned}\langle \Pi^{LSP}_{ab}|V|\Pi^{LSP}_{cd}\rangle &= \frac{\mathcal{N}}{2}\int_\tau d^3r_1 d^3r_2 \Big\{\chi_a(r_1)\chi_b(r_2)\Xi^{L*}_{ab}\left(\frac{1}{r_{12}}\right)\chi_c(r_1)\chi_d(r_2)\Xi^{L}_{cd} \\ &+ (-1)^{L+S+P}\chi_a(r_1)\chi_b(r_2)\Xi^{L*}_{ab}\left(\frac{1}{r_{12}}\right)\chi_d(r_1)\chi_c(r_2)\Xi^{L}_{dc} \\ &+ (-1)^{L+S+P}\chi_b(r_1)\chi_a(r_2)\Xi^{L*}_{ba}\left(\frac{1}{r_{12}}\right)\chi_c(r_1)\chi_d(r_2)\Xi^{L}_{cd} \\ &+ \chi_b(r_1)\chi_a(r_2)\Xi^{L*}_{ba}\left(\frac{1}{r_{12}}\right)\chi_d(r_1)\chi_c(r_2)\Xi^{L}_{dc}\Big\} \qquad (176)\end{aligned}$$

Now we consider just the first term of (176). Using the form for the expansion of the interaction potential, equation (159), we can reexpress that term as

$$\begin{aligned}&\frac{\mathcal{N}}{2}\int_\tau d^3r_1 d^3r_2 \left\{\chi_a(r_1)\chi_b(r_2)\Xi^{L*}_{ab}\left(\frac{1}{r_{12}}\right)\chi_c(r_1)\chi_d(r_2)\Xi^{L}_{cd}\right\} = \\ &\qquad \frac{\mathcal{N}}{2}\int_\tau d^3r_1 d^3r_2 \Big\{\chi_a(r_1)\chi_b(r_2)\Xi^{L*}_{ab}\Big(\sum_{\lambda=0}^{\infty}\sum_{m=-\lambda}^{+\lambda}\frac{4\pi}{2\lambda+1}\frac{(r_<)^\lambda}{(r_>)^{\lambda+1}}Y_{\lambda m}Y^*_{\lambda m}\Big) \\ &\qquad\qquad \times\chi_c(r_1)\chi_d(r_2)\Xi^{L}_{cd}\Big\} \qquad (177)\end{aligned}$$

Rearranging this gives us

$$\begin{aligned}&\frac{\mathcal{N}}{2}\int_\tau d^3r_1 d^3r_2 \left\{\chi_a(r_1)\chi_b(r_2)\Xi^{L*}_{ab}\left(\frac{1}{r_{12}}\right)\chi_c(r_1)\chi_d(r_2)\Xi^{L}_{cd}\right\} = \\ &\qquad \frac{\mathcal{N}}{2}\sum_{\lambda=0}^{\infty}\int\int d\Omega_1 d\Omega_2 \Xi^{L*}_{ab}\left(\sum_{m=-\lambda}^{+\lambda}\frac{4\pi}{2\lambda+1}Y_{\lambda m}Y^*_{\lambda m}\right)\Xi^{L}_{cd} \\ &\qquad \times\int_0^{\bar r} dr_1 r_1^2\int_0^{\bar r} dr_2 r_2^2\chi_a(r_1)\chi_b(r_2)\frac{(r_<)^\lambda}{(r_>)^{\lambda+1}}\chi_c(r_1)\chi_d(r_2) \qquad (178)\end{aligned}$$

The double integral over the angular coordinates is essentially a product of two integrals of three spherical harmonics each. This calculation is shown in Appendix D. The value of the integral, explicitly given in (551), depends on the angular momentum parameters $(L, \lambda, l_a, l_b, L_c, l_d)$ and is denoted by $\mathcal{I}^{L\lambda}_{l_a l_b l_c l_d}$. Using this result, equation (178) can be simplified to

$$\begin{aligned}&\frac{\mathcal{N}}{2}\int_\tau d^3r_1 d^3r_2 \left\{\chi_a(r_1)\chi_b(r_2)\Xi^{L*}_{ab}\left(\frac{1}{r_{12}}\right)\chi_c(r_1)\chi_d(r_2)\Xi^{L}_{cd}\right\} = \\ &\frac{\mathcal{N}}{2}\sum_{\lambda=0}^{\infty}\mathcal{I}^{L\lambda}_{l_a l_b l_c l_d}\int_0^{\bar r} dr_1 r_1^2\int_0^{\bar r} dr_2 r_2^2\chi_a(r_1)\chi_b(r_2)\frac{(r_<)^\lambda}{(r_>)^{\lambda+1}}\chi_c(r_1)\chi_d(r_2) \qquad (179)\end{aligned}$$

Our next step is to make use of the earlier $1e^-$ calculation. The radial integral was previously solved for in equation (163) and the result denoted $[ac|bd]^\lambda$. Using this

result we further simplify the term to

$$\frac{\mathcal{N}}{2}\int_\tau d^3r_1 d^3r_2 \left\{\chi_a(r_1)\chi_b(r_2)\Xi^{L*}_{ab}\left(\frac{1}{r_{12}}\right)\chi_c(r_1)\chi_d(r_2)\Xi^{L}_{cd}\right\} = \frac{\mathcal{N}}{2}\sum_{\lambda=\lambda_{\min}}^{\lambda_{\max}}[ac|bd]^\lambda \mathcal{I}^{L\lambda}_{l_a l_b l_c l_d} \tag{180}$$

where the limits of the summation are determined by the triangular conditions on the Clebsch-Gordon coefficients in $\mathcal{I}^{L\lambda}_{l_a l_b l_c l_d}$, see (502) and (551). These restrict the λ values to be between $\lambda_{\min} = \max(|l_a - l_c|, |l_b - l_d|)$ and $\lambda_{\max} = \min(l_a + l_c, l_b + l_d)$.

We now look at the fourth term in (176). This term gives the same result as the first and can be expressed

$$\frac{\mathcal{N}}{2}\sum_{\lambda=\lambda_{\min}}^{\lambda_{\max}}[bd|ac]^\lambda \mathcal{I}^{L\lambda}_{l_b l_a l_d l_c} = \frac{\mathcal{N}}{2}\sum_{\lambda=\lambda_{\min}}^{\lambda_{\max}}[ac|bd]^\lambda \mathcal{I}^{L\lambda}_{l_a l_b l_c l_d} \tag{181}$$

This is due to the symmetry relation of the angular integral as shown in (552). Considering the radial result in (161), we can see this too is unaffected by the exchange in labeling (remembering that the Sturmians are purely real). Hence we can simplify our result by combining the two.

The second and third terms of (176) can be derived via the same method used above. This yields (neglecting the $(-1)^{L+S+P}$ factor)

$$\frac{\mathcal{N}}{2}\int_\tau d^3r_1 d^3r_2 \left\{\chi_a(r_1)\chi_b(r_2)\Xi^{L*}_{ab}\left(\frac{1}{r_{12}}\right)\chi_d(r_1)\chi_c(r_2)\Xi^{L}_{dc}\right\} = \frac{\mathcal{N}}{2}\int_\tau d^3r_1 d^3r_2 \left\{\chi_b(r_1)\chi_a(r_2)\Xi^{L*}_{ba}\left(\frac{1}{r_{12}}\right)\chi_c(r_1)\chi_d(r_2)\Xi^{L}_{cd}\right\} \tag{182}$$

Or alternatively

$$\frac{\mathcal{N}}{2}\sum_{\lambda=\lambda_{\min}}^{\lambda_{\max}}[ad|bc]^\lambda \mathcal{I}^{L\lambda}_{l_b l_a l_d l_c} = \frac{\mathcal{N}}{2}\sum_{\lambda=\lambda_{\min}}^{\lambda_{\max}}[bc|ad]^\lambda \mathcal{I}^{L\lambda}_{l_b l_a l_c l_d} \tag{183}$$

Again we combine the two results into one term. Finally putting the two remaining terms together, we get for the $2e^-$ Coulomb interaction matrix elements the result

$$\langle \Pi^{LSP}_{ab}|V|\Pi^{LSP}_{cd}\rangle = \mathcal{N}\left\{\sum_{\lambda=\lambda_{\min}}^{\lambda_{\max}}[ac|bd]^\lambda \mathcal{I}^{L\lambda}_{l_a l_b l_c l_d} + (-1)^{L+S+P}\sum_{\lambda=\lambda_{\min}}^{\lambda_{\max}}[ad|bc]^\lambda \mathcal{I}^{L\lambda}_{l_a l_b l_d l_c}\right\} \tag{184}$$

Solving for Pseudostates

Now that we have derived the matrix elements for the $1e^-$ and $2e^-$ Hamiltonians we can calculate the pseudostates for the target. The pseudostates in the $1e^-$ case

are represented in terms of the Sturmian basis functions χ and the usual spherical harmonics,

$$\phi_\mu(\mathbf{r}) = \sum_j \varphi_j(\mathbf{r})\alpha_{j\mu} = \sum_j \chi_j(r)Y_j(\Omega)\alpha_{j\mu} \tag{185}$$

where φ_j is the $1e^-$ basis state as defined in equation (135). We insert this basis function expansion into the Bloch modified $1e^-$ Schrödinger's equation (150) to get

$$H_B\phi_\mu(\mathbf{r}) = E_\mu\phi_\mu(\mathbf{r}) \tag{186}$$

$$\sum_j \left[-T_B - \frac{Z}{r}\right]\varphi_j(r)\alpha_{j\mu} = E_\mu \sum_j \varphi_j\alpha_{j\mu} \tag{187}$$

where E_μ is the energy eigenvalue for the pseudostate ϕ_μ of H_B. We project this onto φ_i^* and integrate over the interior region, 0 to $\bar{r}$ to yield

$$\sum_j \int_0^{\bar{r}} dr\varphi_i^*(r)\left[-T_B - \frac{Z}{r}\right]\varphi_j(r)\alpha_{j\mu} = E_\mu \sum_j \int_0^{\bar{r}} dr\varphi_i^*\varphi_j\alpha_{j\mu} \tag{188}$$

We can simplify this result by defining the following matrices

$$\mathbf{H} = H_{ij} = \int_0^{\bar{r}} dr\varphi_i^*(r)\left[-T_B - \frac{Z}{r}\right]\varphi_j(r) \tag{189}$$

$$\mathbf{D} = D_{ij} = \int_0^{\bar{r}} dr\varphi_i^*\varphi_j \tag{190}$$

where H_{ij} are the matrix elements for the $1e^-$ Hamiltonian and D_{ij} are the elements of the overlap matrix. Both of these results we have calculated in the previous sections. Using these matrices we can reexpress equation (188) as

$$\sum_j H_{ij}\alpha_{j\mu} = E_\mu \sum_j D_{ij}\alpha_{j\mu} \tag{191}$$

or in matrix notation

$$\mathbf{H}\cdot\vec{\alpha}_\mu = E_\mu\mathbf{D}\cdot\vec{\alpha}_\mu \tag{192}$$

where E_μ is the energy for a given vector $\vec{\alpha}_\mu$. This is the generalized eigenproblem [84], using this result we can easily solve for the eigenvectors $\vec{\alpha}_\mu$. The details of this calculation are explained in Appendix E. These can then be used to describe the target state and to perform the close coupling expansion calculation for the channel wave functions.

We repeat this process with the $2e^-$ basis. In this case the eigenstates (which will be used to construct the **R**-matrix in Chapter 5) are of the form

$$\varpi_{\mu'}(\mathbf{r}_1,\mathbf{r}_2) = \sum_i c_i\Pi_i(\mathbf{r}_1,\mathbf{r}_2) \tag{193}$$

where the summation ranges over the list of possible angular momenta combinations. The derivation of the eigenstates is otherwise identical.

IV.3 SUMMARY

We gave an overview of the X2e method, from the inner region to the final calculation of the TDCS and how the boundaries between the regions are established. We also discussed the inner region. We described the Sturmian basis elements we use and how these are used to construct the matrix elements for the $1e^-$ and $2e^-$ Hamiltonians as well as the overlap matrices. We then discussed how the pseudostates were constructed within the inner region.

CHAPTER V

R-OPERATOR THEORY

In this chapter we derive and discuss the most powerful portion of the X2e method, the $\mathcal{R}$-operator. The $\mathcal{R}$-operator is a generalization of the **R**-matrix described in Chapter 1. More over it is a generalization of the variationally derived **R**-matrix which removes several of the problems that hinder the standard **R**-matrix method.

As mentioned in Chapter 1, the principle behind the **R**-matrix approach is to divide the problem into an inner and outer region. The inner region, defined where the escaping particles are within some radius $\bar{r}$, is where all possible interactions, including exchange, are taken into account. In the outer region, exchange effects are ignored. This allows for different computational models to be used in each region thereby allowing for a great potential simplification of the problem. The **R**-matrix portion, itself, allows one to connect the interior region's solutions to the exterior region's.

As mentioned earlier, the strength of the **R**-Matrix method is its flexibility when applied to different processes and targets. The $\mathcal{R}$-operator, as shown later, expands on this by transforming the **R**-matrix into an operator formalism that allows the electrons to be treated symmetrically. This makes the method more flexible in terms of collisional geometry as well as giving us a more powerful tool for connecting to the asymptotic region.

In this chapter we first examine how the variational **R**-Matrix is derived and what its advantages are. We will then derive the $\mathcal{R}$-operator and examine how to do a variational estimate of the operator. Then we project that $\mathcal{R}$-operator into the region $r_1 \geq r_2$ and use it to solve a series of integro-differential equations for the channel wave functions, making use of a close coupling expansion. These channel wave functions will then be used to construct the **R**-Matrix.

V.1 VARIATIONAL R-MATRIX THEORY

The variational derivation of the **R**-Matrix uses an argument based on work by Kohn [85]. Kohn's argument is not directly related to the **R**-Matrix, but instead an attempt to increase accuracy for the **S**-matrix by using a wave function that is close to the exact wave function. The **R**-matrix, however, is linearly related to the

S-matrix and can be derived with relative ease from the same procedure. For the derivation here, only an elastic collision is considered but this can be generalized to excitation or ionization of multiple particles without difficulty. One consequence of our choice is that the **R**-matrix is only a 1×1 matrix or a scalar. It is possible to generalize this derivation to a $N \times N$ matrix as described in [13]. Beginning with Schrödinger's equation in the radial coordinate and an orthonormal basis set, we have:

$$\left(-\frac{\nabla^2}{2} + V(r) - E\right) u(r) = 0 \tag{194}$$

where the wave function u has the following properties, that $u(0) = 0$ and:

$$\lim_{r\to\infty} u(r) = A \sin kr + B \cos kr \quad \text{(finite range potentials)} \tag{195}$$

$$\lim_{r\to\infty} u(r) = AF(kr) + BG(kr) \quad \text{(Coulomb potentials)} \tag{196}$$

where $k = \sqrt{2E}$ and open channels are assumed. F and G are regular and irregular Coulomb functions. Additionally for this example we treat the functions u as real. Later we will see that using complex radial functions will yield the same result.

We next construct a functional to apply the variational argument to:

$$J[u] = \int_0^{\bar{r}} u(r) \left(-\frac{\nabla^2}{2} + V(r) - E\right) u(r)\, dr \tag{197}$$

where we need only integrate from 0 to $\bar{r}$ since we are concerned only with the interior region in establishing our **R**-matrix. For an exact solution this functional J will equal zero. Next we integrate by parts:

$$J = \frac{\lambda}{2} u^2(\bar{r}) + \int_0^{\bar{r}} \left(-\frac{1}{2}(u')^2 - Vu^2 + Eu^2\right) dr \tag{198}$$

where

$$\lambda = u'/u|_{r=\bar{r}}. \tag{199}$$

Now we know from (86), that **R**-Matrix is defined as

$$u(\bar{r}) = \bar{r}\mathbf{R}u'(\bar{r}). \tag{200}$$

Hence we can rewrite (199) as

$$\lambda = 1/(\mathbf{R}\bar{r}). \tag{201}$$

So in solving for λ we will also derive how the **R**-Matrix is defined in terms of the basis set.

Next a trial wave function u_t is introduced and expanded in the basis set:

$$u_t(r) = \sum_i^n a_i x_i(r) \tag{202}$$

where x_i are the elements of an orthonormal basis set that spans the volume. Substituting this into our functional for u:

$$\begin{aligned} J(u_t) &= \frac{\lambda}{2}\sum_{ij} a_i a_j x_i x_j|_{r=\bar{r}} \\ &+ \int_0^{\bar{r}} dr \sum_{ij} a_i a_j \left(-\frac{1}{2}x_i' x_j' + x_i x_j (E-V)\right) \qquad (203) \\ &= \frac{\lambda}{2}\Big(\sum_i a_i x_i(\bar{r})\Big)^2 - \sum_{ij} a_i a_j A_{ij} \qquad (204) \end{aligned}$$

where

$$A_{ij} = \int_0^{\bar{r}} dr \left(\frac{1}{2}x_i' x_j' + x_i x_j (V-E)\right) \tag{205}$$

We note A_{ij} is a symmetric matrix.

The Kohn variational principle works by giving an improvement in scattering phase shifts in the **K**-matrix. As there is a linear relation between the **K**-matrix and the **R**-matrix (as shown explicitly in Chapter 7), this yields an equivalent increase of accuracy for the **R**-matrix.

In Kohn's original argument the improvement is shown by examining a related derivation where we work from equation (197) and make use of a trial function $u_t = u + \delta u$ where u is an exact solution to Schrödinger's equation. u_t has the properties that it is zero at the origin and asymptotically behaves as

$$u_t \to A \sin kr + B_t \cos kr \tag{206}$$

where B would be the correct amplitude for the scattering case. In the case we are examining now, $\bar{r}$ is large and the function can be considered to behave as in the asymptotic limit. We place this trial function into equation (197) and vary our functional J over u_t to find the optimal result. This yields

$$\begin{aligned} \delta J &= \int_0^{\bar{r}} \left(u\frac{d^2}{dr^2}\delta u - \delta u \frac{d^2}{dr^2}u\right) dr \\ &= \left(u\frac{d}{dr}\delta u - \delta u \frac{d}{dr}u\right)_{r=\bar{r}} \\ &= -kA\delta B \qquad (207) \end{aligned}$$

where $\delta B = B_t - B$. Thus

$$\delta(I + kAB_t) = 0 \tag{208}$$

For the true wave function u, $I = 0$, and $B = A\tan\eta$, where η is the scattering phase shift. This means

$$I + kAB_t = kA^2\tan\eta \tag{209}$$

is correct to first order and serves as a variational principle to the scattering phase shifts and hence the **K**-matrix. With this in mind we proceed to apply the variational principle to our functional.

Varying in a_i, we search for a stationary result:

$$\frac{\partial J}{\partial a_i} = \lambda x_i(\bar{r})\sum_j a_j x_j(\bar{r}) - 2\sum_j a_j A_{ij} = 0. \tag{210}$$

Rewriting (210) as

$$\sum_j (A_{ij} - \frac{\lambda}{2}x_i(\bar{r})x_j(\bar{r}))a_j = 0. \tag{211}$$

A nontrivial solution to (211) requires that:

$$A_{ij} - \frac{\lambda}{2}x_i(\bar{r})x_j(\bar{r}) = 0. \tag{212}$$

But to derive λ it is more useful to rewrite (211) as

$$\sum_j a_j A_{ij} = \frac{\lambda}{2}x_i(\bar{r})\beta \tag{213}$$

with

$$\beta = \sum_j a_j x_j(\bar{r}) = u_t(\bar{r}) \tag{214}$$

which is our trial wave function. Then assuming the matrix **A** is non-singular, we can multiply both sides by $\mathbf{A}^{-1}$ to get an expression for a_i:

$$a_i = \frac{\lambda}{2}\sum_j A_{ij}^{-1}x_j(\bar{r})\beta. \tag{215}$$

We can place (215) back into our formulation for the trial wave function, (202) or (214), to get

$$\beta = \frac{\lambda}{2}\sum_{ij} x_i(\bar{r})A_{ij}^{-1}x_j(\bar{r})\beta. \tag{216}$$

This allows us to derive a solution for λ and hence $\mathbf{R}$:

$$\lambda^{-1} = \frac{1}{2}\sum_{ij} x_i(\bar{r})A_{ij}^{-1}x_j(\bar{r}) \tag{217}$$

$$\mathbf{R} = \frac{1}{2\bar{r}}\sum_{ij} x_i(\bar{r})A_{ij}^{-1}x_j(\bar{r}). \tag{218}$$

It should be noted here that the variational value for λ is unique and thus the $\mathbf{R}$-matrix derived from it is as well. This can seen by looking at (212) and seeing that the determinate of the matrix $A_{ij} - \frac{\lambda}{2}x_i(\bar{r})x_j(\bar{r})$ must vanish. This linear equation for λ determines it uniquely.

From here the symmetric matrix $\mathbf{A}$, with elements A_{ij}, can be diagonalized by a unitary transformation, such that $\mathbf{U}^T\mathbf{A}\mathbf{U}$ is a diagonal matrix. This unitary transformation also diagonalizes $\mathbf{A}^{-1}$ since $\mathbf{U}^T\mathbf{A}^{-1}\mathbf{U}\mathbf{U}^T\mathbf{A}\mathbf{U} = I$. Applying this to (218):

$$\begin{aligned}\mathbf{R} &= \frac{1}{2\bar{r}}\sum_{ij} x_i(\bar{r})\Big[\sum_l\sum_k\Big(\sum_c U_{ic}U_{ck}^T\Big)A_{kl}^{-1}\Big(\sum_d U_{ld}U_{dj}^T\Big)\Big]x_j(\bar{r}) \\ &= \frac{1}{2\bar{r}}\sum_{ij} x_i(\bar{r})\Big[\sum_c\sum_d U_{ic}\Big(\sum_l\sum_k U_{ck}^T A_{kl}^{-1}U_{ld}\Big)U_{dj}^T\Big]x_j(\bar{r}).\end{aligned} \tag{219}$$

Using the results of the unitary transformation:

$$\sum_i\sum_j U_{ci}^T A_{ij}^{-1}U_{dj} = \tilde{E}_c^{-1}\delta_{cd} \tag{220}$$

and defining $\tilde{x}_c = \sum_i x_i U_{ic}$, we arrive at an expression for the $\mathbf{R}$-Matrix:

$$\mathbf{R} = \frac{1}{2\bar{r}}\sum_{cd}\frac{\tilde{x}_c(\bar{r})\tilde{x}_d(\bar{r})\delta_{cd}}{\tilde{E}_c} \tag{221}$$

$$= \frac{1}{2\bar{r}}\sum_c\frac{|\tilde{x}_c(\bar{r})|^2}{\tilde{E}_c}. \tag{222}$$

Finally we rewrite (222) using $\tilde{E}_c = E_i - E$, where E_i are the eigenvalues of the symmetric matrix $B_{ij} = \int_0^{\bar{r}} dr[\frac{1}{2}x_i'(r)x_j'(r) + x_i(r)V(r)x_j(r)]$. As can be seen $A_{ij} = B_{ij} - E\delta_{ij}$, thus justifying this approach. This gives a final form for the $\mathbf{R}$-Matrix:

$$\mathbf{R} = \frac{1}{2\bar{r}}\sum_c\frac{|\tilde{x}_c(\bar{r})|^2}{E_i - E}. \tag{223}$$

A few points can be made here about the $\mathbf{R}$-Matrix. We see for single channel scattering, the $\mathbf{R}$-Matrix is a 1×1 matrix. In the case of multichannel scattering it will be an $N \times N$ matrix. Generalizing this result to multiple channels is similar to the process shown here and is discussed in Nesbet [13].

There are also two major advantages of our method. The first is the Bloch operator is a natural addition to the Hamiltonian. The Bloch operator [82] corrects for non-vanishing surface terms on the finite surface. These terms crop up due to the fact that the Hamiltonian is not Hermitian within the finite interior region. The addition of the Bloch operator is necessary to make the final **R**-matrix Hermitian within that region. In our derivation the **R**-matrix is automatically Hermitian. This can be seen in (218) where the **R**-matrix depends on the real and symmetric matrix A_{ij}. In the case of a complex radial function, u_i in A_{ij} would be conjugated and our matrix A_{ij} would be Hermitian. Hence the **R**-matrix would still be Hermitian. This will be shown explicitly when we derive the $\mathcal{R}$-operator.

The other advantage is that the variational **R**-matrix does not require a Buttle correction. This is an advantage of our method over other non-variationally derived **R**-matrices. The Buttle correction resolves the error caused by requiring a fixed boundary condition on the basis elements at $r = \bar{r}$. This of course restricts the value of the wave function there, thus causing a discontinuity in the slope at that point. It was found that this leads to a slow convergence to the solution [86, 87]. Buttle [88] proposed a method, known as the Buttle correction, for approximating the terms excluded from the basis set. To improve the speed of convergence and simplify the actual calculations, many authors developed formalisms where the need for a specific boundary condition was relaxed. The variational **R**-matrix just developed achieves this, resulting in no discontinuity of the radial function at $r = \bar{r}$ by deriving the optimal boundary value λ. This decreases the computational effort of the calculation. These improvements also apply to the $\mathcal{R}$-operator giving us an advantage in calculation of atomic scattering processes.

V.2 $\mathcal{R}$-OPERATOR

The $\mathcal{R}$-operator is an extension of the **R**-matrix method to generalized coordinates [13], allowing the electrons to be treated symmetrically. This allows it to be applied to ionizing collision geometries where there is equal sharing of an energy between the two electrons. A major strength of this method is that it is also valid near threshold. It is for this reason that we move to the $\mathcal{R}$-operator approach.

The $\mathcal{R}$-operator itself is a functional that takes normal derivatives of function values on a hypersurface Σ, which encloses a hypervolume Ω, and maps them to function values elsewhere on the surface:

$$\psi(\sigma_1) = \int_\Sigma R(E, \sigma_1, \sigma_2) \nabla_n \psi(\sigma_2) \cdot d\sigma_2 \tag{224}$$

where σ defines the coordinates of some point on the hypersurface Σ. The hypervolume is the space defined by the coordinates of the escaping particles. Thus the $\mathcal{R}$-operator allows one to relate the inner region results to an outer region.

V.3 VARIATIONAL DERIVATION OF $\mathcal{R}$-OPERATOR

Now we will show that there exists a variational functional for the $\mathcal{R}$-operator which is stationary if and only if the trial wave function satisfies the Schrödinger equation throughout the enclosed volume [13]. Importantly, this provides us with a practical way of calculating the $\mathcal{R}$-operator.

The estimate of the $\mathcal{R}$-operator is done with a variation over a functional J. In defining this functional, we begin with the result of Corollary 1, where we use Ψ and its conjugate as the wave functions:

$$\int_\Omega \Psi^*(\mathbf{r})(H - E)\Psi(\mathbf{r})\, d\tau = A - \frac{1}{2}\int_\Sigma \Psi^*(\mathbf{r}) \nabla_n \Psi(\mathbf{r})\, d\sigma \tag{225}$$

where

$$A = \int_\Omega \left\{ \frac{1}{2} \nabla \Psi^*(\mathbf{r}) \cdot \nabla \Psi(\mathbf{r}) + \Psi^*(\mathbf{r})(V(\mathbf{r}) - E)\Psi(\mathbf{r}) \right\} d\tau. \tag{226}$$

We note that A is real, as $A = A^*$. Rearranging this result we arrive at an expression

$$A = \int_\Omega \Psi^*(\mathbf{r})(H - E)\Psi(\mathbf{r})\, d\tau + \frac{1}{2}\int_\Sigma \Psi^*(\mathbf{r}) \nabla_n \Psi(\mathbf{r})\, d\sigma. \tag{227}$$

Next we see that if $\Psi(\mathbf{r})$ is an exact solution to Schrödinger's equation then A will be equal to the second term on the right hand side of (227). We set the boundary condition $\nabla_n \Psi(\mathbf{r}) = \zeta(\mathbf{r})$ where ζ is an arbitrary well behaved function on the boundary. We then define

$$A_1 = \frac{1}{2}\int_\Sigma \Psi^*(\mathbf{r}) \zeta(\mathbf{r})\, d\sigma. \tag{228}$$

In analogy with the Schwinger variational principle for scattering we create the functional:

$$J[\Psi] = \frac{A_1 A_1^*}{A}. \tag{229}$$

We note that if $\Psi(\mathbf{r})$ is an exact solution then $A_1 = A$ and thus $J = A_1^* = A$. We then insert an approximate solution $\Psi = \Psi_e + \delta\Psi$, where Ψ_e is the exact solution, into J.

First we look at the effect of small variations of Ψ on A about Ψ_e. This yields

$$\begin{aligned}
\delta A &= A[\Psi_e + \delta\Psi] - A[\Psi_e] \\
&= \int_\Omega (\Psi_e^*(\mathbf{r}) + \delta\Psi^*(\mathbf{r}))(H - E)(\Psi_e(\mathbf{r}) + \delta\Psi(\mathbf{r}))\, d\tau \\
&\quad + \frac{1}{2}\int_\Sigma (\Psi_e^*(\mathbf{r}) + \delta\Psi^*(\mathbf{r}))\nabla_n(\Psi_e(\mathbf{r}) + \delta\Psi(\mathbf{r}))\, d\sigma \\
&\quad - \int_\Omega \Psi_e^*(\mathbf{r})(H - E)\Psi_e(\mathbf{r})\, d\tau - \frac{1}{2}\int_\Sigma \Psi_e^*(\mathbf{r})\nabla_n\Psi_e(\mathbf{r})\, d\sigma \\
&= \int_\Omega \Psi_e^*(\mathbf{r})(H - E)\delta\Psi(\mathbf{r})\, d\tau + \int_\Omega \delta\Psi^*(\mathbf{r})(H - E)\Psi_e(\mathbf{r})\, d\tau \\
&\quad + \frac{1}{2}\int_\Sigma \delta\Psi^*(\mathbf{r})\nabla_n\Psi_e(\mathbf{r})\, d\sigma + \frac{1}{2}\int_\Sigma \Psi_e^*(\mathbf{r})\nabla_n\delta\Psi(\mathbf{r})\, d\sigma \\
&= \mathrm{Re}\left(2\int_\Omega \delta\Psi^*(\mathbf{r})(H - E)\Psi_e(\mathbf{r})\, d\tau + \int_\Sigma \delta\Psi^*(\mathbf{r})\nabla_n\Psi_e(\mathbf{r})\, d\sigma\right) \qquad (230)
\end{aligned}$$

For A_1 this same variation yields

$$\delta A_1 = \frac{1}{2}\int_\Sigma \delta\Psi^*(\mathbf{r})\zeta(\mathbf{r})\, d\sigma \qquad (231)$$

With these two results in hand we then examine the effects of the variation on J

$$\begin{aligned}
\delta J &= J\left(\frac{\delta A_1}{A_1} + \frac{\delta A_1^*}{A_1^*} - \frac{\delta A}{A}\right) \\
&= J\,\mathrm{Re}\left(\frac{2\delta A_1}{A_1} - \frac{1}{A}\left[2\int_\Omega \delta\Psi^*(\mathbf{r})(H - E)\Psi(\mathbf{r})\, d\tau\right.\right. \\
&\quad \left.\left. + \frac{1}{2}\int_\Sigma \delta\Psi^*(\mathbf{r})\nabla_n\Psi(\mathbf{r})\, d\sigma\right]\right) \qquad (232)
\end{aligned}$$

As we noted before for exact solutions $J = A = A_1 = A_1^*$. We can use this result in our variations about the exact solutions to yield

$$\delta J = \mathrm{Re}\left(\int_\Sigma \delta\Psi^*(\mathbf{r})(\zeta(\mathbf{r}) - \nabla_n\Psi(\mathbf{r}))\, d\sigma - 2\int_\Omega \delta\Psi^*(\mathbf{r})(H - E)\Psi(\mathbf{r})\, d\tau\right) \qquad (233)$$

Since our variations are unconstrained throughout Ω and Σ, (233) implies that $\delta J = 0$ if and only if

$$\begin{aligned}
&(H - E)\Psi(\mathbf{r}) = 0 \quad \text{in } \Omega, \\
&\zeta(\mathbf{r}) = \nabla_n\Psi(\mathbf{r}) \quad \text{on } \Sigma.
\end{aligned} \qquad (234)$$

These conditions implicitly determine an $\mathcal{R}$-operator. This can be show explicitly by introducing a basis ϕ_a that is linearly independent in the volume Ω. These can then be used to expand Ψ and $\delta\Psi$,

$$\Psi(\mathbf{r}) = \sum_a \phi_a(\mathbf{r})c_a \qquad (235)$$

$$\delta\Psi(\mathbf{r}) = \sum_a \phi_a(\mathbf{r})\delta c_a \tag{236}$$

Using these expansions and assuming δJ vanishes then (233) becomes

$$\sum_b \int_\Omega \phi_a^*(\mathbf{r})(H-E)\phi_b(\mathbf{r})\,d\tau c_b = \frac{1}{2}\int_\Sigma \phi_a^*(\mathbf{r})\left(\zeta(\mathbf{r}) - \sum_b \nabla_n\phi_b(\mathbf{r})c_b\right)d\sigma \tag{237}$$

Next we apply Lemma 1 from Chapter 3 on the left hand side of equation (237) to yield

$$\sum_b A_{ab}c_b = \frac{1}{2}\int_\Sigma \phi_a^*(\mathbf{r})\zeta(\mathbf{r})\,d\sigma \tag{238}$$

where

$$A_{ab} = \int_\Omega \left\{\frac{1}{2}\nabla\phi_a^*(\mathbf{r})\cdot\nabla\phi_b(\mathbf{r}) + \phi_a^*(\mathbf{r})(V(\mathbf{r})-E)\phi_b(\mathbf{r})\right\}d\tau \tag{239}$$

Next we define

$$\zeta_a = \frac{1}{2}\int_\Sigma \phi_a^*(\mathbf{r})\zeta(\mathbf{r})\,d\sigma. \tag{240}$$

Thus arriving at a matrix equation, $\mathbf{Ac} = \bar{\zeta}$, with the matrix and vectors corresponding the terms from equation (238). Solving this equation yields an expression for the expansion coefficients

$$c_a = \sum_b A_{ab}^{-1}\zeta_b \tag{241}$$

with A_{ab}^{-1} being the elements of the inverse of the matrix $\mathbf{A}$ (assuming the matrix $\mathbf{A}$ is non-singular). From this we can derive an expression for $\Psi(\mathbf{r})$:

$$\Psi(\mathbf{r}) = \sum_a \phi_a(\mathbf{r})c_a = \sum_a \phi_a(\mathbf{r})\Big(\sum_b A_{ab}^{-1}\zeta_b\Big) \tag{242}$$

$$= \frac{1}{2}\sum_a\sum_b \int_\Sigma \phi_a^*(\mathbf{r})A_{ab}^{-1}\phi_b^*(\mathbf{r}')\nabla_n\Psi(\mathbf{r}')\,d\sigma'. \tag{243}$$

This allows us to define the $\mathcal{R}$-operator,

$$\mathcal{R}(\mathbf{r},\mathbf{r}',E) = \frac{1}{2}\sum_a\sum_b \phi_a^*(\mathbf{r})A_{ab}^{-1}\phi_b^*(\mathbf{r}'). \tag{244}$$

Rewriting (243) we arrive at

$$\Psi(\mathbf{r}) = \int_\Sigma \mathcal{R}(\mathbf{r},\mathbf{r}',E)\nabla_n\Psi(\mathbf{r}')\,dr' \tag{245}$$

returning us to our definition in (224). As can be seen the $\mathcal{R}$-operator relates the normal derivative of the wave function on some boundary point (denoted by the coordinates $\mathbf{r}'$) to the values on some other surface point $\mathbf{r}$. This removes the restrictions

of the **R**-matrix, by allow us the freedom of relating the wave function at different points on the surface.

We can also use these coefficients in our functional J. Inserting our expansion (235) into A and A_1 yields

$$\begin{aligned} A &= \sum_{ab} c_a A_{ab} c_b^* = \sum_{ab} \sum_c A_{ac}^{-1} \zeta_c A_{ab} \sum_d A_{bd}^{-1} \zeta_d \\ &= \sum_{ab} \zeta_a A_{ab}^{-1} \zeta_b \end{aligned} \tag{246}$$

$$A_1 = \sum_a \zeta_a c_a = \sum_a \zeta_a \sum_b A_{ab}^{-1} \zeta_b = \sum_{ab} \zeta_a A_{ab}^{-1} \zeta_b \tag{247}$$

Thus we can see that the functional J yields

$$J = A = A_1 = A_1^* = \sum_{ab} \zeta_a A_{ab}^{-1} \zeta_b \tag{248}$$

Expanding this out we arrive at the expression

$$J = \frac{1}{4} \sum_{a,b} \frac{\int_\Sigma d\sigma' \phi_b^*(\mathbf{r}') \zeta(\mathbf{r}') \int_\Sigma d\sigma \phi_a(\mathbf{r}) \zeta^*(\mathbf{r})}{\int_\Omega d\tau (\frac{1}{2} \nabla \phi_b^*(\mathbf{r}) \cdot \nabla \phi_a(\mathbf{r}) + \phi_b^*(\mathbf{r}) [V(\mathbf{r}) - E] \phi_a(\mathbf{r}))}. \tag{249}$$

Lastly, we use the definition of the $\mathcal{R}$-operator (244) to get

$$J = \frac{1}{2} \int_\Sigma \int_\Sigma d\sigma \, d\sigma' \zeta^*(\mathbf{r}) \mathcal{R}(\mathbf{r}, \mathbf{r}', E) \zeta(\mathbf{r}'). \tag{250}$$

We note that J is stationary while the boundary functions ζ are arbitrary. This gives us a stationary result for our $\mathcal{R}$-operator. Thus we have variational estimate for the $\mathcal{R}$-operator defined in terms of arbitrary boundary conditions and basis elements.

V.4 $\mathcal{R}$-OPERATOR TO THE R-MATRIX

As noted earlier in equation (244), the $\mathcal{R}$-operator can be expressed as

$$\mathcal{R}^{LSP}(\mathbf{r}, \mathbf{r}', E) = \frac{1}{2} \sum_{i,j} \psi_i^{LSP}(\mathbf{r}) (A_{ab,cd}(E))^{-1} \psi_j^{LSP*}(\mathbf{r}') \tag{251}$$

For the cases we are interested in we will restrict the $\mathcal{R}$-operator to systems with two escaping electrons. This means in equation (251) the vector $\mathbf{r}$ refers to a point in the 6-dimensional space formed by the two electrons. We can reexpress (251) in this case in terms of the radial vectors $\mathbf{r}_1$ and $\mathbf{r}_2$ as

$$\mathcal{R}^{LSP}(\mathbf{r}_1, \mathbf{r}_2, \mathbf{r}_1', \mathbf{r}_2', E) = \frac{1}{2} \sum_{ab,cd} \Pi_{ab}^{LSP}(\mathbf{r}_1, \mathbf{r}_2) (A_{ab,cd}(E))^{-1} \Pi_{cd}^{LSP*}(\mathbf{r}_1', \mathbf{r}_2') \tag{252}$$

where Π_{ab}^{LSP} are our two electron pseudostates. To derive useful results from the $\mathcal{R}$-operator we must first relate it to the **R**-matrix. This result will then be propagated to the asymptotic limit in the later chapters and used to derive the final results as outlined in Chapter 4.

In order to calculate the **R**-matrix we need to first project out the angular dependance of the $\mathcal{R}$-operator. This will leave us with a reduced $\mathcal{R}$-operator that relates the wave function values to their derivatives at a given radial distance. This reduced $\mathcal{R}$-operator can then be used to construct the **R**-matrix by solving for the channel functions by making use of a close coupling expansion. The surface the **R**-matrix is constructed on is composed of two parts σ_I and σ_{II} as show in Fig. 18. In this work we will concentrate on σ_I where $r_1 = \bar{r}$ and $r_2 \leq r_1$. The "missing" data can be derived by making use of the symmetry about the line $r_1 = r_2$.

V.4.1 THE REDUCED $\mathcal{R}$-OPERATOR

We project out the angular dependence of the $\mathcal{R}$-operator with coupled spherical harmonics $\Xi_{l_a l_b}^{LP}(\Omega_1, \Omega_2)$. This will leave us with a reduced $\mathcal{R}$-operator with only radial dependence. We then fix one of the radial coordinates. This means we will have four potentially distinct components of our $\mathcal{R}$-operator: $\mathcal{R}_{I,I}^{LSP}$, $\mathcal{R}_{II,I}^{LSP}$, $\mathcal{R}_{I,II}^{LSP}$, and $\mathcal{R}_{II,II}^{LSP}$. the subscripts refer to which coordinates is fixed, I for r_1 and II for r_2. The order indicates whether we are talking about the unprimed or primed coordinates respectively.

We begin by projecting out the angular dependence with spherical harmonics yielding the initial version of our reduced $\mathcal{R}$-operator, denoted $\mathcal{R}_{\text{red}}^{LSP}$,

$$\begin{aligned}\mathcal{R}_{\text{red}}^{LSP} &= \frac{1}{2}\sum_{ab,cd}\left(\int d\Omega_1 d\Omega_2 \Xi_{l_1 l_2}^{L*}(\Omega_1,\Omega_2)\Pi_{ab}^{LSP}(\mathbf{r}_1,\mathbf{r}_2)|_{r_1,r_2=\bar{r}}\right) \\ &\times \left(A_{ab,cd}(E)\right)^{-1}\left(\int d\Omega_1' d\Omega_2' \Xi_{l_3 l_4}^{L}(\Omega_1',\Omega_2')\Pi_{cd}^{LSP*}(\mathbf{r}_1',\mathbf{r}_2')|_{r_1',r_2'=\bar{r}}\right) \quad (253)\end{aligned}$$

where $r_1, r_2 = \bar{r}$ indicates that either r_1 or r_2 is equal to $\bar{r}$, that is that we are on one of the bounding surfaces σ_I or σ_{II}. Next we expand this result using the form of the $2e^-$ basis elements (140). This gives us

$$\begin{aligned}\mathcal{R}_{\text{red}}^{LSP} &= \frac{1}{2}\sum_{ab,cd}\Big(\frac{1}{2}N_a N_b \int d\Omega_1 d\Omega_2 \Xi_{l_1 l_2}^{L*}\Big\{\chi_a(r_1)\chi_b(r_2)|_{r_1,r_2=\bar{r}}\Xi_{l_a l_b}^{L} \\ &\quad +(-1)^{L+S+P}\chi_b(r_1)\chi_a(r_2)|_{r_1,r_2=\bar{r}}\Xi_{l_b l_a}^{L}\Big\}\Big) \\ &\times \left(A_{ab,cd}(E)\right)^{-1}\Big(\frac{1}{2}N_c N_d \int d\Omega_1' d\Omega_2' \Xi_{l_3 l_4}^{L}\Big\{\chi_c(r_1')\chi_d(r_2')|_{r_1',r_2'=\bar{r}}\Xi_{l_c l_d}^{L*}\end{aligned}$$

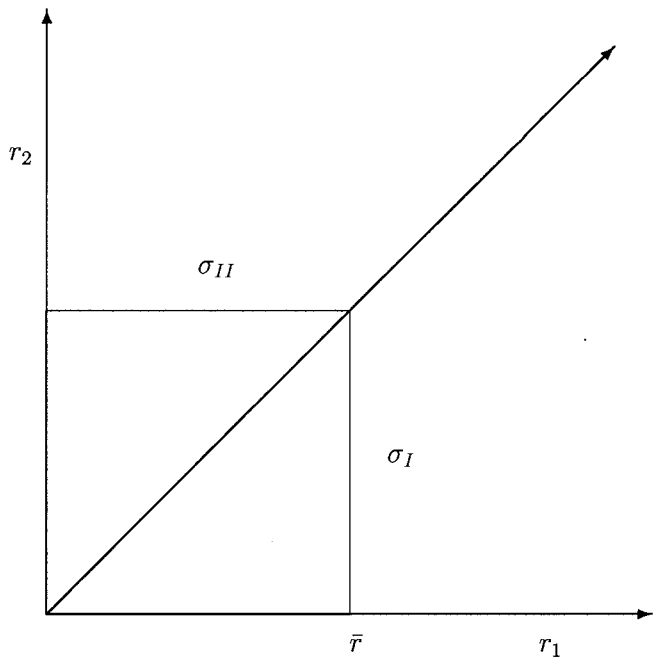

FIG. 18: The radial plane depicting the surfaces on which the **R**-matrix is defined. These are σ_I, where $r_1 = \bar{r}$ where $r_2 \leq r_1$, and surface σ_{II}, which is identical except the radial coordinates are reversed so that $r_2 = \bar{r}$, where $r_1 \leq r_2$. The reduced $\mathcal{R}$-operator can be related from one surface to other by making use of the symmetry about the line $r_1 = r_2$.

$$+(-1)^{L+S+P}\chi_d(r_1')\chi_c(r_2')|_{r_1',r_2'=\bar{r}}\Xi^{L*}_{l_d l_c}\Big\}\Big) \tag{254}$$

Next we use the orthonormality of the coupled spherical harmonics to reduce equation (254) to

$$\begin{aligned}\mathcal{R}^{LSP}_{\rm red} &= \frac{1}{8}\sum_{ab,cd}\mathcal{N}\Big(\chi_a(r_1)\chi_b(r_2)|_{r_1,r_2=\bar{r}}\delta_{l_1 l_a}\delta_{l_2 l_b} \\ &\quad +(-1)^{L+S+P}\chi_b(r_1)\chi_a(r_2)|_{r_1,r_2=\bar{r}}\delta_{l_1 l_b}\delta_{l_2 l_a}\Big) \\ &\times\ (A_{ab,cd}(E))^{-1}\Big(\chi_c(r_1')\chi_d(r_2')|_{r_1',r_2'=\bar{r}}\delta_{l_3 l_c}\delta_{l_4 l_d} \\ &\quad +(-1)^{L+S+P}\chi_d(r_1')\chi_c(r_2')|_{r_1',r_2'=\bar{r}}\delta_{l_3 l_d}\delta_{l_4 l_c}\Big)\end{aligned} \tag{255}$$

where $\mathcal{N} = N_a N_b N_c N_d$. The four reduced $\mathcal{R}$-operator components can be written explicitly as

$$\begin{aligned}&\mathcal{R}^{LSP}_{I,I} = \langle l_1 l_2|\mathcal{R}^{LSP}(r_2, r_2', E)|l_3 l_4\rangle|_{r_1=r_1'=\bar{r}} = \\ &\quad \frac{1}{8}\sum_{ab,cd}\mathcal{N}\left\{\chi_a(\bar{r})\chi_b(r_2)\delta_{l_1 l_a}\delta_{l_2 l_b} + (-1)^{L+S+P}\chi_b(\bar{r})\chi_a(r_2)\delta_{l_1 l_b}\delta_{l_2 l_a}\right\} \\ &\times(A_{ab,cd}(E))^{-1}\left\{\chi_c(\bar{r})\chi_d(r_2')\delta_{l_3 l_c}\delta_{l_4 l_d} + (-1)^{L+S+P}\chi_d(\bar{r})\chi_c(r_2')\delta_{l_3 l_d}\delta_{l_4 l_c}\right\}\end{aligned} \tag{256}$$

$$\begin{aligned}&\mathcal{R}^{LSP}_{I,II} = \langle l_1 l_2|\mathcal{R}^{LSP}(r_2, r_1', E)|l_3 l_4\rangle|_{r_1=r_2'=\bar{r}} = \\ &\quad \frac{1}{8}\sum_{ab,cd}\mathcal{N}\left\{\chi_a(\bar{r})\chi_b(r_2)\delta_{l_1 l_a}\delta_{l_2 l_b} + (-1)^{L+S+P}\chi_b(\bar{r})\chi_a(r_2)\delta_{l_1 l_b}\delta_{l_2 l_a}\right\} \\ &\times(A_{ab,cd}(E))^{-1}\left\{\chi_c(r_1')\chi_d(\bar{r})\delta_{l_3 l_c}\delta_{l_4 l_d} + (-1)^{L+S+P}\chi_d(r_1')\chi_c(\bar{r})\delta_{l_3 l_d}\delta_{l_4 l_c}\right\}\end{aligned} \tag{257}$$

$$\begin{aligned}&\mathcal{R}^{LSP}_{II,I} = \langle l_1 l_2|\mathcal{R}^{LSP}(r_1, r_2', E)|l_3 l_4\rangle|_{r_2=r_1'=\bar{r}} = \\ &\quad \frac{1}{8}\sum_{ab,cd}\mathcal{N}\left\{\chi_a(r_1)\chi_b(\bar{r})\delta_{l_1 l_a}\delta_{l_2 l_b} + (-1)^{L+S+P}\chi_b(r_1)\chi_a(\bar{r})\delta_{l_1 l_b}\delta_{l_2 l_a}\right\} \\ &\times(A_{ab,cd}(E))^{-1}\left\{\chi_c(\bar{r})\chi_d(r_2')\delta_{l_3 l_c}\delta_{l_4 l_d} + (-1)^{L+S+P}\chi_d(\bar{r})\chi_c(r_2')\delta_{l_3 l_d}\delta_{l_4 l_c}\right\}\end{aligned} \tag{258}$$

$$\begin{aligned}&\mathcal{R}^{LSP}_{II,II} = \langle l_1 l_2|\mathcal{R}^{LSP}(r_1, r_1', E)|l_3 l_4\rangle|_{r_2=r_2'=\bar{r}} = \\ &\quad \frac{1}{8}\sum_{ab,cd}\mathcal{N}\left\{\chi_a(r_1)\chi_b(\bar{r})\delta_{l_1 l_a}\delta_{l_2 l_b} + (-1)^{L+S+P}\chi_b(r_1)\chi_a(\bar{r})\delta_{l_1 l_b}\delta_{l_2 l_a}\right\} \\ &\times(A_{ab,cd}(E))^{-1}\left\{\chi_c(r_1')\chi_d(\bar{r})\delta_{l_3 l_c}\delta_{l_4 l_d} + (-1)^{L+S+P}\chi_d(r_1')\chi_c(\bar{r})\delta_{l_3 l_d}\delta_{l_4 l_c}\right\}\end{aligned} \tag{259}$$

We can clearly see that the four reduced $\mathcal{R}$-operator components are related. By examining equations (256) and (257) we see that after we integrate over the primed coordinates from 0 to $\bar{r}$ the two formula will be both be functions of r_2 only. An integration of this sort will done later in this chapter. Thus the effect of $\mathcal{R}^{LSP}_{I,II}$ on subsurface σ_I will be identical to that of $\mathcal{R}^{LSP}_{I,I}$ once the limits on the angular momenta are considered. Hence we can simplify our result for subsurface σ_I by using only $\mathcal{R}^{LSP}_{I,I}$ and multiplying by 2. This reasoning also holds for $\mathcal{R}^{LSP}_{II,II}$ and $\mathcal{R}^{LSP}_{II,I}$ on subsurface σ_{II}.

Additionally a symmetry exists between $\mathcal{R}^{LSP}_{I,I}$ and $\mathcal{R}^{LSP}_{II,II}$. This is easily seen by noting that by reversing the coordinates in $\mathcal{R}^{LSP}_{I,I}$ we get $\mathcal{R}^{LSP}_{II,II}$. Hence the two components yield identical results on their corresponding subsurfaces.

Before moving on we will rearrange our result to a more convenient form. The total reduced $\mathcal{R}$-operator can be expressed as

$$\begin{aligned}
\mathcal{R}^{LSP}_{\text{red}} &= \frac{1}{8}\sum_{n_1n_2}\sum_{n_3n_4}\chi_{n_1}(r_1)\chi_{n_2}(r_2)|_{r_1,r_2=\bar{r}} \\
&\times \Big\{\sum_{n_an_b} N_aN_b \sum_{n_cn_d} N_cN_d\left[\delta_{l_1l_a}\delta_{l_2l_b}\delta_{n_1n_a}\delta_{n_2n_b} + (-1)^{L+S+P}\delta_{l_1l_b}\delta_{l_2l_a}\delta_{n_1n_b}\delta_{n_2n_a}\right] \\
&\times (A_{ab,cd}(E))^{-1}\left[\delta_{l_3l_c}\delta_{l_4l_d}\delta_{n_3n_c}\delta_{n_4n_d} + (-1)^{L+S+P}\delta_{l_3l_d}\delta_{l_4l_c}\delta_{n_1n_a}\delta_{n_2n_b}\delta_{n_3n_d}\delta_{n_4n_c}\right] \\
&\times \chi_{n_3}(r_1')\chi_{n_4}(r_2')|_{r_1',r_2'=\bar{r}} \\
&= \frac{1}{2}\sum_{n_1n_2}\sum_{n_3n_4}\chi_{n_1}(r_1)\chi_{n_2}(r_2)|_{r_1,r_2=\bar{r}} \\
&\times \langle n_1l_1n_2l_2|R|n_3l_3n_4l_4\rangle\chi_{n_3}(r_1')\chi_{n_4}(r_2')|_{r_1',r_2'=\bar{r}} \qquad (260)
\end{aligned}$$

where

$$\begin{aligned}
&\langle n_1l_1n_2l_2|R|n_3l_3n_4l_4\rangle = \\
&\frac{1}{4}\sum_{n_an_b} N_aN_b \sum_{n_cn_d} N_cN_d\left[\delta_{l_1l_a}\delta_{l_2l_b}\delta_{n_1n_a}\delta_{n_2n_b} + (-1)^{L+S+P}\delta_{l_1l_b}\delta_{l_2l_a}\delta_{n_1n_b}\delta_{n_2n_a}\right] \\
&\times(A_{ab,cd}(E))^{-1}\left[\delta_{l_3l_c}\delta_{l_4l_d}\delta_{n_3n_c}\delta_{n_4n_d} + (-1)^{L+S+P}\delta_{l_3l_d}\delta_{l_4l_c}\delta_{n_1n_a}\delta_{n_2n_b}\delta_{n_3n_d}\delta_{n_4n_c}\right] \qquad (261)
\end{aligned}$$

Next we make use of our conclusions about the symmetry between $\mathcal{R}^{LSP}_{I,I}$ and $\mathcal{R}^{LSP}_{I,II}$ to give us a factor of 2. We will limit ourselves for the moment to the consideration of σ_I based on our earlier conclusions of the symmetry of the problem. This gives us a reduced $\mathcal{R}$-operator on σ_I of

$$\mathcal{R}^{LSP}_{\sigma_I} = \sum_{n_1n_2}\sum_{n_3n_4}\chi_{n_1}(\bar{r})\chi_{n_2}(r_2)\langle n_1l_1n_2l_2|R|n_3l_3n_4l_4\rangle\chi_{n_3}(\bar{r})\chi_{n_4}(r_2') \qquad (262)$$

V.4.2 CLOSE-COUPLING EXPANSION

To derive the **R**-matrix, a close coupling expansion of the form shown in equations (129) and (131) is made on the surface σ_I. This will produce a set of linearly independent one-electron radial channel functions which can be used to construct the **R**-matrix. The expansion of the wave functions is

$$\Phi_{\mu}^{LSP}(\mathbf{r}_1, \mathbf{r}_2) = \sum_{\mu'} \frac{u_{\mu\mu'}(r_1)\phi_{\mu'}(r_2)}{r_1} \Xi_{\mu'}^{L}(\Omega_1, \Omega_2) \tag{263}$$

where the subscript μ denotes a particular incident channel and μ' ranges over all the scattering channels. The subscripts also denote a set of quantum numbers n, l_1, and l_2. $\phi_\mu(r)$ are the radial wave functions of the target state, the eigenstates and psuedostates derived in Chapter 4.

If we substitute (263) into the $2e^-$ Schrödinger's equation, with the Hamiltonian given by $H = \frac{1}{2}\nabla_1^2 + \frac{1}{2}\nabla_1^2 - Z/r_1 - Z/r_2 + 1/r_{12}$, we can project out the angular dependence by making use of the coupled spherical harmonics. We can also use the fact that the pseudostates are solutions to the one electron Hamiltonian to further simplify the result. This yields a set of coupled integro-differential equations, as mentioned in Chapter 4, for the radial channel functions for the scattered electron $u_{\mu\mu'}(r_1)$,

$$\left(\frac{d^2}{dr_1^2} - \frac{l_\mu(l_\mu+1)}{r_1^2} + \frac{2Z}{r_1} + k_\mu^2\right) u_{\mu\mu'}(r_1) = 2\sum_{\nu} V_{\mu\nu} u_{\nu\mu'}(r_1) \tag{264}$$

where

$$V_{\mu\mu'} = \langle \phi_\mu^*(r_2)\Xi_\mu(\Omega_1, \Omega_2) | \frac{1}{r_{12}} | \phi_{\mu'}(r_2)\Xi_{\mu'}(\Omega_1, \Omega_2) \rangle \tag{265}$$

This result will be used in Chapter 6 when we propagate the wave function.

V.4.3 $\mathcal{R}$-OPERATOR TO THE CHANNEL FUNCTIONS

We begin the construction of the channel functions by examining the $\mathcal{R}$-operator equation on the surface σ_I:

$$\Psi(\mathbf{r}) = \int_\Sigma d\sigma' \mathcal{R}(\mathbf{r}, \mathbf{r}', E) \nabla_n \Psi(\mathbf{r}') \tag{266}$$

which for a $2e^-$ system can be rewritten as

$$\Psi_\mu(\mathbf{r}_1, \mathbf{r}_2) = \int_\Sigma d^3r_1' d^3r_2' \mathcal{R}^{LSP}(\mathbf{r}_1, \mathbf{r}_2, \mathbf{r}_1'\mathbf{r}_2', E) \nabla_n \Psi_\mu(\mathbf{r}_1', \mathbf{r}_2') \tag{267}$$

Next we make use of the close coupling expansion, equation (263), substituting it into equation (267) to yield

$$\frac{1}{r_1}\sum_{\mu'} u_{\mu\mu'}(r_1)\phi_{\mu'}(r_2)\Xi^L_{\mu'} = \int_\Sigma \mathcal{R}^{LSP}(\mathbf{r}_1,\mathbf{r}_2,\mathbf{r}'_1,\mathbf{r}'_2,E) \times\nabla_n\Big(\sum_\nu \frac{u_{\mu\nu}(r_1)}{r_1}\phi_\nu(r_2)\Xi^L_\nu\Big)\, d^3r'_1 d^3r'_2 \qquad (268)$$

where we have dropped the explicit angular dependence in Ξ. Next we can eliminate the angular variables by projecting onto $\Xi^{L*}_{l_1l_2}(\Omega_1,\Omega_2)\Xi^{L*}_{l_3l_4}(\Omega'_1,\Omega'_2)\Xi^L_{l_3l_4}(\Omega'_1,\Omega'_2)$ and then integrating over all angular space. This results in

$$\begin{aligned}&\frac{1}{r_1}\sum_{\mu'} u_{\mu\mu'}(r_1)\phi_{\mu'}(r_2)\int d\Omega_1 d\Omega_2 \Xi^{L*}_{l_1l_2}\Xi^L_{\mu'}\int d\Omega'_1 d\Omega'_2 \Xi^{L*}_{l_3l_4}\Xi^L_{l_3l_4}\\ &= \int_0^{\bar r} dr'_2 \int d\Omega_1 d\Omega_2 \int d\Omega'_1 d\Omega'_2 \Xi^{L*}_{l_1l_2}\mathcal{R}^{LSP}(\mathbf{r}_1,\mathbf{r}_2,\mathbf{r}'_1,\mathbf{r}'_2,E)\Xi^L_{l_3l_4}\\ &\qquad\times\int d\Omega'_1 d\Omega'_2 \Xi^{L*}_{l_3l_4}\nabla_n\left(\frac{1}{r'_1}\sum_\nu u_{\mu\nu}(r'_1)\phi_\nu(r'_2)\Xi^L_\nu\right)\end{aligned} \qquad (269)$$

The integral involving the $\mathcal{R}$-operator was already considered when we derived the reduced $\mathcal{R}$-operator earlier in this chapter. Making use of equations (260) and (261) we can simplify this result to

$$\begin{aligned}&\frac{1}{r_1}\sum_{\mu'} u_{\mu\mu'}(r_1)\phi_{\mu'}(r_2)\delta_{l_{\mu'_1}l_1}\delta_{l_{\mu'_2}l_2}\\ &= \int_0^{\bar r} dr'_2 \sum_{n_1n_2}\sum_{n_3n_4}\chi_{n_1}(r_1)\chi_{n_2}(r_2)\langle n_1l_1n_2l_2|R|n_3l_3n_4l_4\rangle\chi_{n_3}(r'_1)\chi_{n_4}(r'_2)\\ &\qquad\times\int d\Omega'_1 d\Omega'_2 \Xi^{L*}_{l_3l_4}\nabla_n\left(\frac{1}{r'_1}\sum_\nu u_{\mu\nu}(r'_1)|_{r'_1=\bar r}\phi_\nu(r'_2)\Xi^L_\nu\right)\end{aligned} \qquad (270)$$

where for the delta functions $\delta_{l_{\mu'_1}l_1}$ and $\delta_{l_{\mu'_2}l_2}$, the indexing indicates the restrictions on the l values allowed for a particular channel. $l_{\mu'_1}$ must equal l_1 to yield a non zero result.

Next we deal with the normal gradient ∇_n. On the surface σ_I, the norm is perpendicular to r_2 and the angular coordinates, which means that is purely a derivative in r_1. This allows use to simplify our results (since neither $\Xi^{L*}_{l_3l_4}$ or $\phi_\nu(r'_2)$ is affected by it) to get

$$\begin{aligned}&\frac{1}{r_1}\sum_{\mu'} u_{\mu\mu'}(r_1)\phi_{\mu'}(r_2)\delta_{l_{\mu'_1}l_1}\delta_{l_{\mu'_2}l_2}\\ &= \int_0^{\bar r} dr'_2 \sum_{n_1n_2}\sum_{n_3n_4}\chi_{n_1}(r_1)\chi_{n_2}(r_2)\langle n_1l_1n_2l_2|R|n_3l_3n_4l_4\rangle\chi_{n_3}(r'_1)\chi_{n_4}(r'_2)\\ &\qquad\times\sum_\nu \frac{d}{dr_1}\left(\frac{u_{\mu\nu}(r'_1)}{r'_1}\right)|_{r'_1=\bar r}\phi_\nu(r'_2)\int d\Omega'_1 d\Omega'_2 \Xi^{L*}_{l_3l_4}\Xi^L_\nu\end{aligned} \qquad (271)$$

Then we perform the angular integration to give

$$\frac{1}{r_1}\sum_{\mu'} u_{\mu\mu'}(r_1)\phi_{\mu'}(r_2)\delta_{l_{\mu'_1}l_1}\delta_{l_{\mu'_2}l_2}$$
$$= \int_0^{\bar{r}} dr'_2 \sum_{n_1n_2}\sum_{n_3n_4} \chi_{n_1}(r_1)\chi_{n_2}(r_2)\langle n_1l_1n_2l_2|R|n_3l_3n_4l_4\rangle\chi_{n_3}(r'_1)\chi_{n_4}(r'_2)$$
$$\times \sum_{\nu}\frac{d}{dr_1}\left(\frac{u_{\mu\nu}(r'_1)}{r'_1}\right)|_{r'_1=\bar{r}}\phi_\nu(r'_2)\delta_{l_{\nu_1}l_3}\delta_{l_{\nu_2}l_4} \qquad (272)$$

Next we project out the r_2 dependence by projecting onto a set of pseudostates $\phi^*_{\nu'}(r_2)$ and integrating over r_2. Then we can write equation (272) as

$$\sum_{\mu'}\frac{u_{\mu\mu'}(r_1)}{r_1}\int_0^{\bar{r}} dr_2\phi^*_{\nu'}(r_2)\phi_{\mu'}(r_2)\delta_{l_{\mu'_1}l_1}\delta_{l_{\mu'_2}l_2}$$
$$= \sum_{n_1n_2}\sum_{n_3n_4}\chi_{n_1}(r_1)\left(\int_0^{\bar{r}} dr_2\phi^*_{\nu'}(r_2)\chi_{n_2}(r_2)\right)\langle n_1l_1n_2l_2|R|n_3l_3n_4l_4\rangle\chi_{n_3}(r'_1)$$
$$\times\sum_{\nu}\left(\int_0^{\bar{r}} dr'_2\chi_{n_4}(r'_2)\phi_\nu(r'_2)\right)\frac{d}{dr_1}\left(\frac{u_{\mu\nu}(r'_1)}{r'_1}\right)|_{r'_1=\bar{r}}\delta_{l_{\nu_1}l_3}\delta_{l_{\nu_2}l_4} \qquad (273)$$

which reduces to

$$\sum_{\mu'}\frac{u_{\mu\mu'}(r_1)}{r_1}\delta_{\mu'\nu'}\delta_{l_{\mu'_1}l_1}\delta_{l_{\mu'_2}l_2}$$
$$= \sum_{n_1n_2}\sum_{n_3n_4}\chi_{n_1}(r_1)\left(\int_0^{\bar{r}} dr_2\phi^*_{\nu'}(r_2)\chi_{n_2}(r_2)\right)\langle n_1l_1n_2l_2|R|n_3l_3n_4l_4\rangle\chi_{n_3}(r'_1)$$
$$\times\sum_{\nu}\left(\int_0^{\bar{r}} dr'_2\chi_{n_4}(r'_2)\phi_\nu(r'_2)\right)\frac{d}{dr_1}\left(\frac{u_{\mu\nu}(r'_1)}{r'_1}\right)|_{r'_1=\bar{r}}\delta_{l_{\nu_1}l_3}\delta_{l_{\nu_2}l_4}$$
$$= \sum_{n_1n_2}\sum_{n_3n_4}\chi_{n_1}(r_1)\langle\nu'|n_2\rangle\langle n_1l_1n_2l_2|R|n_3l_3n_4l_4\rangle\chi_{n_3}(r'_1)$$
$$\times\sum_{\nu}\langle\nu|n_4\rangle\frac{d}{dr_1}\left(\frac{u_{\mu\nu}(r'_1)}{r'_1}\right)|_{r'_1=\bar{r}}\delta_{l_{\nu_1}l_3}\delta_{l_{\nu_2}l_4} \qquad (274)$$

where

$$\langle\nu|n\rangle = \int_0^{\bar{r}} dr_2\phi_\nu(r_2)\chi_n(r_2) \qquad (275)$$

Using the delta function relations in equation (274) gives

$$\frac{u_{\mu\nu'}(r_1)}{r_1} = \sum_{n_1n_2}\sum_{n_3n_4}\chi_{n_1}(r_1)\langle n_{\nu'}|n_2\rangle\langle n_1l_{\nu'_1}n_2l_{\nu'_2}|R|n_3l_{\nu_1}n_4l_{\nu_2}\rangle\chi_{n_3}(r'_1)$$
$$\times\sum_{n_\nu}\langle n_\nu|n_4\rangle\frac{d}{dr'_1}\left(\frac{u_{\mu\nu}(r'_1)}{r'_1}\right)|_{r'_1=\bar{r}}\delta_{l_{\nu_1}l_3}\delta_{l_{\nu_2}l_4} \qquad (276)$$

Next we set the normal gradient $(u_{\mu\nu}(r)/r)' = C_\nu\delta_{\mu\nu}$ to define a set of independent radial channel wave functions. The actual value of the normal gradient is unimportant as long as we have this delta function relation. Any value would be canceled

out in the construction of the **R**-matrix. Using this form for the normal gradient in (276) gives us an expression for the radial channel functions $u_{\mu\nu}(r_1)$

$$u_{\mu\nu}(r_1) = \sum_{n_1} r_1 \chi_{n_1}(r_1) \sum_{n_2} \sum_{n_3 n_4} \langle n_\nu | n_2 \rangle \langle n_1 l_{\nu_1'} n_2 l_{\nu_2'} | R | n_3 l_{\nu_1} n_4 l_{\nu_2} \rangle \chi_{n_3}(r_1') \langle n_\mu | n_4 \rangle \quad (277)$$

The derivatives of the radial channel functions are determined by differentiating this equation with respect to r_1. This yields

$$u'_{\mu\nu}(r_1) = \sum_{n_1} r_1 \chi_{n_1}(r_1) \left(\frac{n_1}{r_1} - \alpha \right) \times \sum_{n_2} \sum_{n_3 n_4} \langle n_\nu | n_2 \rangle \langle n_1 l_{\nu_1'} n_2 l_{\nu_2'} | R | n_3 l_{\nu_1} n_4 l_{\nu_2} \rangle \chi_{n_3}(r_1') \langle n_\mu | n_4 \rangle \quad (278)$$

where χ are the normal Sturmian functions. As explained earlier only the subsurface σ_I needs to be considered to completely solve the $2e^-$ problem. The value of the channel wave function on the surface is obtained by setting $r_1 = r_1' = \bar{r}$,

$$u_{\mu\mu'}(\bar{r}) = \sum_{n_1} \bar{r} \chi_{n_1}(\bar{r}) \sum_{n_2} \sum_{n_3 n_4} \langle i | n_2 \rangle \langle n_1 l_{i_1} n_2 l_{i_2} | R | n_3 l_{j_1} n_4 l_{j_2} \rangle \chi_{n_3}(\bar{r}) \sum_{n_\nu} \langle j | n_4 \rangle \quad (279)$$

V.4.4 CONSTRUCTING THE R-MATRIX

With the derivation of the channel functions we can now construct the **R**-matrix. The multichannel $1e^-$ **R**-matrix is defined as

$$u_{\mu\mu'}(\bar{r}) = \sum_k R_{\mu k} u'_{k\mu'}(\bar{r}) \quad (280)$$

which can be rearranged to give

$$R_{\mu\mu'} = \sum_k u_{\mu k}(\bar{r}) [u'(\bar{r})]^{-1}_{k\mu'} \quad (281)$$

which is similar to the single channel definition given in Chapter 1 except for the constant factor of $\bar{r}$. Using equation (281) we can construct the **R**-matrix. Since we are dealing with approximate solutions there are limits to computational accuracy (due to a finite number of significant figures) so we need to insure that the **R**-matrix is constructed so that it is always symmetric. This can be accomplished by constructing the **R**-matrix, in matrix notation, as

$$R = u[u^\dagger u']^{-1} u^\dagger \quad (282)$$

where U now refers to a matrix of channel functions. Additionally for exact solutions of the problem, the matrix $u^\dagger u'$ being inverted is real symmetric but for approximate solutions this may not be the case. We can rewrite (282) as

$$R = u[\frac{1}{2}u^\dagger u' + \frac{1}{2}u'^\dagger u]^{-1}u^\dagger \tag{283}$$

allows us to ensure that the inverted term is always symmetric, even for approximate solutions used in the actual calculations

V.5 SUMMARY

We derived a variational form for the **R**-Matrix and investigated its advantages such as the lack of discontinuity at the boundary and the natural inclusion of the Bloch operator. We have also derived the $\mathcal{R}$-operator and shown how it can be projected into the space where $r_1 \geq r_2$. We showed how this projection can then be used to solve a series of integro-differential equations for the channel wave functions by making use of a close coupling expansion. Finally we showed how these channel wave functions can then be used to construct an **R**-matrix. We note that we can make use of the symmetry about the line $r_1 = r_2$ to account for the region where $r_2 \geq r_1$. With these methods in hand we can construct the **R**-Matrix which can then be used to propagate or interior information to the asymptotic region. Next we will look at how that propagation is effected.

CHAPTER VI

PROPAGATION METHOD

Having constructed our $\mathcal{R}$-operator we need to now extend it to the asymptotic limit, r_g, the Gialitis radius. Expanding our coupling equations to larger and larger radii require larger bases sets which bring with them the problem of spurious linear dependencies developing between basis elements due to the limits of computational accuracy. Dealing with this requires various time consuming stabilization methods. In the interest of speed and stability, a method was developed by Light and Walker [89], as well as others [90], to propagate an **R**-matrix in a way that preserves the information from the solutions of the inner region and quickly translates it to a larger radius. Doing this also allows us to correctly handle those mid range interactions such as the polarization potential until we finally reach the region where only the long range coulomb forces dominate.

Before we do this we must first address the issue with the failure of the Sturmian basis. To correct this problem we convert to a new more robust basis called the spline delta basis s_Δ. This new basis is explicitly linearly independent and is defined in the region $0 \leq r \leq r_g$. It is also simple to convert the **R**-matrix from our Sturmian basis via a linear transformation.

In this chapter we examine the spline delta basis and outline the basis transformation. Then we will review the Light Walker method and then we will show how it has been modified to efficiently make use the geometry we are using. We show it propagates the **R**-matrix from $\bar{r}$ out to the asymptotic radius r_g allowing us to use the **R**-matrix to connect to asymptotic region.

VI.1 SPLINE DELTA BASIS

In our R-matrix calculations we make use of a spline delta (s_Δ) basis to overcome the challenges of linear dependence on the boundary of r_b and out to our final asymptotic boundary, r_g. This resolves the issues with the spurious linear dependencies of the Sturmian basis and allows us to proceed to a region where we can treat the problem asymptotically. Here we will examine the nature and properties of this basis.

As the its name indicates, the basis is constructed from spline interpolation functions. These functions are cubic polynomials, which for the jth interval are defined:

$$g_j(x) = f_j + a_j(x - x_j) + b_j(x - x_j)^2 + c_j(x - x_j)^3 \tag{284}$$

Each interval is defined by a separate equation, each with 4 unknown coefficients to be solved for. For n points along the interpolated interval, this requires $4n - 4$ equations to solve for the unknowns. $4n - 7$ of these are provided by the values at those points and the conditions of smoothness in the first and second derivatives:

$$g_{j+1}(x_j) = g_j(x_j) = f_j \tag{285}$$

$$g'_j(x_j) = g'_{j+1}(x_j) \tag{286}$$

$$g''_j(x_j) = g''_{j+1}(x_j) \tag{287}$$

The remaining equations come from the additional restraints on the endpoints. These restrictions of zero value and vanishing third derivative at the end points are set to help insure smoothness of the interpolation.

$$g_1(x_0) = g_{n-1}(x_n) = 0 \tag{288}$$

$$g''_1(x_0) = g''_{n-1}(x_n) = 0 \tag{289}$$

Using all of these equations and the values at the various points x_j, solutions can be found for the various coefficients, allowing for a cubic spline interpolation to be derived.

The s_Δ basis consists of a set of spline interpolations where the function has zero value at the points x_j, called knot points, except at one knot point where it has the value of 1.

$$u_i(x_j) = \delta_{ij}, \text{ where } i = 1, 2, ..., n \text{ and } j = 0, 1, ..., n + 1 \tag{290}$$

The reason there are more points j than basis functions is to allow for the functions to go to zero at the end points as mentioned above.

In Fig. 19, we see an example of a s_Δ basis function. This one is defined over the interval -1 to 6, with only the values 0 to 5 being used in the actual basis. As can be seen it has the value of zero at every integer point except for 1 where it has the value of unity.

In Fig. 20 through Fig. 22 we see the usage of the s_Δ basis in modeling various functional behaviors. These were all done with a simple 6 element basis. The

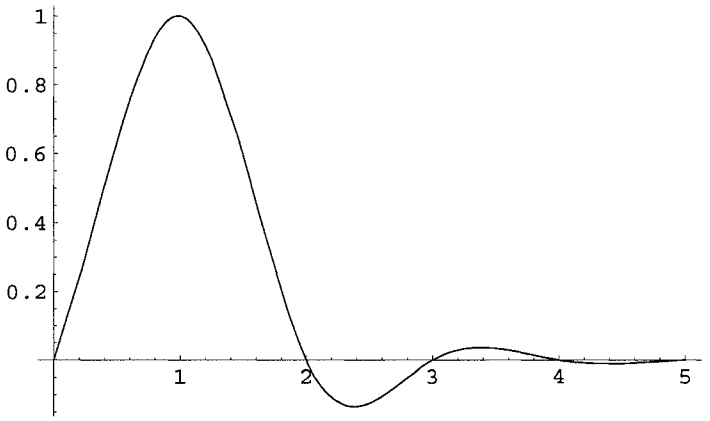

FIG. 19: s_Δ basis element for the range x_j=0 to 5.

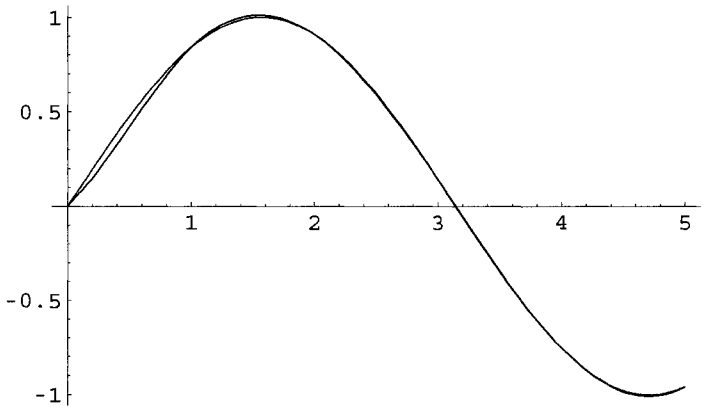

FIG. 20: A representation of $\sin x$ in the s_Δ basis verses the actual. 6 basis elements were used.

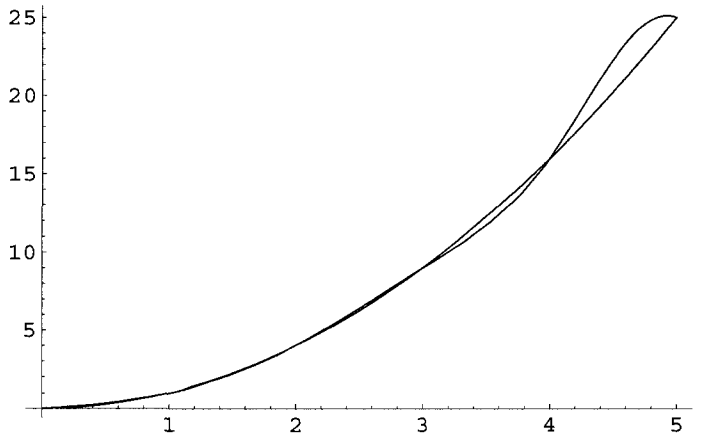

FIG. 21: A representation of x^2 in the s_Δ basis verses the actual. 6 basis elements were used.

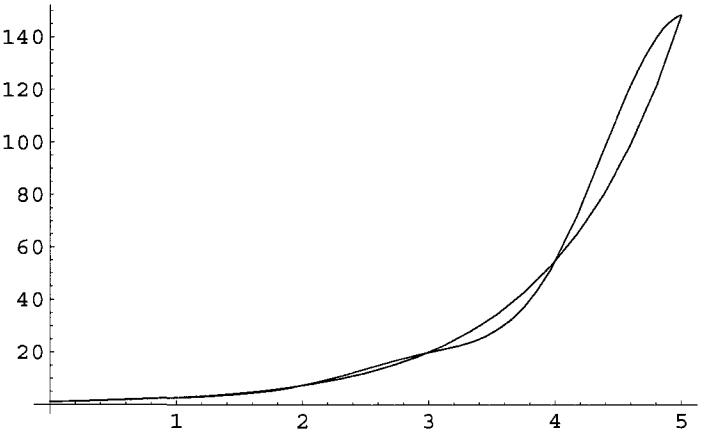

FIG. 22: A representation of e^x in the s_Δ basis verses the actual. 6 basis elements were used.

representations $\tilde{f}(x)$ of the functions $f(x)$ were constructed via

$$\tilde{f}(x) = \sum_i f(x_i) u_i(x) \tag{291}$$

where u_i are the s_Δ functions and x_i the knot points.

As can be seen, except near the end points, the behavior of $\sin x$, x^2, and e^x are all well modeled by this basis. With increasing numbers of knot points, and thus basis functions, the effectiveness of the basis increases. Of particular note to us is the effectiveness in modeling sinusoidal functions.

In actual work, our spline delta basis has the form

$$\eta_i(r) = r^{l+1} u_i(r) \tag{292}$$

where the factor of r^{l+1} is there to account for Coulomb Cusp condition. The basis is defined on the range $0 \leq r \leq r_g$, where r_g, the Gialitis radius, is where we are able to treat our escaping electrons asymptotically and where only the coulomb forces contribute.

The s_Δ basis can be used to replicate the behavior of our pseudostates. With these basis elements in hand we can then construct $1e^-$ pseudostates as well as transform our **R**-matrix from the Sturmian representation into the s_Δ basis. We also calculate the relevant potential matrix elements which will be needed in the propagation region.

VI.1.1 TRANSFORMATION OF BASIS

The pseudostates are constructed in the same way as they were in the Sturmian basis, following the method in the Chapter 4. The $1e^-$ Hamiltonian and overlap matrix elements are constructed using the s_Δ basis elements. Since the s_Δ basis elements are simple polynomials, the integration is quick and analytic. The details of this calculation and the general integration scheme are shown in Appendix F.

In addition to the overlap matrix S and the $1e^-$ Hamiltonian H, the multipole moments of the basis elements are also calculated to be used in the propagation calculations shown later in this chapter. These moments are simply integrals of the form

$$\langle i | r^\lambda | j \rangle = \int_0^{r_g} dr \eta_i r^{\lambda+2} \eta_j \tag{293}$$

and thus are easily solved via the same procedure.

Transformation of the R-matrix

The transformation of the **R**-matrix is relatively straightforward. We begin by expanding the pseudostates in the s_Δ basis in the original Sturmian pseudostate basis (for a given angular momentum l),

$$\phi_j^\Delta(r_2) = \sum_i \phi_i^S(r_2) c_{ij} \tag{294}$$

$$= \sum_i \phi_i^S(r_2) \int_0^{r_b} \phi_i^S(r) \phi_j^\Delta(r) dr \tag{295}$$

where the superscripts Δ and S indicate the basis. We note that the Sturmian pseudostates ϕ^S are orthonormal over $r_2 \leq r_b$ by construction, but the ϕ^Δ functions we use are not. Both bases use the same number of channels, ensuring that the overlap matrix between the two is nonsingular.

Our next step is to determine the linear transformation of **R**-matrix $R^0 = R^S$ to $R^1 = R^\Delta$. This transformation is defined for $r_1 = \bar{r}$, that is on the surface σ_I, and sums over channel indices with the conditions

$$F(\bar{r}, r_2) = \sum_i \phi_i^S(r_2) u_i^S(\bar{r}) \tag{296}$$

$$= \sum_j \phi_j^\Delta(r_2) u_j^\Delta(\bar{r}) \tag{297}$$

and

$$G(\bar{r}, r_2) = \sum_i \phi_i^S(r_2) u_i'^S(\bar{r}) \tag{298}$$

$$= \sum_j \phi_j^\Delta(r_2) u_j'^\Delta(\bar{r}) \tag{299}$$

if the bases are sufficiently complete. F is the coupled radial wave function and its derivative is G. Next we use equation (294) in (297)

$$F = \sum_i \sum_j \phi_i^S c_{ij} u_j^\Delta \tag{300}$$

This condition implies

$$u_i^S = \sum_j c_{ij} u_j^\Delta \tag{301}$$

Similarly we can show that

$$u_j'^S = \sum_{j'} c_{jj'} u_{j'}'^\Delta \tag{302}$$

Using the definition of the **R**-matrix, equation (280),

$$\begin{aligned} u_i^S &= \sum_k R_{ik}^S u_k'^S \\ \sum_j c_{ij} u_j^\Delta &= \sum_k R_{ik}^S \sum_{j'} c_{kj'} u_{j'}'^\Delta \end{aligned} \tag{303}$$

which implies that

$$R_{jj'}^1 = \sum_{i,k} c_{ji}^{-1} R_{ik}^0 c_{kj'} \tag{304}$$

Thus we are able to transform our **R**-matrix from the Sturmian basis to the spline delta basis.

VI.2 LIGHT WALKER PROPAGATION

Developed initially in the area of inelastic scattering calculations, the Light Walker method allows one to propagate an **R**-matrix in a radial coordinate. It does this by dividing up the space between the inner boundary, in our case $\bar{r}$, and the outer boundary, r_g, into evenly spaced sectors, as illustrated in Fig. 23. Using this method we construct sector **R**-matrices that relate solutions from one boundary to the next. These sector **R**-matrices can then be concatenated, or linked together, to create a global **R**-matrix that will be valid on the boundary r_g.

We begin by looking at the standard Light-Walker propagation method. This method makes use of the close coupled equations,

$$\frac{d^2}{dr^2} u_{ij}(r) = \sum_k 2[V_{ik}(r) - E + \epsilon_i] u_{kj}(r) \tag{305}$$

for the channel wave functions u. Our first step is to diagonalize our potential, or interaction, matrix $[V_{ik}(r_x) - E + \epsilon_i]$ at each sector boundary, r_x,

$$\sum_{i,k} x_{\mu i}(r_x) 2[V_{ik}(r_x) - E + \epsilon_i] x_{k\nu}(r_x) = \Gamma_\mu(r_x)\delta_{\mu\nu}. \tag{306}$$

where **X** is the diagonalization matrix and Γ_μ are the values along the diagonal. This also defines the locally (within the sector) decoupled pseudostates for the slower electron:

$$\zeta_\mu(r_2) = \sum_i x_{\mu i} \tilde{\phi}_i(r_2). \tag{307}$$

where $\tilde{\phi}$ is our untransformed pseudostates in the s_Δ basis. Our assumption is that we are at a reasonable distance from our target where the potential function will be

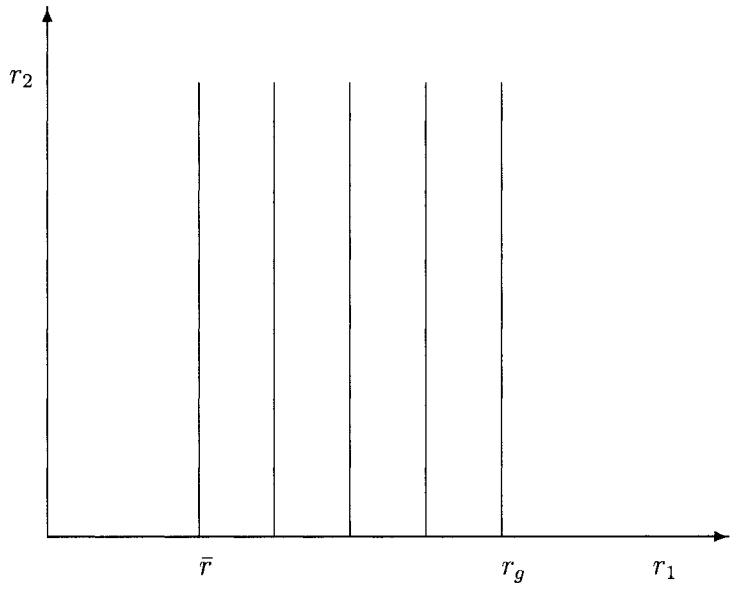

FIG. 23: The Light Walker Propagation Scheme. The propagation region is divided up into sectors, each of which has its own independent sector **R**-matrix.

slowly varying. Thus we will be able to take the potential to be constant over each sector assuming a small enough step size. Using the values of Γ we calculated, we can interpolate average values of Γ for each sector. If the commutator $\left[\frac{d^2}{dr_1^2}, x_{\mu i}\right] \approx 0$, then there are channel wave functions $w_\mu(r_1)$ which satisfy the decoupled equations

$$\frac{d^2}{dr_1^2} w_\mu(r_1) = \Gamma_\mu w_\mu(r_1) \tag{308}$$

where $w_\mu = x_{\mu i} u_{ij} x_{j\mu}$.

These uncouple solutions w are used to construct our sector **R**-matrices. There are two independent solutions for each Γ_μ and any solution to (308) can be constructed from a linear combination of them. As our choice of solution is arbitrary, we choose solutions for their ease in computation. For a sector $[ab]$ (referring to the bounding radii r_a and r_b), we choose two solutions that give us normal gradients of unity on

one boundary and zero on the opposite. Thus we will have a w^a, which has the boundary conditions

$$\frac{d}{dr}w^a(r_a) = -1, \quad \frac{d}{dr}w^a(r_b) = 0, \tag{309}$$

and a solution w^b with the boundary conditions

$$\frac{d}{dr}w^b(r_a) = 0, \quad \frac{d}{dr}w^b(r_b) = 1. \tag{310}$$

Our "left" solution, w_a, has a negative gradient to account for the fact that the normal on the surface is pointing inward toward the origin. Next we use these solutions in the **R**-matrix equation (86) to determine the $2N \times 2N$ coefficients of our sector **R**-matrices.

The forms chosen for the wave functions are

$$w^a_\mu(r) = -\frac{\cos[k_\mu(r_b - r)]}{k_\mu \sin[k_\mu(r_b - r_a)]} \quad w^b_\mu(r) = -\frac{\cos[k_\mu(r - r_a)]}{k_\mu \sin[k_\mu(r_b - r_a)]} \tag{311}$$

for $\Gamma_\mu = \lambda^2_\mu = -k^2_\mu < 0$, and

$$w^a_\mu(r) = \frac{\cosh[\lambda_\mu(r_b - r)]}{\lambda_\mu \sinh[\lambda_\mu(r_b - r_a)]} \quad w^b_\mu(r) = \frac{\cosh[\lambda_\mu(r - r_a)]}{\lambda_\mu \sinh[\lambda_\mu(r_b - r_a)]} \tag{312}$$

for $\lambda^2_\mu > 0$. These can then be used in the **R**-matrix equation as follows:

$$\begin{bmatrix} \mathbf{w}^a(r_a) & \mathbf{w}^b(r_a) \\ \mathbf{w}^a(r_b) & \mathbf{w}^b(r_b) \end{bmatrix} = \begin{bmatrix} \mathbf{r}^{ab}_{aa} & \mathbf{r}^{ab}_{ab} \\ \mathbf{r}^{ab}_{ba} & \mathbf{r}^{ab}_{bb} \end{bmatrix} \begin{bmatrix} -\frac{d}{dr}\mathbf{w}^a|_{r=r_a} & -\frac{d}{dr}\mathbf{w}^b|_{r=r_a} \\ \frac{d}{dr}\mathbf{w}^a|_{r=r_b} & \frac{d}{dr}\mathbf{w}^b|_{r=r_b} \end{bmatrix} \tag{313}$$

Using these functions we can solve for the matrices $\mathbf{r}_i$ and construct our **R**-matrices. Once the sector **R**-matrix is constructed we can simply transform back to the normal representation using our transformation matrices, **X**.

VI.3 MODIFICATION OF THE LIGHT WALKER PROPAGATION

The above solutions w however do not account for the fact that we are propagating in a region where $r_1 \geq r_2$. As seen in Fig. 24, in all our calculations involving the potential we have been working under the assumption that $r_2 \leq r_1$. Hence to account for for the fact that we are not using the correct Hamiltonian in the region above the line $r_1 = r_2$, we must use a modified Light-Walker method, using a technique developed by Temkin [10] and is the basis for the Poet-Temkin model. This technique involves mixing the solutions w^a and w^b and then using the symmetry of the channels about the line $r_1 = r_2$ to determine the best fit, thereby deriving the correct channel functions for the region $r_2 \leq r_1$.

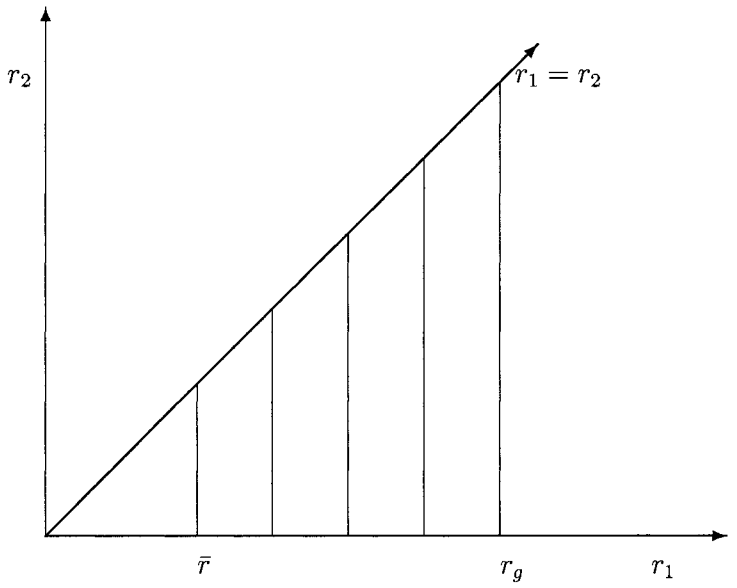

FIG. 24: Modified Light Walker Propagation Scheme. The propagation region $r_1 \geq r_2$ is divided up into sectors, each of which has its own independent sector **R**-matrix.

In this method our full transformed radial functions are

$$\sum_{\mu} \zeta_{\mu} \tilde{w}^{a}_{\mu\nu} = \sum_{\mu} \zeta_{\mu} (w^{a}_{\mu} \delta_{\mu\nu} + w^{b}_{\mu} y_{\mu\nu}) \tag{314}$$

$$\sum_{\mu} \zeta_{\mu} \tilde{w}^{b}_{\mu\nu} = \sum_{\mu} \zeta_{\mu} (-w^{a}_{\mu} z_{\mu\nu} + w^{b}_{\mu} \delta_{\mu\nu}) \tag{315}$$

where y_{ij} and z_{ij} are elements of the coefficient matrices. These allow us to mix elements of the other linearly independent solution to construct the correct sector wave function for the region. We use the boundary conditions to determine the coefficient matrices **Y** and **Z** via a mean square fit along the line $r_1 = r_2$. The boundary conditions for the coupled radial wave function $F^{LSP}(r_1, r_2)$ are

$$F^{LSP}(r_x, r_x) = 0 \tag{316}$$

where the sum $L+S+P$ is odd (i.e. anti-symmetric) and

$$\frac{\partial F^{LSP}}{\partial r_1} - \frac{\partial F^{LSP}}{\partial r_2}|_{r_1=r_2} = 0 \tag{317}$$

where $L+S+P$ is even, or symmetric. This defines the functions $\tilde{w}^a$ and $\tilde{w}^b$ which allows for the construction of the channel wave function matrix U:

$$U = \begin{bmatrix} \tilde{w}^a_{\mu\nu}(r_a) & \tilde{w}^b_{\mu\nu}(r_a) \\ \tilde{w}^a_{\mu\nu}(r_b) & \tilde{w}^b_{\mu\nu}(r_b) \end{bmatrix} \tag{318}$$

and the corresponding matrix U' of outward normal gradients.

From this we can construct a real symmetric **R**-matrix [15, 91]. First we use the generalization of the **R**-matrix equation to multiple channels:

$$U = r^{ab}_{\mu p,\nu q} U' \tag{319}$$

We can rearrange (319) to get a solution for the sector **R**-matrix:

$$r^{ab}_{\mu p,\nu q} = U(U')^{-1} \tag{320}$$

This gives us a solution, but because of the numerical limits of the computational accuracy this result will not be exact. We need to ensure that our **R**-matrices remain real and symmetric. This can be done by including a factor of $U^\dagger$,

$$r^{ab}_{\mu p,\nu q} = U(U^\dagger U')^{-1} U^\dagger \tag{321}$$

We can compare this formula to (218) and we see that if U corresponds to the pseudostates, the factor $U^\dagger U'$ corresponds to the integral over $H_B - E$. As we noted H_B is the Hermitian Bloch-modified Hamiltonian. In our case it is only locally Hermitian but that is sufficient for our purposes. If $U^\dagger U'$ is Hermitian then we can use (321) to derive a real symmetric sector **R**-matrix.

VI.3.1 CONSTRUCTING A GLOBAL R-MATRIX

As mentioned earlier, the sector **R**-matrices can be concatenated to link surfaces bounding the entire volume. This is done by linking two sector **R**-matrices at a time, moving slowly outward in r_1. Connecting two regions is a fairly simple procedure first worked out by Zvijac and Light [92]. We proceed by looking at the connection between the wave functions in the representation of sector $[ab]$ to that of $[bc]$. In

terms of the relevant sector **R**-matrices and wave functions we have the following equations:

$$w^i(r_a) = r^{ab}_{aa} w^{i'}(r_a) + r^{ab}_{ab} w^{i'}(r_b) \quad (322)$$

$$w^j(r_c) = r^{bc}_{cb} w^{j'}(r_b) + r^{bc}_{cc} w^{j'}(r_c). \quad (323)$$

Now if w^i represents the wave function in sector $[ab]$ and w^j in sector $[bc]$, these wave functions of course must transition smoothly along the boundary r_b. This requires that

$$w^{i'}(r_b) = -\Lambda w^{j'}(r_b) \quad (324)$$

and

$$r^{ab}_{ba} w^{i'}(r_a) + r^{ab}_{bb} w^{i'}(r_b) = \Lambda[r^{bc}_{bb} w^{j'}(r_b) + r^{bc}_{bc} w^{j'}(r_c)] \quad (325)$$

where Λ is the matrix relates the different bases used in the sectors. In our case the sector bases are equivalent and $\Lambda = \mathbf{I}$. With (322)-(325) we can solve for $w^{i'}(r_b)$ and $w^{j'}(r_b)$. This gives us

$$w^{i'}(r_b) = w^{j'}(r_b) = (r^{ab}_{bb} + r^{bc}_{bb})^{-1}(r^{ab}_{ba} w^{i'}(r_a) - r^{bc}_{bc} w^{j'}(r_c)) \quad (326)$$

Inserting (326) into (322) and (323) gives us

$$w^i(r_a) = r^{ab}_{aa} w^{i'}(r_a) - r^{ab}_{ab}(r^{ab}_{bb} + r^{bc}_{bb})^{-1}(r^{ab}_{ba} w^{i'}(r_a) - r^{bc}_{bc} w^{j'}(r_c)) \quad (327)$$

$$w^j(r_c) = r^{bc}_{cb}(r^{ab}_{bb} + r^{bc}_{bb})^{-1}(r^{ab}_{ba} w^{i'}(r_a) - r^{bc}_{bc} w^{j'}(r_c)) + r^{bc}_{cc} w^{j'}(r_c) \quad (328)$$

Rearranging this we can derive the forms for the elements of the new sector **R**-matrix r^{ac},

$$r^{ac}_{aa} = r^{ab}_{aa} - r^{ab}_{ab}(r^{ab}_{bb} + r^{bc}_{bb})^{-1} r^{ab}_{ba} \quad (329)$$

$$r^{ac}_{ac} = r^{ab}_{ab}(r^{ab}_{bb} + r^{bc}_{bb})^{-1} r^{bc}_{bc} \quad (330)$$

$$r^{ac}_{ca} = r^{bc}_{cb}(r^{ab}_{bb} + r^{bc}_{bb})^{-1} r^{ab}_{ba} \quad (331)$$

$$r^{ac}_{cc} = r^{bc}_{cc} - r^{bc}_{cb}(r^{ab}_{bb} + r^{bc}_{bb})^{-1} r^{bc}_{bc} \quad (332)$$

Thus we can connect two sector **R**-matrices, quickly linking the whole chain together. Additionally once we have concatenated the sector **R**-matrices, we can transform the result back to our original basis via

$$r^{ab}_{ij} = \sum_{\mu,\nu} x_{\mu i} r^{ab}_{\mu\nu} x_{\nu j} \quad (333)$$

Then we can propagate the global **R**-matrix from $\bar{r}$ at the initial sector to r_g at the nth sector via:

$$R^n = r^{0n}_{nn} - r^{0n}_{n0}(R^0 + r^{0n}_{00})^{-1} r^{0n}_{0n} \tag{334}$$

With this method we can also propagate our wave functions outwards to r_g or if we wish backwards from some larger radius:

$$\begin{aligned} u_n - r^{0n}_{nn} u'_n &= -r^{0n}_{n0} u'_0 \quad \text{Outwards} \\ r^{0n}_{0n} u'_n &= u_0 + r^{0n}_{00} u'_0 \qquad \text{Inwards} \end{aligned} \tag{335}$$

VI.4 SUMMARY

We have accounted for the linear dependencies arising in the Sturmian basis by translating to the spline delta basis. We have described how this basis has been constructed to be explicitly linearly independent and defined throughout the propagation region. We have shown how the linear translation of bases is made.

We have examined the Light Walker propagation method and how it is modified to account for the fact that the Hamiltonian is incorrect for $r_1 < r_2$. We have shown how the line of symmetry $r_1 = r_2$ is used to construct the correct sector r-matrices and how these allow us to construct a global **R**-matrix to take our solutions to the asymptotic region at r_g. Now we must look at how we use this **R**-matrix in the construction of our final results.

CHAPTER VII

CONNECTING TO THE ASYMPTOTIC REGION

Having constructed and propagated our **R**-matrix to the region of long range interactions, we now must connect the wave function it details to this asymptotic region. This is the region where we can derive the cross sections and other relevant details of the $(e, 2e)$ process.

In the first part of this chapter we will examine how to use the **R**-matrix to connect to the elastic scattering region and the construction of the scattering cross sections and phase shifts. We examine how the **S**, **K**, and **T**-matrices are calculated and how these are then used to calculate the scattering phase shifts as well as cross sections for elastic scattering and excitation.

We begin with elastic scattering as this is the easiest process to model and provides us a test of our method. Calculations above the threshold for ionization requires us to deal with electrons in continuum states as well as substantial contributions from higher angular momentum states. This is especially true in the region just above threshold where high order angular momenta make large contributions to the cross section. It is for this reason we begin with the much simpler scattering process.

In preparation for calculations for the ionization case, we will discuss the various asymptotic forms that can be used to characterize the behavior of two free electrons in the field of an ion. We need a form for this to use as our projector to extract that part of propagated wave function that contributes to ionization. A more in depth look at the alternate projectors can be found in Appendix H.

In the third section we will show how to derive the ionization amplitude and examine what form the projector needs to take to extract it. Lastly, we will show how in practice we use this minimum form to extract the triple differential cross section.

VII.1 CONNECTING TO THE SCATTERING REGION

The first step in using the $\mathcal{R}$-operator method to construct scattering results is to construct the **S**-matrix, or scattering matrix, from the propagated **R**-matrix. From this one can build the **T**-matrix, or transmission matrix, and derive the cross sections. Additionally one can construct a **K**-matrix, or reactance matrix, and derive the

scattering phase shifts. This is shown in the sections below.

These results are constructed in the limit where one electron remains close to the atom while the scattered electron goes to infinity. Hence these results are constructed using only one radial coordinate, that of the scattered electron, referred to as r_1.

VII.1.1 DERIVATION OF S-MATRIX AND SCATTERING CROSS SECTIONS

From the **R**-matrix propagated as shown in Chapter 6, it is possible to derive the **S**-matrix, or scattering matrix, which allows for the calculation of the cross section. First we look at the asymptotic form of the channel wave functions $u_\mu(r_1)$ and their derivatives:

$$\lim_{r_1\to\infty} u_\mu(r_1) \to A_\mu f_\mu^{in}(r_1) + B_\mu f_\mu^{out}(r_1) \tag{336}$$

$$\lim_{r_1\to\infty} u'_\mu(r_1) \to A_\mu g_\mu^{in}(r_1) + B_\mu g_\mu^{out}(r_1) \tag{337}$$

where the f functions describe the incoming and outgoing parts of the wave function. the g functions are their derivatives. The coefficients A_μ and B_μ are not independent, as the amplitudes of the outgoing waves, B_μ, are dependent on the amplitudes of the incoming waves, A_μ. The relationship between them is defined by the **S**-matrix:

$$B_\mu = \sum_{\mu'} S_{\mu\mu'} A_{\mu'}. \tag{338}$$

Substituting this into (336) gives

$$\lim_{r_1\to\infty} u_\mu(r_1) \rightarrow \sum_{\mu'} A_{\mu'} \left\{ f_\mu^{in}(r_1)\delta_{\mu\mu'} + f_\mu^{out}(r_1) S_{\mu\mu'} \right\} \tag{339}$$

$$\rightarrow \sum_{\mu'} u_{\mu\mu'} A_{\mu'} \tag{340}$$

where

$$u_{\mu\mu'} = f_\mu^{in}(r_1)\delta_{\mu\mu'} + f_\mu^{out}(r_1) S_{\mu\mu'} \tag{341}$$

and the derivative

$$\lim_{r_1\to\infty} u'_\mu(r_1) \rightarrow \sum_{\mu'} A_{\mu'} \left\{ g_\mu^{in}(r_1)\delta_{\mu\mu'} + g_\mu^{out}(r_1) S_{\mu\mu'} \right\} \tag{342}$$

$$\rightarrow \sum_{\mu'} u'_{\mu\mu'} A_{\mu'} \tag{343}$$

where

$$u'_{\mu\mu'} = g_\mu^{in}(r_1)\delta_{\mu\mu'} + g_\mu^{out}(r_1) S_{\mu\mu'}. \tag{344}$$

From here we can derive the **S**-matrix through the use of the **R**-matrix. Using the **R**-matrix equation, (86), and substituting in the definitions of u_μ and u'_μ:

$$\begin{aligned}
&\sum_{\mu'} A_{\mu'}\Big\{f^{in}_{\mu}(r_1)\delta_{\mu\mu'} + f^{out}_{\mu}(r_1)S_{\mu\mu'}\Big\} \\
&\quad = \sum_{\nu} R_{\mu\nu} \sum_{\mu'} A_{\mu'}\Big\{g^{in}_{\nu}(r_1)\delta_{\nu\mu'} + g^{out}_{\nu}(r_1)S_{\nu\mu'}\Big\} \\
&\quad = \sum_{\mu'} A_{\mu'}\Big\{\sum_{\nu} R_{\mu\nu}g^{in}_{\nu}(r_1)\delta_{\nu\mu'} + \sum_{\nu} R_{\mu\nu}g^{out}_{\nu}(r_1)S_{\nu\mu'}\Big\}. \qquad (345)
\end{aligned}$$

As can be seen the factors inside the brackets must be equal to each other for a nontrivial solution. Bringing the incoming functions to one side yields:

$$f^{in}_{\mu}(r_1)\delta_{\mu\mu'} - \sum_{\nu} R_{\mu\nu}g^{in}_{\nu}(r_1)\delta_{\nu\mu'} = -f^{out}_{\mu}(r_1)S_{\mu\mu'} + \sum_{\nu} R_{\mu\nu}g^{out}_{\nu}(r_1)S_{\nu\mu'} \qquad (346)$$

which can be rewritten

$$\begin{aligned}
f^{in}_{\mu}(r_1)\delta_{\mu\mu'} - R_{\mu\mu'}g^{in}_{\mu'}(r_1) &= -\sum_{\nu}\Big\{f^{out}_{\mu}(r_1)\delta_{\mu\nu}S_{\nu\mu'} - R_{\mu\nu}g^{out}_{\nu}(r_1)S_{\nu\mu'}\Big\} \\
&= -\sum_{\nu}\Big\{f^{out}_{\mu}(r_1)\delta_{\mu\nu} - R_{\mu\nu}g^{out}_{\nu}(r_1)\Big\}S_{\nu\mu'}. \qquad (347)
\end{aligned}$$

This can then be solved via matrix algebra to get the **S**-matrix.

VII.1.2 THE T-MATRIX AND THE TOTAL CROSS SECTION

The **T**-matrix is derived from the **S**-matrix by subtracting the portion corresponding to the incoming waves, thereby taking into account only that portion corresponding to transmission. Thus the **T**-matrix is [13]:

$$\mathbf{T} = \frac{\mathbf{S} - \mathbf{I}}{2i} \qquad (348)$$

where **I** is the identity matrix. Using the **T**-matrix one can then construct the scattering cross sections. We first note that the **T**-matrix can be expressed as

$$T_{ij}\sum_{k=1}^{n} x_{ik}x_{jk}e^{i\delta_k}\sin\delta_k \qquad (349)$$

where the matrices x_{ij} contain the eigenstates of the **T**-matrix and δ_k are the eigenphases, or phase shifts, of the system [13]. We already know that

$$d\sigma/d\Omega = |f(\theta)|^2 \qquad (350)$$

for the case of scattering, as discussed in Chapter 1. The scattering amplitude $f(\theta)$ can be expressed in terms of the phase shifts δ_k as [93]

$$f(\theta) = \frac{1}{k}\sum_{l=0}^{\infty}(2l+1)e^{i\delta_l}\sin\delta_l P_l(\cos\theta) \tag{351}$$

Blatt and Biedenharn [93] have shown that from (350) and (351) one can derive

$$\sigma_{ij} = \frac{4\pi}{k_j^2}|T_{ij}|^2 \tag{352}$$

which gives us the partial cross section for scattering from channel i to channel j. The total cross section is obtained by summing over degenerate final states and averaging over the initial states. The degeneracies in the initial state give factors of $2l_j+1$ and $2S_j+1$ due to possible initial state values of angular momentum l_j and spin S_j. An additional factor of 2 occurs for the degeneracy of spin of the incident electron. The final states contribute degeneracy factors of $2L+1$ and $2S+1$ based on the total angular momentum L and spin S. We sum over LSP as the **T**-matrix is independent of the total M_s and M_L. Putting this all together, the total cross section for a transition $i \rightarrow j$ is

$$\sigma_{ij} = \frac{4\pi}{k_j^2}\sum_{LSP}\frac{(2S+1)(2L+1)}{2(2l_j+1)(2S_j+1)}|T_{ij}^{LSP}|^2 \tag{353}$$

In our calculation we examine specific LSP cases and the summation is suppressed.

VII.1.3 DERIVING THE K-MATRIX AND THE SCATTERING PHASE SHIFTS

From the **S**-matrix, the **K**-matrix can be derived in straightforward manner [15]. The **K**-matrix, much like the **S**-matrix, relates the components of the asymptotic radial wave functions u_μ. In the **K**-matrix formulation, u_μ can be written as

$$\lim_{r_1\rightarrow\infty} u_\mu(r_1) = \frac{1}{\sqrt{k_\mu}}(C_\mu\sin\theta_\mu + D_\mu\cos\theta_\mu) \tag{354}$$

where $\theta_\mu = k_\mu r_1 - l_\mu\pi/2 - \eta\ln 2k_\mu r_1 + \sigma_{l_\mu}$. $\sigma_l = \arg[\Gamma(l+1-i\eta)]$, $\eta = Z/k_\mu$, and l is the angular momentum. The **K**-matrix then relates the coefficients of the even and odd parts of the asymptotic wave function:

$$D_\mu = \sum_{\mu'} K_{\mu\mu'}C_{\mu'}. \tag{355}$$

To relate this to the **S**-matrix, we first use (355) in (354) to get

$$\lim_{r_1\to\infty} u_\mu(r_1) = \sum_{\mu'} \frac{C_{\mu'}}{\sqrt{k_\mu}}(\delta_{\mu\mu'}\sin\theta_\mu + K_{\mu\mu'}\cos\theta_\mu) \tag{356}$$

$$= \sum_{\mu'} u_{\mu\mu'}C_{\mu'} \tag{357}$$

where

$$u_{\mu\mu'} = \frac{1}{\sqrt{k_\mu}}(\delta_{\mu\mu'}\sin\theta_\mu + K_{\mu\mu'}\cos\theta_\mu). \tag{358}$$

As we can see (358) is very similar in form to (340) and we can use these two equations to relate the **K**-matrix to the **S**-matrix. By manipulating the vectors of the elements $A_{\mu'}$ and $C_{\mu'}$, we can construct the equation

$$\sum_\nu \left[\frac{1}{\sqrt{k_\mu}}(\delta_{\mu\mu'}\sin\theta_\mu + K_{\mu\mu'}\cos\theta_\mu)\right]\beta_{\nu\mu'} = f_\mu^{in}\delta_{\mu\mu'} + f_\mu^{out}S_{\mu\mu'} \tag{359}$$

where the incoming and outgoing waves, f_μ^{in} and f_μ^{out}, can be expressed asymptotically

$$f_\mu^{in}(k_\mu r_1) = \frac{-e^{-i\theta_\mu}}{\sqrt{k_\mu}} \tag{360}$$

$$f_\mu^{out}(k_\mu r_1) = \frac{e^{i\theta_\mu}}{\sqrt{k_\mu}}. \tag{361}$$

Substituting (360) and (361) into equation (359) yields

$$\sum_\nu(\delta_{\mu\mu'}\sin\theta_\mu + K_{\mu\mu'}\cos\theta_\mu)\beta_{\nu\mu'} = -e^{-i\theta_\mu}\delta_{\mu\mu'} + e^{i\theta_\mu}S_{\mu\mu'} \tag{362}$$

where we have also multiplied by $\sqrt{k_\mu}$. If we expand the exponentials into sine and cosine functions we get

$$\sum_\nu(\delta_{\mu\mu'}\sin\theta_\mu + K_{\mu\mu'}\cos\theta_\mu)\beta_{\nu\mu'} = -(\cos\theta_\mu - i\sin\theta_\mu)\delta_{\mu\mu'} + (\cos\theta_\mu + i\sin\theta_\mu)S_{\mu\mu'}. \tag{363}$$

From here we can compare the coefficients of the sine and cosine terms. This gives us two equations:

$$\beta_{\mu\mu'} = i\delta_{\mu\mu'} + iS_{\mu\mu'} \tag{364}$$

$$\sum_\nu K_{\mu\nu}\beta_{\nu\mu'} = -\delta_{\mu\mu'} + S_{\mu\mu'}. \tag{365}$$

Putting (364) into (365) we arrive at

$$i\sum_{\nu} K_{\mu\nu}(\delta_{\nu\mu'} + S_{\nu\mu'}) = -\delta_{\mu\mu'} + S_{\mu\mu'}. \tag{366}$$

This expression can be written in matrix notation as

$$i\mathbf{K}(\mathbf{I} + \mathbf{S}) = -\mathbf{I} + \mathbf{S}. \tag{367}$$

Rewriting this yields a solution for the **K**-matrix in terms of the **S**-matrix:

$$\mathbf{K} = \frac{i(\mathbf{I} - \mathbf{S})}{\mathbf{I} + \mathbf{S}}. \tag{368}$$

In a similar way the **S**-matrix can be expressed in terms of the **K**-matrix:

$$\mathbf{S} = \frac{\mathbf{I} + i\mathbf{K}}{\mathbf{I} - i\mathbf{K}}. \tag{369}$$

In this work, the **S**-matrix is calculated directly from the **R**-matrix as outlined above. Having calculated the **S**-matrix the corresponding **K**-matrix is then derived as in (368). From the **K**-matrix one can then easily derive the scattering phase shifts.

The scattering phase shifts are derived from the eigenvalues of the **K**-matrix [13]. In terms of the eigenchannels, or eigenvectors of the **K**-matrix, the matrix can be expressed:

$$K_{ij} = \sum_{k}^{n} x_{ik}x_{jk}\tan\delta_k \tag{370}$$

where x_{ij} is the jth element of the ith eigenchannel. δ_k are the eigenphases corresponding to the scattering phase shifts.

VII.2 $(E, 2E)$ ASYMPTOTIC BEHAVIOR

In Chapter 1 we briefly discussed the form of the wave function in the asymptotic region. In this section we review fully the various forms that one can choose to describe the behavior of the two escaping electrons. In previous work in this area, there was considerable interest in finding a valid asymptotic form for use in calculating the full problem [20]. For our needs however we need only a solution sufficiently valid to extract the ionization amplitude needed to construct the TDCS.

In this section we discuss the asymptotic form of the escaping two electrons as developed by Rudge, Seaton, and Peterkop. Though we do not use the form presented here as our projector for extracting the ionization cross section we did at one point

consider using such as projector and others like it. These other asymptotic forms explored in Appendix H. As discussed there we later determined that these functions were more complicated than our needs. Indeed in the X2c method we use a much simpler projector which was discussed in Chapter 1 and consists of two Coulomb waves.

Note that in this section we use the notation for hyperspherical coordinates extensively. Hyperspherical coordinates is a convenient way to express the radial coordinates in a two electron system. With any two particles, one can specify their position in terms of six coordinates, such as a pair of spherical coordinates $(\mathbf{r}_1, \mathbf{r}_2) = (r_1, \theta_1, \phi_1, r_2, \theta_2, \phi_2)$.

In hyperspherical notation the radial coordinates are converted into a hyperradius ρ and a hyperspherical angle α. In this notation $r_1 = \rho \cos\alpha$ and $r_2 = \rho \sin\alpha$ where $\rho = r_1^2 + r_2^2$ and $\alpha = \tan^{-1}(r_2/r_1)$. This notation allows one to easily define an asymptotic condition where both electrons are far from the nucleus (i.e. $\rho \to \infty$).

VII.2.1 SEMICLASSICAL DETERMINATION OF THE ASYMPTOTIC FORM

We begin by examining a solution for where all three particles are far from each other. This is done using the formalism of Rudge, Seaton, and Peterkop (RSP) [11, 12]. As usual we start with the Schrödinger equation:

$$(-\frac{\nabla_1^2}{2} - \frac{\nabla_2^2}{2} + V + E)\Psi(r_1, r_2) = 0 \tag{371}$$

with

$$V = -\frac{Z}{r_1} - \frac{Z}{r_2} + \frac{1}{r_{12}} \tag{372}$$

and

$$2E = k_1^2 + k_2^2 = \kappa^2. \tag{373}$$

Since the situation is that of an incoming electron of momentum $\mathbf{k}_0$ followed by the excitation or ionization of an electron, the wave function can be described asymptotically as:

$$\lim_{r_1 \to \infty} \Psi \sim e^{i\mathbf{k}_0 \cdot \mathbf{r}_1} \Phi_0(\mathbf{r}_2) + \sum_{nlm} \Phi_{nlm}(\mathbf{r}_2) f_{nlm}(\mathbf{k}_2, k_2 \hat{\mathbf{r}}_1) \frac{e^{ik_{1n} r_1}}{r_1}$$

$$+ \int_{k_2 \leq \kappa = \sqrt{2E}} \Phi_{k_2}(\mathbf{r}_2) f(\mathbf{k}_2, k_2\hat{\mathbf{r}}_1) \frac{e^{ik_1 r_1 + i\eta(\mathbf{k}_2, \mathbf{r}_1)}}{r_1} d\mathbf{k}_2 \tag{374}$$

$$\lim_{r_2 \to \infty} \Psi \sim \sum_{nlm} \Phi_{nlm}(\mathbf{r}_1) g_{nlm}(\mathbf{k}_2, k_2\hat{\mathbf{r}}_2) \frac{e^{ik_{1n} r_2}}{r_2}$$
$$+ \int_{k_2 \leq \kappa = \sqrt{2E}} \Phi_{k_2}(\mathbf{r}_1) g(\mathbf{k}_2, k_2\hat{\mathbf{r}}_2) \frac{e^{ik_1 r_2 + i\eta(\mathbf{k}_2, \mathbf{r}_2)}}{r_2} d\mathbf{k}_2 \tag{375}$$

where (374) refers to the ionization process and (375) to the exchange process (where the two electrons exchange states). In the ionization process, $e^{i\mathbf{k}_0 \cdot \mathbf{r}_1} \Phi_0(\mathbf{r}_2)$ is the target state multiplied by the plane wave which represents the incident electron. The scattered electron is treated as an outgoing spherical wave. As one can see there are contributions from both the excitation and ionization states, though for the case we are considering the excitation states do not contribute. f and g are the ionization and exchange amplitudes respectively and the η factor in the exponent is due to Coulomb interactions with the unscreened nucleus. The question then becomes what are $f(\mathbf{k}_2, \mathbf{k}_1)$ and $g(\mathbf{k}_1, \mathbf{k}_2)$ for the ionization process?

We note that their absolute values should be equivalent. Both processes should result in the same cross section due to the indistinguishability of the electrons. For a more persuasive argument of why this is so, we first need to examine some of the formalisms and assumptions in the case of finite range potentials. By finite range, we mean that $V(r) = 0$ for very large but finite r. This is opposed to asymptotic range potentials such as the coulomb potential Z/r which cannot be ignored in our calculations even at extremely large distances.

Finite Range Potentials

For finite ranged potentials (where $V(r) = 0$ for large r) the solution for the continuum can take the form of a plane wave plus a diverging or converging wave. Using the converging wave form for ease of use, we look at the solution for large r.

$$\lim_{r \to \infty} \Phi(\mathbf{k}, \mathbf{r}) \sim (2\pi)^{-3/2} \{e^{i\mathbf{k}\cdot\mathbf{r}} + \phi^*(|k|\hat{\mathbf{r}}; -k) \frac{e^{-ikr}}{r}\} \tag{376}$$

where ϕ^* is a distortion on the incoming waves due to the interactions with the nucleus. We expand the plane wave, $e^{i\mathbf{k}\cdot\mathbf{r}}$, into its asymptotic form [94]:

$$\lim_{r \to \infty} e^{i\mathbf{k}\cdot\mathbf{r}} \sim \frac{2\pi}{ikr} \{\delta(\hat{\mathbf{k}} - \hat{\mathbf{r}}) e^{ikr} - \delta(\hat{\mathbf{k}} + \hat{\mathbf{r}}) e^{-ikr}\}. \tag{377}$$

This is derived in Appendix G. Putting this into (376) yields

$$\lim_{r\to\infty}\Phi(\mathbf{k},\mathbf{r}) \sim \frac{(2\pi)^{-1/2}}{ikr}\{\delta(\hat{\mathbf{k}}-\hat{\mathbf{r}})e^{ikr}+a(\hat{\mathbf{r}})e^{-ikr}\} \tag{378}$$

where

$$a(\hat{\mathbf{r}}) = \frac{ik}{2\pi}\phi^*(|k|\hat{\mathbf{r}};-k)+\delta(\hat{\mathbf{k}}+\hat{\mathbf{r}}). \tag{379}$$

Next we insert this into (374) for the case of $r_1, r_2 \to \infty$, or $\rho \to \infty$. Since we are interested in the asymptotic form we drop the summation over the bound states.

$$\begin{aligned}\lim_{\rho\to\infty}\Psi(\mathbf{r}_1,\mathbf{r}_2) \quad \sim \quad & \frac{(2\pi)^{-1/2}}{ir_1r_2}\int_0^{\sqrt{2E}} k_2dk_2\int d\hat{\mathbf{k}}_2\{\delta(\hat{\mathbf{k}}_2-\hat{\mathbf{r}}_2)e^{ik_2r_2} \\ & +a(\hat{\mathbf{r}}_2)e^{-ik_2r_2}\}e^{ik_1r_1}f(\mathbf{k}_2,k_2\hat{\mathbf{r}}_1).\end{aligned} \tag{380}$$

Next we make use of the stationary phase theorem which we introduced in Chapter 1, that is equations (29) and (30). Applying these to (380), we first make use of Theorem 1, equation (29):

$$\lim_{\rho\to\infty}\Psi(\mathbf{r}_1,\mathbf{r}_2) \sim \frac{(2\pi)^{-1/2}}{ir_1r_2}\int_0^{\sqrt{2E}} k_2dk_2e^{ik_2r_2+ik_1r_1}f(\mathbf{k}_2,k_2\hat{\mathbf{r}}_1). \tag{381}$$

The term with the incoming wave $e^{-ik_2r_2}$ has been lost since the wave function is the same at $k_2 = 0$, corresponding to the scattering of electron 1 with $k_1 = \sqrt{2E}$, and at $k_2 = \sqrt{2E}$, or $k_1 = 0$ and the case of scattering of electron 2. Hence the integral is zero and only the outgoing wave contributes.

We next note that in the limit we are working in, $(r_1, r_2 \to \infty)$, we assume that momentum is directly proportional to the distance that electron has traveled. Hence $r_1/k_1 \cong r_2/k_2 \cong \rho/\kappa$. This follows from an argument based on the phase of the ionization amplitude. This will shown later when we deal with the long range potentials.

Next we apply Theorem 2, equation (29), to the (381) integral. We first find the point k_x where $\xi' = 0$.

$$\xi'\rho = \frac{\partial}{\partial k_2}(k_1r_1+k_2r_2) = r_2 - \left(\frac{k_2}{k_1}\right)r_1 = 0. \tag{382}$$

where we have used equation (373) to express $k_1 = \sqrt{\kappa^2-k_2^2}$. Solving this for k_2 gives $k_2 = k_x = \kappa r_2/\rho$. For this k_2, $k_1 = \kappa r_1/\rho$. ξ'' in this case is

$$\xi''(k_x) = \frac{1}{\rho}\frac{\partial^2}{\partial k_2^2}(k_1r_1+k_2r_2) = -\frac{1}{\rho}\left(\frac{r_1}{k_1}+\frac{k_2^2r_1}{k_1^3}\right) = -\frac{1}{\kappa}\left(1+\frac{r_2^2}{r_1^2}\right) = -\frac{\rho^2}{\kappa r_1^2}. \tag{383}$$

Thus:

$$\lim_{\rho\to\infty}\Psi(\mathbf{r}_1,\mathbf{r}_2) \sim \frac{(2\pi)^{-1/2}}{ir_1r_2}\frac{(2\pi\kappa r_1^2)^{1/2}}{\rho^{3/2}}\frac{\kappa r_2}{\rho}f(\mathbf{k}_0,\mathbf{k}_1)e^{i\kappa(r_1^2+r_2^2)/\rho+i\pi/4}$$
$$\sim -i^{1/2}\frac{\kappa^{3/2}}{\rho^{5/2}}f(\mathbf{k}_0,\mathbf{k}_1)e^{i\kappa\rho}. \quad (384)$$

The same reasoning can be applied to (375) to yield:

$$\lim_{\rho\to\infty}\Psi(\mathbf{r}_1,\mathbf{r}_2) \sim -i^{1/2}\frac{\kappa^{3/2}}{\rho^{5/2}}g(\mathbf{k}_1,\mathbf{k}_0)e^{ik\rho}. \quad (385)$$

Thus $|f(\mathbf{k}_0,\mathbf{k}_1)| = |g(\mathbf{k}_1,\mathbf{k}_0)|$, showing that they are equivalent in absolute value as we stated earlier.

Long Ranged Solution

Next we attempt to solve the problem with long range potentials. We are looking for the asymptotic form of the solution to (371). We reexpress the wave function as

$$\Psi(\rho,\Omega_1,\Omega_2,\alpha) = \frac{\Theta(\rho,\Omega_1,\Omega_2,\alpha)}{\rho^{5/2}\sin\alpha\cos\alpha}. \quad (386)$$

In hyperspherical notation Schrödinger's equation is

$$\left(\frac{1}{\rho^5}\frac{\partial}{\partial\rho}\left(\rho^5\frac{\partial}{\partial\rho}\right) + \frac{1}{\rho^2\sin^2\alpha\cos^2\alpha}\frac{\partial}{\partial\alpha}\left(\sin^2\alpha\cos^2\alpha\frac{\partial}{\partial\alpha}\right)\right.$$
$$\left. -\frac{L_2^2}{\rho^2\sin^2\alpha} - \frac{L_1^2}{\rho^2\cos^2\alpha} + \frac{2\zeta(\Omega_1,\Omega_2,\alpha)}{\rho} + \kappa^2\right)\Theta = 0 \quad (387)$$

where

$$\zeta(\Omega_1,\Omega_2,\alpha) = \frac{Z}{\sin\alpha} + \frac{Z}{\cos\alpha} - \frac{1}{\sqrt{1-\hat{\mathbf{r}}_1\cdot\hat{\mathbf{r}}_2\sin 2\alpha}} \quad (388)$$

$$L^2 = -\frac{1}{\sin\theta}\frac{\partial}{\partial\theta}\left(\sin\theta\frac{\partial}{\partial\theta}\right) - \frac{1}{\sin^2\theta}\frac{\partial}{\partial\phi^2}. \quad (389)$$

We plug (386) into (387) to get

$$\left(\frac{\partial^2}{\partial\rho^2} + \frac{1}{\rho}\left[\frac{1}{4} - \frac{L_2^2}{\sin^2\alpha} - \frac{L_1^2}{\cos^2\alpha} + \frac{\partial^2}{\partial\alpha^2}\right] + \frac{2\zeta(\Omega_1,\Omega_2,\alpha)}{\rho} + \kappa^2\right)\Theta = 0 \quad (390)$$

Next we substitute the form:

$$\Theta(\rho,\Omega_1,\Omega_2,\alpha) = G(\rho,\Omega_1,\Omega_2,\alpha)e^{iU(\rho,\Omega_1,\Omega_2,\alpha)} \quad (391)$$

where G and U are real valued, into (390). This yields the real and imaginary parts:

$$\frac{1}{G}\left[\frac{\partial^2 G}{\partial\rho^2}+\frac{1}{\rho^2}D^2G\right]+\frac{1}{4\rho^2}=\left(\frac{\partial U}{\partial\rho}\right)^2+\frac{1}{\rho^2}(DU)^2-\left(\kappa^2+\frac{2\zeta}{\rho}\right) \tag{392}$$

with

$$D^2=-\frac{L_1^2}{\cos^2\alpha}-\frac{L_2^2}{\sin^2\alpha}+\frac{\partial^2}{\partial\alpha^2} \tag{393}$$

$$(DU)^2=(\frac{\partial U}{\partial\alpha})^2-(\frac{L_1U}{\cos\alpha})^2-(\frac{L_2U}{\sin\alpha})^2 \tag{394}$$

and

$$\frac{\partial}{\partial\rho}\left(G^2\frac{\partial U}{\partial\rho}\right)+\frac{1}{\rho^2}D(G^2DU)=0 \tag{395}$$

with

$$D=\frac{\partial}{\partial\alpha}-\frac{L_1}{\cos\alpha}-\frac{L_2}{\sin\alpha}. \tag{396}$$

L_i are the standard angular momentum operators.

So starting with the real part (392), we set the left hand side to zero (we can show later that this result will be small for large ρ). We get:

$$\left(\frac{\partial U}{\partial\rho}\right)^2+\frac{1}{\rho^2}(DU)^2=\kappa^2+\frac{2\zeta}{\rho}. \tag{397}$$

Neglecting $\frac{1}{\rho^2}(DU)^2$ as small in the first approximation means:

$$\frac{\partial U_1}{\partial\rho}=\sqrt{\kappa^2+\frac{2\zeta}{\rho}}. \tag{398}$$

Letting $x=\kappa^2\rho/\zeta$, we arrive at a first approximation of

$$U_1=\frac{\zeta}{\kappa}[\sqrt{x^2+2x}+\ln(1+x+\sqrt{x^2+2x})]+c(\Omega_1,\Omega_2,\alpha). \tag{399}$$

Putting this result into $\frac{1}{\rho^2}(DU)^2$ we see

$$\begin{aligned}\frac{1}{\rho^2}(DU_1)^2 &= \left(\frac{\kappa}{\zeta}\right)^2\left(\frac{\ln(1+x+\sqrt{x^2+2x})}{x}\right)^2(D\zeta)^2\\ &\sim \left(\frac{\kappa}{\zeta}\right)^2\left(\frac{\ln(x)}{x}\right)^2(D\zeta)^2 \text{ for } |x|\gg 1.\end{aligned} \tag{400}$$

The constant c has been left out but we can see that it is even smaller than the first term in the large x limit. This justifies our neglection of the $\frac{1}{\rho^2}(DU_1)^2$ term. We then look at the limit for (399) as $\rho\to\infty$,

$$U_1\sim\kappa\rho+\frac{\zeta}{\kappa}\ln(2\kappa^2\rho/\zeta). \tag{401}$$

Next we solve for G using (395). First we note that the outward directed current for our problem is proportional to

$$\{\Psi^* \frac{\partial \Psi}{\partial \rho} - \Psi \frac{\partial \Psi^*}{\partial \rho}\} \rho^5 \sin^2 \alpha \cos^2 \alpha d\alpha d\alpha d\Omega_1 d\Omega_2. \tag{402}$$

Using (386) and (391), we that this is equivalent to

$$\left(G^2 \frac{\partial U}{\partial \rho} \right) d\alpha d\Omega_1 d\Omega_2. \tag{403}$$

Now this should be independent of ρ asymptotically. Our final answer should be independent of radius. Thus

$$\frac{\partial}{\partial \rho} \left(G_1^2 \frac{\partial U}{\partial \rho} \right) = 0. \tag{404}$$

So using U_1, we can solve for G

$$G_1 = \frac{b(\Omega_1, \Omega_2, \alpha)}{\sqrt[4]{\kappa^2 + 2\zeta/\rho}}. \tag{405}$$

Looking at the limit as $\rho \rightarrow \infty$ we see

$$\lim_{\rho \rightarrow \infty} G \sim \kappa^{-1/2} b(\Omega_1, \Omega_2, \alpha) \text{ with } \kappa > 0. \tag{406}$$

With this result we can now illustrate that asymptotically the left hand side of (392) will be very small. The terms $\frac{1}{4\rho^2}$ and $\frac{1}{G\rho^2} D^2 G$ will of course be very small for large ρ and so can be neglected. Using (406), we also see that the remaining term, $\frac{1}{G} \frac{\partial^2 G}{\partial^2 \rho}$, will be close to zero in the asymptotic limit.

Putting (406) and (401) together we arrive at a functional form for the asymptotic behavior of the wave functions. Using the work from the finite range potentials, specifically (384), we can construct the full form of the asymptotic wave function in terms of the ionization amplitude

$$\lim_{\rho \rightarrow \infty} \Psi \sim -i^{1/2} \left(\frac{\kappa^3}{\rho^5} \right)^{1/2} f(\mathbf{k}_0, \mathbf{k}) e^{i(\kappa\rho + \frac{\zeta}{\kappa} \ln(2\kappa\rho))}. \tag{407}$$

Thus we have established an asymptotic form for the escaping electrons.

VII.3 SURFACE INTEGRAL

In Chapter 1 we showed how one could extract the ionization amplitude from the interior wave function via the flux projector method. In this section we will show

how the calculation is done in practice. This section repeats and expands on some of our recent work [95].

First we will look at the form of the interior wave function and that of the projector used to derive the ionization amplitude. We will also discuss the effect of exchange on our calculations. Then we will show how we convert the volume integral of (37) into a much simpler surface integral. Then we will examine the methods used to calculate the angular and radial portions of the integral.

Reconstructing the Interior Wave Function

Our interior solution is constructed from the pseudostate functions described in Chapter 4. The total wave function has the form:

$$\psi(\mathbf{r}_1,\mathbf{r}_2)=\frac{1}{r_1 r_2}\sum_n u^{LSP}_{nl_2,\,l_1}(r_1)\phi_{nl_2}(r_2)\Xi^{LM}_{l_1,l_2}(\hat{\Omega}_1,\hat{\Omega}_2) \tag{408}$$

where ϕ_{nl_2} are the hydrogenic radial pseudostates and where $u^{LSP}_{nl_2,l_1}$ are the channel orbitals. $\Xi^{LM}_{l_1,l_2}$ are the couple spherical harmonics as discussed in Chapter 4. The channel orbitals on the boundary are outgoing plane waves with momenta k_{nl} and weighted by the corresponding **T**-matrix element. For a target in the ground state, they are:

$$u_{nl}(r_1)=T_{1n}\frac{i^l}{\sqrt{k_{nl}}}e^{ik_{nl}r_1}. \tag{409}$$

As noted in Chapter 4, l_1 and l_2 are restricted by the boundary conditions along $r_1=r_2$, ensuring that the wave function has the proper symmetry.

Projector Wave Function

As mentioned earlier our projecting wave function is the product of two Coulomb wave functions with effective charges. The Coulomb wave function is a solution to the equation

$$[\nabla^2+\frac{2Z}{r}+k^2]\chi=0. \tag{410}$$

This equation has solutions of the form

$$\chi(Z,-\mathbf{k}|\mathbf{r})=e^{-i\mathbf{k}\cdot\mathbf{r}}\phi(\gamma,kr+\mathbf{k}\cdot\mathbf{r}) \tag{411}$$

where

$$\phi(\gamma,y)=\sqrt{\frac{2\pi\gamma}{1-\exp(-2\pi\gamma)}}e^{i\eta_0(\gamma)}{}_1F_1(i\gamma;1;iy) \tag{412}$$

with $\gamma = \frac{Z}{k}$ and $\eta_l = \arg[\Gamma(l+1-i\gamma)]$. ${}_1F_1$ is the confluent hypergeometric function. Of interest to us is that equation (410) also admits a partial wave solution of the form

$$\chi(Z,k,l,m|\mathbf{r}) = Y_{lm}(\hat{\mathbf{r}})\frac{1}{r}\mathcal{F}(Z,k,l|r) \tag{413}$$

where the function, $\mathcal{F}$, has the asymptotic form

$$\mathcal{F} \rightarrow \sin(kr - l\pi/2 + \gamma\ln(2kr) + \eta_l(\gamma)). \tag{414}$$

These two forms are related via the equation [96]

$$\chi(Z,-\mathbf{k}|\mathbf{r}) = \frac{4\pi}{k}\sum_{lm} Y_{lm}{}^*(\hat{\mathbf{k}})i^l e^{i\eta_l}\chi(Z,klm|\mathbf{r}). \tag{415}$$

Putting equations (413) and (415) together we arrive at a form for our projectors decomposed by spherical harmonics,

$$\chi(Z,-\mathbf{k}|\mathbf{r}) = \frac{4\pi}{\sqrt{k}}\sum_{lm} Y_{lm}{}^*(\hat{\mathbf{k}})Y_{lm}(\hat{\mathbf{r}})i^l e^{i\eta_l}\frac{1}{r}F_l(Z/k,k_1r_1) \tag{416}$$

where we have used that fact that asymptotically, the Coulomb wave goes as (414) with an added factor of $k^{-1/2}$. As our interior solution is already broken down into spherical harmonics, this allows for efficient extraction of the differential cross section as shown later.

Exchange Processes

Before dealing with the surface integral it is important to first discuss exchange. We have been treating the electrons as if they were distinguishable and now we need to consider spin. We first note that the electrons have spin eigenvalues of $s_z^{(2)}$ and $s_z^{(1)}$. We define $\mathbf{x_i} = (\mathbf{r}_i, s_z^{(i)})$, where $i = s$ or f, to denote both space and spin coordinates. A total spin wave function for the two electrons can be written $\chi(S, M_S|s_z^{(f)}, s_z^{(s)})$ where S takes the values, 1 and 0 and

$$\chi(S,M_s|s_z^{(1)},s_z^{(2)}) = (-)^{S+1}\chi(S,M_s|s_z^{(2)},s_z^{(1)}). \tag{417}$$

Adding this to (407), we see that the asymptotic form of the outgoing wave function is given by

$$\begin{aligned}\lim_{\rho\rightarrow\infty}\Psi \;\sim\; & -i^{\frac{1}{2}}\sqrt{\frac{X^2}{\rho^5}}\chi(S,M_S|s_z^{(1)}s_z^{(2)})f(S|\hat{\mathbf{r}}_2,\hat{\mathbf{r}}_1,\alpha) \\ & \times\exp\{i[X\rho + \frac{\Xi}{X}ln(2X\rho)]\}\end{aligned} \tag{418}$$

where

$$f(S|\hat{\mathbf{r}}_1,\hat{\mathbf{r}}_2,\alpha) = f(\hat{\mathbf{r}}_1,\hat{\mathbf{r}}_2,\alpha) + (-1)^S f(\hat{\mathbf{r}}_2,\hat{\mathbf{r}}_1,\frac{\pi}{2}-\alpha). \tag{419}$$

Note that $\tan\alpha = r_2/r_1$, consequently $\tan(\pi/2-\alpha) = \cot\alpha = r_1/r_2$, and the integral expression for $f(S|\mathbf{k}_1,\mathbf{k}_2))$ becomes

$$\begin{aligned} f(S|\mathbf{k}_f,\mathbf{k}_s) &= -\frac{1}{2}(2\pi)^{-5/2}e^{i\Delta(\mathbf{k}_f,\mathbf{k}_s)} \\ &\times \int \Phi(H-E)[\Psi(\mathbf{r}_f,\mathbf{r}_s) \\ &+ (-1)^S\Psi(\mathbf{r}_s,\mathbf{r}_f)]d^3\mathbf{r}_f d^3\mathbf{r}_s. \end{aligned} \tag{420}$$

With this form, the triple differential cross section (TDCS) then becomes

$$\begin{aligned} \frac{d^3\sigma}{d\Omega_f d\Omega_s dE} &= \frac{(2\pi)^4 k_f k_s}{4k_0}[|f(S=0|\mathbf{k}_f,\mathbf{k}_s)|^2 \\ &\quad +3|f(S=1|\mathbf{k}_f,\mathbf{k}_s)|^2]. \end{aligned} \tag{421}$$

Another way to express $f(S|\mathbf{k}_f\mathbf{k}_s)$ is [11, 97]

$$f(S|\mathbf{k}_f\mathbf{k}_s) = f(\mathbf{k}_f,\mathbf{k}_s) + (-1)^S g(\mathbf{k}_f,\mathbf{k}_s). \tag{422}$$

Thus with this small alteration to the TDCS and the calculation of f we can properly account for exchange.

Surface Integral

With these ideas in mind, we return to (37), where we have

$$\begin{aligned} f(\mathbf{k}_f,\mathbf{k}_s) &= -\frac{e^{i\Delta}}{(2\pi)^{5/2}}\int \Phi(\mathbf{k}_s,\mathbf{r}_s,\mathbf{k}_f,\mathbf{r}_f) \\ &\times (H-E)\Psi^+(\mathbf{r}_f,\mathbf{r}_s)d^3\mathbf{r}_s d^3\mathbf{r}_f \end{aligned} \tag{423}$$

and where Φ, our projector, is

$$\Phi(\mathbf{k}_s,\mathbf{r}_s,\mathbf{k}_f,\mathbf{r}_f) = \chi^*(z_s,\mathbf{k}_s,\mathbf{r}_s)\chi^*(z_f,\mathbf{k}_f,\mathbf{r}_f). \tag{424}$$

Ψ^+ is the outgoing solution of the Schrödinger's equation in the form $(H-E)\Psi^+ = 0$. In our case this is the solution from the interior region. Our Hamiltonian is

$$H = -\frac{1}{2}\vec{\nabla}^2 - \frac{1}{r_s} - \frac{1}{r_f} + V_{sf} \tag{425}$$

where $\vec{\nabla}^2 = {\nabla_f}^2 + {\nabla_s}^2$ and $\vec{\nabla} = \nabla_f + \nabla_s$.

Now we consider the function

$$\Theta = \frac{1}{2}[\Psi^+\vec{\nabla}\Phi - \Phi\vec{\nabla}\Psi^+] \tag{426}$$

then we can see that

$$\vec{\nabla}\Theta = 2\Psi^+(H-E)\Phi. \tag{427}$$

Now assuming (423) is valid in some very large volume, V, with surface, S, then we can apply the 6-dimensional analog of the divergence theorem to derive

$$f(\mathbf{k}_f,\mathbf{k}_s) = -\frac{1}{2}\frac{e^{i\Delta}}{(2\pi)^{5/2}}\oint_S[\Phi\vec{\nabla}\Psi^+ - \Psi^+\vec{\nabla}\Phi]\cdot d\mathbf{S}. \tag{428}$$

Next we define

$$\tilde{\Phi}_S = \Phi(\mathbf{r}_f,\mathbf{r}_s) + (-1)^S\Phi(\mathbf{r}_s,\mathbf{r}_f) \tag{429}$$

to account for exchange. Now (429) clearly satisfies

$$\left(-\frac{1}{2}\vec{\nabla}^2 - \left(\frac{z_s}{r_s}+\frac{z_f}{r_f}\right)\right)\tilde{\Phi}_S(\mathbf{r}_f,\mathbf{r}_s) = E\tilde{\Phi}_S(\mathbf{r}_f,\mathbf{r}_s) \tag{430}$$

so the analysis leading to (428) may be repeated, resulting in

$$f(S|\mathbf{k}_f,\mathbf{k}_s) = -\frac{1}{2}\frac{e^{i\Delta}}{(2\pi)^{5/2}}\oint_S[\tilde{\Phi}_S\vec{\nabla}\Psi^+ - \Psi^+\vec{\nabla}\tilde{\Phi}_S]\cdot d\mathbf{S}. \tag{431}$$

Using this result it is possible to determine the ionization amplitude and thus determine the TDCS as mentioned earlier.

Our choice of the surface to conduct our integral on is a 6-dimensional box. As seen in Fig. 25, the surface integral occurs along the line $r_1 = r_g$ in r_2 and $r_2 = r_g$ in r_1. Re-examining our surface integral in (431), we see that this divides the procedure into two distinct parts, a surface term and a radial integral. This division occurs because $\vec{\nabla} = \hat{\mathbf{r_1}}\nabla_1 + \hat{\mathbf{r_2}}\nabla_2$, and the surface we have chosen is always tangential to one of the those terms.

Using the form of our interior solution (408) and our projector (416), the surface integral (431) takes the form:

$$\begin{aligned} f(S|\mathbf{k}_1,\mathbf{k}_2) &= -\frac{1}{2}\frac{e^{i\Delta}}{(2\pi)^{5/2}}\sum_n\Big[\int\int d\Omega_1 d\Omega_2\Xi(\Omega_1,\Omega_2)[\chi(z_1,\mathbf{k}_1,\mathbf{r}_1)\nabla_1 u_n(r_1) \\ &\quad -u_n(r_1)\nabla_1\chi(z_1,\mathbf{k}_1,\mathbf{r}_1)]|_{r_1=\bar{r}}\int_0^{\bar{r}}\phi_n(r_2)\chi(z_2,\mathbf{k}_2,\mathbf{r}_2)dr_2 \\ &+ (-1)^S\int\int d\Omega_1 d\Omega_2\Xi(\Omega_1,\Omega_2)[\chi(z_2,\mathbf{k}_2,\mathbf{r}_1)\nabla_1 u_n(r_1) \\ &\quad -u_n(r_1)\nabla_1\chi(z_2,\mathbf{k}_2,\mathbf{r}_1)]|_{r_1=\bar{r}}\int_0^{\bar{r}}\phi_n(r_2)\chi(z_1,\mathbf{k}_1,\mathbf{r}_2)dr_2. \end{aligned} \tag{432}$$

This is the formulation used for all our calculations.

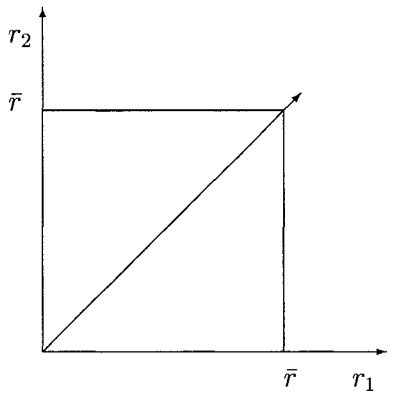

FIG. 25: A depiction of the surface integral in the radial space of the two escaping electrons. The solid line denotes the surface that the integral occurs on. As can seen it runs from 0 to $\bar{r}$ in r_2 at $r_1 = \bar{r}$ and the continues in a symmetric path for r_1.

Angular Integral

The surface integral (432) can be broken up into a radial and angular portion by expanding the projecting wave function in spherical harmonics as shown in (416). We know that Ξ is

$$\Xi^{L0}_{l_a,l_b}(\hat{\Omega}_1,\hat{\Omega}_2) = \sum_{m=-l_{\min}}^{l_{\min}} C(l_a l_b m{-}m, L0) Y_{l_a m}(\hat{\mathbf{r}}_1) Y_{l_b -m}(\hat{\mathbf{r}}_2) \tag{433}$$

where $l_{\min}$ is the smaller of l_a and l_b.

We can combine this with the angular portion of our projector to derive an analytic solution to these integrals. For an integral over a single channel n, the angular integrals reduce to

$$\begin{aligned}\int d\Omega_1 d\Omega_2 \Xi^{L0*}_{l_a l_b}(\hat{\Omega}_1,\hat{\Omega}_2)\Phi(\mathbf{r}_1,\mathbf{r}_2) = \frac{(4\pi)^2}{r_1 r_2\sqrt{k_1 k_2}} \sum_{m=-l_{\min}}^{l_{\min}} Y^*_{l_a m}(\hat{\mathbf{k}}_1) Y^*_{l_b -m}(\hat{\mathbf{k}}_2) \\ \times e^{i\sigma(\gamma_1)+i\sigma(\gamma_2)} i^{l_a+l_b} F_{l_a}(\gamma_1,-k_1 r_1) F_{l_b}(\gamma_2,-k_2 r_2) C(l_a l_b m{-}m, L0)\end{aligned} \tag{434}$$

where we have made use of the orthogonality properties of the spherical harmonics. This provides us with a straightforward and efficient way to calculate the this portion of the integral.

Radial Integral

The radial part of the integral is broken up into a constant surface term and a radial integral in one coordinate. The radial integral is simply

$$\int_0^{\bar{r}} \phi_n(r_2) F_{l_b}(\gamma_2, -k_2 r_2) dr_2 \tag{435}$$

and is sufficiently non-oscillatory that it may be accurately calculated via a 5-point Simpson's rule (Boole's rule). The surface term is equally simple

$$F_{l_a}(\gamma, -kr_1)\nabla_1 u_n(r_1) - u_n(r_1)\nabla_1 F_{l_a}(\gamma, -kr_1)|_{r_1=\bar{r}} \tag{436}$$

where as indicated the entire expression is evaluated at the final radius.

VII.4 SUMMARY

We have shown how to use the propagated **R**-matrix to connect our results to the asymptotic regions. In the $1e^-$ asymptotic region, we showed how to calculate the **S**, **K**, and **T**-matrices. We then showed how these are used to construct the cross sections and phase shifts for scattering.

In the $2e^-$ asymptotic region, we derived the RSP wave function for the escaping electrons. We have also derived and detailed a surface integral that allows us to determine the ionization amplitude and using that to calculate the Triple Differential Cross Section.

CHAPTER VIII

POET-TEMKIN MODEL

In this chapter we provide a proof of principle for our X2e method. This takes the form of the simplified case called the Poet-Temkin model. Derived by Temkin [10] and extended by Poet [9], this model has been examined extensively using variational methods [98, 99] as well as several numerical methods, in the case of elastic scattering, excitation and double ionization [36, 100, 101, 102]. This makes it a perfect first test of the method by providing us with ample comparison while at the same time reducing the computational complexity.

The crux of the Poet-Temkin model is a simplification of the three body problem via the elimination of higher angular momenta. This was undertaken historically to establish a lower bound on cross sections results for electron scattering. As argued by Temkin [10], progress in theoretical calculations of electron scattering was hampered by a lack of a minimum principle to establish limits (upper or lower) on the values of phase shifts and other descriptors of the scattering process. To establish this lower bound he investigated a simplified model of the scattering problem.

The true importance of the Poet-Temkin model for us however is that which drew Poet to the problem. His interest was drawn to the possibility of using the simplified case as a test of pseudostate bases. Though one could test the completeness of a basis by examining its polarizability (for example via the real part of the second Born term) [103], this crucially fails to take into account the correlation effects between elements of the pseudostate basis. These effects turn out to have substantial effect of the usefulness of the basis [104]. Thus by making use of this simplified model we gain a much better test of the effectiveness of our basis.

For the X2e method, this simplified model also allows us to test the method without the additional complication and computational effort of the higher order momentum states. Below we will examine Temkin and Poet's original derivations. In the second section we will compare the $\mathcal{R}$-operator calculations for phase shift and cross section to those of other methods for this special case. We also calculate elastic phase shifts for the full problem as a test of our method.

VIII.1 POET-TEMKIN MODEL

In this section we examine the theory behind the Poet-Temkin model and illustrate how it simplifies the calculation of the total scattering (or ionization) wave function and the associated cross sections and scattering phase shifts.

As mentioned earlier, Temkin proposed the zeroeth order solution to establish a lower limit on the size of the scattering phase shift. He began with the three body Schrödinger's equation confined to a plane [105]:

$$\Big\{-\frac{1}{2r_1}\frac{\partial^2 r_1}{\partial r_1^2}-\frac{1}{2r_2}\frac{\partial^2 r_2}{\partial r_2^2}-\left(\frac{1}{r_1^2}+\frac{1}{r_2^2}\right)\frac{1}{\sin\theta_{12}}\frac{\partial}{\partial\theta_{12}}\sin\theta_{12}\frac{\partial}{\partial\theta_{12}} + \frac{Z}{r_1}+\frac{Z}{r_2}+\frac{1}{r_{12}}-E\Big\}\Psi(r_1,r_2,\theta_{12})=0 \tag{437}$$

where θ_{12} is the angle between the two electrons. His next step was to expand the wave function in terms of Legendre polynomials:

$$\Psi(r_1,r_2,\theta_{12})=\frac{1}{r_1 r_2}\sum_{l=0}^{\infty}(2l+1)\Phi_l(r_1,r_2)P_l(\cos\theta_{12}) \tag{438}$$

where $\Phi_l(r_1,0)=\Phi_l(0,r_2)=0$ to ensure the proper boundary condition at the origin. This is to account for the factor of $1/r_1r_2$ in our wave function Ψ. Substituting this into Schrödinger's equation and restricting the problem to Hydrogen ($Z=1$) gives a set of coupled equations:

$$\Big\{\frac{\partial^2}{\partial r_1^2}+\frac{\partial^2}{\partial r_2^2}-l(l+1)\left(\frac{1}{r_1^2}+\frac{1}{r_2^2}\right)+\frac{2}{r_1}+\frac{2}{r_2} +E-M_{ll}\Big\}\Phi(r_1,r_2)=\sum_{m=0}^{\infty}M_{lm}\Phi_m(r_1,r_2). \tag{439}$$

Note that we have multiplied equation (437) by 2 on both sides to simplify the final formula. M_{lm}, in the region $r_1>r_2$, is defined as

$$M_{lm}=(2l+1)^{1/2}(2m+1)^{1/2}\sum_{n=0}^{l+m}\frac{r_2^n}{r_1^{n+1}} \times\int_0^{\pi}P_l(\cos\theta)P_m(\cos\theta)P_n(\cos\theta)\sin\theta d\theta. \tag{440}$$

The wave function is restricted by the condition that it be symmetric or antisymmetric with the switch of the two electrons. In the case we have thus presented, this switch results results in the exchange of coordinates $r_1\leftrightarrow r_2$ and $\theta_{12}\leftrightarrow+\theta_{12}$. For

the symmetric case this means that the wave function should be perfectly reflected in the line $r_1 = r_2$, or

$$\Phi^{\text{sym}}(\mathbf{r}_1, \mathbf{r}_2) = \Phi^{\text{sym}}(\mathbf{r}_2, \mathbf{r}_1) \tag{441}$$

More over the total wave function must converge smoothly along that line with no discontinuity in the derivative. In other words there should be a local extremum along that line at all points. One way to approach this is to require that the difference between the derivative of the wave function on both sides of the boundary goes to zero as you converge on the line. To simplify matters if we conduct our derivative along the line normal to the line $r_1 = r_2$, we get the simplest expression of this, the singlet, boundary condition.

In the case of antisymmetric wave functions the value of the wave function on one side of the line $r_1 = r_2$ is reversed in sign to that on the other side, or

$$\Phi^{\text{anti}}(\mathbf{r}_1, \mathbf{r}_2) = -\Phi^{\text{anti}}(\mathbf{r}_2, \mathbf{r}_1) \tag{442}$$

This merely requires that the wave function go to zero along that line. These two arguments yield the following boundary conditions along the region $r_1 = r_2$:

$$\Phi_l(r_1, r_2)|_{r_1=r_2} = 0, \text{ triplet} \tag{443}$$

$$(\partial/\partial n)\Phi_l(r_1, r_2)|_{r_1=r_2} = 0, \text{ singlet} \tag{444}$$

where $\partial/\partial n$ is the normal derivative along $r_1 = r_2$. Additionally as mentioned earlier there is the boundary condition that the wave function ϕ_l goes to zero as $r_1, r_2 \to 0$ that must be accounted for so that the total wave function is regular at the origin.

In his original paper, Temkin restricted the problem to elastic scattering on the ground state. This establishes an asymptotic condition that the wave function is also required to go to zero for $l > 0$ as the scattered electron goes out to infinity. For $l = 0$ Temkin states this restriction as

$$\lim_{r_1 \to \infty} \Phi_0(r_1, r_2) = \sin(kr_1 + \delta) R_{1s}(r_2) \tag{445}$$

where δ is the phase shift, k is the momentum of the scattered electron, and R_{1s} is the Hydrogen ground state. The problem as a whole is restricted to a region where $r_1 \geq r_2$. Using the symmetric properties of the wave function about the line $r_1 = r_2$, this yields the correct overall solution for all regions.

The zeroth order solution for s-wave scattering involves neglecting the right hand side of (439) and restricting the problem to $l = 0$. In this case

$$M_{ll} = (2l+1)\sum_{n=0}^{2l} \frac{r_2^n}{r_1^{n+1}} \int_0^\pi P_l(\cos\theta) P_l(\cos\theta) P_n(\cos\theta) \sin\theta d\theta \tag{446}$$

reduces to

$$\begin{aligned} M_{00} &= \frac{1}{r_1} \int_0^\pi P_0(\cos\theta) P_0(\cos\theta) P_0(\cos\theta) \sin\theta d\theta \\ &= 2/r_1 \end{aligned} \tag{447}$$

where we have made use of the rule for integration of three spherical harmonics [106]. Thus the problem is then reduced to finding a solution to the equation

$$\left\{ \frac{\partial^2}{\partial r_1^2} + \frac{\partial^2}{\partial r_2^2} + \frac{2}{r_2} + E \right\} \Phi_0^{(0)}(r_1, r_2) = 0 \tag{448}$$

thus greatly simplifying the computational task of calculating the cross section and phase shifts. As illustrated in the next section, this allows use to derive complete analytic solutions for the individual channels that go into constructing the total wave function.

VIII.1.1 POET'S WAVE FUNCTION

It was illustrative in the course of this work to compare our $\mathcal{R}$-operator wave function to that derived for the Poet-Temkin model. The cleanest derivation of that function is via the later derivations of Poet [9]. It is also through this way that we can most clearly see how to derive the phase shift and associated cross sections.

In Poet's derivation, he expands the solution $\Phi_0^{(0)}$ into incident and reflected (or scattered) states:

$$\Phi_0^{(0)} = u_{\epsilon_0}^I + \sum C_{\epsilon\epsilon_0} u_\epsilon^R d\epsilon \tag{449}$$

where the summation includes an integration over the continuum. In practice this is only a summation over a set of pseudostates that converge on the correct wave functions with a sufficient number of channels. u^I and u^R are the incident and reflected solutions to (448), respectively, and are expressed:

$$\begin{aligned} u_\epsilon^I &= e^{-ik_1 r_1} R_\epsilon(r_2) \\ u_\epsilon^R &= e^{ik_1 r_1 + \delta_0} R_\epsilon(r_2) \quad \text{where } k_1^2 = E - \epsilon > 0 \\ u_\epsilon^R &= e^{-k_1 r_1 + \delta_0} R_\epsilon(r_2) \quad \text{where } k_1^2 = \epsilon - E \geq 0 \end{aligned} \tag{450}$$

where the reflected solutions correspond to open and closed channels, respectively. Note that we have altered our asymptotic conditions for this variant of the model. The scattered electron is treated as a plane wave. The hydrogenic wave functions, $R_\epsilon(r_2)$, are

$$R_\epsilon(r_2) = r_2 e^{-qr_2} {}_1F_1(1-(1/q), 2; 2qr_2) \tag{451}$$

where $q^2 = -\epsilon$, and

$$\begin{aligned} q &= 1/n \quad \text{for a bound state where } n = 1, 2, 3, ... \\ q &= \pm ik_2 \quad \text{for a free state,} \end{aligned} \tag{452}$$

This can be characterized, at least for the free states, as the product of a plane wave and a Coulomb wave.

These functions satisfy (448) but to satisfy the boundary condition on the line $r_1 = r_2$ we need to use a linear combination of these separable solutions. To achieve this Poet used a variational method. He defined functions $v(r_1)$ for the singlet and triplet cases

$$v(r_1, r_2)|_{r_1=r_2} = u, \text{ triplet} \tag{453}$$

$$v(r_1, r_2)|_{r_1=r_2} = \left(\frac{\partial u}{\partial r_1} - \frac{\partial u}{\partial r_2}\right), \text{ singlet.} \tag{454}$$

These functions should go to zero for the correct solution along the border. Equivalently the function,

$$\chi = v^I_{\epsilon_0} + \sum C_{\epsilon\epsilon_0} v^R_\epsilon d\epsilon \tag{455}$$

should equal 0. With this in mind we see the integral over $|\chi|^2$ will also be zero, i. e.

$$I = \int_0^\infty |\chi|^2 dx = 0. \tag{456}$$

We can then minimize that integral with respect $C_{\epsilon\epsilon_0}$, i. e.

$$\begin{aligned} \frac{\partial I}{\partial C_{\epsilon\epsilon_0}} &= \frac{\partial}{\partial C_{\epsilon\epsilon_0}} \int_0^\infty |\chi|^2 dx = 0 \\ &= \frac{\partial}{\partial C_{\epsilon\epsilon_0}} \int_0^\infty \left(v^{I*}_{\epsilon_0} + \sum C^*_{\epsilon'\epsilon_0} v^{R*}_{\epsilon'} d\epsilon\right)\left(v^I_{\epsilon_0} + \sum C_{\epsilon\epsilon_0} v^R_\epsilon d\epsilon\right) dx \\ &= \int_0^\infty \left(v^{I*}_{\epsilon_0} v^R_\epsilon + \sum C^*_{\epsilon'\epsilon_0} v^{R*}_{\epsilon'} v^R_\epsilon d\epsilon'\right) dx \end{aligned} \tag{457}$$

This is equivalent to acting on χ with $\int_0^\infty dx v^{R*}_{\epsilon'}$. This allows us to state that

$$\sum A_{\epsilon\epsilon'} C_{\epsilon'\epsilon_0} d\epsilon' = b_{\epsilon\epsilon_0} \tag{458}$$

where

$$A_{\epsilon\epsilon'} = \int_0^\infty v_\epsilon^{R*} v_{\epsilon'}^R dx \tag{459}$$

and

$$b_{\epsilon\epsilon_0} = -\int_0^\infty v_\epsilon^{R*} v_{\epsilon_0}^I dx. \tag{460}$$

If (458) is true then $\chi = 0$, establishing the minimum case and a solution that satisfies the boundary condition along $r_1 = r_2$. Crucially this give us a way to solve for the total wave function.

The integrals for A and b can be done analytically [9]. The first step in the analytic solution for $A_{\epsilon\epsilon'}$ and $b_{\epsilon\epsilon_0}$ is to restate the wave functions as

$$u = e^{-px} x e^{-qx} {}_1F_1(1-(1/q), 2; 2qx) \tag{461}$$

with $p = \pm ik_1$, for open channels, and $p = k_1$ for closed channels. q is defined as earlier. x is the radial coordinate with $x = r_1 = r_2$. To simplify notation we will define

$$X = e^{-px} \tag{462}$$

$$X' = -pe^{-px} = -pX \tag{463}$$

$$Y = xe^{-qx} {}_1F_1(1-(1/q), 2; 2qx) \tag{464}$$

Thus $u = XY$. Putting this form and its derivative into the integrals (459) and (460) we are able to derive the form for the singlet and triplet integrals. The singlet integral is:

$$\begin{aligned}
{}^1J &= \int_0^\infty dx (X_1'Y_1 - X_1Y_1')(X_2'Y_2 - X_2Y_2') e^{-x/r_c} && (465)\\
&= p_1p_2 \int_0^\infty dx e^{-x/r_c} X_1X_2Y_1Y_2 + p_1 \int_0^\infty dx e^{-x/r_c} X_1X_2Y_1Y_2' \\
&\quad + p_2 \int_0^\infty dx e^{-x/r_c} X_1X_2Y_1'Y_2 + \int_0^\infty dx e^{-x/r_c} X_1X_2Y_1'Y_2' && (466)\\
&= p_1p_2 \int_0^\infty dx e^{-x/r_c} X_1X_2Y_1Y_2 + p_1 \int_0^\infty dx e^{-x/r_c} X_1X_2Y_1Y_2' \\
&\quad + p_2 \int_0^\infty dx e^{-x/r_c} X_1X_2Y_1'Y_2 - \int_0^\infty dx e^{-x/r_c} X_1X_2Y_1''Y_2 \\
&\quad + (p_1+p_2) \int_0^\infty dx e^{-x/r_c} X_1X_2Y_1'Y_2 && (467)\\
&= p_1p_2 \int_0^\infty dx e^{-x/r_c} X_1X_2Y_1Y_2 + p_1 \int_0^\infty dx e^{-x/r_c} X_1X_2Y_1Y_2' \\
&\quad + p_2 \int_0^\infty dx e^{-x/r_c} X_1X_2Y_1'Y_2 + \int_0^\infty dx e^{-x/r_c} \frac{2}{x} X_1X_2Y_1Y_2 \\
&\quad - q_1^2 \int_0^\infty dx e^{-x/r_c} X_1X_2Y_1Y_2 + (p_1+p_2) \int_0^\infty dx e^{-x/r_c} X_1X_2Y_1'Y_2 && (468)
\end{aligned}$$

where to avoid singularities in the A integrals a cut off radius r_c is introduced, which is much larger than the radii of the low level states. The derivation above uses integration by parts twice and the formula:

$$Y_1'' + \left(\frac{2}{x} - q_1^2\right) Y_1 = 0. \tag{469}$$

Those terms resulting from the differentiation of e^{-x/r_c} are dropped as it is assumed that $1/r_c$ is small.

The triplet integrals are simply:

$${}^3J = \int_0^\infty dx e^{-x/r_c} X_1 X_2 Y_1 Y_2. \tag{470}$$

All of these integrals have the same basic form:

$$J = \int_0^\infty dx x^l e^{-rx} {}_1F_1(a_1, m_1; 2q_1 x) {}_1F_1(a_2, m_2; 2q_2 x) \tag{471}$$

which has a solution in the form of the F_2 Appell function [107]. The solution is

$$J = \frac{l!}{r^{l+1}} F_2\left(l+1, a_1, a_2, m_1, m_2; \frac{2q_1}{r}, \frac{2q_2}{r}\right). \tag{472}$$

Additionally, Appel functions of the form $F_2(m, a_1, a_2, m, m; z_1, z_2)$ can be expressed in terms of a hypergeometric function, ${}_2F_1$, by [107]

$$\begin{aligned} F_2(m, a_1, a_2, m, m; z_1, z_2) &= (1-z_1)^{-a_1}(1-z_2)^{-a_2} \\ &\quad \times {}_2F_1\left(a_1, a_2, m; \frac{z_1 z_2}{(1-z_1)(1-z_2)}\right) \end{aligned} \tag{473}$$

We can use the recurrence relations for the F_2 functions to transform the various solutions into the required form above. These recurrence relations are

$$\begin{aligned} F_2(3, a_1, a_2, 2, 2; z_1, z_2) &= (1 - \frac{1}{2}a_1 - \frac{1}{2}a_2) F_2(2, a_1, a_2, 2, 2; z_1, z_2) \\ &\quad + \frac{1}{2} a_1 F_2(2, a_1+1, a_2, 2, 2; z_1, z_2) \\ &\quad + \frac{1}{2} a_2 F_2(2, a_1, a_2+1, 2, 2; z_1, z_2) \end{aligned} \tag{474}$$

$$\begin{aligned} F_2(3, a_1, a_2, 3, 2; z_1, z_2) &= (1 - \frac{1}{2}a_2) F_2(3, a_1, a_2, 3, 3; z_1, z_2) \\ &\quad + \frac{1}{2} a_2 F_2(3, a_1, a_2+1, 3, 3; z_1, z_2) \end{aligned} \tag{475}$$

for the cases $(l, m_1, m_2) = (2, 2, 2)$ and $(l, m_1, m_2) = (2, 3, 2)$ respectively.

Using these formulae we get expressions for the singlet and triplet integrals:

$$
\begin{aligned}
{}^1J &= A\left\{p_1p_2T_1 + p_1T_2 + p_2T_3 + T_4\right\} && (476)\\
{}^3J &= AT_1 && (477)
\end{aligned}
$$

where

$$
\begin{aligned}
A &= \frac{2(1-z_1)^{-a_1-1}(1-z_2)^{-a_2-1}}{r^3} && (478)\\
T_1 &= (1-\frac{1}{2}a_1-\frac{1}{2}a_2)_1F_2(a_1,a_2,2;z)(1-z_1)(1-z_2)\\
&\quad +\frac{1}{2}a_{11}F_2(a_1+1,a_2,2;z)(1-z_2)+\frac{1}{2}a_{21}F_2(a_1,a_2+1,2;z)(1-z_1) && (479)\\
T_2 &= \frac{1}{2}r_1F_2(a_1,a_2,2;z)(1-z_1)(1-z_2)-q_2T_1\\
&\quad +(q_2-1)\Big[(1-\frac{1}{2}a_1)_1F_2(a_1,a_2+1,3;z)(1-z_1)\\
&\quad +\frac{1}{2}a_{11}F_2(a_1+1,a_2+1,3;z)\Big] && (480)\\
T_3 &= \frac{1}{2}r_1F_2(a_1,a_2,2;z)(1-z_1)(1-z_2)-q_1T_1\\
&\quad +(q_1-1)\Big[(1-\frac{1}{2}a_2)_1F_2(a_1+1,a_2,3;z)(1-z_2)\\
&\quad +\frac{1}{2}a_{21}F_2(a_1+1,a_2+1,3;z)\Big] && (481)\\
T_4 &= PT_2-q_1^2T_1+r_1F_2(a_1,a_2,2;z)(1-z_1)(1-z_2) && (482)\\
P &= \frac{1}{r_c}+p_1+p_2 && (483)\\
r &= \frac{1}{r_c}+p_1+p_2+q_1+q_2 && (484)\\
a_i &= 1-\frac{1}{q_i} && (485)\\
z_i &= \frac{2q_i}{r} && (486)\\
z &= \frac{z_1z_2}{(1-z_1)(1-z_2)} && (487)
\end{aligned}
$$

Using these formulae, we can solve for the coefficients $C_{\epsilon\epsilon_0}$ and reconstruct the wave function.

These coefficients can also be related directly to the **S**-matrix:

$$S_{ij} = -\left(\frac{k_i}{k_j}\right)^{1/2}\left(\frac{n_i}{n_j}\right)^{3/2}C_{ij} \qquad (488)$$

where j refers to the incoming state and n is the normalization for the states. The

TABLE 1: Comparison with Temkin scattering phase shift. The subscript a denotes our phase shift results using the $\mathcal{R}$-operator approach and the subscript b denotes the variational calculations of Temkin [10].

k	^1S_a	^1S_b	^3S_a	^3S_b
0.01	3.0637	3.0638	3.1181	3.1182
0.05	2.7586	2.7595	3.0242	3.0247
0.1	2.4168	2.4207	2.9075	2.9084
0.2	1.8952	1.8949	2.6778	2.6806
0.3	1.5338	1.5350	2.4611	2.4634
0.4	1.2685	1.2694	2.2579	2.2582
0.5	1.0652	1.0667	2.0706	2.0715
0.75	0.75450	0.7556	1.6804	1.6914
0.8	0.72188	0.7289	1.6151	1.6166

cross section is then:

$$Q(j \to i) = \frac{2S+1}{4k_j^2}|\delta_{ij} - S_{ij}|^2 \tag{489}$$

where S is the total spin.

From this one can also derive the **K**-matrix and thus obtain the zeroth order phase shift, δ_0. Finally as shown by Temkin [10], there is a relation between δ_0 and the true phase shift, δ:

$$\begin{aligned} \sin(\delta - \delta_0) &= -\frac{1}{k}\sum_{m=1}^{\infty}\frac{2}{\sqrt{2m+1}} \\ &\quad \times \int_0^{\infty} dr_1 \int_0^{r_1} dr_2 \Phi_0^{(0)} \frac{r_2^m}{r_1^{m+1}} \Phi_m \end{aligned} \tag{490}$$

which illustrates the minimum principle that was the initial impulse to the derivation of this model.

VIII.2 RESULTS

Here we present of preliminary results for the X2e method in comparison with the Poet-Temkin model. In our calculations this is done by limited the maximum l value for our pseudostates to zero and then proceeding as normal. In Table 1, we have replicated the Temkin's scattering phase shifts using our method. We have good agreement despite using only a small basis and a minimal final radius ($r_g = 10$ a.u.).

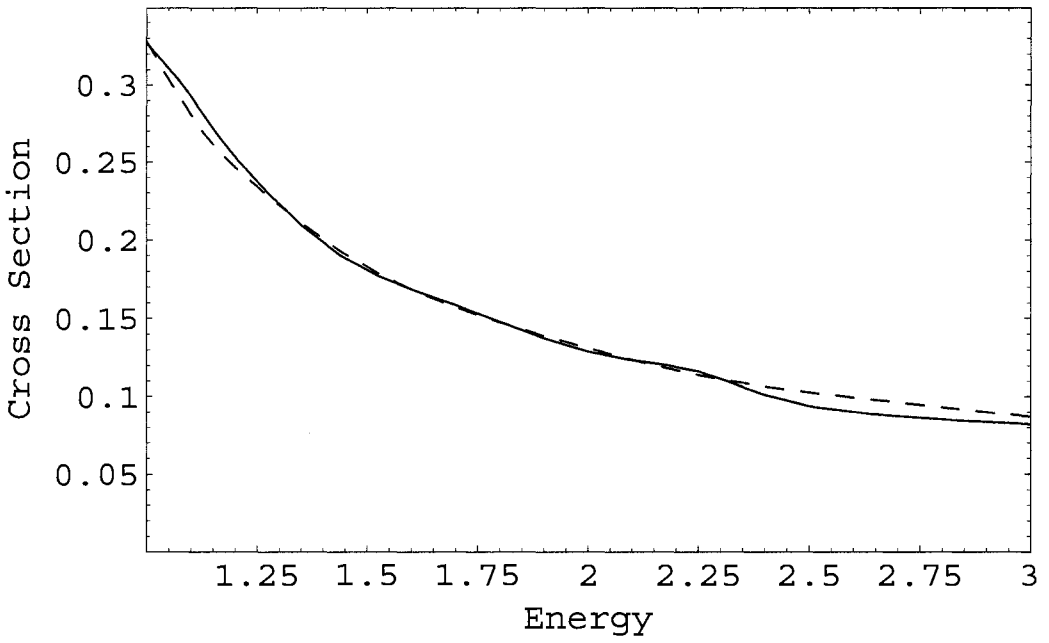

FIG. 26: Plot of $1s \rightarrow 1s$ cross sections (in πa_0^2) by X2e (solid) against those of Callaway (dashed)[99]. The energy is in terms k^2.

Figure 26 shows further results where we compare our $1S \rightarrow 1S$ cross sections for energies above threshold to the calculations of Callaway and Oza [99]. Again we use only a small basis and final radius.

We have also generated results for elastic scattering of hydrogen for energies below threshold. In Tables 2 and 3 we compare our calculations with the variational calculations of Schwartz [108], Armstead [109], and Chen [98]. We get good agreement for almost all cases except for those where the phase shift is very small.

VIII.3 SUMMARY

In this chapter we have described the Poet-Temkin model in detail. We have also presented a comparison of our results to those of other accepted theory and shown that the X2e is in excellent agreement for both phase shift calculations and total scattering cross sections. Additionally we have also provided calculation of elastic

TABLE 2: Comparison with elastic scattering phase shift. The subscript a denotes our phase shift results using the X2e method and the subscript b denotes the variational calculations of Schwartz (S) [108], Armstead (P) [109], and Chen (for $k = 0.8$) [98].

k	^1S_a	^1S_b	^3S_a	^3S_b	^1P_a	^1P_b	^3P_a	^3P_b
0.1	2.5474	2.553	2.9296	2.938	0.0041	0.0070	0.0078	0.0114
0.2	2.0601	2.0673	2.7126	2.7171	0.0110	0.0147	0.0411	0.0450
0.3	1.6903	1.6964	2.4977	2.4996	0.0439	0.0170	0.1032	0.1063
0.4	1.4097	1.4146	2.2935	2.2938	0.0082	0.0100	0.1862	0.1872
0.5	1.1961	1.202	2.1036	2.1046	-0.0023	-0.0007	0.2696	0.2705
0.6	1.0358	1.041	1.9320	1.9329	-0.0133	-0.009	0.3449	0.3412
0.7	0.92504	0.930	1.7786	1.7797	-0.0171	-0.0013	0.3913	0.3927
0.8	0.87506	0.886	1.6426	1.643	-0.0096	-0.007	0.4251	0.426

TABLE 3: Comparison with elastic scattering phase shift for D waves. The subscript a denotes our phase shift results using the R-operator approach and the subscript b denotes the variational calculations of Chen [98].

k	^1D_a	^1D_b	^3D_a	^3D_b	k	^1D_a	^1D_b	^3D_a	^3D_b
0.1	0.0010	0.0011	0.0008	0.0012	0.5	0.0264	0.027	0.0291	0.030
0.2	0.0034	0.0056	0.0012	0.0059	0.6	0.0375	0.038	0.0416	0.042
0.3	0.0087	0.011	0.0087	0.011	0.7	0.0514	0.052	0.0546	0.055
0.4	0.0176	0.018	0.0178	0.019	0.8	0.0719	0.074	0.0675	0.069

scattering phase shifts for Hydrogen in comparison with the best variational calculations. In this case we again have good agreement. The good agreement with the Poet-Temkin model proves that the basic techniques and structure of X2e method are functioning as they should and that we can expect that this method can successfully applied to calculations of the full $(e, 2e)$ TDCS. Further proofs of individual parts of the X2e method will be presented in the next chapter.

CHAPTER IX

TESTS OF THE $X2E$ METHOD

Thus far we have shown the details of the X2e method and in Chapter 8 showed some preliminary results that illustrate the method's validity. In this chapter we will examine several tests of the method that indicate key calculations are done correctly. We will also discuss what work is still necessary to bring the method to fruition.

First we show the convergence of our 1 electron pseudostates to the true bound and continuum electron wave functions for hydrogen. This will be done both for the Sturmian basis and the spline delta basis. We will also present the stability of the modified Light Walker propagation technique and discuss whether we have truly reached the asymptotic region.

In the second section, we will discuss what problems remain with the X2e method and what further work is necessary to correct for these issues. We will discuss two methods this might be accomplished and outline how this might be implemented.

IX.1 TESTS OF THE $X2E$ METHOD

In constructing the X2e method we conducted many tests of individual subroutines. Here we will present several results that clearly indicate that certain key section of the method are performed correctly.

First we examine the 1 electron pseudostates. In the case of the correct result these should converge on the correct bound states of the hydrogen wave functions. Figure 27 shows a comparison of the pseudostates in the spline delta basis to the theoretical results for hydrogen [73]. There is no difference between the two curves, proving that our $1e^-$ pseudostates have converged. As another test we also note that for the cases in Fig. 27, the energies for the bound states have converged onto the true bound states. That is for the $1s$ state $E_1 = 0.5$ atomic units and on up to the $5s$ state which is $E_5 = 0.1$ atomic units.

The picture is a little different for the Sturmian basis. In Fig. 28, we can see a comparison between the first two bound states and the pseudostates generated with the Sturmian basis. Due to the limits of the Sturmian basis, we are limited to a radius of only 10 atomic units and the limitations this imposes can be seen in the discrepancies in the $2s$ curve. This distorts not only the shape of the curve but also

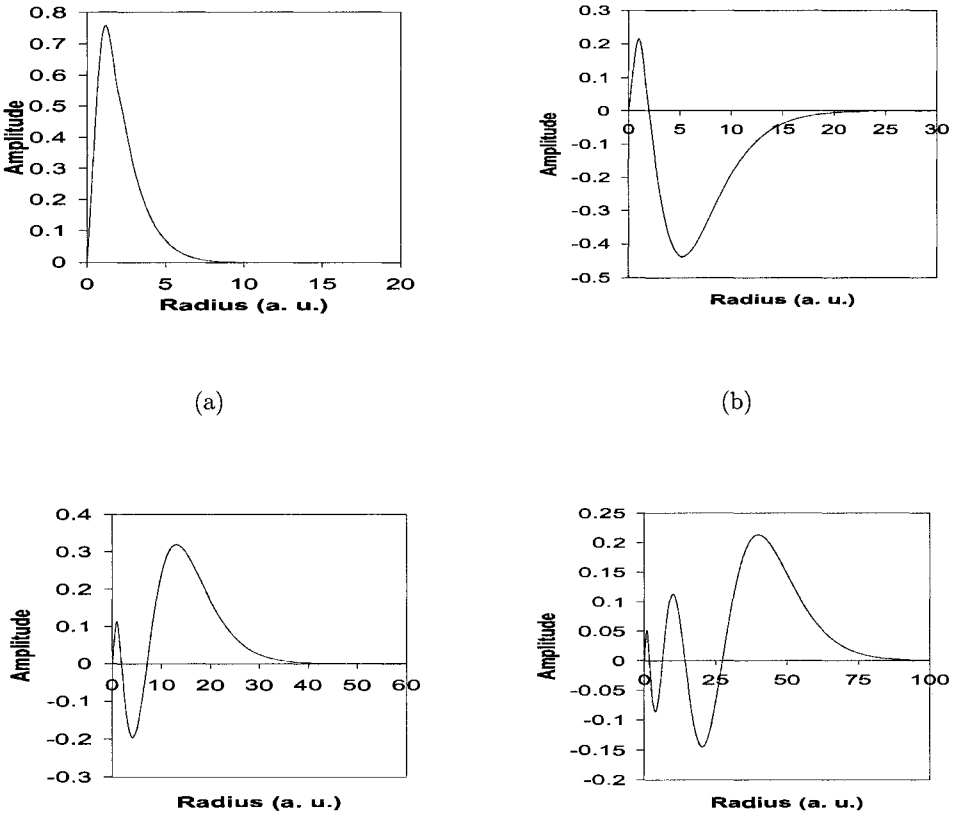

FIG. 27: Comparison of $1e^-$ spline delta pseudostates against the corresponding hydrogen bound states. Here we compare the pseudostates (dashed lines) against the radial portion of the bound states (solid lines) for (a) $1s$, (b) $2s$, (c) $3s$ and (d) $5s$ states. These calculations were done with an impact energy of 1.1 atomic units and a radius of 100 atomic units.

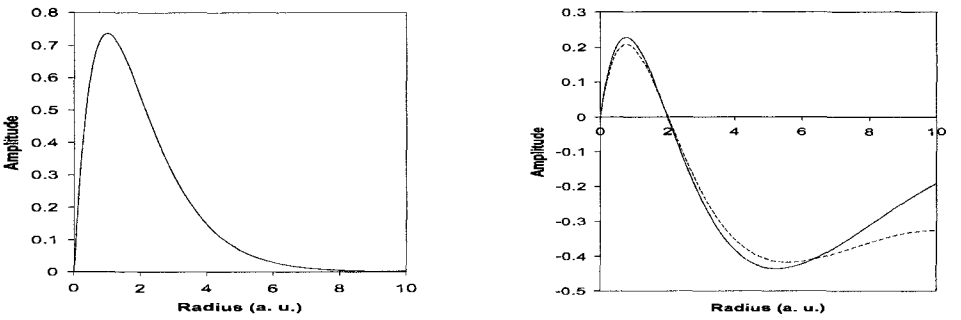

(a) (b)

FIG. 28: Comparison of $1e^-$ Sturmian pseudostates against the corresponding hydrogen bound states. Here we compare the pseudostates (dashed lines) against the radial portion of the bound states (solid lines) for $1s$ (left) and $2s$ (right) states. These calculations were done with an impact energy of 1.1 atomic units and a radius of 10 atomic units.

throws off the bound state energy. For the $2s$ state this yields an energy value of 0.134 atomic units verses the standard value of 0.125 atomic units. The squeezing of the state due to the small radius causes this effect. This problem will be discussed further in the next section. We note however that we can get good agreement with the ground state.

We have also performed a number of tests of the modified Light Walker propagation method to ensure stability. In Table 4 we show the propagation of the results for a calculation at $r_g = 40$ in the Poet-Temkin model with an impact energy of $k = 1.1$ atomic units. In normal calculation the **R**-matrix would be propagated from $\bar{r}$ to r_g and the cross sections determined at the final radius. For the results shown in Table 4, we truncated the propagation artificially and generated the results at an intermediate radius. Thus they are all generated with the same set of pseudostates. As the table shows the results are relatively stable. Some limited variance can be attributed to the fact that the sector size is constant throughout and hence our assumption that the potential is slowly varying may not be accurate. this could be solved by using a variable sector size. For the $3s$ results we note that we are not able to generate converged results. The reasons for this are discussed in the next section and are tied

TABLE 4: A test of the stability of the modified Light Walker technique. Shown are the elastic and inelastic cross sections at various 'final' radii. The results are generated in the Poet-Temkin model with an impact energy of $k = 1.1$ atomic units with the actual final radius of $r_g = 40$. The other values are generated by truncating the propagation early and generating the final cross section results.

σ	$r_g = 12$	$r_g = 14$	$r_g = 16$	$r_g = 30$	$r_g = 40$	σ_T
1s	0.252	0.252	0.252	0.245	0.243	0.244
2s	0.033	0.033	0.034	0.038	0.039	0.035
3s	0.00084	0.00068	0.00065	0.00013	0.00054	0.008

to the squeezing of the inner region states.

Lastly we explored the question of what is the limit for the asymptotic behavior of our wave functions. That is, what is the minimum distance at which we need to be to have the correct final state behavior. To determine this we explored using several formulations of the final channel wave functions u_μ. In Chapter 7 we presented an extreme asymptotic form of a plane wave in equation (409). But one could also use the obvious Coulomb wave function $\mathcal{F}$ or its asymptotic form,

$$\mathcal{F} \rightarrow \sin(kr - l\pi/2 + \gamma \ln(2kr) + \eta_l(\gamma)). \tag{491}$$

where $\gamma = \frac{Z}{k}$, $\eta_l = \arg[\Gamma(l + 1 - i\gamma)]$, and l is the angular momentum. There is also an asymptotic expansion used in the FARM (Flexible Asymptotic R-Matrix) package [110] and based on an asymptotic expansion developed by Gailitis and others [111, 112]. All of these were used and compared with each other for several different cases. In all cases the results were found to be identical thus showing that we were indeed in the asymptotic regime even at a minimal radius of a few tens of atomic units.

IX.2 AREAS FOR FURTHER WORK

Despite the good results for elastic scattering and the Poet-Temkin model, there is much work that needs to be done to allow X2e method to calculate accurate TDCS. The previous section shows us that the issues do not lie in the pseudostate bases themselves or in the propagation techniques. On the other hand we can see that we are failing to get convergence for the total cross sections for inelastic collisions despite good convergence for the $1e^-$ pseudostates. This issue also ruins our TDCS,

regardless of whether we use the flux projector method outlined in Chapter 7 or the pure flux method of Chapter 1.

The cause of this failure is due to the limited size of the interior region. Specifically the fact that the Sturmians quickly develop false linear dependencies due to our computational limits, means that the $2e^-$ pseudostates (which are calculated entirely in the Sturmian basis) are grossly wrong for any state above the ground state. This is understandable in light of the squeezing we see for the $1e^-$ pseudostates for the Sturmians in Fig. 28. It is important to note that the $2e^-$ pseudostates which are used to construct the **R**-matrix and hence the issue propagates despite our change of basis.

There are several ways this problem can be rectified. The easiest conceptually is to expand the interior region. This can be done by replacing the Sturmians with a more robust basis. The logical candidate is the spline delta basis. In retrospect it is lamentable that we discovered this basis so late in the design process while at the same time failing to account for the pervasive influence of the Sturmian's failure. Replacing the Sturmians with the spline delta basis will remove the linear dependencies that limit the size of the inner region. We can then construct an initial **R**-matrix on a much larger initial radius with much improved results for the $2e^-$ pseudostates. It may even prove unnecessary for us to propagate further.

The other possible solution is to follow the example of Malegat. The hypersphrical **R**-matrix with semiclassical outgoing waves method [40, 41, 42] uses an internal region of roughly the same size as ours. Their region is highly inaccurate for anything beside total cross section and elastic scattering, thus even less accurate than ours. They deal with the issue via their propagation technique which carries to the solution to millions of atomic units. Essentially they account for the missing internal information by accounting for the final coulomb interactions to a much higher degree.

It should be possible for us to propagate our result further as well. Currently we are limited to 100 atomic units due to the memory structure used in the X2e code (which consists of a large dynamical array). If we could restructure that memory to allow for an arbitrary number of propagation regions we should be able to propagate far enough to achieve convergence of the TDCS despite the flaws of our inner region.

Both these methods should allow the X2e method to generate accurate TDCS. Both require substantial effort to bring the method to completion but given the advantages of this method in terms of flexibility of target and kinematics, they are

well worth pursuing.

IX.3 SUMMARY

In this chapter we presented tests for intermediate portions of the X2e code. We showed the convergence of the 1 electron pseudostates to the bound and continuum states of hydrogen, both for the Sturmian and spline delta basis. We tested the stability of the modified Light Walker propagation technique and showed that we had indeed reached the asymptotic region as far as our projectors and outgoing wave function was concerned.

We also discussed how the failure for the $2e^-$ pseudostates to converge limits our ability to calculate the TDCS. We explained how the limited size of the inner region generated inaccuracies in the pseudostates that make up the basis of the **R**-matrix. Faced with this, we discussed two methods that can rectify these problems. We described how replacing the Sturmian basis would improve the 2 electron wave function by increasing a larger more complete inner region. We also pointed out that the properties of the spline delta basis would make it ideal for constructing this larger interior region and thus allowing for greater convergence of the final wave function. We also noted that we could use our current small and limited inner region and instead modify the code for a much larger propagation region and thereby extract an accurate TDCS.

Ultimately by pursuing some combination of these corrections, the X2e method will reach fruition. We note that the X2e method is readily applicable to $(e, 2e)$ for hydrogenic ions and there exists easily implementable subroutines (discussed in [15]) that will allow the X2e method to be applied to $(\gamma, 2e)$ for helium and helium-like targets. Thus with completion of this (substantial) work the X2e method with be able to provide an efficient and flexible method of calculating $(e, 2e)$ and $(\gamma, 2e)$ TDCS for a wide variety of systems.

CHAPTER X

CONCLUSIONS

In this thesis we investigated electron impact ionization using a several methods. We first examined the problem using first order perturbation calculations such as the Distorted Wave Born Approximation (DWBA). We used this method to calculate the TDCS for $(e, 2e)$ processes for inner shell ionization of Argon in both the $2s$ and $2p$ case as well as for inner and outer shell ionization of Magnesium (for $3s$ and $2p$). In both cases our results compared well with experiment, particularly the recent data for Magnesium [48, 60]. We were able to use the plane wave born approximation to show that the trough in the recoil peak was in fact due to the momentum distribution of the target wave function.

We were also able to use the DWBA to examine hydrogen-like and helium-like ions near threshold. In particular because of the simple approximations used we were able to examine the dominate processes that caused the central peak in the case of $(e, 2e)$ in helium and were able to determine that it is caused by incident channel effects such as correlation and exchange despite the literature that shows that final state processes dominate at low energies.

In the second half of this thesis we developed the variational $\mathcal{R}$-operator approach, or X2e method, an *ab initio* calculation applicable to electron impact ionization and double photo-ionization for all kinematics. We gave a detailed accounting of the techniques used within the method, including derivations of the crucial theoretical concepts. We presented early results using the simplified model called the Poet-Temkin model [9, 10]. We also noted the current limitations of the X2e method due to the limited size of the inner region, which generates inaccuracies in the pseudostates that make up the basis of the $\mathbf{R}$-matrix.

We have outlined two methods of rectifying these problems, either implementing the spline delta basis throughout the inner region , replacing the Sturmian basis or by modifying the code for a much larger propagation region. Either of these corrections will allow us to calculate accurate TDCS for $(e, 2e)$ for hydrogen. The X2e method is already readily applicable to $(e, 2e)$ for hydrogenic ions and the necessary subroutines for $(\gamma, 2e)$ on helium already exist [15]. It is easy to see that with the implementation of these (non-trivial) corrections the X2e method with be an efficient and flexible method of calculating TDCS $(e, 2e)$ and $(\gamma, 2e)$ for a wide variety of systems in

relatively short order. The computational savings over other methods should prove extremely useful in the quest to extend *ab initio* calculations to more complex target atoms and ions.

BIBLIOGRAPHY

[1] C. T. Whelan, in *(e,2e) in New Directions in Atomic Physics*, edited by C. T. Whelan *et al.* (Kluwer/Plenum, New York, 1999) p87.

[2] http://www.gsi.de/fair/

[3] E. Hinnov, in *Atomic Physics of Highly Ionized Atoms*, edited by R. Marrus (Plenum Press, New York, 1983), p.49.

[4] M. E. Foord, S. H. Glenzer, R. S. Thoe, K. L. Wong, K. B. Fournier, B. G. Wilson, and P. T. Springer, *Phys. Rev. Lett.* **85**, 992 (2000).

[5] D. E. Osterbrock *Astrophysics of Gaseous Nebulae and Active Galactic Nuclei*, (University Science Books, Mill Valley, CA, 1989).

[6] I. E. McCarthy and E. Weigold, *Rep. Prog. Phys.* **51**, 299 (1998).

[7] G. C. King and L. Avaldi, *J. Phys. B* **31**, R215 (2000).

[8] P. J. Marchalant, C. T. Whelan, and H. R. J. Walters, *J. Phys. B* **31**, 1141 (1998).

[9] R. Poet, *J. Phys. B* **11**, 3081 (1978).

[10] A. Temkin, *Phys. Rev.* **126**, 130 (1962).

[11] R. K. Peterkop, *Theory of ionization of atoms by electron impact* (Colorado Associated University Press, Boulder, 1977).

[12] M. R. H. Rudge and M. J. Seaton, *Proc. Roy. Soc. A* **283**, 262 (1965).

[13] R. K. Nesbet, *Phys. Rev. B* **30**, 4230 (1984).

[14] H. Jeffreys and B. Jeffreys, *Methods of Mathematical Physics* (Cambridge University Press, Cambridge, 1956).

[15] P. J. Roche, PhD thesis, University of Cambridge, Cambridge, 2003.

[16] X. Zhang, C. T. Whelan, H. R. J. Walters, R. J. Allan, P. Bickert, W. Hink and S. Schonberger, *J. Phys. B* **25**, 4325 (1992).

[17] H. R. J. Walters, *J. Phys. B* **6**, 1003 (1973).

[18] H. R. J. Walters, *J. Phys. B* **8**, L54 (1975).

[19] D. H. Madison, R. V. Calhoun, and W. N. Shelton, *Phys. Rev. A* **16**, 552 (1977).

[20] S. P. Lucey, J. Rasch, and C. T. Whelan, *Proc. Roy. Soc. A* **455**, 349 (1999).

[21] C. T. Whelan, R. J. Allan, and H. R. J. Walters, *J. de Physique IV* **3**, 39 (1993).

[22] C. T. Whelan, R. J. Allan, H. R. J. Walters, and X. Zhang, in *(e,2e) & related processes*, edited by C T Whelan, H. R. J. Walters, A. Lahmam-Bennani, and H. Ehrhardt (Kluwer Academic, New York, 1993), p1.

[23] H. R. J. Walters, X. Zhang, and C. T. Whelan, in *(e,2e) & Related Processes* edited by C T Whelan, H. R. J. Walters, A. Lahmam-Bennani, and H. Ehrhardt (Kluwer Academic, New York, 1993), p33.

[24] E. Clementi and C. Roetti, *Atomic Data and Nuclear Tables* **14**, 177 (1974).

[25] J. Rasch, PhD thesis, University of Cambridge, Cambridge, 1996.

[26] J. B. Furness and I. E. McCarthy, *J. Phys. B* **6**, 2280 (1973).

[27] I. Bray and A. T. Stelbovics, *Phys. Rev. Lett.* **70**, 746 (1993).

[28] I. C. Percival and M. J. Seaton, *Proc. Cambridge Phil. Soc.* **53**, 654 (1957).

[29] E. P. Curran and H. R. J. Walters, *J. Phys. B* **20**, 337 (1987).

[30] P. G. Burke and W. D. Robb, *Adv. At. Mol. Phys.* **11**, 143 (1975).

[31] D. V. Fursa and I. Bray, *Phys. Rev. A.* **54**, 2991 (1996).

[32] K. Bartschat and I. Bray, *Phys. Rev. A* **54**, R1002 (1996).

[33] T. N. Rescigno, M. Baertschy, W. A. Isaacs and C. W. McCurdy, *Science* **286**, 2474 (1999).

[34] P. L. Bartlett, A. T. Stelbovics, and I. Bray, *J. Phys. B* **37**, L69 (2004).

[35] R. Poet, *J. Phys. B* **13**, 2995 (1980).

[36] P. L. Bartlett and A. T. Stelbovics, *Phys. Rev. A* **69**, 22703 (2004).

[37] K. Bartschat, I. Bray, D. V. Fursa, and A. T. Stelbovics, *Phys. Rev. A* **76**, 024703 (2007).

[38] D. V. Fursa and I. Bray, *Phys. Rev. Lett.* **100**, 113201 (2008).

[39] E. P. Wigner and L. Eisenbud, *Phys. Rev.* **72**, 29 (1947).

[40] L. Malegat, P. Selles, and A. Kazansky, *Phys. Rev. A* **60**, 3667 (1999).

[41] L. Malegat, P. Selles, and A. Kazansky, in *Many-Particle Quantum Dynamics in Atomic and Molecular Fragmentation*, edited by J. Ullrich and V. P. Shelvelko (Berlin, Springer, Berlin , 2003), p103.

[42] A. K. Kazansky, P. Selles, and L. Malegat, *Phys. Rev. A* **68**, 052701 (2003).

[43] R. V. Calhoun, D. H. Madison, and W. N. Shelton, *J. Phys. B* **10**, 3523 (1977).

[44] A. Lahmam-Bennani, H. F. Wellenstein, A. Duguet, and A. Daoud, *Phys. Rev. A* **30**, 1511 (1984).

[45] G. Stefani, L. Avaldi, A. Lahman-Bennani and A. Duguet, *J. Phys. B* **19**, 3787 (1986).

[46] S. Cavanagh and B. Lohmann, *J. Phys. B* **30**, L231 (1997).

[47] I. Taouil, A. Duguet, A. Lahmam-Bennani, B. Lohmann, J. Rasch, C. T. Whelan, and H. R. J. Walters, *J. Phys. B* **32**, L5 (1999).

[48] P. Bolognesi *et al.*, in *Proceedings of the 9th European Conference on Atomic and Molecular Physics*, edited by D. Charalambidis, S. Farantos and P. Lambropoulos (E.P.S., 2007), TU1.

[49] H. A. Bethe, *Annalen der Physiks* **5**, 325 (1930).

[50] B. H. Bransden and C. J. Joachain, *Physics of Atoms and Molecules* (Prentice Hall, Harlow, 2003).

[51] E. Weigold and I. E. McCarthy, *Electron Momentum Spectroscopy* (Kluwer/Plenum, New York, 1999).

[52] J. Rasch *et al.*, in *Coincidence Studies of Electron and Photon Impact Ionization*, edited by C. T. Whelan and H. R. J. Walters (New York, Plenum, New York, 1997), p305.

[53] D. R. Hartree, *Proc. Comb. Phil. Soc* **89**, 111 (1928).

[54] J. C. Slater, *Phys. Rev.* **34**, 1293 (1929).

[55] C. Froese-Fischer, *The Hartree Fock Method for Atoms* (New York, Wiley, New Yrok, 1977).

[56] M. Riley and D. Truhlar, *J. Chem. Phys.* **63**, 2182 (1975).

[57] M. Riley and D. Truhlar, *J. Chem. Phys.* **65**, 792 (1976).

[58] P. Selles, A. Huetz and J. Mazeau, *J. Phys. B* **20**, 5195 (1987).

[59] J. Martinez, C. T. Whelan, and H. R. J. Walters, *Eur. Phys. J. D* **46**, 409 (2008).

[60] P. Bolognesi, L. Pravica, S. Veronesi, E. Fainelli, J. Martinez, C. T. Whelan, H. Bohachov, A. Borovik and L. Avaldi, *Phys. Rev. A* (2008, in press)

[61] J. Rasch *et al.*, *Phys. Rev. A* **56**, 1379 (1997).

[62] M. Cherid, A. Lahmam-Bennani, A. Duguet, R. W. Zurales, R. R. Lucchese, M. C. Dal Cappello and C. Dal Cappello, *J. Phys. B* **22**, 3483 (1989).

[63] C. T. Whelan *et al.*, *Phys. Rev. A* **50**, 4394 (1994).

[64] A. Müller, *Nucl. Inst. Meth. B* **87**, 34 (1994).

[65] S. Hagmann, invited talk at the *20th International Symposium on Ion-Atom Collisions*, available online at http://isiac-2007.physics.uoc.gr/XX_ISIAC_program_withPDFs.html, (2007).

[66] P. Schlemmer, T. Rösel, K. Jung, and H. Ehrhardt, *Phys. Rev. Lett.* **63**, 252 (1989).

[67] T. Rösel, J. Röder, K. Jung, H. Ehrhardt, S. Jones, and D. H. Madison, *Phys. Rev. A* **46**, 2539 (1992).

[68] H. Ehrhardt and T. Rösel, in *(e,2e) & related processes* edied by C. T. Whelan, H. R. J. Walters, A. Lahmam-Bennani, and H. Ehrhardt (Kluwer Academic, New York, 1993), pp 75.

[69] G. H. Wannier, *Phys. Rev.* **90**, 817 (1953).

[70] C. Pan and A. F. Starace, *Phys. Rev. A* **45**, 4588 (1992).

[71] J. M. Martinez, H. R. J. Walters, and C. T. Whelan, *J. Phys. B* **41**, 065202 (2008).

[72] S. Jones, D. H. Madison, and M. K. Srivastava, *J. Phys. B* **25**, 1899 (1992).

[73] D. J. Griffiths, *Introduction to Quantum Mechanics* (Addison-Wesley, New York, 2004).

[74] F. W. Byron and C. J. Joachain, *Phys. Rev. Lett.* **16**, 1139 (1966).

[75] T. Koga, H. Tatewaki and A. J. Thakkar, *Phys. Rev. A* **47**, 4510 (1993).

[76] T. J. Hawley-Jones, F. H. Read, S. Cvejanovic, P. Hammond and G. C. King, *J. Phys. B* **25**, 2393 (1992).

[77] J. W. McGowan and E. M. Clarke, *Phys. Rev.* **167**, 43 (1968).

[78] P. L. Bartlett, A. T. Stelbovics, and I. Bray, *Phys. Rev. A* **68**, 030701 (2003).

[79] E. P. Wigner, *Phys. Rev.* **73**, 1002 (1948).

[80] F. H. Read, in *Electron Impact Ionization*, edited by T. D. Märk and G. H. Dunn (Springer-Verlag, Wein, 1985), p42.

[81] K. Smith, *The Calculation of Atomic Collision Processes* (John Wiley and Sons, New Yrok, 1971).

[82] C. Bloch, *Nuclear Physics* **4**, 503 (1957).

[83] P. G. Burke and W. C. J. Noble, and P. Scott, *Proc. Roy. Soc. A* **410**, 289 (1986).

[84] G. H. Golub and C. F. Van Loan, *Matrix Computations* (John Hopkins University Press, Baltimore, 1989), section 7.7.

[85] W. Kohn, *Phys. Rev.* **74**, 1763 (1948).

[86] P. G. Burke, A. Hilbert, and W. D. Robb, *J. Phys. B* **4**, 153 (1971).

[87] P. G. Burke and W. D. Robb, *J. Phys. B* **5**, 44 (1972).

[88] P. J. A. Buttle, *Phys. Rev.* **160**, 719 (1967).

[89] J. C. Light and R. B. Walker, *J. Chem. Phys.* **65**, 4272 (1976).

[90] E. B. Stechel, R. B. Walker, and J. C. Light, *J. Chem. Phys.* **69**, 3518 (1978).

[91] R. K. Nesbet (unpublished).

[92] D. J. Zvijac and J. C. Light, *J. Chem. Phys.* **12**, 237 (1976).

[93] J. M. Blatt and L. C. Biedenharn, *Rev. Mod. Phys.* **24**, 258 (1952).

[94] I. C. Percival and M. J. Seaton, *Phil. Trans. A* **251**, 113 (1958).

[95] C. T. Whelan, R. K. Nesbet, and J. M. Martinez, *J. Elec. Spec.* **161**, 67 (2007).

[96] A. Burgess and M. R. H. Rudge, *Proc. Roy. Soc. A* **273**, 372 (1963).

[97] M. R. H. Rudge, *Rev. Mod. Phys.* **40**, 564 (1968).

[98] Ming-Ken Chen, C. D. Lin, and J. Z. Tang, *Phys. Rev. A* **56**, 2435 (1997).

[99] J. Callaway and D. H. Oza, *Phys. Rev. A* **29**, 2416 (1984).

[100] S. Jones and A. T. Stelbovics, *Aust. J. Phys.* **52**, 621 (1999).

[101] S. Jones and A. T. Stelbovics, *Phys. Rev. A* **66**, 32717 (2002).

[102] T. N. Rescigno, M. Baertschy, and C. W. McCurdy, *Phys. Rev. A* **68**, 20701 (2003).

[103] H. R. J. Walters, *Phys. Reports* **116**, 1 (1984).

[104] C. T. Whelan, M. R. C. McDowell, and P. W. Edmunds, *J. Phys. B* **20**, 1587 (1987).

[105] P. M. Morse and H. Feshbach, *Method of Theoretical Physics* (McGraw-Hill Book Company, Inc., New Yrok, 1953), p1725.

[106] G. B. Arfken and H. J. Weber, *Mathematical Methods for Physicists* (Harcourt Academic Press, San Diego, 2001).

[107] K. Alder, A. Bohr, T. Huus, B. Mottleson and A. Winter, *Rev. Mod. Phys.* **28**, 432 (1956).

[108] C. Schwartz, *Phys. Rev.* **124**, 1468 (1961).

[109] R. L. Armstead, *Phys. Rev.* **171**, 91 (1968).

[110] V. M. Burke and C. J. Noble, *Comp. Phys. Comm.* **85**, 471 (1995).

[111] M. Gailitis, *J. Phys. B* **9**, 843 (1976).

[112] C. J. Noble and R. K. Nesbet, *Comp. Phys. Comm* **33**, 399 (1984).

[113] M. E. Rose, *Elementary Theory of Angular Momentum* (Dover Publications Inc., New York, 1957).

[114] B. W. Shore and D. H. Menzel, *Principles of Atomic Spectra* (John Wiley and Sons, Inc., New York, 1968).

[115] M. Abramowitz and I. Stegun, *Handbook of Mathematical Functions* (Dover Publications, New York, 1970).

[116] W. H. Press, S. A. Teukolsky, W. T. Vetterling, and B. P. Flannery, *Numerical Recipes in Fortran 77: the Art of Scientific Computing* (Cambridge University Press, USA, 1992).

[117] H. J. Weber and G. B. Arfken, *Essential Mathematical Methods for Physicists* (Elsevier, Amsterdam, 2004).

[118] E. T. Copson, *Introduction to the Theory of Functions of a Complex Variable* (The Clarendon Press, Oxford, 1935).

[119] J. Martinez, *Nucl. Inst. Meth. B* **241**, 30 (2005).

[120] E. O. Alt and A. Mukhamedzhanov, *Phys. Rev.* A **47**, 2004 (1993).

[121] A. Engelns, H. Klar, and A. W. Malcherek, *J. Phys. B* **30**, L811 (1997).

[122] M. Brauner, J. S. Briggs, and H. Klar, *J. Phys. B* **22**, 2265 (1989).

APPENDIX A

HYPERSPHERICAL SURFACE ELEMENTS

In this appendix we show how the hyperspherical surface elements are derived. Hyperspherical coordinates transform the radial coordinates of the two escaping electrons into a hyper radius, $\rho = \sqrt{r_1^2 + r_2^2}$, and hyperspherical angle, $\alpha = \arctan(r_1/r_2)$. Beginning with the standard 6-dimensional volume integral, we have

$$\begin{aligned} d\mathbf{r}_1 d\mathbf{r}_2 &= r_1^2 r_2^2 dr_1 d\theta_1 d\phi_1 dr_2 d\theta_1 d\phi_1 \\ &= r_1^2 r_2^2 dr_1 d\Omega_1 dr_2 d\Omega_1 \end{aligned} \tag{492}$$

where Ω represents the standard spherical angles θ and ϕ. Next we note that in hyperspherical notation $r_1 = \rho\cos\alpha$ and $r_1 = \rho\sin\alpha$. This is analogous to polar coordinates and uses the same transformation. That is

$$dr_1 dr_2 = \rho d\rho d\alpha \tag{493}$$

Inserting (493) into (492) we get

$$d\mathbf{r}_1 d\mathbf{r}_2 = \rho^5 \sin^2\alpha \cos^2\alpha d\rho d\alpha d\Omega_1 d\Omega_1 \tag{494}$$

which is the 6-dimensional volume element in hyperspherical coordinates. To derive the surface element we remove differential element in ρ,

$$d\Sigma = \rho^5 \sin^2\alpha \cos^2\alpha d\alpha d\Omega_1 d\Omega_1 \tag{495}$$

Next we wish to derive a surface element that is differential in energy and the angular coordinates for use in deriving the TDCS. First we note that asymptotically $\hat{\mathbf{r}}_i = \hat{\mathbf{k}}_i$. This means that $\tan^2\alpha = k_1^2/k_2^2 = E_1/E_2$ where E_1 and E_2 are the asymptotic energies of the escaping electrons, which satisfy $E_1 + E_2 = E$. Using this result in equation (495),

$$\begin{aligned} d\Sigma &= \frac{\rho^5}{4} \sin^2 2\alpha d\alpha d\Omega_1 d\Omega_1 \\ &= \frac{\rho^5}{4} \sin 2\alpha \left(\frac{2\tan\alpha}{1+\tan^2\alpha}\right) d\alpha d\Omega_1 d\Omega_1 \\ &= \frac{\rho^5}{4} \sin 2\alpha \left(\frac{2E_2 \tan\alpha}{E_2 + E_1}\right) d\alpha d\Omega_1 d\Omega_1 \\ &= \frac{\rho^5 \sin 2\alpha}{4E} 2E_2 \tan\alpha d\alpha d\Omega_1 d\Omega_1 \end{aligned} \tag{496}$$

To simplify this we consider the derivative of $\tan^2\alpha = E_1/E_2$,

$$\begin{aligned}(\tan^2\alpha)' &= \left(\frac{E_1}{E_2}\right)' = \left(\frac{E_1}{E-E_1}\right)' \\ \frac{2\tan\alpha d\alpha}{\cos^2\alpha} &= dE_1\left(\frac{1}{E-E_1}+\frac{E_1}{(E-E_1)^2}\right) = \frac{E}{E_2^2}dE_1 \end{aligned} \tag{497}$$

We can simplify this by considering

$$\begin{aligned}\frac{E}{E_2^2} &= \frac{E_1+E_2}{E_2^2} = \left(\frac{E_1}{E_2}+1\right)\frac{1}{E_2} \\ &= \left(\tan^2\alpha+1\right)/E_2 \\ &= \frac{1}{E_2\cos^2\alpha}\end{aligned} \tag{498}$$

Substituting (498) into (497) we are able to derive

$$\frac{dE_1}{E_2\cos^2\alpha} = \frac{2\tan\alpha d\alpha}{\cos^2\alpha} \tag{499}$$

and thus

$$dE_1 = 2E_2\tan\alpha d\alpha \tag{500}$$

Finally we can use the relation (500) in (496) to get

$$d\Sigma = \frac{\rho^5}{4E}\sin 2\alpha dE_1 d\Omega_1 d\Omega_1 \tag{501}$$

which is a surface element differential in energy and angle.

APPENDIX B

ANGULAR MOMENTUM COUPLING TERMS

This appendix reviews the relations and identities for the Clebsch-Gordan coefficients as well as their relationship to the Wigner $3j$ and $6j$ symbols and the Racah W symbol [113, 114]. These coefficients are used extensively in calculating the coupling of the angular momentum terms presented throughout this thesis.

B.1 CLEBSCH-GORDAN COEFFICIENTS

The Clebsch-Gordan coefficients, $c(j_1 j_2 m_1 m_2|jm)$, are zero unless $m = m_1 + m_2$. Additionally the triangular condition, $\triangle(j_1 j_2 j_3)$, must hold:

$$j_1 \leq j_2 + j, \qquad j_2 \leq j_1 + j, \qquad j \leq j_1 + j_2. \tag{502}$$

The pertinent relationships for Clebsch-Gordan coefficients used in this thesis include:

$$c(j_1 j_2 00|j0) = 0 \quad \text{unless} \quad j_1 + j_2 + j \quad \text{is even} \tag{503}$$

$$c(j_1 j_2 m_1 m_2|jm) = (-1)^{j_2+m_2}\left(\frac{2j+1}{2j_1+1}\right)^{1/2} c(jj_2 - m - m_2|j_1 - m_1) \tag{504}$$

$$c(j_1 j_2 m_1 m_2|jm) = (-1)^{j_1+j_2-j} c(j_1 j_2 - m_1 - m_2|j - m) \tag{505}$$

$$c(j_1 j_2 m_1 m_2|jm) = (-1)^{j_1+j_2-j} c(j_2 j_1 m_2 m_1|j - m) \tag{506}$$

$$c(j_1 j_2 m_1 m_2|jm) = (-1)^{j_1-m_1}\left(\frac{2j+1}{2j_2+1}\right)^{1/2} c(j_1 j m_1 - m|j_2 - m_2) \tag{507}$$

We also make extensive use of the orthogonality relations for Clebsch-Gordan coefficients:

$$\sum_{m_1,m_2} c(j_1 j_2 m_1 m_2|jm) c(j_1 j_2 m_1 m_2|j'm') = \delta_{mm'}\delta_{jj'} \tag{508}$$

$$\sum_{j,m} c(j_1 j_2 m_1 m_2|jm) c(j_1 j_2 m_1' m_2'|jm) = \delta_{m_1 m_1'}\delta_{m_2 m_2'} \tag{509}$$

B.2 CLEBSCH-GORDAN COEFFICIENTS AND THE WIGNER $3J$ SYMBOL

The Clebsch-Gordan coefficients can be easily related to the Wigner $3j$ symbols, or Wigner coefficients, by

$$c(j_1 j_2 m_1 m_2|jm) = (-1)^{m+j_1+j_2}\sqrt{2j+1}\begin{pmatrix} j_1 & j_2 & j \\ m_1 & m_2 & -m \end{pmatrix} \tag{510}$$

and conversely,

$$\begin{pmatrix} j_1 & j_2 & j \\ m_1 & m_2 & m \end{pmatrix} = \frac{(-1)^{m+j_1-j_2}}{\sqrt{2j+1}} c(j_1 j_2 m_1 m_2|j-m) \tag{511}$$

Using the Wigner $3j$ symbols we can make use of its symmetry relations:

$$\begin{pmatrix} j_1 & j_2 & j \\ m_1 & m_2 & m \end{pmatrix} = \begin{pmatrix} j_2 & j & j_1 \\ m_2 & m & m_1 \end{pmatrix} = \begin{pmatrix} j & j_1 & j_2 \\ m & m_1 & m_2 \end{pmatrix} \tag{512}$$

$$\begin{pmatrix} j_1 & j_2 & j \\ m_1 & m_2 & m \end{pmatrix} = (-1)^{j_1+j_2+j}\begin{pmatrix} j_1 & j & j_2 \\ m_1 & m & m_2 \end{pmatrix} \tag{513}$$

$$\begin{pmatrix} j_1 & j_2 & j \\ m_1 & m_2 & m \end{pmatrix} = (-1)^{j_1+j_2+j}\begin{pmatrix} j_1 & j_2 & j \\ -m_1 & -m_2 & -m \end{pmatrix} \tag{514}$$

As well as its special cases and orthogonality relations:

$$\begin{pmatrix} j_1 & j_2 & j \\ 0 & 0 & 0 \end{pmatrix} = 0 \qquad \text{if } j_1+j_2+j \text{ is odd} \tag{515}$$

$$\sum_{j,m}(2j+1)\begin{pmatrix} j_1 & j_2 & j \\ m_1 & m_2 & m \end{pmatrix}\begin{pmatrix} j_1 & j_2 & j \\ m_1' & m_2' & m \end{pmatrix} = \delta_{m_1 m_1'}\delta_{m_2 m_2'} \tag{516}$$

B.3 CLEBSCH-GORDAN COEFFICIENTS, THE RACAH W SYMBOL AND THE WIGNER $6J$ SYMBOL

Next we relate the Clebsch-Gordan coefficients and the Racah W Symbol. This can be done via [15]

$$\begin{aligned}[(2j_5+1)(2j_6+1)]^{1/2} & W(j_1 j_2 j_3 j_4|j_5 j_6) c(j_1 m_1 j_6(m_2+m_3)|j_3 m) \\ &= \sum_{m_2} c(j_1 m_1 j_2 m_2|j_5(m_1+m_2)) c(j_5(m_1+m_2) j_4 m_3|j_3 m) \\ &\times c(j_2 m_2 j_4 m_3)|j_6(m_2+m_3)).\end{aligned} \tag{517}$$

where $m = m_1 + m_2 + m_3$. The Wigner $6j$ symbols have the following symmetry relations:

$$\left\{ \begin{array}{ccc} j_1 & j_2 & j_3 \\ j_4 & j_5 & j_6 \end{array} \right\} = \left\{ \begin{array}{ccc} j_2 & j_1 & j_3 \\ j_5 & j_4 & j_6 \end{array} \right\} = \left\{ \begin{array}{ccc} j_1 & j_3 & j_2 \\ j_4 & j_6 & j_5 \end{array} \right\} \tag{518}$$

$$\left\{ \begin{array}{ccc} j_1 & j_2 & j_3 \\ j_4 & j_5 & j_6 \end{array} \right\} = \left\{ \begin{array}{ccc} j_4 & j_5 & j_3 \\ j_1 & j_2 & j_6 \end{array} \right\} = \left\{ \begin{array}{ccc} j_1 & j_5 & j_6 \\ j_4 & j_2 & j_3 \end{array} \right\} \tag{519}$$

Additionally we can easily relate the Wigner $6j$ symbol and the Racah W symbol via

$$W(j_1 j_2 j_3 j_4 | j_5 j_6) = (-1)^{j_1+j_2+j_3+j_4} \left\{ \begin{array}{ccc} j_1 & j_2 & j_3 \\ j_4 & j_5 & j_6 \end{array} \right\} \tag{520}$$

B.4 EVALUATION OF THE INTEGRAL OF THREE SPHERICAL HARMONICS

We can use the Wigner $3j$ symbols to express the result of an integral of three spherical harmonics:

$$\int_\Omega d\Omega Y_{l_1 m_1}(\Omega) Y_{l_2 m_2}(\Omega) Y_{l_3 m_3}(\Omega) = \sqrt{\frac{(2l_1+1)(2l_2+1)(2l_3+1)}{4\pi}} \left(\begin{array}{ccc} l_1 & l_2 & l_3 \\ m_1 & m_2 & m_3 \end{array} \right) \left(\begin{array}{ccc} l_1 & l_2 & l_3 \\ 0 & 0 & 0 \end{array} \right) \tag{521}$$

APPENDIX C

BASIC RADIAL INTEGRALS

In this appendix we cover the details for the radial integrals. Specifically we show the numerical methods used to efficiently calculate these integrals.

In conducting the integrals for the Sturmian basis, we need to do numerous integrals of the form:

$$U_{\bar{r}}(n,\alpha) = \int_0^{\bar{r}} r^n e^{-\alpha r} dr \tag{522}$$

where $\alpha > 0$ and n is a positive integer (in actual calculations n was at most 30). These integrals are solved via the simple analytic formulae outlined here.

We begin by noting that the incomplete gamma function $\gamma(\alpha, x)$ is defined [115] as

$$\gamma(m,\beta) = \int_0^{\beta} e^{-x} x^{m-1} dx. \tag{523}$$

Via a change of variables, $r' = \alpha r$, we can reexpress equation (522) in terms of the incomplete gamma function. In this way $U_{\bar{r}}(n,\alpha)$ can be written:

$$\begin{aligned} U_{\bar{r}}(n,\alpha) &= \int_0^{\alpha\bar{r}} \left(\frac{r'}{\alpha}\right)^n e^{-r'} \frac{dr'}{\alpha} \\ &= \frac{1}{\alpha^{n+1}} \int_0^{\alpha\bar{r}} r'^n e^{-r'} dr' \\ &= \frac{1}{\alpha^{n+1}} \gamma(n+1, \alpha\bar{r}) \end{aligned} \tag{524}$$

The incomplete gamma function itself can be represented via a Kummer confluent hypergeometric function [115],

$$\begin{aligned} \gamma(a,x) &= a^{-1} x^a e^{-x} M(1, 1+a, x) \\ &= a^{-1} x^a M(a, 1+a, -x). \end{aligned} \tag{525}$$

We can use this to rewrite equation (524) as

$$U_{\bar{r}}(n,\alpha) = \frac{\bar{r}^{n+1}}{n+1} e^{-\alpha\bar{r}} M(1, n+2, \alpha\bar{r}). \tag{526}$$

To speed the calculation of these integrals we can make use of a downward recursion formula. This can be derived from (522) via an integration by parts,

$$U_{\bar{r}}(n,\alpha) = \int_0^{\bar{r}} r^n e^{-\alpha r} dr$$

$$= \frac{1}{\alpha}[\bar{r}^n e^{-\alpha\bar{r}} + n\int_0^{\bar{r}} r^{n-1}e^{-\alpha r}dr]$$
$$= \frac{1}{\alpha}[\bar{r}^n e^{-\alpha\bar{r}} + nU_{\bar{r}}(n-1,\alpha)] \quad (527)$$

and thus

$$U_{\bar{r}}(n-1,\alpha) = \frac{1}{n}[\alpha U_{\bar{r}}(n,\alpha) + \bar{r}^n e^{-\alpha\bar{r}}]. \quad (528)$$

To determine the initial value for our downward recursion, the particular integral $U_{\bar{r}}(n,\alpha)$ can be calculated via the closed formula finite series

$$U_{\bar{r}}(n,\alpha) = \frac{n!}{\alpha^{n+1}}[1 - e^{-\alpha\bar{r}}(1 + \alpha\bar{r} + \cdots + \frac{(\alpha\bar{r})^n}{n!})] \quad (529)$$

or by the power series

$$U_{\bar{r}}(n,\alpha) = \frac{\bar{r}^{n+1}}{n+1}e^{-\alpha\bar{r}}\sum_{k=0}^{\infty}\frac{(n+1)!}{(n+k+1)!}(\alpha\bar{r})^k. \quad (530)$$

In the limit $\bar{r} \to \infty$ however the integral is greatly simplified. In this case we have a complete gamma function and the integral becomes

$$U_{\infty}(n,\alpha) = \frac{n!}{\alpha^{n+1}}. \quad (531)$$

APPENDIX D

ANGULAR INTEGRALS

This appendix reviews the integration of coupled spherical harmonics that arise out of the evaluation of the $2e^-$ matrix elements used to construct the $\mathcal{R}$-operator. These integrals are also important when generating the radial channel solutions for propagating the wave function.

The integrals of interest are those associated with the $1/r_{12}$ operator. So first we will investigate how this operator can be expanded into spherical harmonics to allow for easier integration. In the second section we will investigate how we can perform the angular integrals associated with this integration.

D.1 TRANSFORMATION OF THE $1/R_{12}$ OPERATOR

One of the key integrals to be performed is the interaction between the two electrons, the $1/r_{12}$ potential. To aid in our integration over this term, we will expand it in terms of spherical harmonics. First we we reexpress the Coulomb interaction as

$$\begin{aligned} \frac{1}{r_{12}} &= \frac{1}{|\mathbf{r}_1 - \mathbf{r}_2|} = \frac{1}{\sqrt{r_1^2 + r_2^2 - 2r_1 r_2 \cos\theta_{12}}} \\ &= \frac{1}{r_> \sqrt{1 + (r_</r_>)^2 - 2(r_</r_>)\cos\theta_{12}}} \end{aligned} \tag{532}$$

where $r_< = \min(r_1, r_2)$ and $r_> = \max(r_1, r_2)$. θ_{12} is the angle between the two electrons. We expand this form in a Taylor series,

$$\begin{aligned} \frac{1}{\sqrt{1 + x^2 - 2x\cos\theta}} &= 1 + \cos\theta x + \frac{1}{2}(3\cos^2\theta - 1)x^2 + \ldots \\ &= \sum_{\lambda=0}^{\infty} x^\lambda P_\lambda(\cos\theta) \end{aligned} \tag{533}$$

where $P_\lambda(\cos\theta)$ are the Legendre polynomials [115]. Using equation (533) in equation (532) yields

$$\frac{1}{r_{12}} = \sum_{\lambda=0}^{\infty} \frac{r_<^\lambda}{r_>^{\lambda+1}} P_\lambda(\cos\theta_{12}). \tag{534}$$

Next we use the addition theorem of spherical harmonics [106],

$$P_\lambda(\cos\theta_{12}) = \frac{4\pi}{2\lambda + 1} \sum_{m=-\lambda}^{+\lambda} Y^*_{\lambda,m}(\theta_1, \phi_1) Y_{\lambda,m}(\theta_2, \phi_2) \tag{535}$$

in equation (534) to get

$$\frac{1}{r_{12}} = \sum_{\lambda=0}^{\infty} \frac{r_<^\lambda}{r_>^{\lambda+1}} \frac{4\pi}{2\lambda+1} \sum_{m=-\lambda}^{+\lambda} Y^*_{\lambda m}(\theta_1,\phi_1) Y_{\lambda m}(\theta_2,\phi_2) \tag{536}$$

which gives us an expression for the Coulomb interaction in terms of spherical harmonics.

D.2 ANGULAR INTEGRALS

The integral of interest to us is the angular integral over the $1/r_{12}$ operator or

$$\mathcal{I}^{L\lambda}_{abcd} = \int\int d\Omega_1 d\Omega_2 \Xi^{L*}_{ab}(\Omega_1,\Omega_2) P_\lambda(\cos\theta_{12}) \Xi^L_{cd}(\Omega_1,\Omega_2) \tag{537}$$

where Ω_n denotes the angular coordinates for the nth electron and θ_{12} is the angle between the two electrons. $P_\lambda(\cos\theta)$ are the Legendre polynomials and $\Xi^L_{ab}(\Omega_1,\Omega_2)$ are the coupled spherical harmonics, discussed in Chapter 4, which have the form

$$\Xi^L_{ab}(\Omega_1,\Omega_2) = \sum_{m_a,m_b} Y_{l_a,m_a}(\Omega_1) Y_{l_b,m_b}(\Omega_2) c(l_a l_b m_a m_b | LM). \tag{538}$$

Using equation (535) we can rewrite equation (537) as

$$\begin{aligned}\mathcal{I}^{L\lambda}_{abcd} &= \int\int d\Omega_1 d\Omega_2 \Big\{ \Xi^{L*}_{ab}(\Omega_1,\Omega_2) \left(\frac{4\pi}{2\lambda+1} \sum_{m=-\lambda}^{+\lambda} Y_{\lambda,m}(\theta_1,\phi_1) Y_{\lambda,m}(\theta_2,\phi_2) \right) \\ &\quad \times \Xi^L_{cd}(\Omega_1,\Omega_2) \Big\}. \end{aligned} \tag{539}$$

Incorporating equation (538) as well, this yields

$$\begin{aligned}\mathcal{I}^{L\lambda}_{abcd} &= \frac{4\pi}{2\lambda+1} \sum_{m_a,m_b} \sum_{m_c,m_d} \sum_{m=-\lambda}^{+\lambda} c(l_a l_b m_a m_b | LM) c(l_c l_d m_c m_d | LM) \\ &\quad \times (-1)^{m_a} \int d\Omega_1 Y_{l_a - m_a}(\Omega_1) Y_{\lambda m}(\Omega_1) Y_{l_c m_c}(\Omega_1) \\ &\quad \times (-1)^{m_b+m} \int d\Omega_2 Y_{l_b - m_b}(\Omega_2) Y_{\lambda - m}(\Omega_2) Y_{l_d m_d}(\Omega_2) \end{aligned} \tag{540}$$

where we have made us of the relation $(-1)^{-m} Y_{l-m} = Y^*_{lm}$. Next we use equation (521), to evaluate the integrals over three spherical harmonics in terms of Wigner $3j$ symbols. This yields

$$\mathcal{I}^{L\lambda}_{abcd} = \frac{4\pi}{2\lambda+1} \sum_{m_a,m_b} \sum_{m_c,m_d} \sum_{m=-\lambda}^{+\lambda} c(l_a l_b m_a m_b | LM) c(l_c l_d m_c m_d | LM)$$

$$\times(-1)^{m_a+m_b+m}\sqrt{\frac{(2l_a+1)(2\lambda+1)(2l_c+1)}{4\pi}}$$
$$\times\begin{pmatrix} l_a & \lambda & l_c \\ -m_a & m & m_c \end{pmatrix}\begin{pmatrix} l_a & \lambda & l_c \\ 0 & 0 & 0 \end{pmatrix}\sqrt{\frac{(2l_b+1)(2\lambda+1)(2l_d+1)}{4\pi}}$$
$$\times\begin{pmatrix} l_b & \lambda & l_d \\ -m_b & -m & m_d \end{pmatrix}\begin{pmatrix} l_b & \lambda & l_d \\ 0 & 0 & 0 \end{pmatrix} \tag{541}$$

The Wigner $3j$ symbols can then be expressed in terms of Clebsch-Gordan coefficients. Using equation (511) in equation (541) we get

$$\begin{aligned}\mathcal{I}^{L\lambda}_{abcd} &= \sum_{m_a,m_b}\sum_{m_c,m_d}\sum_{m=-\lambda}^{+\lambda} c(l_a l_b m_a m_b|LM)c(l_c l_d m_c m_d|LM)\\ &\quad\times(-1)^{m_a+m_b+m_c+m_d+m}\sqrt{\frac{(2l_a+1)(2l_b+1)}{(2l_c+1)(2l_d+1)}}\\ &\quad\times c(l_a\lambda - m_a m|l_c - m_c)c(l_a\lambda 00|l_c 0)\\ &\quad\times c(l_b\lambda - m_b m|l_d - m_d)c(l_b\lambda 00|l_d 0)\end{aligned} \tag{542}$$

Next we note that $m_a + m_b = M$ and $m_c = m_d = M$. This reduces the exponent of (-1) in equation (542) to simply m. Next we rearrange the fifth and sixth Clebsch-Gordan coefficients using equation (504). This adds another factor of $(-1)^m$ yielding

$$\begin{aligned}\mathcal{I}^{L\lambda}_{abcd} &= \sum_{m_a,m_b}\sum_{m_c,m_d}\sum_{m=-\lambda}^{+\lambda} c(l_a l_b m_a m_b|LM)c(l_c l_d m_c m_d|LM)\\ &\quad\times\sqrt{\frac{(2l_a+1)(2l_b+1)}{(2l_c+1)(2l_d+1)}}c(l_a\lambda - m_a m|l_c - m_c)c(l_a\lambda 00|l_c 0)\\ &\quad\times c(l_d\lambda m_d m|l_b m_b)c(l_d\lambda 00|l_b 0)\end{aligned} \tag{543}$$

We then use equation (505) to rearrange the third Clebsch-Gordan coefficient in equation (543) to give

$$\begin{aligned}\mathcal{I}^{L\lambda}_{abcd} &= \sum_{m_a,m_b}\sum_{m_c,m_d}\sum_{m=-\lambda}^{+\lambda} c(l_a l_b m_a m_b|LM)c(l_c l_d m_c m_d|LM)\\ &\quad\times(-1)^{l_a+\lambda-l_c}\sqrt{\frac{(2l_a+1)(2l_b+1)}{(2l_c+1)(2l_d+1)}}c(l_a\lambda m_a - m|l_c m_c)c(l_a\lambda 00|l_c 0)\\ &\quad\times c(l_d\lambda m_d m|l_b m_b)c(l_d\lambda 00|l_b 0)\end{aligned} \tag{544}$$

Our next step is to use equation (506) to rearrange the first and third Clebsch-Gordan coefficients in equation (544) to give

$$\mathcal{I}^{L\lambda}_{abcd} = \sum_{m_a,m_b}\sum_{m_c,m_d}\sum_{m=-\lambda}^{+\lambda}(-1)^{l_a+l_b-L+l_a+\lambda-l_c+l_a+\lambda-l_c}\sqrt{\frac{(2l_a+1)(2l_b+1)}{(2l_c+1)(2l_d+1)}}$$

$$\times c(l_b l_a m_b m_a | LM) c(l_c l_d m_c m_d | LM) c(\lambda l_a - m m_a | l_c m_c) c(l_a \lambda 00 | l_c 0)$$
$$\times c(l_d \lambda m_d m | l_b m_b) c(l_d \lambda 00 | l_b 0) \quad (545)$$

Next we look at the first, third and fifth Clebsch-Gordan coefficients in equation (546) and see that we can use equation (517) to express these in terms of the product of a Racah W coefficient and a Clebsch-Gordan coefficient,

$$\begin{aligned} \mathcal{I}^{L\lambda}_{abcd} &= \sum_{m_c, m_d} (-1)^{l_a + l_b - L} \sqrt{(2l_a+1)(2l_d+1)} W(l_d \lambda L l_a | l_b l_c) \\ &\quad \times c(l_d \lambda 00 | l_b 0) c(l_a \lambda 00 | l_c 0) c(l_c l_d m_c m_d | l_L M) c(l_d l_c m_d m_c | LM) \end{aligned} \quad (546)$$

where we have used the constraint for equation (517), $m = m_1 + m_2 + m_3$ or $M = m_d + m + M$. This reduced the possible values for the angular momentum projections m_i thus simplifying the summation. Next we use equation (506) to rearrange the fourth Clebsch-Gordan coefficient in equation (546) to yield

$$\begin{aligned} \mathcal{I}^{L\lambda}_{abcd} &= \sum_{m_c, m_d} \sqrt{(2l_a+1)(2l_d+1)} W(l_d \lambda L l_a | l_b l_c) \\ &\quad \times c(l_d \lambda 00 | l_b 0) c(l_a \lambda 00 | l_c 0) c(l_c l_d m_c m_d | l_L M) c(l_c l_d m_c m_d | LM) \\ &\quad \times (-1)^{l_a + \lambda + l_c} (-1)^{l_b - \lambda - l_d} (-1)^{-L-L} \end{aligned} \quad (547)$$

We can remove the factor of (-1) by noting that by equation (503) when the first and second Clebsch-Gordan coefficients are non-zero the exponents must be even. We can also eliminate the remaining summation by making use of the orthogonality of Clebsch-Gordan coefficients illustrated in equation (508). This reduces equation (548) to

$$\mathcal{I}^{L\lambda}_{abcd} = \sqrt{(2l_a+1)(2l_d+1)} W(l_d \lambda L l_a | l_b l_c) c(l_d \lambda 00 | l_b 0) c(l_a \lambda 00 | l_c 0) \quad (548)$$

At this point we have eliminated any angular momentum projections and we can alter the indices *abcd* to reflect the fact we are only referencing the angular momenta. Hence we change our notation from $\mathcal{I}^{L\lambda}_{abcd}$ to $\mathcal{I}^{L\lambda}_{l_a l_b l_c l_d}$.

Next we use equation (507) to rearrange the remaining Clebsch-Gordan coefficients in equation (548) to yield

$$\begin{aligned} \mathcal{I}^{L\lambda}_{l_a l_b l_c l_d} &= (-1)^{l_a + l_d} (2\lambda + 1)^{-1} \sqrt{(2l_a+1)(2l_b+1)(2l_c+1)(2l_d+1)} \\ &\quad \times W(l_d \lambda L l_a | l_b l_c) c(l_d l_b 00 | \lambda 0) c(l_a l_c 00 | \lambda 0) \end{aligned} \quad (549)$$

and then use equation (506) to rearrange the second Clebsch-Gordan coefficient in equation (549) to give

$$\begin{aligned}\mathcal{I}^{L\lambda}_{l_a l_b l_c l_d} &= (-1)^{l_a+l_b-\lambda}(2\lambda+1)^{-1}\sqrt{(2l_a+1)(2l_b+1)(2l_c+1)(2l_d+1)} \\ &\quad \times W(l_d\lambda L l_a|l_b l_c)c(l_b l_d 00|\lambda 0)c(l_a l_c 00|\lambda 0) \end{aligned} \tag{550}$$

Lastly we can use the relation between the Racah W coefficient and the Wigner $6j$ symbol, equation (520), as well as the symmetry relations for the Wigner $6j$ symbol, equations (518) and (519), to rewrite the Racah W cofficient $(-1)^{l_a+l_b-\lambda}W(l_d\lambda L l_a|l_b l_c)$ as $(-1)^{l_a+l_c-L}W(l_a l_b l_c l_d|L\lambda)$. Using this equation (550) yields

$$\begin{aligned}\mathcal{I}^{L\lambda}_{l_a l_b l_c l_d} &= (-1)^{l_a+l_b-\lambda}(2\lambda+1)^{-1}\sqrt{(2l_a+1)(2l_b+1)(2l_c+1)(2l_d+1)} \\ &\quad \times W(l_a l_b l_c l_d|L\lambda)c(l_b l_d 00|\lambda 0)c(l_a l_c 00|\lambda 0) \end{aligned} \tag{551}$$

Additionally we note a few useful symmetry relations for the $\mathcal{I}^{L\lambda}_{l_a l_b l_c l_d}$ coefficients which are easily derived from equation (551). These are:

$$\mathcal{I}^{L\lambda}_{l_a l_b l_c l_d} = \mathcal{I}^{L\lambda}_{l_c l_d l_a l_b} = \mathcal{I}^{L\lambda}_{l_b l_a l_d l_c} \tag{552}$$

This relation makes use of the fact that due to parity conservation $(-1)^{l_a+l_b} = (-1)^{l_c+l_d}$.

APPENDIX E

PSEUDOSTATE CALCULATIONS

In this appendix we show explicitly the construction of the psuedostates and their corresponding energies from the Hamiltonian and overlap matrices.

We refer back to equation (191),

$$\mathbf{H} \cdot \alpha_\mu = E_\mu \mathbf{D} \cdot \alpha_\mu \tag{553}$$

where $\mathbf{H}$ is the Hamiltonian matrix, $\mathbf{D}$ is the overlap matrix, α_μ is an eigenstate that will be part of our pseudostate basis, and E_μ is an eigenvalue which is also the energy of the pseudostate α_μ. All matrices are constructed in the Sturmian basis as outlined in Chapter 4.

We begin the process of deriving the α coefficients as well as the energy eigenvalues by first factorizing the $\mathbf{H}$ and $\mathbf{D}$ matrices into the forms

$$\mathbf{H} = \mathbf{T} \cdot \mathbf{A} \cdot \mathbf{T}^\dagger \quad \mathbf{D} = \mathbf{T} \cdot \mathbf{T}^\dagger \tag{554}$$

where $\mathbf{T}$ is the matrix generated via a Cholesky decomposition [116]. $\mathbf{A}$ is a real symmetric matrix.

The Cholesky decomposition is valid because we could if we wished translate our Sturmian basis into an orthonormal basis via a unitary transformation. Indeed our pseudostates will form just such a basis. Under such a transformation the overlap matrix would be transformed into a diagonal matrix with eigenvalues along the diagonal. These eigenvalues are positive by construction thus satisfying the requirements that the matrix be positive definite.

Next we insert the result of equation (554) for $\mathbf{D}$ into (553) to get

$$\mathbf{H} \cdot \alpha_\mu = E_\mu \mathbf{T} \cdot \mathbf{T}^\dagger \cdot \alpha_\mu \tag{555}$$

Next we insert a factor of $(\mathbf{T}^\dagger)^{-1} \cdot \mathbf{T}^\dagger$ between $\mathbf{H}$ and α_μ and multiply by a factor of $\mathbf{T}^{-1}$ on both sides. This yields

$$\mathbf{T}^{-1} \cdot \mathbf{H} \cdot (\mathbf{T}^\dagger)^{-1} \cdot \mathbf{T}^\dagger \cdot \alpha_\mu = E_\mu \mathbf{T}^\dagger \cdot \alpha_\mu \tag{556}$$

Next we make use of the other part of equation (554) to get

$$\mathbf{T}^{-1} \cdot \mathbf{T} \cdot \mathbf{A} \cdot \mathbf{T}^\dagger \cdot (\mathbf{T}^\dagger)^{-1} \cdot \mathbf{T}^\dagger \cdot \alpha_\mu = E_\mu \mathbf{T}^\dagger \cdot \alpha_\mu \tag{557}$$

or more simply

$$\mathbf{A} \cdot \mathbf{T}^{\dagger} \cdot \alpha_{\mu} = E_{\mu} \mathbf{T}^{\dagger} \cdot \alpha_{\mu} \tag{558}$$

Our next step is to decompose $\mathbf{A}$ via spectral decomposition. Looking at equation (558), we see that the eigenvalues of $\mathbf{A}$ are the same as those of equation (553) and the eigenvectors are $\mathbf{T}^{\dagger} \cdot \alpha_{\mu}$. By spectral decomposition $\mathbf{A}$ can be expressed as

$$\mathbf{A} = \mathbf{X} \cdot \mathbf{E} \cdot \mathbf{X}^{\dagger} \tag{559}$$

where $\mathbf{X}$ is the matrix made up of the eigenvectors of $\mathbf{A}$ and $\mathbf{E}$ is a diagonal matrix containing the eigenvalues. This gives us the energies of our pseudostates but we still need to solve for the vectors α_{μ}. This can be done by solving

$$\mathbf{X} = \mathbf{T}^{\dagger} \cdot \alpha \tag{560}$$

where α now refers to that matrix made up of the eigenvectors α_{μ}. After making sure they are correctly normalized, this yields the eigenvectors of our Hamiltonian. These eigenvectors are the pseudostate basis we use in our close coupling expansion.

APPENDIX F

SPLINE DELTA S_Δ INTEGRALS

In this appendix we review how the integrals over the spline delta basis elements are conducted. As we know from Chapter 6, the actual basis elements have the form

$$\eta_i(r) = r^{l+1} u_i(r) \tag{561}$$

where l is the angular momentum which is included to ensure the correct Coulomb Cusp conditions. u_i is a cubic spline function with values of zero at each knot point except for the ith one where it has a value of one. Within a given interval j, the spline delta function has the form

$$u_{ij}(r) = f_{ij} + a_{ij}(r - r_j) + b_{ij}(r - r_j)^2 + c_{ij}(r - r_j)^3 \tag{562}$$

where $r_j \leq r \leq r_{j+1}$ and the second subscript refers to the interval in question.

Now we look at the inner product of two basis elements. Due to the orthogonality of the spherical harmonics our integrals will be confined to the case where $l_a = l_b$. The general form of this integral for a given interval is

$$\begin{aligned}
&\int_{r_j}^{r_{j+1}} r^{2l+2} dr u_i^j(r) u_k^j(r) = \\
&\int_{r_j}^{r_{j+1}} r^{2l+2} dr \Big(f_{ij} + a_{ij}(r - r_j) + b_{ij}(r - r_j)^2 + c_{ij}(r - r_j)^3 \Big) \\
&\qquad \times \Big(f_{kj} + a_{kj}(r - r_j) + b_{kj}(r - r_j)^2 + c_{kj}(r - r_j)^3 \Big)
\end{aligned} \tag{563}$$

We can simplify this expression if we expand u_{ij} in powers of r, this yields

$$\begin{aligned}
u_{ij}(r) &= (f_{ij} - a_{ij} r_j + b_{ij} r_j^2 - c_{ij} r_j^3) + (a_{ij} - 2 b_{ij} r_j + 3 c_{ij} r_j^2) r \\
&\quad + (b_{ij} - 3 c_{ij} r_j) r^2 + c_{ij} r^3 \\
&= \tilde{f}_{ij} + \tilde{a}_{ij} x + \tilde{b}_{ij} x^2 + c_{ij} x^3
\end{aligned} \tag{564}$$

where

$$\tilde{f}_{ij} = f_{ij} - a_{ij} x_j + b_{ij} x_j^2 - c_{ij} x_j^3 \tag{565}$$

$$\tilde{a}_{ij} = a_{ij} - 2 b_{ij} x_j + 3 c_{ij} x_j^2 \tag{566}$$

$$\tilde{b}_{ij} = b_{ij} - 3 c_{ij} x_j \tag{567}$$

We insert (564) into (563) to get

$$\begin{aligned}\int_{r_j}^{r_{j+1}} r^{2l+2}dru_i^j(r)u_k^j(r) &= \int_{r_j}^{r_{j+1}} r^{2l+2}dr\Big(\tilde{f}_{ij}+\tilde{a}_{ij}r+\tilde{b}_{ij}r^2+c_{ij}r^3\Big)\\ &\quad\times\Big(\tilde{f}_{kj}+\tilde{a}_{kj}r+\tilde{b}_{kj}r^2+c_{kj}r^3\Big)\\ &= \int_{r_j}^{r_{j+1}} dr\Big(\tilde{f}_{ij}\tilde{f}_{kj}r^{2l+2}+(\tilde{a}_{ij}\tilde{f}_{kj}+\tilde{f}_{ij}\tilde{a}_{kj})r^{2l+3}\\ &\quad+(\tilde{b}_{ij}\tilde{f}_{kj}+\tilde{f}_{ij}\tilde{b}_{kj}+\tilde{a}_{ij}\tilde{a}_{kj})r^{2l+4}\\ &\quad+(c_{ij}\tilde{f}_{kj}+\tilde{f}_{ij}c_{kj}+\tilde{b}_{ij}\tilde{a}_{kj}+\tilde{a}_{ij}\tilde{b}_{kj})r^{2l+5}\\ &\quad+(c_{ij}\tilde{a}_{kj}+\tilde{a}_{ij}c_{kj}+\tilde{b}_{ij}\tilde{b}_{kj})r^{2l+6}\\ &\quad+(c_{ij}\tilde{b}_{kj}+\tilde{b}_{ij}c_{kj})r^{2l+7}+c_{ij}c_{kj}r^{2l+8}\Big) \qquad (568)\end{aligned}$$

Looking at (568) we see that the integral is easily solved to yield

$$\begin{aligned}\int_{r_j}^{r_{j+1}} r^{2l+2}dru_i^j(r)u_k^j(r) &= \tilde{f}_{ij}\tilde{f}_{kj}s(2l+2)+(\tilde{a}_{ij}\tilde{f}_{kj}+\tilde{f}_{ij}\tilde{a}_{kj})s(2l+3)\\ &\quad+(\tilde{b}_{ij}\tilde{f}_{kj}+\tilde{f}_{ij}\tilde{b}_{kj}+\tilde{a}_{ij}\tilde{a}_{kj})s(2l+4)\\ &\quad+(c_{ij}\tilde{f}_{kj}+\tilde{f}_{ij}c_{kj}+\tilde{b}_{ij}\tilde{a}_{kj}+\tilde{a}_{ij}\tilde{b}_{kj})s(2l+5)\\ &\quad+(c_{ij}\tilde{a}_{kj}+\tilde{a}_{ij}c_{kj}+\tilde{b}_{ij}\tilde{b}_{kj})s(2l+6)\\ &\quad+(c_{ij}\tilde{b}_{kj}+\tilde{b}_{ij}c_{kj})s(2l+7)+c_{ij}c_{kj}s(2l+8) \qquad (569)\end{aligned}$$

where

$$s(l)=\int_{r_j}^{r_{j+1}} r^l dr \qquad (570)$$

Using this calculation we can construct the overlap matrix D. To solve for the pseudostates we also need to construct the $1e^-$ Hamiltonian H. This is simply a sum of a Coulomb potential, a Centrifugal term, and a Bloch modified kinetic energy operator. The Coulomb element can be integrated over the intervals and has the form

$$\begin{aligned}\int_{r_j}^{r_{j+1}} r^{2l+2}dru_i^j(r)\frac{Z}{r}u_k^j(r) &= Z\Big(\tilde{f}_{ij}\tilde{f}_{kj}s(2l+1)+(\tilde{a}_{ij}\tilde{f}_{kj}+\tilde{f}_{ij}\tilde{a}_{kj})s(2l+2)\\ &+ (\tilde{b}_{ij}\tilde{f}_{kj}+\tilde{f}_{ij}\tilde{b}_{kj}+\tilde{a}_{ij}\tilde{a}_{kj})s(2l+3)\\ &+ (c_{ij}\tilde{f}_{kj}+\tilde{f}_{ij}c_{kj}+\tilde{b}_{ij}\tilde{a}_{kj}+\tilde{a}_{ij}\tilde{b}_{kj})s(2l+4)\\ &+ (c_{ij}\tilde{a}_{kj}+\tilde{a}_{ij}c_{kj}+\tilde{b}_{ij}\tilde{b}_{kj})s(2l+5)\\ &+ (c_{ij}\tilde{b}_{kj}+\tilde{b}_{ij}c_{kj})s(2l+6)+c_{ij}c_{kj}s(2l+7)\Big) \qquad (571)\end{aligned}$$

in a given interval. The same formula holds up for the centrifugal term except the

constant factor is $l(l+1)$ instead of Z. Lastly the Bloch modified kinetic energy is

$$\begin{aligned}\frac{1}{2}\int_{r_j}^{r_{j+1}} dr \nabla\eta_i^j(r)\cdot\nabla\eta_k^j(r) &= \Big(\tilde{f}'_{ij}\tilde{f}_{kj'}s(2l)+(\tilde{a}'_{ij}\tilde{f}'_{kj}+\tilde{f}'_{ij}\tilde{a}'_{kj})s(2l+1)\\ &+ (\tilde{b}'_{ij}\tilde{f}'_{kj}+\tilde{f}'_{ij}\tilde{b}'_{kj}+\tilde{a}'_{ij}\tilde{a}'_{kj})s(2l+2)\\ &+ (c'_{ij}\tilde{f}'_{kj}+\tilde{f}'_{ij}c'_{kj}+\tilde{b}'_{ij}\tilde{a}'_{kj}+\tilde{a}'_{ij}\tilde{b}'_{kj})s(2l+3)\\ &+ (c'_{ij}\tilde{a}'_{kj}+\tilde{a}'_{ij}c'_{kj}+\tilde{b}'_{ij}\tilde{b}'_{kj})s(2l+4)\\ &+ (c'_{ij}\tilde{b}'_{kj}+\tilde{b}'_{ij}c'_{kj})s(2l+5)+c'_{ij}c'_{kj}s(2l+6)\Big) \quad (572)\end{aligned}$$

where

$$\tilde{f}'_{ij} = (l+1)\tilde{f}_{ij} \quad (573)$$

$$\tilde{a}'_{ij} = (l+2)\tilde{a}_{ij} \quad (574)$$

$$\tilde{b}'_{ij} = (l+3)\tilde{b}_{ij} \quad (575)$$

$$c'_{ij} = (l+4)c_{ij} \quad (576)$$

for a given interval. Thus we solve for the matrix elements, adding up the contributions from each interval and then solve the eigenvector equation as outlined in Appendix E.

APPENDIX G

MATHEMATICAL RESULTS

In this appendix we derive various minor mathematical results for our derivations.

G.1 ASYMPTOTIC FORM OF THE PLANE WAVE

Many times in describing an escaping or incoming particle we approximate its behavior as that of a plane wave $e^{i\mathbf{k}\cdot\mathbf{r}}$. It is thus of interest to us to determine what the asymptotic behavior of a plane wave is. In terms of spherical waves, a plane wave asymptotically behaves as

$$\lim_{r\to\infty} e^{i\mathbf{k}\cdot\mathbf{r}} \sim \frac{2\pi}{ikr}\{\delta(\hat{\mathbf{k}}-\hat{\mathbf{r}})e^{ikr} - \delta(\hat{\mathbf{k}}+\hat{\mathbf{r}})e^{-ikr}\} \tag{577}$$

This unintuitive result may be proven as follows. We begin with the Raliegh expansion of the plane wave in terms of spherical waves [106]

$$e^{i\mathbf{k}\cdot\mathbf{r}} = \sum_l (2l+1)P_l(\hat{\mathbf{k}}\cdot\hat{\mathbf{r}})i^l j_l(kr) \tag{578}$$

where $j_l(kr)$ are spherical bessel functions and P_l are the Legendre functions. We can make use of the spherical harmonic addition theorem [106] to write

$$P_l(\hat{\mathbf{k}}\cdot\hat{\mathbf{r}}) = \frac{4\pi}{2l+1}\sum_m Y^*_{lm}(\hat{\mathbf{k}})Y_{lm}(\hat{\mathbf{r}}) \tag{579}$$

With this we can write

$$e^{i\mathbf{k}\cdot\mathbf{r}} = 4\pi\sum_{lm} Y^*_{lm}(\hat{\mathbf{k}})Y_{lm}(\hat{\mathbf{r}})i^l j_l(kr) \tag{580}$$

Asymptotically the spherical bessel functions behave as

$$\begin{aligned}\lim_{r\to\infty} j_l(kr) &\sim (kr)^{-1}\sin(kr - l\pi/2) \\ &\sim (2ikr)^{-1}(i^{-l}e^{ikr} - i^l e^{-ikr})\end{aligned} \tag{581}$$

Combining (581) and (580) we get

$$\lim_{r\to\infty} e^{i\mathbf{k}\cdot\mathbf{r}}\,\frac{2\pi}{ikr}\sum_{lm} Y^*_{lm}(\hat{\mathbf{k}})Y_{lm}(\hat{\mathbf{r}})(e^{ikr} - (-1)^l e^{-ikr}) \tag{582}$$

Next we make use of the fact that the spherical harmonics y_{lm} form an orthonormal set

$$\sum_{lm} Y^*_{lm}(\hat{\mathbf{k}}) Y_{lm}(\hat{\mathbf{r}}) = \delta(\hat{\mathbf{k}} - \hat{\mathbf{r}}) \tag{583}$$

and the fact that $(-1)^l Y_{lm}(\hat{\mathbf{r}}) = Y_{lm}(-\hat{\mathbf{r}})$. Using these two results (582) becomes

$$\lim_{r\to\infty} e^{i\mathbf{k}\cdot\mathbf{r}} \sim \frac{2\pi}{ikr}\{\delta(\hat{\mathbf{k}} - \hat{\mathbf{r}})e^{ikr} - \delta(\hat{\mathbf{k}} + \hat{\mathbf{r}})e^{-ikr}\} \tag{584}$$

G.2 SUMMATION RULE FOR SPHERICAL HARMONICS

Here we will present a simple derivation of a summation rule for spherical harmonics. We begin with the general addition theorem for spherical harmonics [117],

$$P_l(\cos\gamma) = \frac{4\pi}{2l+1} \sum_{m=-l}^{m} Y^*_{lm}(\theta', \phi') Y_{lm}(\theta, \phi) \tag{585}$$

where

$$\cos\gamma = \cos\theta\cos\theta' + \sin\theta\sin\theta'\cos(\phi - \phi') \tag{586}$$

If we let $\theta = \theta', \phi = \phi'$ the equation (585) becomes

$$P_l(1) = \frac{4\pi}{2l+1} \sum_{m=-l}^{m} |Y_{lm}(\theta, \phi)|^2 \tag{587}$$

but $P_l(1) = 1 \ \forall\, l$ [118] hence (587) becomes

$$\sum_m |Y_{lm}|^2 = \frac{2l+1}{4\pi} \tag{588}$$

thus yielding the summation rule.

APPENDIX H

ALTERNATE ASYMPTOTIC FORMS

In developing the X2e method we considered several possible projectors [119] for use in the asymptotic region in addition to the form developed by Rudge and Seaton [12]. In this appendix we review these other methods examining their strengths and weaknesses. We begin with the special case formula by Alt and Mukhamedzhanov. Then we look at the form developed by Engelns as a general case solution. We compare the two forms and examine the relative merits. Then we discuss why in practical calculations we have no need for them.

H.1 ASYMPTOTIC SOLUTION FOR $R_{12} \not\to \infty$

Special care must be taken in deriving the asymptotic expansion for double ionization in the case where the distance between the two electrons remains small. As described in Alt and Mukhamedzhanov's paper (AM) [120] keeping terms of only leading order in the derivation of an asymptotic form (such as we did in the RSP derivation of Chapter 7) yields unsatisfactory results in such a case. Their solution rectifies this issue.

The AM asymptotic form is derived using a center of mass approach with respect to the coordinates. For two electrons the vector $\mathbf{R}$ joining the their center of mass to ion equals $\frac{1}{2}(\mathbf{r}_1 + \mathbf{r}_2)$. The canonically conjugated relative momentum is $\mathbf{q} = \mathbf{k}_1 + \mathbf{k}_2$. The vector connecting the two electrons is defined as $\mathbf{r}_{12} = \mathbf{r}_1 - \mathbf{r}_2$ and their relative momentum $\mathbf{k}_{12} = \frac{1}{2}(\mathbf{k}_1 - \mathbf{k}_2)$.

The Schrödinger equation describing this system (in the coordinates described above) is:

$$\{T_{r_{12}} + T_R + V - E\}\Psi_{\mathbf{k}_{12},\mathbf{q}}(\mathbf{r}_{12}, \mathbf{R}) = 0 \tag{589}$$

with

$$V = -\frac{Z}{r_1} - \frac{Z}{r_2} + \frac{1}{r_{12}} \tag{590}$$

$$T_{r_{12}} = -\nabla^2_{\mathbf{r}_{12}} \tag{591}$$

$$T_R = -\frac{\nabla^2_{\mathbf{R}}}{4} \tag{592}$$

$$E = \frac{q^2}{4} + k_{12}^2. \tag{593}$$

There are two asymptotic regions to consider. In the Ω_0 case all interparticle distances go to infinity. In hyperspherical notation this corresponds to the case where $\rho \to \infty$ and $\alpha \neq 0, \frac{\pi}{2}, \frac{\pi}{4}$.

In the other case, Ω_1, the distance between the atom and the center of mass for the two electron subsystem goes to infinity but the relative distance between them stays finite, thus $r_{12}/R \to 0$. This corresponds to $\rho \to \infty$, $\alpha \to \pi/4$, where the anglar coordinates of the electrons are similar.

The solution for Ω_1 should match up with Ω_0 as r_{12} is allowed to expand to infinity. The form of the solution to the Ω_0 case is taken by AM to be a product of Coulomb-distorted waves, much like the form we just derived. Excepting in the singular directions ($\mathbf{k}_\nu \cdot \mathbf{r}_\nu = -1$), this takes the form:

$$\Psi_0^{as}(r) = e^{i\mathbf{k}_{12}\cdot\mathbf{r}_{12} + i\mathbf{q}\cdot\mathbf{R}} \prod_{\nu=1}^{3} e^{i\eta_\nu \ln(k_\nu r_\nu + \mathbf{k}_\nu \cdot \mathbf{r}_\nu)} + O(1/r) \tag{594}$$

with

$$\eta_\alpha = e_b e_c \mu_a / k_a, \text{ and } \quad \mu_{1,2} = 1, \quad \mu_3 = \mu_{12} = 1/2. \tag{595}$$

In the notation above, the subscripts α denote are defined as $A_a = A_{bc}$ where $a \neq b \neq c$. For example, $\mu_3 = \mu_{12}$. μ are the reduced masses and e are the electric charge of the particle.

In determining the general form of the solution we note that $R \to \infty$ implies $r_1 \to \infty$ and $r_2 \to \infty$. Thus with respect to the motion of each electron to the ion, Ω_1 coincides with Ω_0. Thus we can represent the relative motion of these two subsystems with the same Coulomb-distortion factors as for the asymptotic solution for Ω_0, as long we stay away from the singular directions. Hence the form of the solution for Ω_1 should be:

$$\Psi^{as}_{\mathbf{k}_{12},\mathbf{q}}(\mathbf{r}_{12}, \mathbf{R}) = e^{i(\mathbf{k}_{12}\cdot\mathbf{r}_{12} + \mathbf{q}\cdot\mathbf{R})} F(\mathbf{r}_{12}; \mathbf{R}) e^{i\eta_1 \ln(k_1 r_1 + \mathbf{k}_1 \cdot \mathbf{r}_1)} e^{i\eta_2 \ln(k_2 r_2 + \mathbf{k}_2 \cdot \mathbf{r}_2)}. \tag{596}$$

where F is the function that remains to be determined that depends on the relative motion of the electrons, possibly modified by the interaction with the ion. It is assumed that a solution can be found such that:

$$\nabla_R F(\mathbf{r}_{12}; \mathbf{R}) = O(\frac{1}{R^2}) \tag{597}$$

so that the transition from Ω_1 to Ω_0 is smooth.

The first step is to write the Coulomb-distortion factors in terms of $\mathbf{R}$ and $\mathbf{r}_{12}$ in the limit $r_{12}/R \to 0$, discarding terms of $O(1/R^2)$. This has the form

$$e^{i\eta_1 \ln(k_1 r_1 + \mathbf{k}_1 \cdot \mathbf{r}_1)} \approx e^{i\eta_1 \ln(k_1 R + \mathbf{k}_1 \cdot \mathbf{R}) + i\mathbf{a}^{(1)}(\hat{\mathbf{R}}) \cdot \mathbf{r}_1 / R} \tag{598}$$

with

$$\mathbf{a}^{(1)}(\hat{\mathbf{R}}) = \eta_1 \frac{\hat{\mathbf{R}} + \hat{\mathbf{k}}_1}{1 + \hat{\mathbf{R}} \cdot \hat{\mathbf{k}}_1}. \tag{599}$$

The result for the second Coulomb-distortion term, with 2 instead of 1, differs by an overall sign. Putting these results back into our formula we have

$$\begin{aligned} \Psi^{as}_{\mathbf{k}_{12},\mathbf{q}}(\mathbf{r}_{12}, \mathbf{R}) &= e^{i(\mathbf{k}_{12}(\mathbf{R}) \cdot \mathbf{r_{12}} + \mathbf{q} \cdot \mathbf{R})} F(\mathbf{r}_{12}; \mathbf{R}) e^{i\eta_1 \ln(k_1 R + \mathbf{k}_1 \cdot \mathbf{R})} \\ &\quad \times e^{i\eta_2 \ln(k_2 R + \mathbf{k}_2 \cdot \mathbf{R})} + O(\frac{1}{R^2}) \end{aligned} \tag{600}$$

with

$$\mathbf{k}_{12}(\mathbf{R}) = \mathbf{k}_{12} + \frac{\mathbf{a}(\hat{\mathbf{R}})}{R} \tag{601}$$

$$\mathbf{a}(\hat{\mathbf{R}}) = \eta_1 \frac{\hat{\mathbf{R}} + \hat{\mathbf{k}}_1}{1 + \hat{\mathbf{R}} \cdot \hat{\mathbf{k}}_1} - \eta_2 \frac{\hat{\mathbf{R}} + \hat{\mathbf{k}}_2}{1 + \hat{\mathbf{R}} \cdot \hat{\mathbf{k}}_2}. \tag{602}$$

The next step is to return to the Schrödinger equation and divide the Hamiltonian into a R part (center of mass relation) and r_{12} part corresponding to the electron interaction:

$$H^{as} = \tilde{H}^{as}_{\mathbf{R}} + \tilde{H}^{C}_{\mathbf{r}_{12}}(\mathbf{R}) \tag{603}$$

$$\tilde{H}^{as}_{R} = T_R + v^C(\mathbf{R}) - \tilde{V}^{C}_{12}(\mathbf{R}) \tag{604}$$

$$\tilde{H}^{C}_{\mathbf{r}_{12}} = T_{\mathbf{r}_{12}} + V^C(\mathbf{r}_{12}) + \tilde{V}^{C}_{12}(\mathbf{R}). \tag{605}$$

with

$$\tilde{V}^{C}_{12}(\mathbf{R}) = -2\frac{\mathbf{a}(\hat{\mathbf{R}}) \cdot \mathbf{k}_{12}}{R} \tag{606}$$

$$V^C(\mathbf{r}_{12}) = \frac{1}{r_{12}} \tag{607}$$

$$v^C(\mathbf{R}) = \lim_{R \to \infty, r_{12}/R \to 0} (\frac{Z}{r_1} + \frac{Z}{r_2}) = \frac{2Z}{R}. \tag{608}$$

Next we define a function $\chi^{as}_{\mathbf{k}_{12},\mathbf{q}}(\mathbf{R})$ as

$$\chi^{as}_{\mathbf{k}_{12},\mathbf{q}}(\mathbf{R}) = e^{i\mathbf{q} \cdot \mathbf{R}} e^{i\eta_1 \ln(k_1 R + \mathbf{k}_1 \cdot \mathbf{R})} e^{i\eta_2 \ln(k_2 R + \mathbf{k}_2 \cdot \mathbf{R})}. \tag{609}$$

As can be seen this corresponds to portion of our wave function directly related to R. Applying it to $\tilde{H}_R^{as}$ portion of the Schrodinger equation:

$$\begin{aligned}
&\{T_R + v^C(\mathbf{R}) - \tilde{V}_{12}^C(\mathbf{R}) - \frac{q^2}{4}\}\chi_{\mathbf{k}_{12},\mathbf{q}}^{as}(\mathbf{R}) \\
&\qquad = e^{i\mathbf{q}\cdot\mathbf{R}}\{-\frac{i\mathbf{q}\cdot\nabla_{\mathbf{R}}}{2} + \frac{2Z}{R} - \tilde{V}_{12}^C(\mathbf{R}) \\
&\qquad\quad +O(1/R^2)\}e^{i\eta_1 \ln(k_1 R + \mathbf{k}_1\cdot\mathbf{R})}e^{i\eta_2 \ln(k_2 R + \mathbf{k}_2\cdot\mathbf{R})} \\
&\qquad = \{-\frac{\mathbf{q}}{R}\cdot[-\mathbf{a}^{(1)}(\hat{\mathbf{R}}) + \mathbf{a}^{(2)}(\hat{\mathbf{R}})] + \frac{2Z}{R} - \tilde{V}_{12}^C(\mathbf{R}) \\
&\qquad\quad +O(1/R^2)\}\chi_{\mathbf{k}_{12},\mathbf{q}}^{as}(\mathbf{R}) \\
&\qquad = O(1/R^2). \qquad (610)
\end{aligned}$$

Thus (609) satisfies the R portion of the Hamiltonian to $O(1/R^2)$. We can use this result to simplify the asymptotic Schrodinger equation.

$$\begin{aligned}
&\{H^{as} - E\}e^{i\mathbf{k}_{12}(\mathbf{R})\cdot\mathbf{r}_{12}}F(\mathbf{r}_{12};\mathbf{R})\chi_{\mathbf{k}_{12},\mathbf{q}}^{as}(\mathbf{R}) \\
&\qquad = e^{i\mathbf{k}_{12}(\mathbf{R})\cdot\mathbf{r}_{12}}F(\mathbf{r}_{12};\mathbf{R})\{\tilde{H}_{\mathbf{R}}^{as} - \frac{q^2}{4}\}\chi_{\mathbf{k}_{12},\mathbf{q}}^{as}(\mathbf{R}) \\
&\qquad\quad +\chi_{\mathbf{k}_{12},\mathbf{q}}^{as}(\mathbf{R})\{\tilde{H}_{\mathbf{k}_{12}}^C - k_{12}^2\}e^{i\mathbf{k}_{12}(\mathbf{R})\cdot\mathbf{r}_{12}}F(\mathbf{r}_{12};\mathbf{R}) \\
&\qquad\quad +O(\frac{1}{R^2}) \\
&\qquad = \chi_{\mathbf{k}_{12},\mathbf{q}}^{as}(\mathbf{R})\{\tilde{H}_{\mathbf{k}_{12}}^C - k_{12}^2\}e^{i\mathbf{k}_{12}(\mathbf{R})\cdot\mathbf{r}_{12}}F(\mathbf{r}_{12};\mathbf{R}) \\
&\qquad\quad +O(\frac{1}{R^2}). \qquad (611)
\end{aligned}$$

In the first equality the $H_{\mathbf{R}}^{as}$ could be shifted through the first two terms since the result would be of $O(1/R^2)$ as assumed in (597). Hence we now need to solve the following equation to derive a solution:

$$\{\tilde{H}_{\mathbf{k}_{12}}^C - k_{12}^2\}e^{i\mathbf{k}_{12}(\mathbf{R})\cdot\mathbf{r}_{12}}F(\mathbf{r}_{12};\mathbf{R}) = O(\frac{1}{R^2}). \qquad (612)$$

This can be adjusted as follows:

$$\begin{aligned}
\{\tilde{H}_{\mathbf{k}_{12}}^C - k_{12}^2\} &= \{T_{\mathbf{r}_{12}} + V^C(\mathbf{r}_{12}) + \tilde{V}_{12}^C(\mathbf{R}) - k_{12}^2\} \\
&= \{T_{\mathbf{r}_{12}} + V^C(\mathbf{r}_{12}) - 2\frac{\mathbf{a}(\hat{\mathbf{R}})\cdot\mathbf{k}_{12}}{R} - k_{12}^2\} \\
&= \{T_{\mathbf{r}_{12}} + V^C(\mathbf{r}_{12}) - k_{12}^2(\mathbf{R}) + O(\frac{1}{R^2})\}. \qquad (613)
\end{aligned}$$

where $k_{12}(\mathbf{R})$ is the modified momentum dependent on the direction of the individual electrons relative to the center of mass.

This yields a 2 body problem in a Coulomb potential to order $1/R^2$, where the energy is now the local energy of the 2 electron subsystem. An exact solution to this problem can immediately be found:

$$\begin{aligned}\psi_{C,\mathbf{k}_{12}(R)}(\mathbf{R}) &= e^{i\mathbf{k}_{12}(\mathbf{R})\cdot\mathbf{r_{12}}}N(\mathbf{R}) \\ &\quad \times {}_1F_1(-i\eta_{12}(\mathbf{R}),1;i[k_{12}(\mathbf{R})r_{12}+\mathbf{k}_{12}(\mathbf{R})\cdot\mathbf{r}_{12}]) \qquad (614)\end{aligned}$$

with

$$\eta_{12}(\mathbf{R}) = \frac{1}{2k_{12}(\mathbf{R})} \qquad \text{and} \qquad N(\mathbf{R}) = e^{-\pi\eta_{12}(\mathbf{R})/2}\Gamma(1+i\eta_{12}(\mathbf{R})). \qquad (615)$$

Thus our final wave function is:

$$\begin{aligned}\Psi^{as}_{\mathbf{k}_{12},\mathbf{q}}(\mathbf{r}_{12},\mathbf{R}) &= \psi_{C,\mathbf{k}_{12}(\mathbf{R})}(\mathbf{r}_{12})\chi^{as}_{\mathbf{k}_{12},\mathbf{q}}(\mathbf{R}) \\ &= e^{i(\mathbf{k}_{12}(\mathbf{R})\cdot\mathbf{r_{12}}+\mathbf{q}\cdot\mathbf{R})}{}_1F_1(-i\eta_{12}(\mathbf{R}),1;i[k_{12}(\mathbf{R})r_{12}+\mathbf{k}_{12}(\mathbf{R})\cdot\mathbf{r}_{12}]) \\ &\quad \times N(\mathbf{R})e^{i\eta_1\ln(k_1R+\mathbf{k}_1\cdot\mathbf{R})}e^{i\eta_2\ln(k_2R+\mathbf{k}_2\cdot\mathbf{R})}. \qquad (616)\end{aligned}$$

Comparing this result to (594) we see that if $r_{12}\rightarrow\infty$ the two results match up since:

$$\lim_{r_{12}\rightarrow\infty} N_1F_1(-i\eta_{12},1;i[k_{12}r_{12}+\mathbf{k}_{12}\cdot\mathbf{r}_{12}]) \approx e^{i\eta_{12}\ln(k_{12}r_{12}+\mathbf{k}_{12}\cdot\mathbf{r}_{12}])} \qquad (617)$$

Now for the boundary conditions to be satisfied the wave function and its derivative should be zero when $\mathbf{r}_1$ equals $\mathbf{r}_2$ (i.e. when $\alpha=\pi/4$). In this case $\mathbf{r}_{12}$ is zero and it can easily be seen that the wave function itself is zero. Looking at the derivative with respect to r_1:

$$\begin{aligned}\frac{\partial\Psi}{\partial r_1}\Big|_{r_{12}=0} &= A\Psi + B_1F_1(1-i\eta_{12}(\mathbf{R}),2;i[k_{12}(\mathbf{R})r_{12}+\mathbf{k}_{12}(\mathbf{R})\cdot\mathbf{r}_{12}]) \\ &= 0 \qquad (618)\end{aligned}$$

where A is a factor derived from the derivatives of the exponentials and B are the various factors attached to the derivative of the hypergeometric function. As can be seen each term becomes zero when $r_{12}=0$. The same result follows a derivative with respect to r_2.

H.2 COMPARISON OF $R_{12}\not\rightarrow\infty$ SOLUTION TO ENGELNS ET AL. ASYMPTOTIC SOLUTION

Recently Engelns [121] and others have proposed an asymptotic solution to the double ionization problem that would cover all asymptotic domains. This form would be

valid in both the case were the interparticles distances become infinite and when the two escaping electron are close (becoming the AM form in that limit). There has been some interest [119] in using this form as an asymptotic form to use in an $\mathcal{R}$-operator formalism. Here we will discuss its relative merits.

The form itself is derived from the Schrödinger equation for the system through the use of the eikonal equation. In its most general form it can be expressed:

$$\begin{aligned}\Psi &= e^{i(\mathbf{k}_1\cdot\mathbf{r}_1+\mathbf{k}_2\cdot\mathbf{r}_2)}{}_1F_1\left(-i\frac{Z}{k_{2\text{eff}}},1;-i(k_{2\text{eff}}r_2+\mathbf{k}_{2\text{eff}}\cdot\mathbf{r}_2)\right)\\ &\quad\times{}_1F_1\left(-i\frac{Z}{k_1},1;-i(k_1r_1+\mathbf{k}_1\cdot\mathbf{r}_1)\right)B(r_{12})\end{aligned}\tag{619}$$

with

$$B(r_{12})={}_1F_1\left(-i\frac{1}{2\kappa_{\text{eff}}},1;-i(\kappa_{\text{eff}}r_{12}+\kappa_{\text{eff}}\cdot\mathbf{r}_{12})\right).\tag{620}$$

As can be seen the Engelns form uses two modified momenta as opposed to the AM form which only has one. Curiously Engelns asserts that AM modifies the momenta of both outgoing particles which as can be seen from the previous section is not the case. The modified momenta used by Engelns are:

$$\mathbf{k}_{2\text{eff}}=\mathbf{k}_2+\nabla_2\Phi\tag{621}$$

where

$$\Phi=-\frac{Z}{k_1}\ln(r_1+\hat{\mathbf{k}}_1\cdot\mathbf{r}_1)+\frac{1}{k_{12}}\ln(r_{12}+0.5\hat{\mathbf{k}}_{12}\cdot\mathbf{r}_{12})\tag{622}$$

and r_1 denoting the position of the farther particle in this case, and:

$$\kappa_{\text{eff}}=\mathbf{k}_{12}+0.5(\nabla_1\Lambda-\nabla_2\Lambda)\tag{623}$$

where

$$\Lambda=-\frac{Z}{k_1}\ln(r_1+\hat{\mathbf{k}}_1\cdot\mathbf{r}_1)-\frac{Z}{k_2}\ln(r_2+\hat{\mathbf{k}}_2\cdot\mathbf{r}_2)\tag{624}$$

and k_{12} is defined as in the previous section.

As one can see in the limit of $r_2\to\infty$, $\mathbf{k}_{2\text{eff}}$ will reduce to k_2. As noted earlier in (617), as $r\to\infty$ the hypergeometric functions become approximately exponentials. This brings us close to the AM form and we can see B should be identified with the hypergeometric term in that form. Comparing the two requires us to take a close look at κ_{eff} to ensure that it corresponds to $k_{12}(\mathbf{R})$ when $r_{12}\not\to\infty$. As mentioned earlier

$$k_{12}(\mathbf{R})=\mathbf{k}_{12}-\frac{Z}{R}\left(\frac{\hat{\mathbf{R}}-\hat{\mathbf{k}}_1}{k_1-\hat{\mathbf{R}}\cdot\mathbf{k}_1}-\frac{\hat{\mathbf{R}}-\hat{\mathbf{k}}_2}{k_2-\hat{\mathbf{R}}\cdot\mathbf{k}_2}\right)\tag{625}$$

The first difference of note is a factor 1/2 for the second term. But a more important concern is that the relationship of the momentum and radial vectors is preserved. Using the form of Λ in the equation for κ_{eff}:

$$\kappa_{\text{eff}} = \mathbf{k}_{12} - 0.5\left(\frac{Z}{k_1}\frac{\hat{\mathbf{r}}_1 + \hat{\mathbf{k}}_1}{r_1 + \hat{\mathbf{k}}_1 \cdot \mathbf{r}_1} - \frac{Z}{k_2}\frac{\hat{\mathbf{r}}_2 + \hat{\mathbf{k}}_2}{r_2 + \hat{\mathbf{k}}_2 \cdot \mathbf{r}_2}\right) \tag{626}$$

Only in the case of $\mathbf{r}_1 \approx \mathbf{r}_2 \approx \mathbf{R}$ do we have direct correspondence. This is a more extreme condition than that used by AM who require that the difference between $\mathbf{r}_1$ and $\mathbf{r}_2$ be small relative to the $\mathbf{R}$. The Engelns form is not a perfect correspondence to the AM form in the $r_{12}/R \rightarrow 0$ limit.

In the limit that all the particles become separated however the transition is much smoother. κ_{eff} goes smoothly over to k_{12} for large radii and the result is clearly a product of the three Coulomb waves, the BBK form derived by Brauner, Brigggs, and Klaur [122]:

$$\Psi(\mathbf{r}_1, \mathbf{r}_2) = e^{i(\mathbf{k}_1 \cdot \mathbf{r}_1 + \mathbf{k}_2 \cdot \mathbf{r}_2)} F(Z/k_1, \mathbf{k}_1, \mathbf{r}_1) F(Z/k_2, \mathbf{k}_2, \mathbf{r}_2) F(1/k_{12}, \mathbf{k}_{12}, \mathbf{r}_{12}) \tag{627}$$

where F is a Coulomb wave. If we look at (617) we can see that the Engelns form and the BBK form go over to that of the RSP derivation.

H.3 CONCLUSION

After having reviewed these various forms including the RSP form of Chapter 7, we must choose one for our calculations. Though ideally there would be a solution that satisfied the conditions in all regions, ultimately we want a solution that is valid for the calculations we can compare with experiment. Also we want a solution that is simple if possible.

For experimental purposes there is a lower limit on how close two electrons can be detected. The detectors used to find these electrons in coincidence are physical objects and therefore must have some volume. This forces some space between the two detected electrons and a thus a minimum distance between them. This distance will be many times larger than the distance considered in AM solution.

For this reason and the interests of a simple solution that we discard the AM and Engelns forms as more complex than our needs. Returning to the RSP form (407) we find that we can in fact derive an even simpler solution through the use of effective charges. This is shown in Chapter 6, when we develop our surface integral for the ionization amplitude.

H.4 SUMMARY

We reviewed the other methods considered for the X2e asymptotic projectors. We showed the special case formula by Alt and Mukhamedzhanov, discussing its motivation and deriving the result. We looked at the form developed by Engelns as a general case solution. We compared it to the AM form and to the BBK form. We tested the claims made by Engelns. Lastly we discussed why in practical calculations we do not need these complicated asymptotic projectors.

VITA

Jason Manuel Martinez
Department of Physics
Old Dominion University
Norfolk, VA 23529

Jason Manuel Martinez was born on January 27, 1979 in Bayshore, New York. He grew up on Long Island and attended the Sachem Central School District where he excelled in mathematics and the sciences. He earned his Bachelor of Arts in Physics in May of 2001 from Reed College in Portland, Oregon. His senior thesis was entitled "Classical and Quantum Features of a Localized Wave Packet in a Coulombic Potential." He earned his Master of Science degree in Physics at Old Dominion University in May of 2005.

Typeset using LaTeX.